UNIVERSITY OF BIRMINGHAM

The Crystallization of Poly(ethylene terephthalate) Studied by Thermal Analysis and FTIR Spectroscopy

ZIYU CHEN

A thesis submitted to the

University of Birmingham

For the degree of

Doctor of Philosophy

School of Metallurgy and Materials

College of Engineeting and Physical Sciences

University of Birmingham

December 2012

Synopsis

This thesis concerns the thermal behaviour and properties, isothermal crystallization kinetics and seeded crystallization study of poly(ethylene terephthalate) (PET) using thermal analysis Fourier transform infrared spectroscopy (TA-FTIR), two-dimensional infrared correlation spectroscopy (2D-FTIR) and differential scanning calorimetry (DSC).

TA-FTIR has been used to characterize phase transitions by a change in the absorbance or peak position with temperature in thermal cycling. It provides more information in assigning the phase transition temperature to an individual chain segment rather than other TA techniques. It also observes two different types of thermal behaviours, Type I and Type II, of the functional groups during thermal treatment.

The most significant achievement of this project assign to find out that the carbonyl stretching band has an amorphous band at 1727 cm^{-1} in the melt and a crystalline band at 1717 cm^{-1} by TA-FTIR. It was then successfully analyzed by 2D correlation spectroscopy and presented “angel” pattern and two cross peaks on synchronous and asynchronous correlation spectra respectively.

The isothermal crystallization kinetics of PET were measured from 230 to 240^{o}C by FTIR focusing on the carbonyl ester group. The deconvolution of the 1727 and 1717 cm^{-1} overlapping absorption bands makes it possible to analyze the kinetics of both primary and secondary crystallization by Avrami equations. The Avrami exponents n were determined as 2.0 for primary and 1.0 for secondary process.

Melting behaviour studies were carried out by DSC observing that crystallinity, melting temperature and calculated lamellar thickness of PET increase with the extending time period of isothermal crystallization in secondary process.

Seeded crystallization provides for the possibility of crystallizing polymers at higher temperatures, even located in the normal melting temperature region, to produce greater lamellae thicknesses and higher melting temperature and to consider the effect of this morphology on their mechanical and physical properties. However, the mechanism of growth rate of seeded crystallization is questionable that requires further research.

Acknowledgement

Firstly, I sincerely appreciate my supervisors Prof. James N. Hay and Dr. Michel J. Jenkins. I am deeply indebted their patient guidance, profound expertise and wisdom throughout these years. They were always willing to answer my questions, provide valuable advice and support in difficulty during the study. I feel extremely honoured to work under their great guidance. Without their help and support, this work would never have been accomplished.

I would like to give a very special thanks to Mr. Frank Biddlestone for his technical support. His broad experience, logical way of thinking and constructive comment has been of great value for me in doing the experimental part of the research.

I am deeply grateful to all my colleagues and friends for supports, sharing their knowledge and precious friendship that made my life in UK enjoyable in these years. Especially to Dr. Abdul G. AL Lafi, Dr Samsudin S. Amril, Dr. Jin Tang, Dr. ZhenHua Hu and Dr. DeJing Kong.

The most important, I would above all like to thank my parents. Their endless love, support and truth is my motivity helping me through the time of this degree and I can never thank them enough. Finally to my fiancée Yi Huang, thank you for your love, understanding, encouragement that support me over this period.

Contents

List of Figures

List of Tables

Abbreviations

2D	*Two-dimensional*
3D	*Three-dimensional*
2D-IR	*Two-dimensional infrared*
2D-FTIR	*Two-dimensional Fourier transform infrared correlation spectroscopy*
ATR	*Attenuated total reflectance*
BHET	*Bis-(2-hydroxyethyl) terephthalate*
CCD	*Charge-coupled device*
DMT	*Dimethyl terephthalate*
DSC	*Differential scanning calorimetry*
DTGS	*Detector triglycine sulfate*
EG	*Ethylene glycol,*
FTIR	*Fourier transform infrared spectroscopy*
IR	*infrared*
KBr	*Potassium bromide*
PET	*Poly(ethylene terephthalate)*
SEM	*Scanning electron microscope*
WAX	*Wide-angle X-ray*
UV-fluorescence	*Ultraviolet fluorescence*

Symbols

%	Percentage
σ	Surface free energy
σ_e	Fold surface free energy of the critical size nucleus
π	Circumference ratio
λ	Wavelength
ε	Molar extinction coefficient of the absorption band
ε_c	Molar extinction coefficient of cis functional group
ε_t	Molar extinction coefficient of trans functional group
^oC	Degree Celsius
μm	Micron $10^{-6}m$
Å	Ångström $10^{-10}m$
A	Surface area / Absorbance
$A_{a,o}$	Absorbance of the amorphous band at initial time
$A_{a,t}$	Absorbance of the amorphous band at time t
$A_{a,T}$	Value of the absorbance at temperature T on the extrapolated amorphous line
A_c	Absorbance of cis functional group
A_t	Absorbance of trans functional group
a	Unit cell dimension along the growing plane
b	Lateral side of the unit cell
C_p	Specific heat
c	Unit cell dimension along the lamella thickness / velocity of light / concentration of the substance
d	constant thickness of disc
ΔE	Activation energy for viscous flow
f	A correction factor $(2T/(T_m^o + T))$

g	Steady state growth rate of a crystal
g_0	Temperature independent constant
ΔG_c	Difference of free energy between the solid and liquid
ΔG_n	Free energy of nucleus formation
ΔG^*	Free energy of formation of a critical size nucleus
h	Planck constant
ΔH_f	Enthalpy of fusion per unit volume perfect crystal
ΔH_v	Enthalpy of fusion per unit volume
I	Intensity of the transmitted light
I_0	intensity of the incident light
K	Kelvin / equilibrium constant
K_g	Nucleation constant
k	Boltzman constant
L	Nucleation density
l	Sample thickness / lamellae thickness / nucleation rate
N	Density of heterogeneous nuclei
n	Avrami exponent / number repeat monomer units
n_p	Avrami exponent of primary crystallization
n_s	Avrami exponent of secondary crystallization
R	Rate of heating / gas constant ($8.314 JK^{-1} mol^{-1}$)
R^2	Sum of the square of the residuals
r	Constant radius of rods
T	Temperature
T_c	Crystallization temperature
T_g	Glass transition temperature
T_m	Melting temperature
T_m^o	Equilibrium melting point
T_∞	Temperature below which the motion of crystallisable segment to the crystallization face cease ($(T_g–30)K$)

t	Time
t_i	Induction time
$t_{p,f,}$	Time corresponding to the value of $X_{p,f}$
$t_{1/2}$	Half-life of crystallization
ΔT	Degree of supercooling ($\Delta T = T_m^o - T_c$)
W	Wavenumber
X_a	Amorphous weight fraction,
$X_{a,t}$	Amorphous weight fraction at time t
X_c	Crystalline weight fraction
$X_{c,t}$	Fractional crystallinity at time t
$X_{p,t,}$	Fractional crystallinity developed at time t of primary process
$X_{p,\ inf}$	Fractional crystallinity developed at the end of primary process
$X_{p,f}$	Residual crystallinity left after partial melting
$X_{s,f}$	Final crystallinity achieved by the seeded crystallization
$X_{s.\infty}$	Fractional crystallinity at the end of secondary process
X_t	Fractional crystallinity
ν	Frequency
U^*	Activation energy for viscous flow (6300 J/mol)
Z	Composite rate constant
Z_p	Composite rate constant of primary crystallization
Z_s	Composite rate constant of secondary crystallization / composite rate constant of seed crystallization

Chapter One

Introduction

1.1 Poly(ethylene terephthalate)

Poly(ethylene terephthalate), PET, is a well established engineering polymer used in the manufacture of fibres, films, tapes, and bottles as well as in moulding powders and the production of composite materials. Amorphous, un-oriented PET is of little commercial interest because of its poor mechanical properties, higher gas permeation, lower dimensional stability and higher extensibility. The physical and mechanical properties of PET, however, can be significantly improved by crystallization and orientation. Modification of the microstructure can be achieved by changing the crystallization rate, the extent of crystallinity and orientation. The degree and quality of crystallinity have long been recognized as having a dominant influence upon the properties of PET.

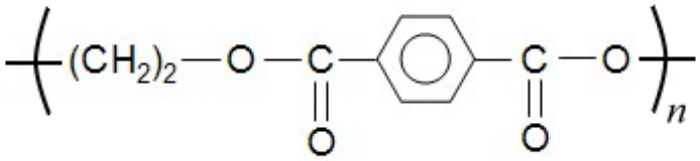

Figure 1.1 The Chemical Repeat Unit of Poly(ethylene terephthalate).

1.1.1 Production of PET

There are several current manufacturing techniques used to produce PET. One of the commonest is synthesizing it from dimethyl terephthalate, DMT, and ethylene glycol, EG, by transesterification [1, 2], carried out with a catalyst, to produce bis-(2-hydroxyethyl) terephthalate, (BHET), i.e.

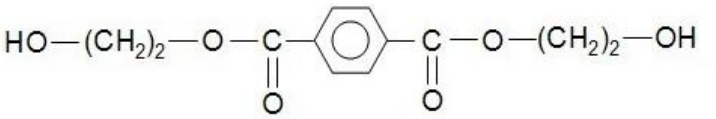

Figure 1.2 Chemical Structure of BHET.

and by subsequent condensation steps BHET reacts further to produce oligomers and then polymers of ethylene terephthalate by the elimination of ethylene glycol units.

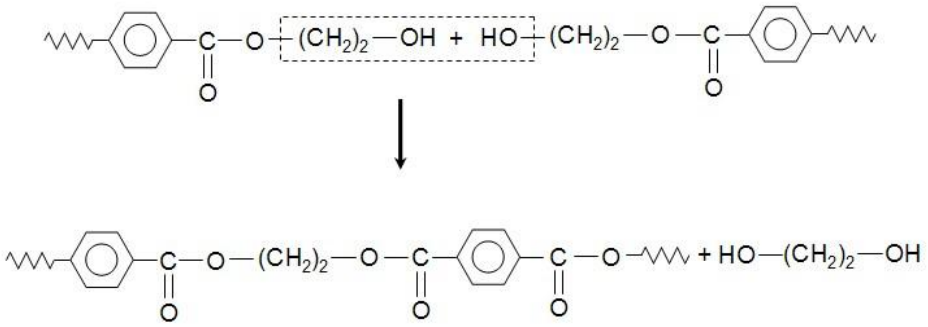

Figure 1.3 Polymerization of Ethylene Terephthalate.

Catalysts used in the condensation reaction are usually blends of antimony trioxide with manganese acetate, calcium acetate, zinc acetate or cobalt acetate. The amount of catalyst is controlled to 0.01-0.05% of the mass of DMT. It has been reported [3] that the first step is catalyzed mainly by the acetates and the second step by the antimony trioxide. A by-product of the first step, methanol, is kept to a minimum and distilled from the reactor.

The initial product is then heated under reduced pressure to eliminate ethylene glycol. The viscous molten mass is extruded using nitrogen pressure from the reaction vessel in the form of a ribbon at about 275^{o}C and is quenched with cold water. The amorphous ribbon is broken into small pieces mechanically or further fabricated into moulding pellets [4].

1.1.2 Commercial Uses of PET.

PET is of great commercial importance, being produced with one of the highest tonnage of all polymer products in the world. It is a hard, stiff, strong, dimensionally stable material that absorbs very little water and is used in the production of synthetic fibre, textiles and fabrics [5]. Synthetic fibres have been produced for many years with some of the most famous commercial names, such as Dacron, Trevira and Terylene. Although in comparison with natural fibres such as cotton, linen and hemp,

PET fabrics have a somewhat synthetic feel athough they do have the advantage of better crease and wrinkle resistance. However, PET is widely mixed with natural fibres to produce a product with the advantages of both fibres.

With the properties being lightweight, strong and transparent when oriented amorphous along with excellent barrier properties for oxygen and carbon dioxide PET has increasingly dominated the bottle market for carbonated soft drinks and bottled water [5, 6]. For similar reasons it has been used for manufacturing food container and packaging material. With increasing recycling of PET bottle and container many of the initial criticisms of the use of such an expensive material as PET has been silenced and accounts for the increasing consumption of the polymer worldwide [7].

The biaxially orientated and thermally stabilized films of PET have found an important commercial market for capacitors, graphics, film base and recording tapes etc [5]. In recent years, PET has increasingly been used in manufacturing fibre reinforced composites and with high tensile fibres should find important applications in the defence industry for body protection applications.

1.2 Kinetics of Polymer crystallization

1.2.1 Polymer crystallization

Crystallization process involves the transformation of a liquid phase into a crystalline phase associated with partial alignment of its molecular chains. It normally happens in the temperature range between the glass transition temperature, T_g, and the melting point of the polymer. In this temperature region the chain segments are sufficiently mobile to adopt the required conformations for crystallization, i.e. trans conformation. Below T_g, the conformational motion is frozen but becomes highly mobile above T_m [8].

Generally, bulk crystallized polymer can attain 10-80% crystallinity and is considered to be semi-crystalline. The crystallization abilities depend on the polymer tacticity, the stiffness of the chain, bulkiness, polarity of side groups and microstructure of polymers. External factors also affect the overall rate of crystallization and degree of crystallinity, such as cooling rate, nucleating agents, orientation and drawing rate in the melt [8]. Polymer chains with symmetrical structure or a high degree of stereoregularity and strong polar interactions are more readily crystallized while atactic, branched, cross-linked polymer chains or those containing impurities groups such as comonomer units will retard the crystallization process [8].

1.2.2 Nucleation.

When a molten polymer is cooled the polymer chains tend to align and form small ordered regions, called nuclei, within the disordered melt. The spontaneous process of forming an ordered domain is called homogeneous nucleation and refers to the first act of developing a new phase from another phase. The ordering process can occur on the surface of heterogeneous particles, e.g. dust and other solid impurities and this is referred to as heterogeneous nucleation. Heterogeneous nucleation is thermodynamically more favorable than homogeneous and occurs at lower degree of super-cooling than homogeneous as a result it is the most commonly encountered form of nucleation in polymer crystallization.

The initial production of the nucleus is called primary nucleation but growth occurs by nucleation of layers on the surface by the formation of secondary and tertiary nuclei. Figure 1.4 distinguishes between the three types of nucleation.

Primary nucleation refers to the first formation of a polymer crystal by a few molecules in the liquid state beginning to pack parallel to another and form small embryos of the crystalline state when there is no preformed nucleus or foreign surface present [9].

Secondary nucleation is similar to primary nucleation, but it takes place on a molecularly smooth crystal surface, building up a new layer. Secondary nucleation

has a lower free energy of formation than primary since it has a lower surface area to volume ratio and will develop at lower degree of super-cooling.

Tertiary nucleation occurs along an existing crystal edge and involves two neighbouring surfaces of a crystal. It has the lowest free energy barrier to growth as the two crystal faces provide a sufficient number of irregularities to be new crystallization sites.

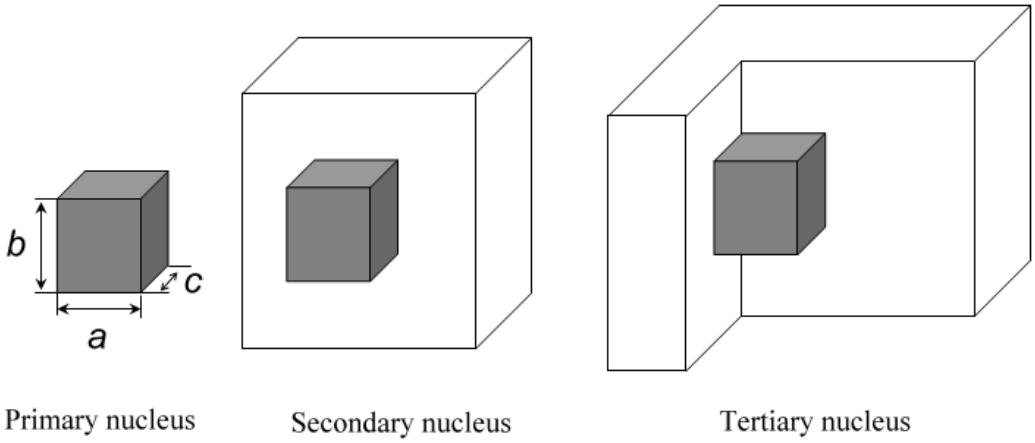

Figure 1.4 Types of Crystal Nuclei.

Crystallization is unable to start in the melt unless the temperature of the melt, T, drops below the melting point, T_m, and there is some supercooling, $\Delta T = T_m - T$,

The free energy of formation of the nucleus,

$$\Delta G_{nuclei} = \Delta G_c + \Sigma \sigma A \qquad (1.1)$$

contains two competing free energy terms, ΔG_c and $\Sigma\sigma A$. The first is the volume free energy difference between the solid (nuclei) and liquid. Below the melting point this is negative in value as the free energy of the melt is greater than that of the crystal and also increases with decreasing temperature. The second is the surface free energy, σ, multiplied by the surface area, A, and is always positive in value. σ and A are the surface free energy derived from the various crystal surface present and the corresponding surface area. The production of a surface between the melt and the nucleus requires the expenditure of the surface free energy and is proportional to the surface area. Accumulating more molecules to the crystal causes the decrease in free energy proportional to the volume of the nucleus. Depending on the geometric shape of the nucleus, the volume term will eventually dominate over the surface and a point is reached, called the critical size when further accumulation of material into the nucleus reduces the free energy of formation. The overall free energy change size during nucleation is shown in Figure 1.5.

Heterogeneous nucleation requires much lower energy barrier than homogeneous nucleation because of differences in the surface energy and the lower surface area to volume ratio. Accordingly heterogeneous occurs at lower degree of supercooling than homogeneous nucleation.

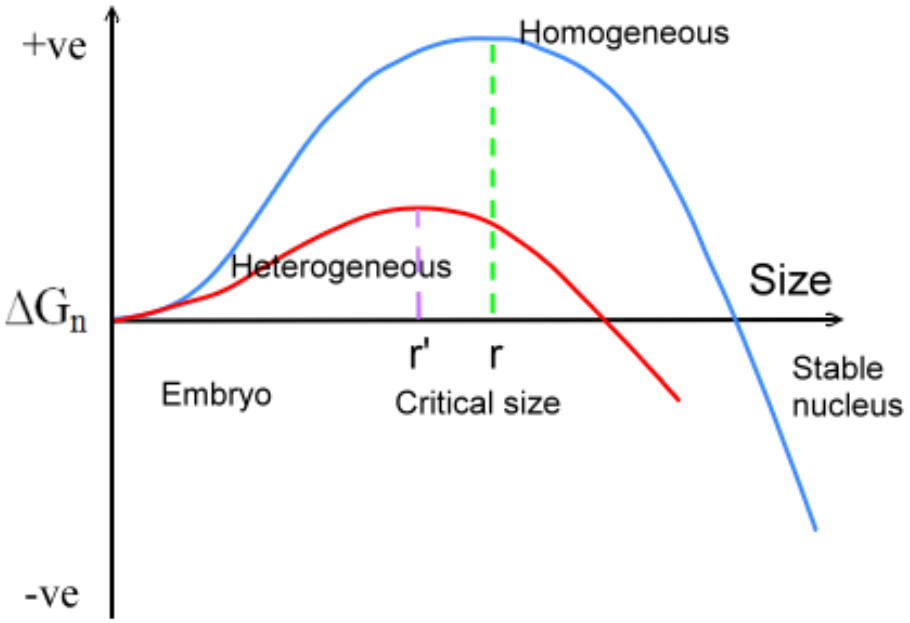

Figure 1.5 Schematic Representation of Variation of Free Energy with Nucleus Size for the Formation of a Stable Polymer Crystal Nucleus [8].

1.2.3 Crystal Growth.

The growth of crystals takes place by the incorporation of the molecular chains on to surface by secondary nucleation. Assume the cross sectional area of the polymer chain is denoted as ($a \times c$), see figure 1.6, where a and c are the unit cell dimensions along the growing plane and the lamella thickness in the chain direction respectively. The chain spreads gradually across the substrate subsequently by laying down a molecular strand on a smooth crystal surface, associated by adding further segments to this interface [8, 10-12].

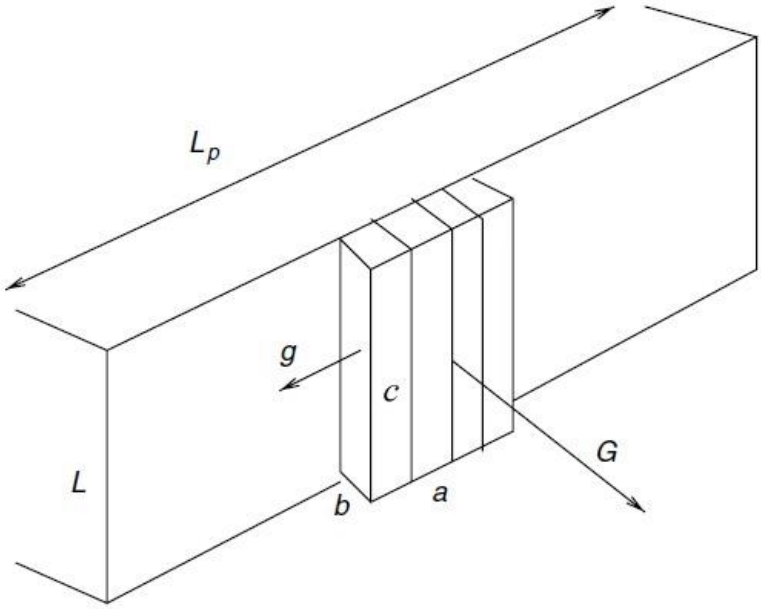

Figure 1.6 Model of the Growth Front [10].

1.2.4 The temperature Dependence of Growth Rate.

Kinetic theories of crystallization lead naturally to predictions of the temperature dependence of crystal growth rates. Turnbull and Fisher [13] derived and expression for the temperature dependence of growth rates in condensed systems in the form

$$g = g_0 \exp\left(-\frac{\Delta E}{RT}\right) \exp\left(-\frac{\Delta G^*}{RT}\right) \quad (1.2)$$

where, g is the steady state growth rate of a crystal at the crystallization temperature, T, g_0 is a temperature independent constant, ΔE represents the activation energy for viscous flow, i.e. the energy barrier for the transport of material to the crystal-liquid

interface, ΔG* is free energy of formation of a critical size nucleus and R is the gas constant (8.314 JK^{-1} mol^{-1}). At low crystallization temperatures close to the T_g, the first term is dominant and the crystal growth rate is determined by chain diffusion to the growth front. At much higher temperatures close to T_m, the second term is the primary factor and nucleation is the controlling factor. The growth rate g of a crystal has a bell shaped dependence on temperature as predicted by Gibbs Thomson equation [14].

Hoffman and Lauritzen [8, 15-22] have modified the Turnbull-Fisher equation for polymer crystallization and describe the temperature dependence of linear growth rate as

$$g = g_0 \exp\left(-\frac{U^*}{R\,(T_c - T_\infty)}\right) \exp\left(-\frac{K_g}{T(\Delta T) f}\right) \qquad (1.3)$$

where, g is the crystal growth rate, g_0 is the jump rate pre-exponential constant, i.e. kT/h; U^* is the activation energy for the transport of crystallizing units across the liquid-solid interfaces (assigned a value of 6300 $Jmol^{-1}$ by Hoffman); T is the crystallization temperature; T_∞ is the hypothetical temperature where segmental chain motion ceases (usually assumed to be equivalent to (T_g–30) K); ΔT is the degree of supercooling, equal to ($T_m^o - T_c$); f is a correction factor which reflects the

reduction in the latent enthalpy of fusion, Δh_f as temperature is decreased given by $2T/(T_m^o + T)$; T_m^o is the equilibrium melting point.

K_g is the nucleation constant whose value depends on the type of nucleation adopted and includes molecular structure information, i.e.

$$K_g = \frac{nb\sigma\,\sigma_e T_m^o}{\Delta H_f k} \tag{1.4}$$

where b is the lateral side of the unit cell; k is Boltzman constant; ΔH_f is the heat of fusion per unit volume perfect crystal; σ and σ_e are the lateral and fold surface free energy of the critical size nucleus respectively. The value of n depends on the nucleation regime as defined by Hoffman and Lauritzen [15, 23, 24]. Accordingly, the dependence of the radial growth of spherulites on the degree of supercooling, ΔT, were analyzed by Eq.[1.4], assuming that the fold length is the same and it grew at the same rate as the radial expansion of the spherulite; there was no imperfect growth of crystal face and no crystal thickening.

Base on these assumptions, Lauritzen and Hoffman created three regimes to describe three different nucleation mechanisms according to the relative rates of the secondary nucleation on the surface and extension of the polymer chain growth along the surface after nucleation has occurred. The three regimes are designated I, II and III, as shown in Figure 1.7.

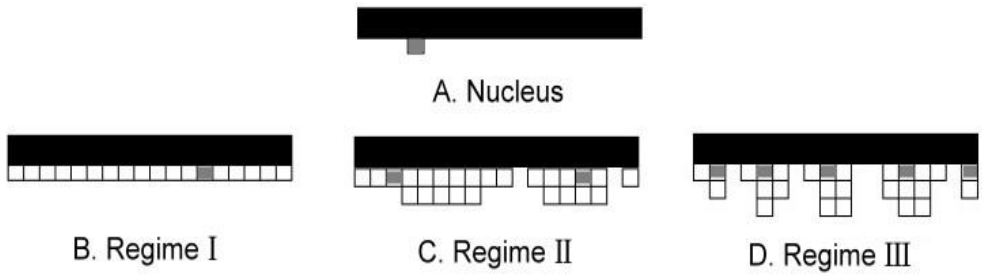

Figure 1.7 Laurizen-Hoffman Model [10].

Regime I occurs when the degree of supercooling is small and the rate of nucleation is low compared to the rate of covering the surface. In this case, secondary nucleation dominates linear growth. In other word, the crystal growth rate is significantly greater than secondary nucleation rate. Once a single surface nucleus has formed, the chains will be fully incorporated on to the growing crystal surface before another nucleus occurs (figure 1.7B). The n value in Eq.[1.4] is 4.

Regime II occurs at higher supercooling and when the crystal growth rate becomes comparable to or smaller than the secondary nucleation rate, i.e. the extension rate of the polymer folding along the surface is approximately equal with the secondary nucleation rate. Each crystal surface will experience some covering due to nucleation and these formed nuclei will have time to cover the remainder of the surface. The value of n is equal to 2.

On further supercooling, regime II can occur in which case, nucleation is so fast that the nucleation rate is much greater than the crystal growth rate. The crystal surface is more or less fully covered by nucleation without any significant coverage by extension of the molecular chain folding. The n value is also 4.

Equation [1.4] is rewritten into the following form

$$\ln g + \frac{U^*}{R(T-T_\infty)} = \ln g_0 - \frac{K_g}{T\Delta T f} \qquad (1.5)$$

K_g can be determined from the slope by plotting the left hand side against $1/(T\ \Delta T f)$. Regime transition can be observed by the abrupt changes in K_g value. Figure 1.8 schematically illustrates the regime transitions from I to III, with K_g^{III}/K_g^{II} and K_g^{I}/K_g^{II} equal to 2.

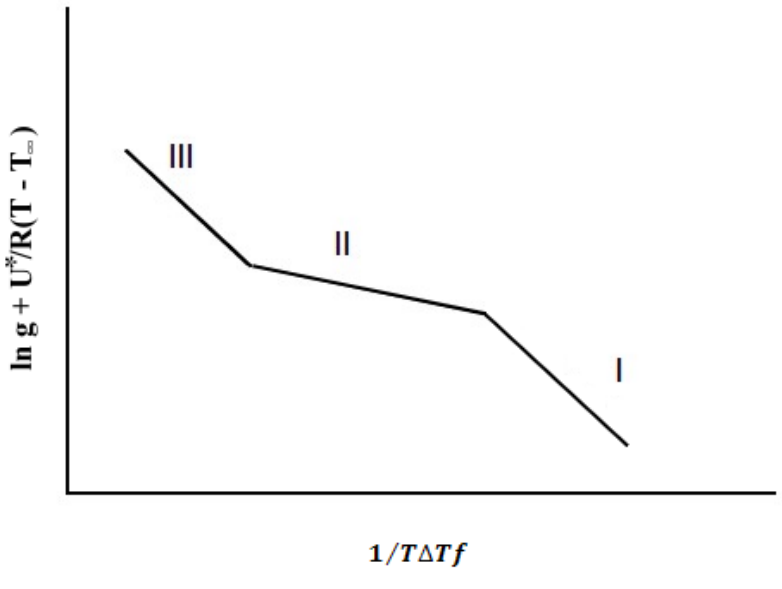

Figure 1.8 Three Regimes in the Nucleation [10].

1.2.5 The Avrami Equation.

The kinetics of phase change on crystallization has been described by the Avrami model [25, 26]. Many people research on it [27-34] in which the approach has been highly successful in describing crystallization of polymers [35]. The model relates the fractional crystallinity to time [25, 26, 36], such that

$$1 - X_t = \exp(-Zt^n) \quad (1.6)$$

In which X_t is the fractional crystallinity, which has developed at time t, Z is a composite rate constant incorporating nucleation and growth characteristics. The Avrami exponent, n, is a constant depending on the crystallization mechanism and the geometry of the growing crystal. Table 1.1 lists the corresponding expressions for the listed mechanisms n and Z below [8, 35].

However, the Avrami equation has many limitations. The variation in the crystalline density within the spherulite boundary throughout the crystallization process give fractional n values and this value assumed to be constant in the Avrami equation. In addition to assuming random nucleation in a super cooled melt, Avrami equation was derived with the following assumption [8, 35, 37]:

1. The rates of nucleation and growth are constant with time.

2. Only primarily and no secondary crystallization process is present

3. The volume of the system remains constant during crystallization.

4. When crystallites impinge with one another growth ceases.

5. The crystallites keep their shape in one, two or three dimension (rods, discs or sphere, respectively) until impingement take place.

6. There is no induction time before crystallization.

Table 1.1 Avrami Parameters for Different Crystallization Mechanisms [35].

Crystallization mechanism		n	Z	Geometry
Spheres	Sporadic	4.0	$2/3\pi\ g^3 l$	3 dimensions
	Predetermined	3.0	$4/3\pi\ g^3 L$	3 dimensions
Discs	Sporadic	3.0	$1/3\pi\ g^2 ld$	2 dimensions
	Predetermined	2.0	$\pi\ g^2 Ld$	2 dimensions
Rods	Sporadic	2.0	$1/4\pi\ glr^2$	1 dimensions
	Predetermined	1.0	$1/2\pi\ gLr^2$	1 dimensions

where g is crystal growth rate; l is nucleation rate; L is nucleation density; d is constant thickness of discs and r is constant radius of rods.

1.3 Morphology of Crystalline Polymers

1.3.1 Single crystals

Extremely small lozenge shaped crystals of the order of a few μm in length and breadth and a few tens of nm in thickness are produced by crystallizing many

polymers from dilute solutions. These crystals has a unique morphology in that the polymer chains lie parallel to the thickness of the lamellae and since the extended chain length is many times the thickness of the lamellae the polymer molecules has to fold regularly backwards and forwards across the lamellae thickness. The chains are observed to fold by adjacent re-entry into the crystal and a very regular fold surface is produced. Using this as a model for the lamellae produced from melt crystallized polymers three structures have been adopted for the lamellae crystallized from the melt [38].

(a) The regular model, with adjacent re-entry folds; (Figure 1.9 upper right)

(b) The irregular model, with some limited amount of adjacent re-entry fold (Figure 1.9 right mid) and

(c) The switchboard model, with non-adjacent re-entry folds and an amorphous layer on either side of the lamellae. (Figure 1.9 lower right)

The fold length increases with increasing crystallization temperature, or decreasing supercooling and also increasing pressure. Usually, the thicknesses of the lamellae are of the order of 10 nm, whereas the other dimensions of the lamella are very larger, typically of the order of several μm.

It is normally the case that the more dilute solutions produce the least complicated crystal. Concentration of 0.01% usually gives monolayers, 0.1%

produces some multilayer development while 1% gives rather complicated structure of a branching lamellar structure, suggestive of melt-grown spherulites.

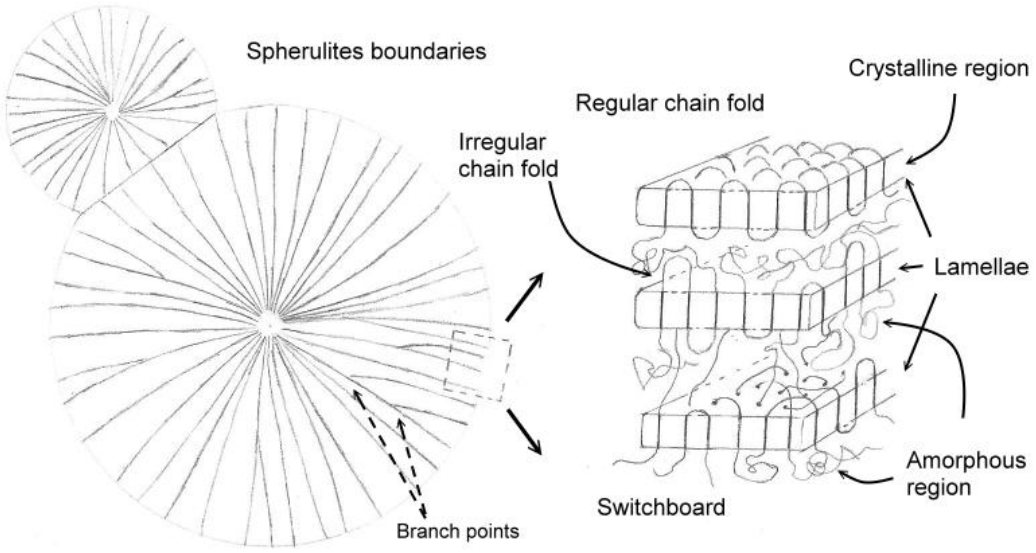

Figure 1.9 Schematic Structure of Spherulites, Lamellae with Regular and Irregular Chain Folds and Switchboard Lamellae [39-41].

1.3.2 Spherulites

Spherulites are made up of polycrystalline fibrils, very similar in structure to the lamellar single crystals, but arranged in a radial pattern which splay out from the centre of the spherulite, see Figure 1.9. These fibrils branch and twist initially until, eventually a spherical particle is produced. Each fibril has the molecular chain perpendicular to the fibril length, (Figure 1.10).

Generally, spherulitic growth proceeds in two different ways:

(a) Primary crystallization. The spherulite is considered to grow from an initial fibril, or lamella, produced as a primary nucleus. Crystal growth is favoured along the crystallographic a and b axis of the unit cell and is restricted in the c axis to a few nm such that the nucleus grows into a thin fibre or sheet. Branching occurs repeatedly at the growth fronts and a branching lamellar structure is produced. These branches bend and twist as they grow, and also branch further to produce a spherical boundary growing radial from the initial primary nucleus. The final result is the production of spherical particles which develop radially outwards from the nucleus until stopped by impinging with neighbouring particles.

(b) Secondary crystallization. This process is growth by filling in the interstices between the lamellae, transforming a portion of the remaining amorphous material between the lamellae and thickening the lamellae or producing new lamellae between the original lamellae. The two effects must be reflected in the isothermal growth kinetics and the relative importance of the two depends on the constitution of the melt and thermal history.

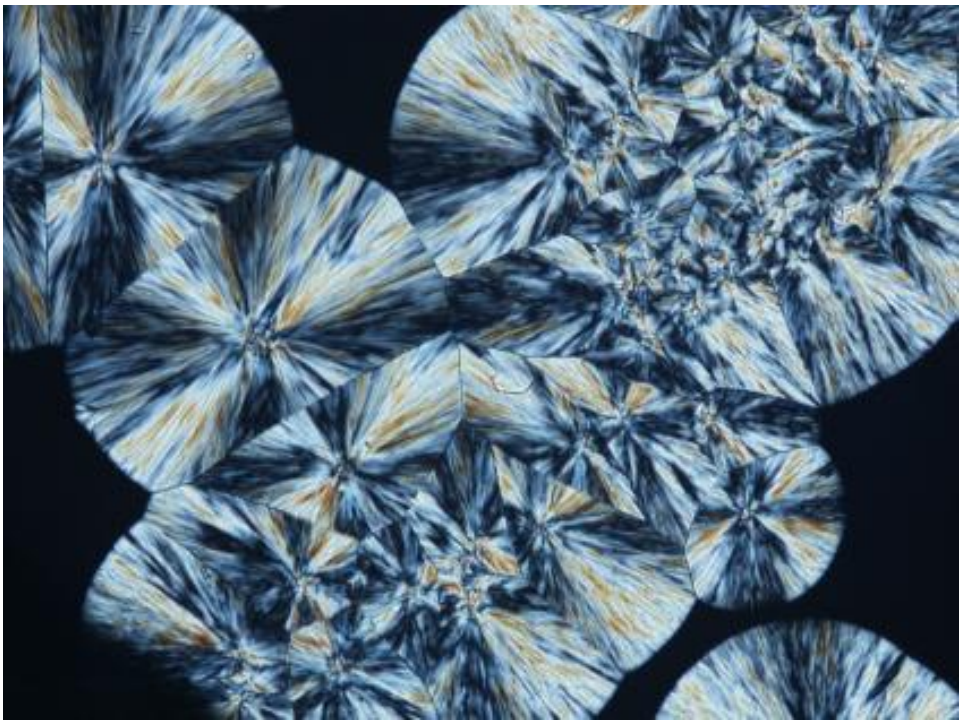

Figure 1.10 Optical Micrograph of Polymer Spherulites

Figure 1.11 depicts the development of a spherulite at various stages in its growth. The growth of a spherulite initially begins with a bundle of lamellae, which evolves into a sheaf. The sheaf keeps growing and spreading laterally by branching, of the lamellae until it ultimately develops a spherical contour [42]. Growth of the spheres continues radially until the spherulite impinges with its neighbours when it stops at the point of contact.

Most spherulites viewed under polarized light exhibit Maltese cross birefringence which is evidence for the above radiating lamellar structure. The Maltese cross indicates that the spherulite has radial symmetry [43], see Figure 1.13. The initial and final stages in the development of a spherulite are referred to as

immature and mature spherulites. Mature spherulites have the same crystallographic axis in the radial direction and immature structure and also dendrites possess a common single crystal orientation although they are also highly branched particles.

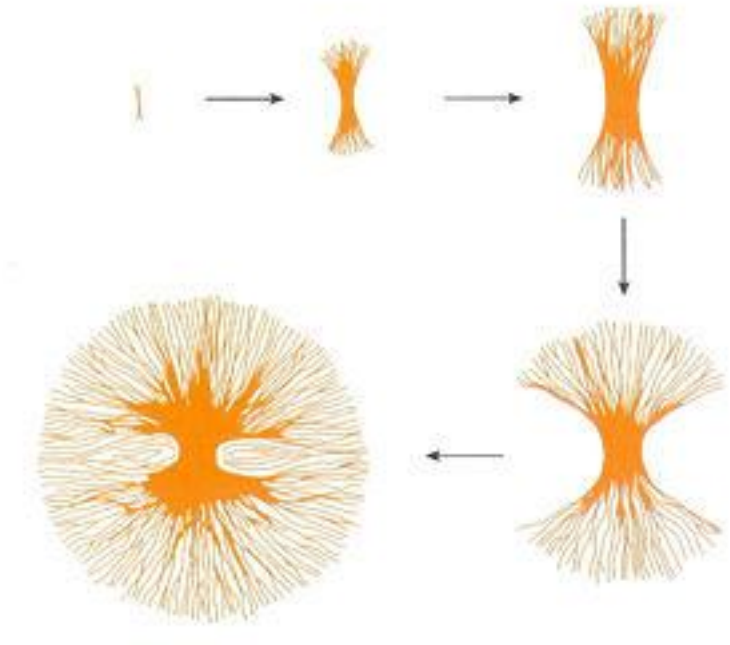

Figure 1.11 Five Stages in the Formation of a Spherulite from Packing of Lamellae.

The development of spherulites also depends on the relative rate of nucleation and growth. In the condition of low nucleation density and high growth rate, a few mature spherulites will result [44]. Conversely, rapid growth and very high nucleation density leads to a profusion of spherulites which may well be immature. Under extremely high nucleation density a spherical contour may not develop. In

polymers spherulite diameters are normally in the range 0.5 to 1000 μm and are observable with a light microcope.

Polymers crystallized from flowing melt or drawn solid produces deformed spherulites or a micro-fibril texture. Preferential growth along the flow or stress direction lead to the growth of fibrils or shish-kebabs [45] and the morphology is sensitive to the rate of flow or strain [46]. Correspondingly, in the absence of flow or strain growth occurs freely in all directions producing a spherulitic morphology. In the presence of flow or applied strain the crystallization mechanism changes progressively, from spherulites, to deformed spherulites oriented in the flow direction, to micro-fibrillar with the molecular chains aligned in the flow direction through an intermediate stage in which shish-kebabs are produced. The exact structure of the microfibrils and their growth mechanism are controversial [47] in that both chain-folded and chain-extended [9, 46] shish-kebabs structure [48] have been invoked.

1.4 The Melting of Polymers.

Unlike small organic molecules which have a precise melting point, polymers melt over a broad temperature range that varies with the crystallization temperature or thermal history. The lamellar crystals are extremely thin and the thickness

determines their thermal stability and since the crystallization temperature or annealing temperature determines the thickness of the crystal; the melting point varies with crystallization temperature and thermal history. Conventionally the temperature corresponding to the last trace of crystallinity is taken to be the melting point of the polymer crystallized at the crystallization temperature [12] and this reflects the thicker lamellae present in the sample as they are able to persist to a higher melting point than thinner ones.

The equilibrium melting temperature, T^o_m, is defined as the melting temperature of lamellar crystals which are infinitely thick and their melting temperature is not suppressed by surface energy terms [49]. However, as a chain-folded lamellar crystal grows with a finite thickness during the crystallization process, T^o_m is not able to be directly measured by experiment and has to be determined by extrapolation of experimentally observed melting temperatures. Establishment of the degree of supercooling and ($\Delta T = T^o_m - T_c$) and determination of T^o_m help to understand the temperature dependence of the crystallization rates.

The most common way to determine T^o_m was proposed by Hoffman and Weeks [12]. They derived a relationship between melting point, T_m, and crystallization temperature, T_c, which enables T^o_m to be determined from the observed melting point, T_m,

$$T_m = T_m^o(1 - 1/2\beta) + T_c/2\beta \quad (1.7)$$

where $\beta = (\sigma_e l/\sigma l_e)$ and σ is the fold surface free energy, l is the lamellae thickness and the subscript *e* refers to equilibrium conditions. Under ideal condition without any re-crystallization or annealing during melting, β is equal to 1.0 and a plot of T_m against T_c is linear with a slope of $1/2\beta$. This line interpolates to the equilibrium condition of $T_m = T_c$ at T^o_m, but only with a slope of 0.5. Eq.[1.7] was derived on the basis that no annealing or secondary crystallization has occurred during the crystallization or subsequent heating to melting.

1.5 Aims and Objectives of the Project.

PET occupies a unique position in the study of polymer crystallization kinetics as it was one of the first polymers to be studied by dilatometry and the crystallization – time data interpreted in terms of the Avrami equation [50], as the growth of spherulites. Since then it has been widely studied by many other techniques, WAX diffraction, IR spectroscopy and more recently DSC [51-70]. The amount of interest in the crystallization behaviour of this polymer reflects its commercial importance and the realization that material properties are closely associated with the degree of crystallinity. This research project focuses on the use of a variety of analytical

techniques to obtain a deeper understanding the thermal behaviour of PET and the effect on material and physical properties.

Thermal analysis Fourier transform infrared spectroscopy (TA-FTIR) has been utilized to examine the thermal behaviour of PET at the molecular level of individual functional groups during heating and cooling.

Fourier transform infrared spectroscopy (FTIR) combined with a novel analysis technique of two-dimensional infrared correlation spectroscopy (2D-FTIR) will be applied to present the close view of thermal behaviour of PET in non-isothermal and isothermal crystallization. These analyses will help to explore the crystallization kinetics of PET, particular by the secondary crystallization process and will be compared with the traditional analysis by differential scanning calorimetry (DSC).

Isothermal and seeded crystallization will be explored using DSC and FTIR spectroscopy to study the effect of temperature and time on the melting behaviour. The secondary crystallization of PET will be more extensively studied than previously with the object of determining its mechanism. Several other characterization techniques, such as hot-stage optical microscopy and scanning electron microscopy (SEM) will be used for a better understanding of the overall crystallization mechanism.

Chapter Two

Materials, Experimental Techniques and Procedures

2.1 Materials.

2.1.1 Poly(ethylene terephthalate) (PET).

Poly(ethylene terephthalate), PET, films, thickness 1.5, 6 and 13 μm, were supplied by Goodfellow Co., UK, and used as received. Commercial Laser PET with a number average molecular weight of 16 kg mol^{-1} and polydispersity of 2.2 was supplied by DuPont Chemical Co. as moulding pellets.

All samples were dried in a vacuum oven at 100 °C for 12 hours before use. Disc specimens, 5.0 mm in diameter and 1.5 mm in thickness were cut from moulded sheets and used for all DSC.

Useful physical properties are listed in Table 2.1.

Table 2.1 Physical Properties of PET [71-74].

Property	Value
Appearance	White pellets or clear film
Density(amorphous)	1.335 gcm^{-3}
Density(crystalline)	1.420 gcm^{-3}
Glass Transition Temperature (amorphous)	67 ^{o}C
Glass Transition Temperature (crystalline)	81 ^{o}C
Melting point	250-265 ^{o}C
Water absorption	0.16 %
Specific heat	1.0 $Jg^{-1}K^{-1}$
Elastic limit	50-150 %
Young's modulus	2.8-3.1 GPa
Tensile strength	55-75 MPa

2.2 Experimental Techniques and Procedures.

2.2.1 Infrared Spectroscopy.

2.2.1.1 Introduction

Infra-red spectroscopy is a branch of molecular vibrational spectroscopy where by infra-red light is used to excite the vibrational/rotational energy modes of in molecular solids, such as polymers. The chemical bonds absorb infra-red light of

characteristic wavelengths associated with the energy differences between the levels involved in the excitation and to different extents depending on the relative ease of the transition [75-81].

Each covalent bond in a molecule has different vibrational, rotational, torsional and bending modes with characteristic quantum energy levels and fixed energy differences, ΔE between adjacent levels. If the energy difference corresponds exactly with the energy of a photon, the light of that wavelength, λ, is strongly absorbed. For the vibrational/rotational energy levels this occurs in the infrared region of the electro-magnetic spectrum and in line with Planck Law [75, 82], the differences in energy correlate to the wavelength of the absorbed light, i.e.

$$\mathbf{\Delta E = h\nu = hc/\lambda} \qquad (2.1)$$

where ν is the frequency, h Planck constant, c the velocity of light and λ the wavelength. Each covalent bond has characteristic energy levels and precise differences between the energy levels such that covalent bond absorbs infrared light, at characteristic wavelengths.

The IR spectrum of a material is a plot of the fraction of the incident light absorbed i.e. the transmittance, $T = (I/I_0)$, where I and I_o are the intensities of the transmitted and incident light as a function of reciprocal wavelength, or wavenumber.

The spectrum is unique to the molecule and can be used to determine its structure, and also by comparing it with spectra of known materials confirm the presence and absence of these materials.

The spectrum is also quantitative as the amount of light absorbed depends on the amount of material present, according to the Beer-Lambert Law [75-79], i.e.

$$\mathbf{I = I_0 \exp(-\varepsilon cl)} \qquad (2.2)$$

where ε is the molar extinction coefficient of the absorption band, c the concentration and l the sample thickness.

There are two different types of spectrometers used to measure the IR spectra of materials,

a) a dispersive double beam spectrometer

b) a Fourier Transform spectrometer.

In the first the IR beam is split into two; one beam passes through the sample and the other does not before both impinge on the light detector. A comparison is made between the light intensities of the two beams as a function of wavenumber. The FTIR spectrometer is a single beam instrument in which an IR laser is used as the radiation source. A schematic diagram of the optics is shown in Figure 2.1. The radiation is split by a beam splitter which is a half-silvered mirror and which splits

the beam equally between a fixed and a moving mirror. The mirrors in turn reflect the beams back to the beam splitter where they recombine constructively and destructively producing an interferogram. When the sample is placed in the beam it absorbs some of the radiation at fixed frequencies reducing the intensities in the interferogram. A Fourier transform on the interferogram is then carried out to produce the IR spectrum of the sample. The time taken to measure an IR Spectrum depends on the scanning time of the moving mirror but it is faster than the dispersive instrument. FTIR spectroscopy is a convenient method for measuring the infrared spectrum of polymers. It is rapid and there are a number of analytical procedures available for sample preparation which makes it convenient to use. The FTIR spectrometer first repeatedly collects, usually 100-400, interferograms in digital form and this is repeated with the sample removed [75]. Subtraction of the two and Fourier transforming the interferograms produces the IR spectrum of the sample. The Fourier transformed interferogram of the sample contains a unique characteristic spectrum of the sample and subtraction of the baseline removes absorption bands characteristic of atmospheric water vapour and carbon dioxide.

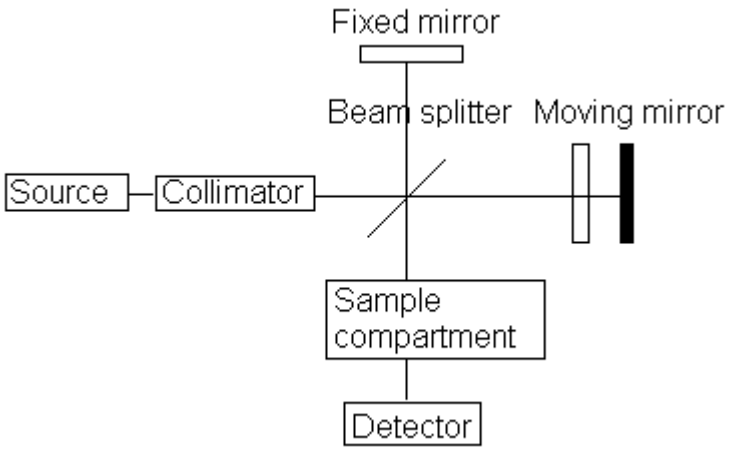

Figure 2.1 A Diagram of the Michelson Interferometer [75].

2.2.1.2 Experimental Procedures.

FTIR spectroscopic measurements were performed using Nicolet Spectrophotometers, model Magna IR 860 and 8700 (see Figure 2.2), each equipped with a DTGS-KBR detector [83]. All spectra were recorded at a resolution of 1-4 cm^{-1} and total of a 100 scans were accumulated for each spectrum along with a background spectrum. The spectra and data were analyzed by Omnic 8.0 software [83, 84]. Before analyzing individual spectra automatic smooth and baseline corrections were made. Two instrumental methods, attenuated total reflectance (ATR) and transmission were used to measure the FTIR spectra of polymer samples.

Figure 2.2 Nicolet Spectrophotometer, model Magna IR 8700.

In the ATR technique, the IR radiation was reflected backwards and forwards between a diamond crystal and the surface of the sample. The depth of penetration which the IR radiation penetrated into the sample was half the wavelength of the incident radiation but also depended on the incident angle and the refractive index difference between the crystal and the sample. The transmission of the absorption bands in an ATR spectrum accordingly depends on experimental parameters as well as the wavelength of the incident radiation. ATR FTIR spectra were not considered to be quantitative and the technique was only used for qualitative measurements.

In the transmission technique, the IR radiation passed directly through the sample contained within a potassium bromide (KBr) disc, or as a thin film. Since the transmission of the sample was dependent on the molar extinction coefficient and sample thickness, there was a severe restriction in examining thick polymer samples greater than 10 μm for the main functional groups and 100 μm for secondary functional groups.

KBr powder was pre-dried in an air oven for 12 hours to remove moisture. 300 mg of KBr powder was weigh and compressed into a disc of 16 mm diameter and used as a reference sample. Two further discs of 150 mg KBr discs were made and used to sandwich PET thin films. A slightly smaller area of PET thin film was cut then sandwiched between two KBr plates. The thickness of the PET thin film was adjusted to maintain absorbances value below 1.0 for the absorption band being analyzed. Thicknesses between 1.5 – 6 μm were chosen for most experiments.

The PET film sandwiched between KBr discs was heated to 265 ^{o}C for 2 minutes within the Linkam THM600 hot-stage cell to melt the PET film. This firmly attached the film to the surface of the KBr discs, removed any orientation or shrinkage, and enabled reproducible spectra of the film to be measured on cooling, or with time at various preset temperatures during isothermal crystallization rate studies. Prior to these rate studies the time scale was fixed and spectra measured at fixed

intervals over the range. The baseline spectrum was also measured and stored for subtracting from the sample interferograms. The spectrum could then be measured on cooling and mounting in the sample chamber of the spectrometer or in the cell of the hot-sage as a function of temperature and time.

TA-FTIR spectra were collected when the sample was heated from room temperature to above the melting point 275 ^{o}C at 4 ^{o}C min^{-1} heating rate and then cooled step-wise in 10 ^{o}C intervals using 20 ^{o}C min^{-1} cooling rate between steps.

In isothermal crystallization experiments, PET film sample was heated to 270 ^{o}C at 50 ^{o}C min^{-1} to melt and maintained at this temperature for 2 minutes. It was then immediately quenched to the isothermal crystallization temperature from 228 to 240 ^{o}C at 60 ^{o}C min^{-1}. Once the sample had reached the isothermal crystallization temperature, a series of spectra were collected at constant time intervals. By this means IR transmission spectra could readily be measured for 3 minutes to unlimited time at the isothermal temperature over the crystallization range studied.

Changes in the IR spectra of PET on melting were also followed by heating the film sandwiched at preset rates of heating to 270 ^{o}C by collecting the spectra at constant time intervals.

In seeded crystallization experiments, PET samples were prepared as described above, a background spectrum of KBr discs was also measured, the time scale of the

experiment set, usually to 1200 minutes, and stored in the Omnic software. The sample was heated to 270 ^{o}C at 50 ^{o}C min^{-1} and held for 2 minutes to melt the PET. This was followed by quench-cooling to 234 ^{o}C at 60 ^{o}C min^{-1} and a series of spectra collected to follow the development of crystallization over 50 minutes. Once the primary crystallization had been completed, the temperature increased at 50 ^{o}C min^{-1} to 244 ~ 250 ^{o}C. This temperature was in the range in which melting was observed to occur and after a set time periods the sample was cooled to the isothermal crystallization temperature. By this means crystallization from seeds produced were studied isothermally.

The quality control of FTIR results and samples thickness have been selected 1720 cm^{-1} and 1410 cm^{-1} as the references for main peaks and secondary peaks respectively. The standard value of absorbance of 1720 cm^{-1} and 1410 cm^{-1} were set as 1.3 ±10% at room temperature and 1.0 ±10% in the melt.

2.2.1.3 Peak Resolution in a FTIR Spectrum.

In measuring the development of crystallinity in PET it was essential to separate the two overlapping carbonyl bands at 1727 and 1717 cm^{-1} attributed to the amorphous and crystalline regions. The amorphous peak maximum was determined initially in the melt where a single band was measure with maximum at 1727 cm^{-1}.

The spectral region from 1650 to 1800 cm^{-1} was selected for peaks resolving and the Omnic baseline function set at the extremes of the range. Using the programmes "Find Peak" (Figure 2.3A) and "Fit Peaks" (Figure 2.3B), the original absorption band was resolved automatically into several smaller peaks by the software. A series of ideal peaks was then selected in the programme "Edit Peaks" with fixed peak maxima. This reduced the number of small peaks, set and locked in the wavenumbers of peak maxima as well as verified the two main peaks, the amorphous band at 1727 cm^{-1} and the crystalline at 1717 cm^{-1}, see Figure 2.3C. Rerunning the "Fit Peaks" gave a better fit to the absorption band and resolution of the two peaks, see Figure 2.3D. The peaks were further edited by adjusting the value of half wave width using a Lorentzian shape for the two absorption curves. Repeating the steps of the "Fit Peaks" and "Edit Peaks" programmes gave the best fit to the absorption band and the best resolution of the two main and other secondary peaks or noise peaks. Normally, the result with a degree of fitting over 97 % and noise peaks area less than 5 % of total peak area is acceptable.

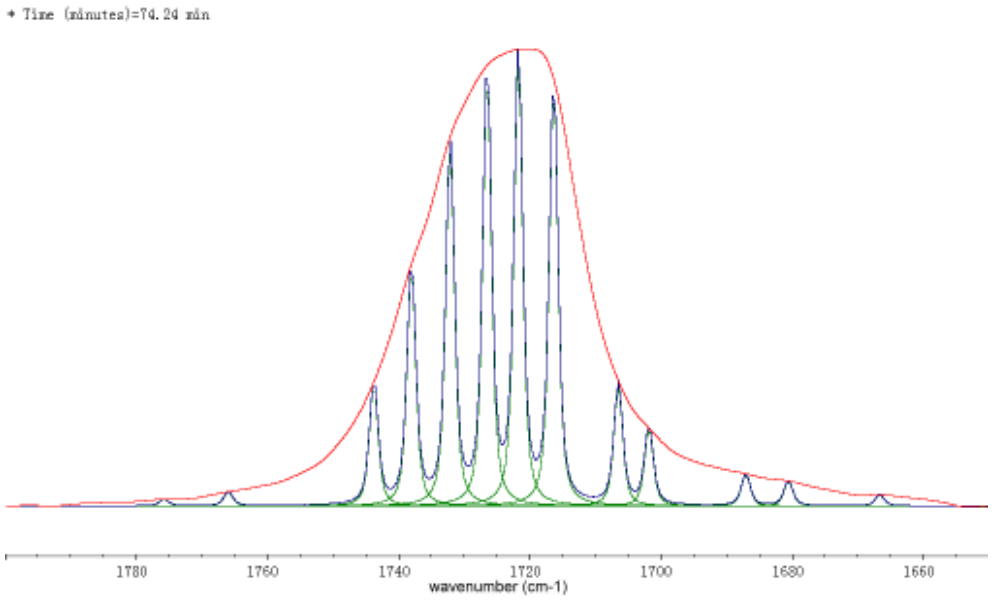

Figure 2.3A Use "Find Peaks" Function of Omnic.

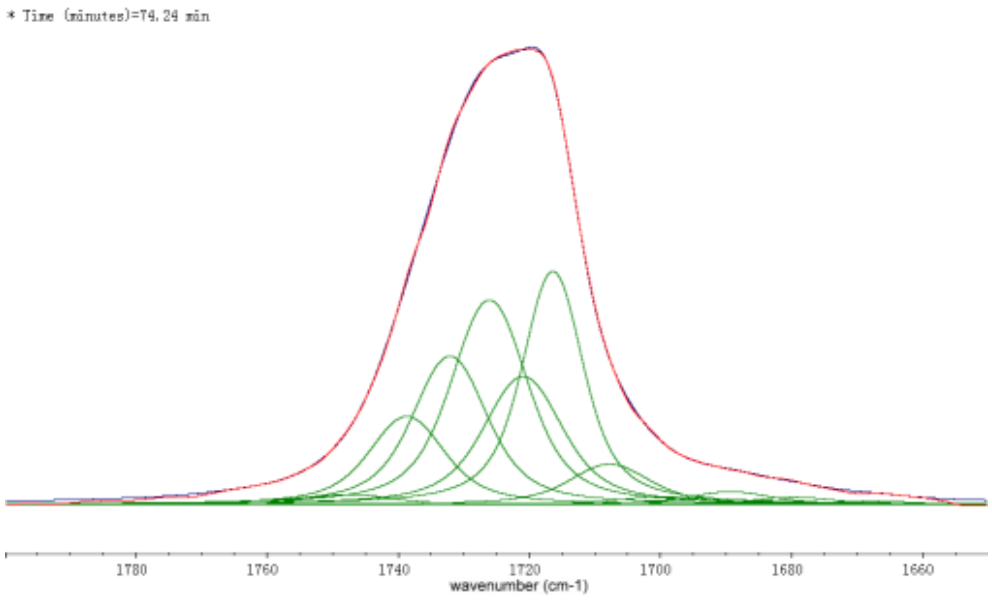

Figure 2.3B First Time to Run Omnic "Fix Peaks" Function.

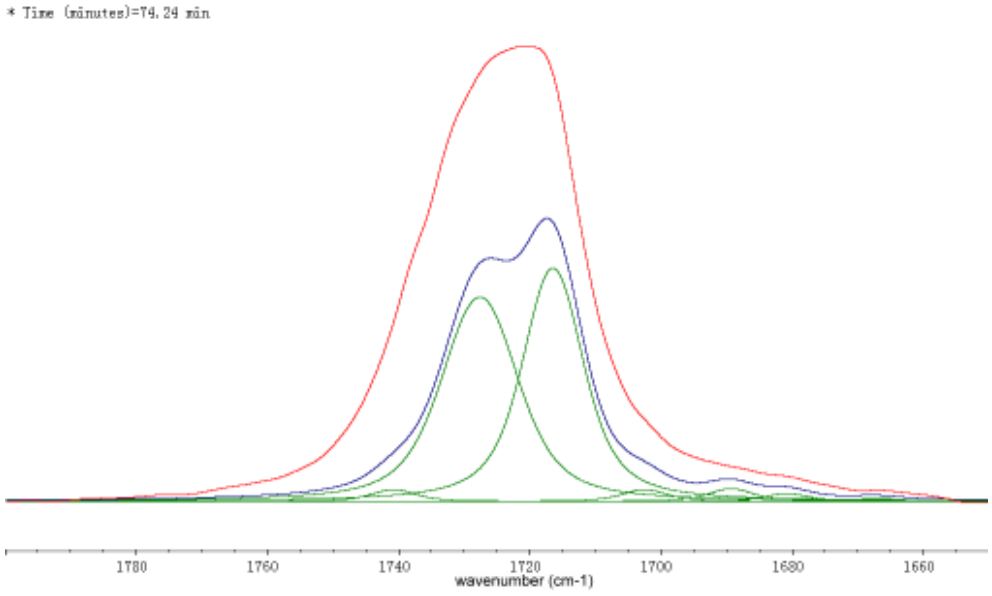

Figure 2.3C Lock the Position of Main Peaks and Reduce the Number of Small Peaks.

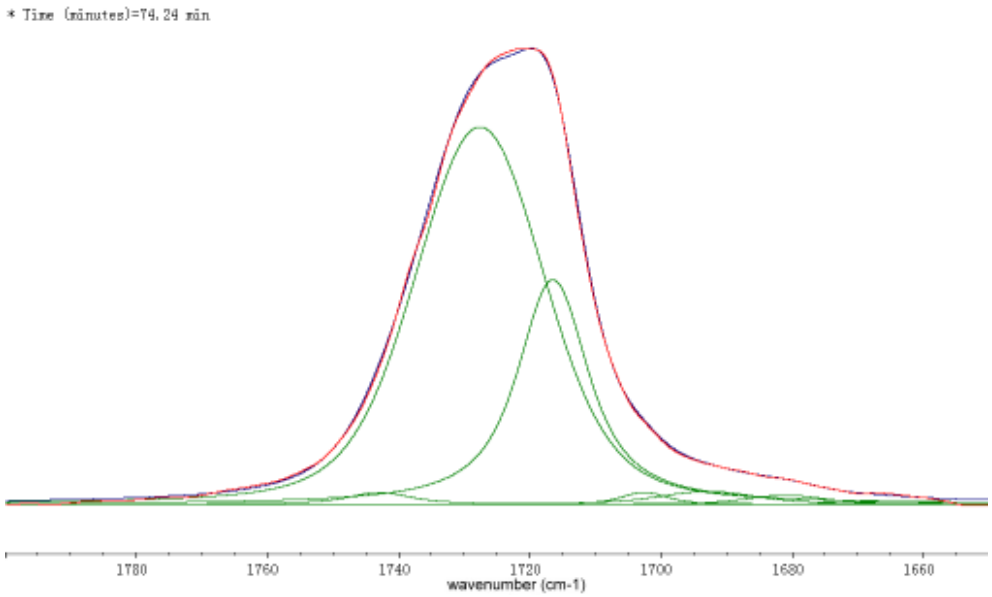

Figure 2.3D Rerun Omnic "Fix Peaks" Function.

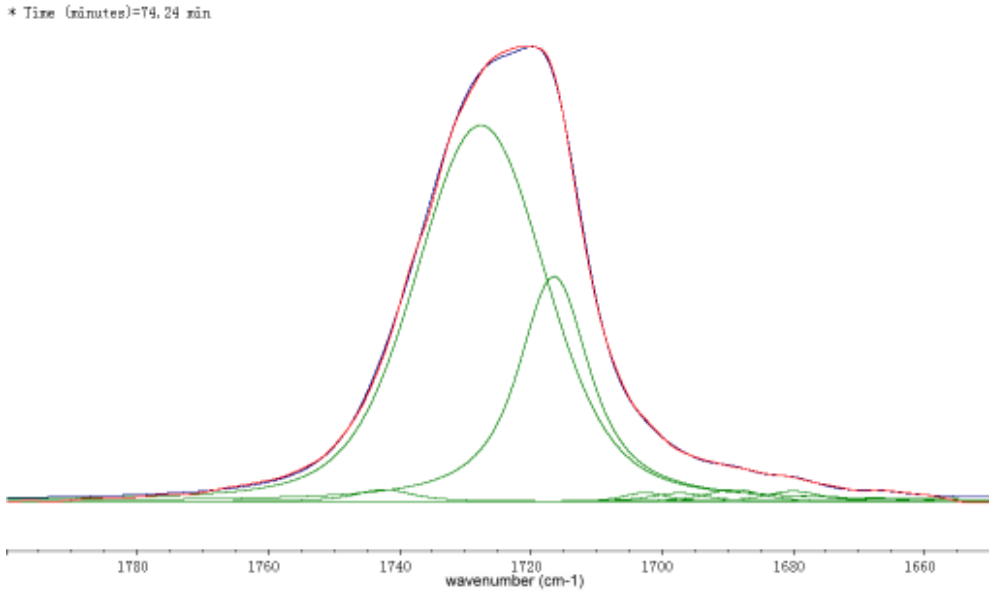

Figure 2.3E Adjust the Half Wave Width and Lorentzian Shape of Peaks then Repeat "Fix Peaks" Function.

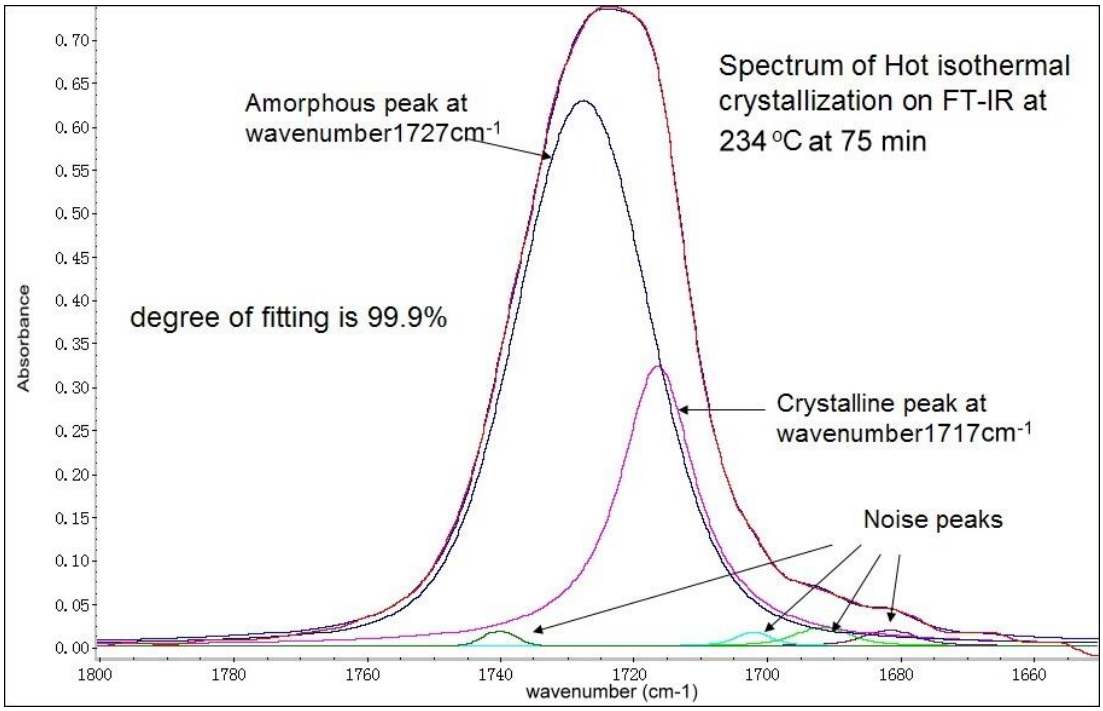

Figure 2.4 Spectrum of Isothermal Crystallization on FT-IR at 234 ^{o}C at 75 Minute Showing How the Overlapped Peaks is Divided.

2.2.2 Differential Scanning Calorimetry (DSC).

2.2.2.1 Introduction.

Differential Scanning Calorimetry, DSC, is a thermal analytical technique which measures thermal events, such as phase transitions, chemical reactions, thermal conductivity and specific heats as a function of temperature [85]. It finds wide application in characterizing polymers, particularly in measuring melting points, crystallization and glass transition temperatures, and specific heats [86].

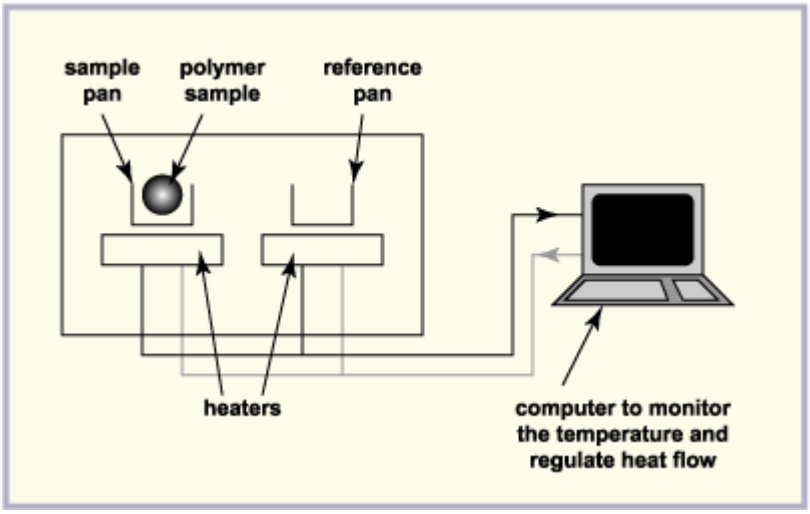

Figure 2.5 A Schematic Diagram of DSC System.

In this project, DSC was chosen to study the crystallization of PET. Although it has been used by previous research workers DSC was used for comparison with the crystallization rate measurement made by FTIR spectroscopy. PET samples, obtained from different manufacturers, were considered to differ in molecular weight,

branching and extent of copolymerization and it was essential to measure their crystallization rate-temperature dependence prior to a detailed study of changes to the IR spectra on crystallization.

DSC is designed to measure the difference in the rate of heat flow required to heat or cool a sample and reference at a defined rate of heating. It therefore measures changes in heat flow, dH/dt of materials as a function of temperature. The heat flow at temperature T is described as below,

$$\left(\frac{dH}{dt}\right)_T = \frac{(dH/dT)_T}{(dT/dt)_T} = C_{p,T}/R \tag{2.3}$$

where C_p and R are the specific heat and the rate of heating respectively.

DSC measures the specific heat of a material as a function of temperature and by integration can be used to measured enthalpy and entropy of phase transitions and chemical reactions. The basic role of this technique is to maintain the sample and reference at the same temperature while at the same time changing the temperature at a controlled rate. When a sample undergoes a phase transition, endothermic or exothermic, more or less heat is required to alter the temperature of the sample relative to that of the reference and the heat flow is adjusted accordingly [86]. The heat flow difference is recorded by the DSC as a function of temperature and displayed against temperature or time.

DSC contains two separate thermal sensors; one for the sample and the second the reference. During a DSC program, heating, cooling or at constant temperature the differences in heat flow between the two sensors are monitored. The instrument maintains sample and reference at exactly the same temperature and records the difference in heat flow rate as a function of time or temperature. Integration of the heat flow data over time enables the enthalpy of the transition to be directly measured, after a correction is made for baseline differences between the sample and reference. In this way the crystallization kinetics of PET over a range in temperature have been studied [86].

2.2.2.2 Experimental Procedures.

A Perkin-Elmer differential scanning calorimeter, DSC-7 with a thermal analyzer TAC 7/DZ [87], interfaced to a computer was used to follow the variation of the rate of heat evolution with time during the crystallization or melting of PET.

The temperature scale of the DSC was calibrated from the melting point of high purity (99.999%) metals: tin (231.93 ^{o}C) and indium (156.60 ^{o}C). The power response of the calorimeter was calibrated from the enthalpy of fusion of indium, taken to be 28.47Jg^{-1}.

Samples were weighed accurately using a Perkin-Elmer microbalance to 10 μg. About 15.0 mg was used encapsulated in an aluminum pan and an empty aluminum pan was used as reference.

In measuring the crystallization rate behaviour of PET as a function of temperature the sample initially was heated to 275 ^{o}C at 10 ^{o}C min^{-1} heating rate and kept for 2 minutes at 275 ^{o}C. It was subsequently cooled to 30 ^{o}C at 10 ^{o}C min^{-1}. The temperature of the onset of crystallization was noted and used to determine the temperature range in which the sample crystallize at rates which could conveniently be measured in the DSC.

Isothermal crystallization studies were carried out by heating a sample at 10 ^{o}C min^{-1} to 275 ^{o}C. The sample was held at this temperature for 2 minutes to ensure complete melting and then quenched to the isothermal crystallization temperature at 160 ^{o}C min^{-1}. It was subsequently held at that temperature until crystallization was observed to be complete by the return of the thermal response to the calorimeter baseline. The resulting exothermic trace was analyzed in terms of the Avrami equation to determine half-lives, rate constants and the rate parameter, n, in the temperature range 224 to 240 ^{o}C as described later. In this way the temperature dependent rate parameters were determined and analyzed in terms on nucleation control of the transition.

Once the isothermal crystallization process was completed, the sample was heated to 280 ^{o}C at 10^{o}C min^{-1} to determine the melting behaviour of the crystallized sample.

Samples for seeded crystallization experiments were prepared in the same way. The DSC samples, heated up to 275 ^{o}C and held for 2 minutes to completely melt, were quenched to 234 ^{o}C and held for 50 minutes so that they could be crystallized to the end of the primary crystallization stage, i.e. pre-crystallization. These were then heated at 50 ^{o}C min^{-1} to 244~258 ^{o}C for partial melting and subsequent seeded crystallization. The time-scale of seeded stage varied from 1 to 1000 minutes. Once the seeded crystallization process was finished, the sample was heated to 280^{o}C at 10^{o}C min^{-1} to determine the melting behaviour.

Figure 2.6 The Perkin-Elmer DSC-7 and TAC 7/DZ.

2.2.3 Hot-stage Microscopy.

2.2.3.1 Optical Microscopy.

Optical microscopy provides a magnified view of the sample under transmitted or reflected light. The magnified view could be detected by human eye, imaged on a photographic plate or captured and displayed on a digital camera.

A digital microscope containing a charge-coupled device (CCD) camera to focus the object was used to study the morphology of crystalline PET. The CCD camera captured a digital image as a function of temperature and time, which could be displayed dynamically on a computer screen for measurement of the image size.

2.2.3.2 Hot-stage Microscopy.

The hot-stage of the microscope included a specimen chamber mounted on the microscope stage, a thermal control unit, cooling unit and computer thermal control software [88, 89]. Hot-stage could be set up on high quality transmitted, reflected and UV-fluorescence microscopes and the Laser-Raman microprobe to investigate the changes and properties of materials [90-94]. The heating and cooling units and specimen chamber provided a broad temperature range from -196 ^{o}C to 500 ^{o}C. The computer software supports computer-controlled x-y stage and heating/cooling rates could be set to 0.1 ^{o}C to 100 ^{o}C min^{-1}.

The optical hot-stage microscopy allowed specimens to be studied with magnification up to 500X using long working distance objective lenses. [88, 89].

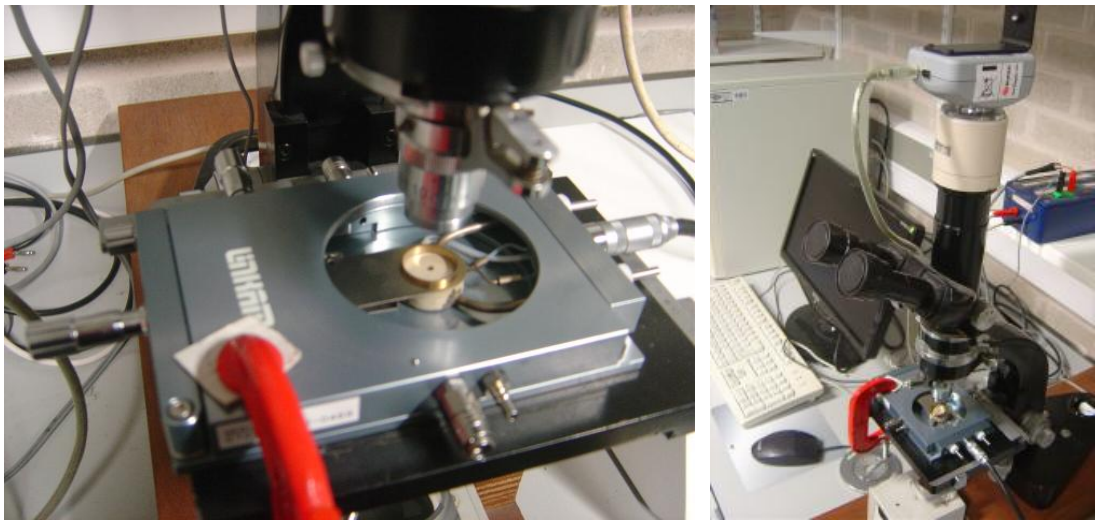

Figure 2.7 The Hot-stage Chamber with Optical Microscope.

2.2.3.3 Experimental Procedures.

Isothermal and seeded crystallization studies were carried out on a Leitz Wetzlar optical/digital microscopy system with a Linkam THMS600 hot-stage coupled to a thermal control unit, TMS94, and cooling unit, LNP94/2, along with a digital camera Olympus, PL-A662, and a light resistance monitor. This was computer controlled supported by Linksys32 software.

PET thin film samples were heated in the hot-stage chamber from room temperature to 275 ^{o}C at 100 ^{o}C min^{-1} and held at this temperature for 2 minutes. to ensure complete melting. The cooling unit enabled the samples to be cooled from

250 ^{o}C to 230 ^{o}C at 80 ^{o}C min^{-1} for isothermal crystallization at that temperature. During crystallization the birefringence of the specimen was measured with a photo-resist meter and the signal recorded by the light current sensor. Alternatively a series of images could be recorded on the digital camera as a function of time. This enabled the spherulitic growth of PET to be measured during the crystallization.

Samples for seeded crystallization experiments were prepared in the same way. The thin film was heated to 275 ^{o}C and held for 2 minutes to melt the sample completely. This was followed by quenching to 234 ^{o}C and holding the sample for 50 minutes to enable pre-crystallization to occur. The sample was the heated at 50 ^{o}C min^{-1} to 244~250 ^{o}C where partial melting and seeded crystallization was followed up to 1200 minutes. Images of the sample were taken at various to follow the development of partial melting and seeded crystallization.

Chapter Three

Thermal Analysis of PET by DSC and FTIR Spectroscopy

3.1 Introduction.

Thermal analysis FTIR spectroscopy, TA-FTIR, has been widely used to study polymer degradation and changes in to chain conformation with temperature. In studying polymer degradation it enables changes in chemical composition and chain structure to be followed as a function of temperature and time. The kinetics of reactions are followed by the change in the concentration of functional groups [95-101] and significant changes in chemical composition determined from the appearance and disappearance of absorption bands. In this way the relative importance of competing reactions can be established as well as the build up and disappearance of transient species.

The chain conformation of PET is closely associated with the ratio of cis and trans rotational isomers present in the sample. In the un-oriented amorphous polymer below the glass transition this ratio is invariant with temperature due to restricted chain mobility. Above the glass transition the ratio is in thermal equilibrium due to the onset of rotational modes in the chain. Accordingly the temperature dependence of the cis/trans ratio has been used to measure the glass transition temperature, T_g and follow the development of physical ageing with time at temperatures below T_g.

Recently [102] the kinetics of isothermal crystallization of poly (ethylene terephthalate) by TA-FTIR have been measured by separating the crystalline and amorphous components of the carbonyl absorption bands as a function of time over a range of temperatures. This enabled the weight fraction crystallinity to be measured well into the secondary crystallization process over a greater time scale and wider temperature range than was possible by differential scanning calorimetry, DSC. The later technique by measuring the rate of crystallization rather than the fractional crystallinity was limited by the sensitivity of the calorimeter to measuring heat flow. As a result it was not possible to measure the kinetics of secondary crystallization with sufficient accuracy for kinetic analysis [103-106].

This chapter considers the value of TA-FTIR to measure phase transitions which occurs in an amorphous/crystallizable polymer and makes a direct comparison with DSC.

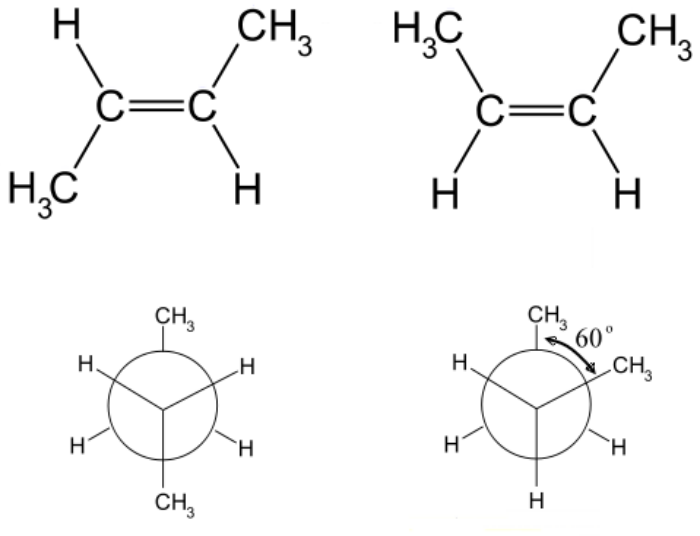

Figure 3. 1 Trans-2-Butene (left) and Cis-2-Butene (right) Structure.

3.2 DSC Thermal Analysis of PET.

Amorphous DSC samples were initially heated from room temperature to 275^{o}C at 10 ^{o}C min^{-1}, and then maintained at 275 ^{o}C for 2 minutes ensuring completed melting. They were subsequently cooled to 30 ^{o}C at 10 ^{o}C min^{-1} for re-crystallization. The thermal procedure detected the measured glass-transition, crystallization, melting and re-crystallization temperatures.

A typical thermal cycling curve of amorphous PET is shown in Figure 3.2. A well-defined glass transition appears at 78 ^{o}C, followed by a sub-transition peak with

rapid quenching from the melt which is the cold crystallization procedure. The onset, T_{c1}, and peak temperature of cold crystallization are 115 and 130 ^{o}C respectively. Melting happens in the range 225-260 ^{o}C with peak melting temperature at 255 ^{o}C.

On cooling to room temperature, crystallization of the sample occurs at about 230 ^{o}C in the high temperature region. The reset smooth curve shows no obvious glass transition which is consistent with the sample being partially crystalline.

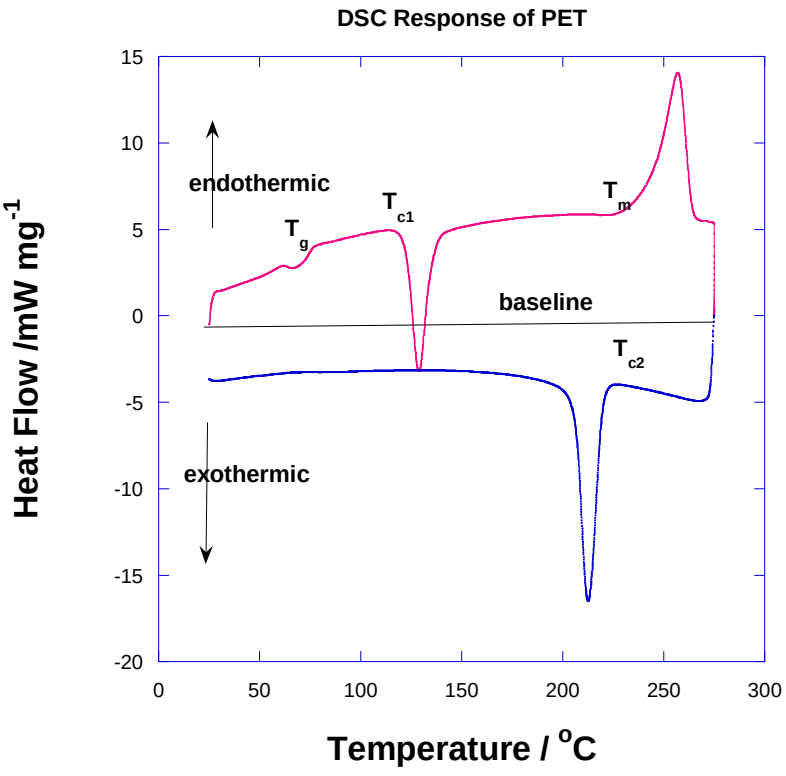

Figure 3.2 The DSC Analysis of PET.
(Red line indicates heating, blue cooling at 10 K min^{-1})

The heat flow-temperature curves in Figure 3.2 were integrated above the instrument baseline generating corresponding change in enthalpy curves [107] associated with the various transitions. These are shown in Figure 3.3 for the heating and cooling curves. The glass transition is seen as a change in slope of the enthalpy of the liquid line at about 75 ^{o}C. There is a linear increase in heat capacity with temperature until the sample starts crystallizing at 115 ^{o}C. This is accompanied by the evolution of heat corresponding to the enthalpy of crystallization at T_{c1}. The enthalpy of the partially crystalline sample also increases linearly until the onset of melting at 230 ^{o}C and melting continued up to 260^{o}C, at which the enthalpy attains the value of the liquid phase. Thereafter the enthalpy increases linearly with a slope which is the heat capacity of the liquid.

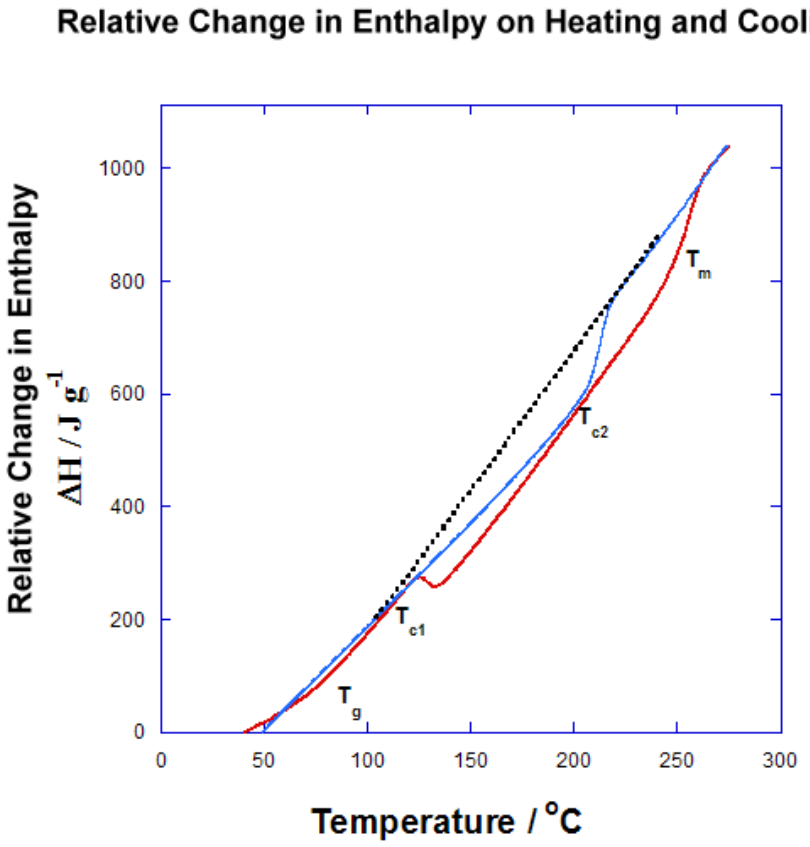

Figure 3.3 The Relative Enthalpy Change on Heating and Cooling PET. 320 K was used as the Reference Temperature. (Red line indicates heating, blue cooling at 10 K min^{-1})

On cooling from above the melting point to 30 ^{o}C, the enthalpy of the liquid decreases linearly with temperature and this extrapolates linearly to the liquid line above the glass transition temperature, as shown by the dotted line in Figure 3.3. Since there is no difference between the extrapolated entropy of the liquid and the original sample at $T_{g,}$ the original sample is amorphous [106]. On further cooling the sample starts to crystallize at about 230^{o}C with the evolution of the enthalpy of crystallization at $T_{c2,}$ and this is complete at 200 ^{o}C. The enthalpy then decreases

linearly with a slope corresponding to the specific heat of the partially crystalline material. There was no evidence, such as a slope change, for a glass transition on cooling in the semi-crystalline sample.

3.3 Typical FTIR Spectrum of PET.

Figure 3.4 shows a typical FTIR spectrum of amorphous PET. The main absorption bands in the spectrum have been assigned [108-111] as follows, 3100-2800 cm^{-1} to aromatic and aliphatic –C-H bond stretching, 1780-1650 cm^{-1} to the ester carbonyl bond stretching, 1470-1350 cm^{-1} to bending and wagging vibrational modes of the ethylene glycol segment, 1235 cm^{-1} to the ester group stretching, 1090cm^{-1} to the methylene group and aromatic bands in-plane/out-plane bending at 1016 and 725 cm^{-1}. Many of the medium and weaker bands have been attributed to chain conformation and are sensitive to whether the sample is amorphous, oriented, or crystalline [111-114], which will be discussed in detail in later chapter. Differences are due to conformation of the ethylene glycol group (cis/trans isomers) and also phenylene carbonyl bonds (cis-trans isomers).

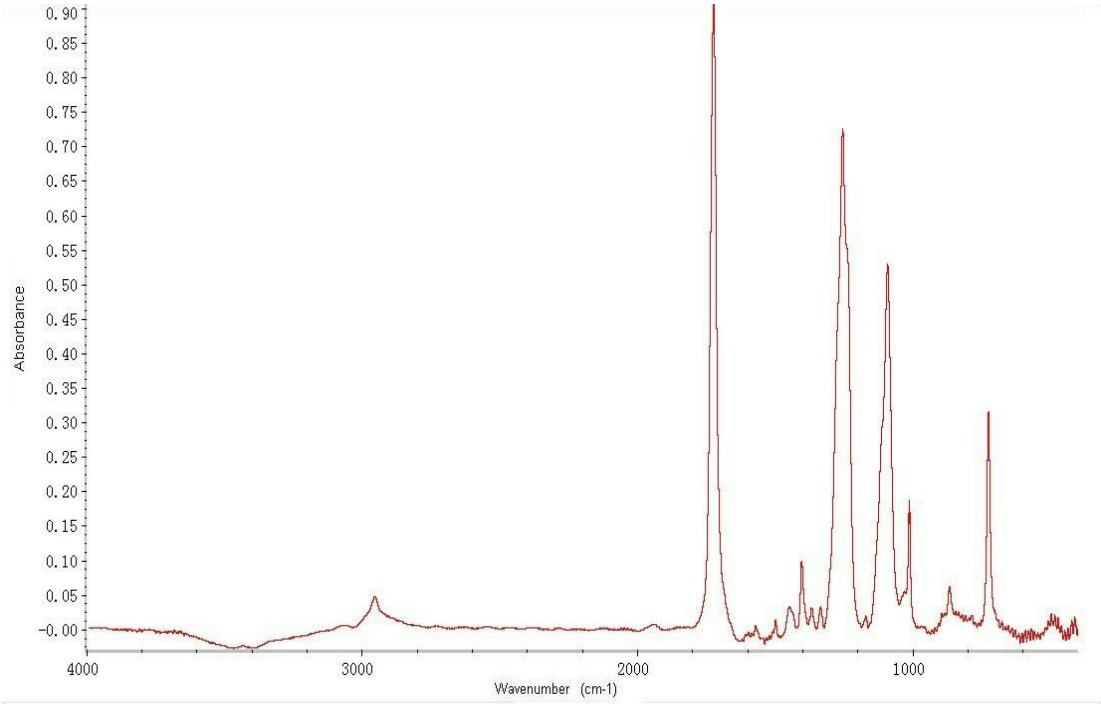

Figure 3.4 The FTIR Spectrum of Amorphous PET, 1.5 µm Thick Film.

3.4 Thermal Analysis PET on FTIR Spectrum.

3.4.1 On cooling PET from the Melt.

An amorphous PET sample was cooled from the melt - from 270 to 160 ^{o}C. Infrared spectra were recorded at intervals and the changes in the peak position, height and breadth on crystallization noted, see Figure 3.4. Particular attention was taken of the carbonyl band at 1727 cm^{-1} as it decreased in intensity on cooling and a second band at 1717 cm^{-1} developed on crystallization. The ratio of the intensities of the two bands was a measure of the crystalline and amorphous content of the PET sample [102]. Other significant changes included an increase in intensity, change in

shape and shift in wavenumber of the bands at 1340, 1235, 1090 and 724 cm^{-1} as can be seen in Figure 3.5.

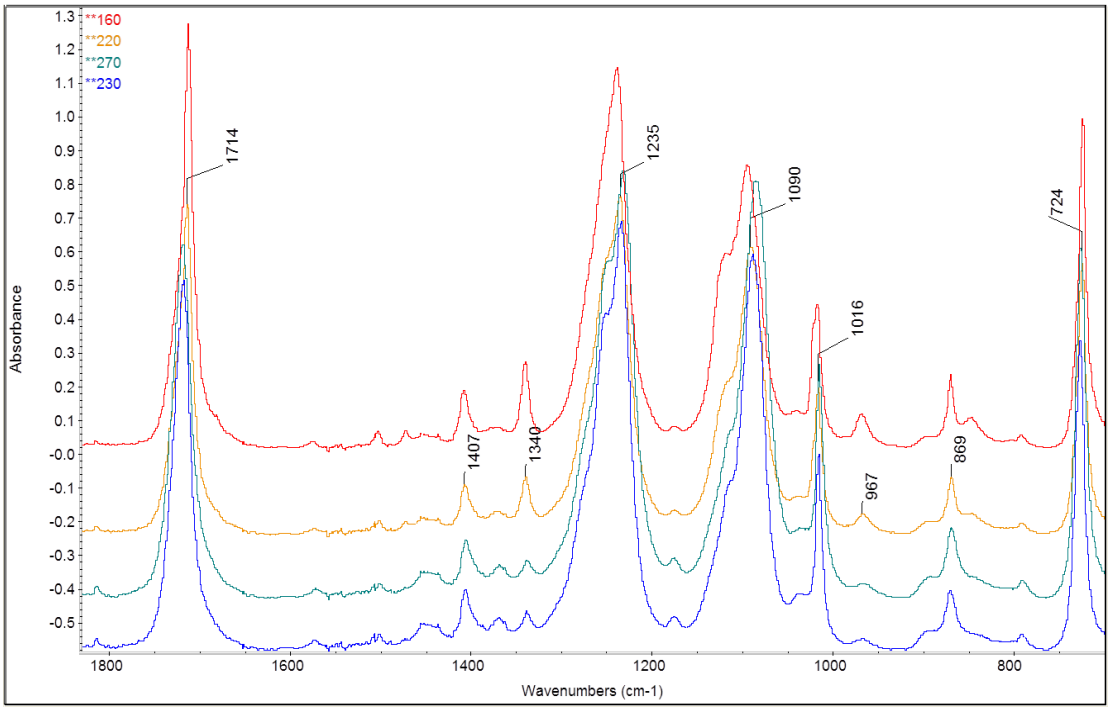

Figure 3.5 Changes in the FTIR Spectra of Amorphous PET on Crystallization on Cooling from 270 to 160^{o}C.

3.4.2 The Effect of Thermal Cycling on the FTIR Spectra

The same thermal cycle as used above in recording the DSC response of amorphous PET was also used in heating from room temperature to 270 ^{o}C and cooling to 40^{o}C. Similar changes were observed in the shape, breadth, peak position and relative intensities of the major bands during this thermal treatment. The cycle was separated into four distinct temperature regions and accompanied with phase transitions in the polymer, i.e. room temperature to T_g, T_g to cold crystallization

temperature T_{c1}, T_{c1} to melting temperature T_m and on cooling from above the melting point down to 40 ^oC. Figure 3.6 exhibits the peak absorbance against wavelength in the region 1350-1600 cm^{-1} while the third axis displays the sample temperature on heating to the melting point and on subsequent cooling. This is an example of a waterfall spectrum in which each spectrum is displaced laterally and vertically by the same amount to display a trend in intensity with temperature. Although the changes of peak 1507 and 1575 cm^{-1} were significant, they seem to be small compared with others. Figure 3.7 provides a 3D model to help highlight these differences.

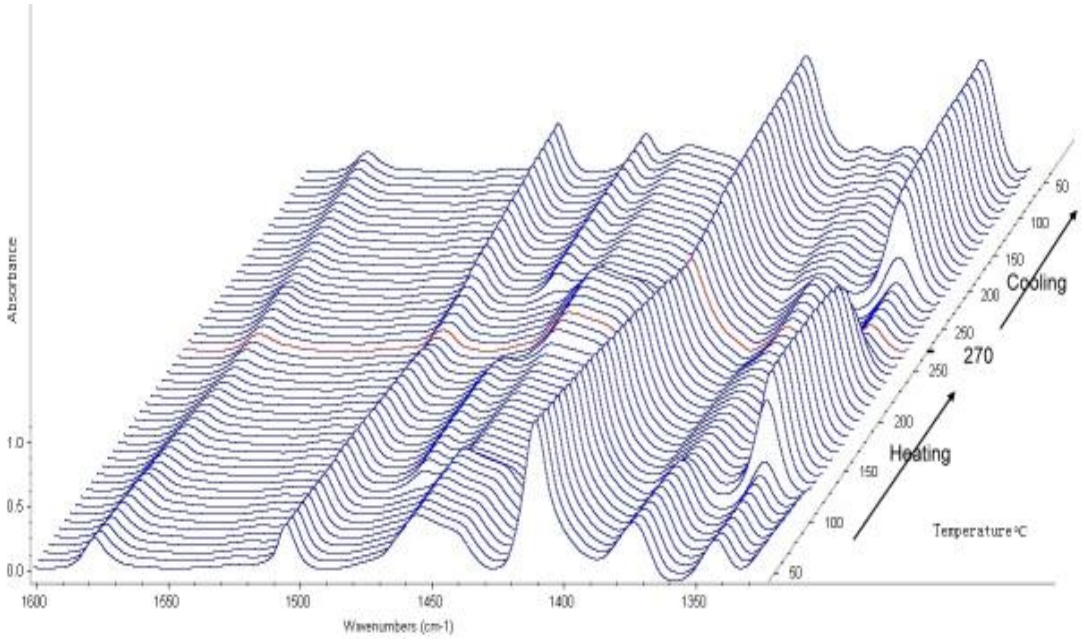

Figure 3.6 The Development of the Absorbances of the Bands in the Region 1350-1600 cm^{-1} with Temperature on Heating and Cooling.

Two different and opposite trends were observed in the way the absorbance of the peaks changed on crystallization and melting on heating and cooling. For example, the bands at 1472 and 1342 cm^{-1} increased in intensity at 110-120 ^{o}C and decreased at 240^{o}C on heating and increased again on cooling at 230^{o}C. This increase is associated with the polymer crystallizing and the decrease with melting. The reverse change was observed by the peaks at 1458-1440 and 1370 cm^{-1} i.e. an increase in absorbance on melting and a decrease on crystallizing.

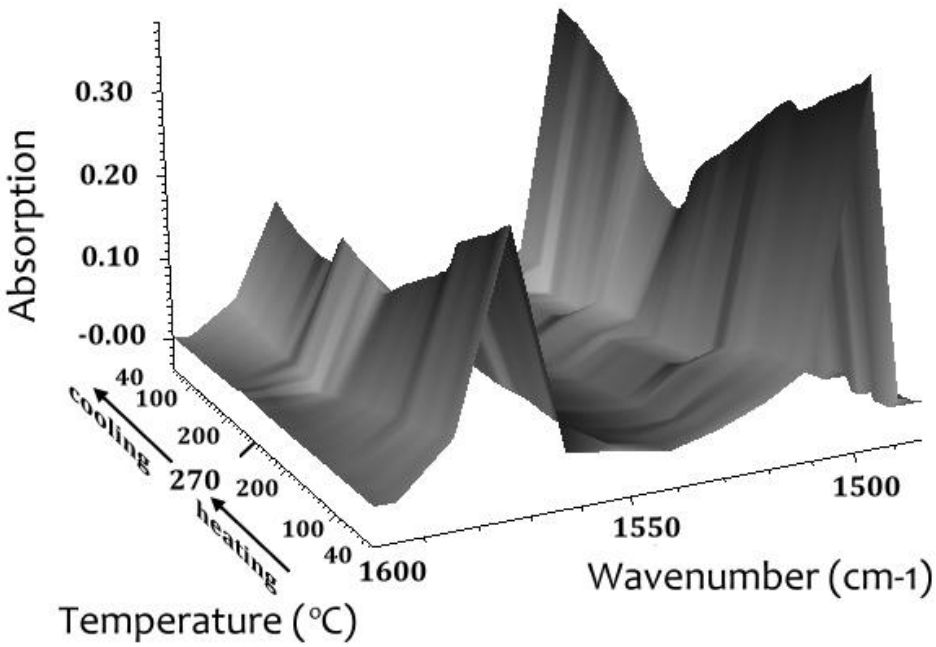

Figure 3.7 A 3D Representation of the Region 1480-1600 cm^{-1} with Temperature on Heating and Cooling.

The pair of bands at 1472 and 1458-40 cm^{-1} have been assigned to the bending modes of the trans and cis conformational isomers of the ethylene segments respectively and the pair at 1342 and 1370 cm^{-1} to the wagging mode of this segment.

Since in the crystalline phase the chain conformation must be trans on crystallization the trans isomer must increase at the expense of the cis and the reverse occurs on melting. These increase and decrease of the peak intensities at each phase transition have been designated as Type I behaviour, since they are the most commonly encountered.

The band at 1410 cm^{-1}, however, was observed to show a different type of behaviour in that the absorbance decreased smoothly with temperature in heating and there was no abrupt change at phase transitions. This band has been assigned to the stretching mode of –C-H bond in the aromatic ring. For convenience this has been designated Type II behaviour and is discussed in section 3.4.4.

3.4.3 Type I Behaviour.

The effect of crystallization, melting and re-crystallization during thermal cycling on the conformation of the molecular chain was studied by considering the behaviour of the bending mode of the glycol methylene groups at 1470 and 1450 cm^{-1}. These two bands have been attributed to the trans and cis conformation isomers [102]. The change in absorbances of the bands in the four temperature regions can be seen in Figures 3.8 and 3.9. For comparison the T_g, T_{c1}, T_{c2}, and T_m determined by DSC are marked on the figures. On heating the absorbances of the two

bands decreased with increasing temperature but the decrease was less marked with the trans than the cis isomer. The Beer-Lambert law defines the absorbance of an IR band as, $A= \varepsilon[c]l$. It was not possible to separate the temperature dependence of the concentration and extinction coefficient in this experimment. However, both must contribute since the absorbance of the two bands decrease with increasing temperature while the concentration of the one of the species must increase and the other decrease depending on which predominates at low temperature, so that ε must have some temperature dependence.

In the region of the glass transition temperature, as measured by DSC at 78 ^{o}C, the cis isomer only shows a step change in the absorbance with temperature and this was attributed to the glass transition. Below the glass transition temperature, PET is a rigid glass that and the chains cannot rotate, and the cis/trans ratio is constant, independent of temperature. The chain conformation is not in thermal equilibrium and does not change with temperature [101, 102]. Above the glass transition, the amorphous polymer becomes a viscous liquid and its molecular chains have some mobility due to the onset of bond rotation. The cis/trans ratio which define the chain conformation is then in thermal equilibrium. The trans isomer does not show any significant change in the glass transition region due to its very low absorption and minor variations are difficult to separate from random fluctuations.

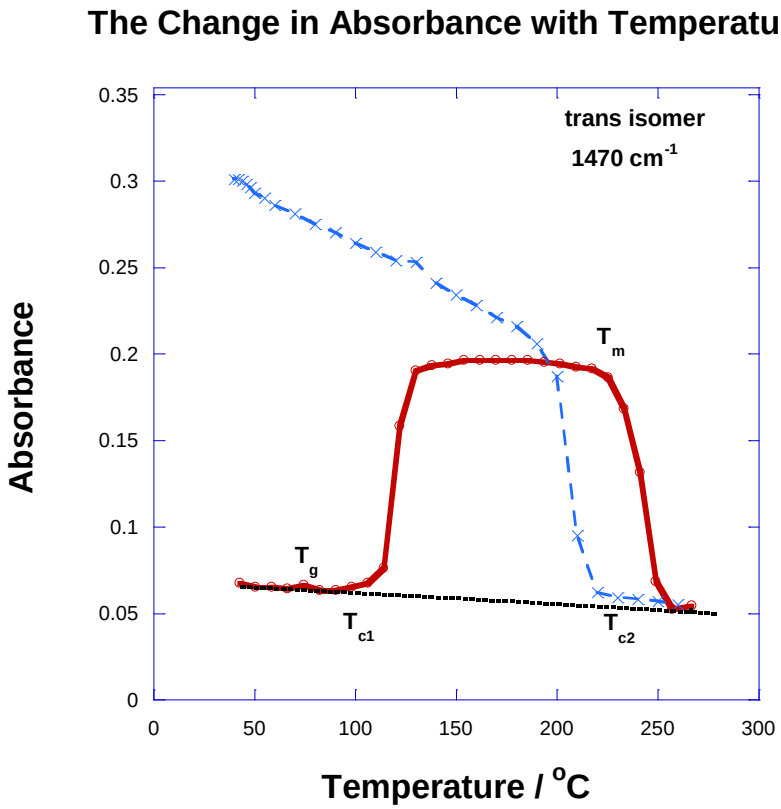

Figure 3.8 The Change in Absorbance of the Trans Isomer at 1470 cm^{-1} with Temperature Showing the Glass Transition Temperature, T_g, Cold Crystallization Temperature, T_{c1}, and Melting Point, T_m on Heating and the Crystallization Temperature, T_{c2}, on Cooling.
(Red line indicates heating, blue cooling)

On heating low temperature crystallization occurs at T_{c1} and it is accompanied by a marked increase in absorption of the trans isomer, Figure 3.8, and a corresponding decrease in the cis, Figure 3.9. This is due to the onset of crystallization. In the crystal the chain must adopt the fully extended all trans conformation and the cis form cannot be accommodated within the crystal but is restricted to the amorphous regions. The overall trans and cis content increases and decreases respectively proportional to the crystallinity.

On further heating the cis intensity continues to decrease due to further crystallization, a change in the cis concentration in the amorphous regions due to the cis/trans isomerisation as cis changes to trans and a decrease in the extinction coefficient. At the same time the absorbance of the trans band does not change substantially due to a balance between the concentration increasing and a decrease in the extinction coefficient.

When the temperature reaches the onset of melting temperature at 230 ^{o}C, the absorbance of cis isomer increase and the trans decreases until the melting is complete at 260 ^{o}C. Above 260 ^{o}C, the absorbance of the trans and cis isomers have returned to the extrapolated values obtained from the amorphous sample at low temperature region between the glass transition and the cold crystallization temperature, T_{c1}, as shown by the dotted lines in Figures 3.8 and 3.9. The dotted lines represents the change in absorbance of the isomers in the amorphous polymer sample.

On cooling, the absorbance follow the linear dependence of the extrapolated line until the sample crystallizes at about 220 ^{o}C, T_{c2}, with a drop in the cis and a rise in the trans absorbance. Since the re-crystalline sample is more crystalline than the cold crystallized sample, it has a higher trans content, which is consistent with a higher fractional crystallinity. The absorbance of trans continues to increase as the temperature decreases, while the cis remain effectively constant.

The general behaviour of the absorbance of the bands changing with temperature and an increasing or decreasing on crystallization and melting was observed with many of the absorption bands in PET, particularly those associated with chain conformation, cis/trans transitions, ie. 2960/2970 cm^{-1}, 1575/1505 cm^{-1}, 1370/1340 cm^{-1} and 1120/1100 cm^{-1} pairs. They could equally have been used to monitor the phase transitions and the crystallinity of PET.

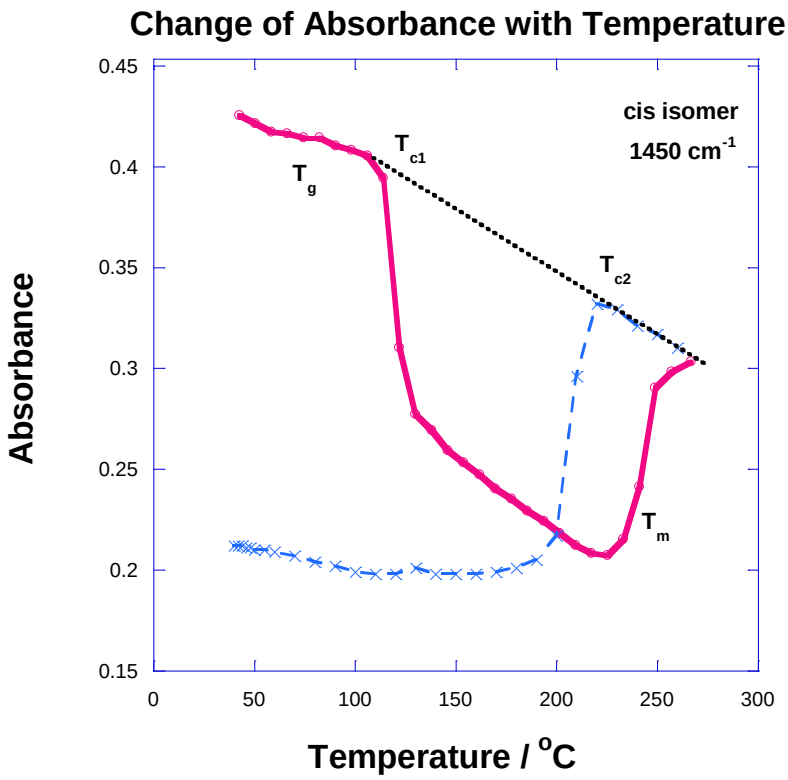

Figure 3.9 The Change in Absorbance of the Cis Isomer at 1350 cm^{-1} with Temperature Showing the Glass Transition Temperature, T_g, Cold Crystallization Temperature, T_{c1}, and Melting Point, T_m, on Heating and the Crystallization Temperature, T_{c2}, on Cooling.
(Red line indicates heating, blue cooling)

3.4.4 Type II Behaviour.

The absorption band at 1410 cm^{-1} has been assigned to –C-H bond of aromatic ring stretching. It has played an important role in the characterization of the structure of PET by IR spectroscopy since it has generally been used as an internal reference against which all others can be ratioed [114]. It is also considered as being effectively constant independent of crystallinity, orientation and in particular temperature while all other bands change. The absorbance and peak maximum is considered invariant with fractional crystallinity and degree of orientation and a useful guide for changes in sample dimensions. It is thus important to establish effect of temperature and thermal treatment on the shape, absorbance and position of the band.

The temperature dependence of the absorbance of the 1410 cm^{-1} band was very different from that observed from the Type I behaviour, see Figure 3.10. In the heating run, a smooth drop with temperature was observed with a change in slope on crystallization or melting instead of discontinuous jump during crystallization or melting. On cooling the absorbance increased linearly with decreasing temperature until the sample crystallized. The absorbance increased on further cooling but at a much lower rate than before re-crystallization also with much lower value than on initial heating.

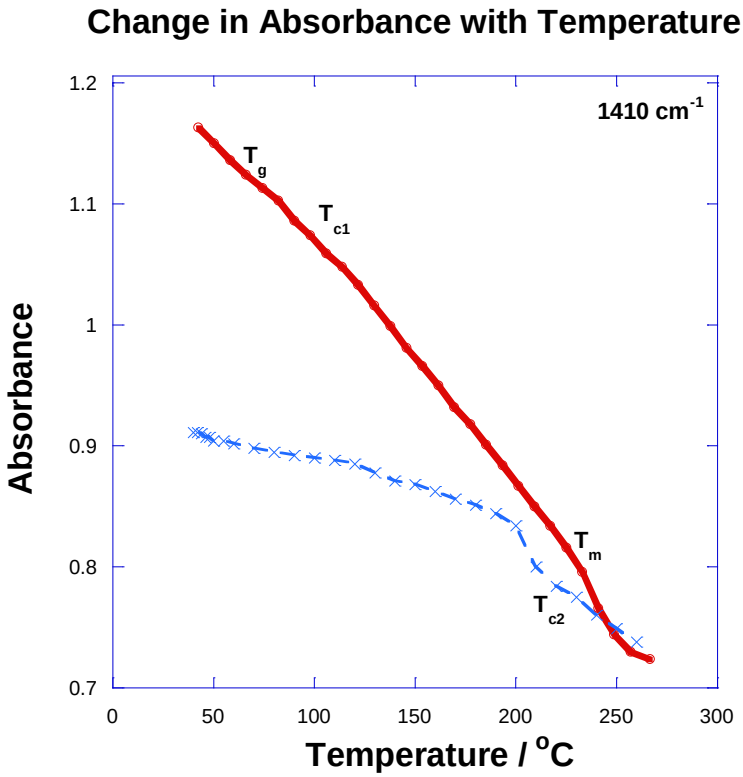

Figure 3.10 The Change in Absorbance of 1410 cm^{-1} Band with Temperature. (Red line indicates heating, blue cooling)

The absorption band was observed to shift progressively to lower wavenumbers with increasing temperature, see Figure 3.11, and there is a marked increase on crystallization at T_{c1}. There was a further linear decrease with temperature until the onset of melting where the peak position dropped sharply until melting was complete at which point it returned to the values obtained by the linear extrapolation of the liquid value against temperature. This shift to the lower wavenumber with increasing temperature was not fully reversible on cooling. The peak position followed the extrapolated liquid line until the sample crystallized at T_{c2}. On further cooling the

peak position continued to increase linearly in wavenumber but at higher values than observed in the cold crystallization sample.

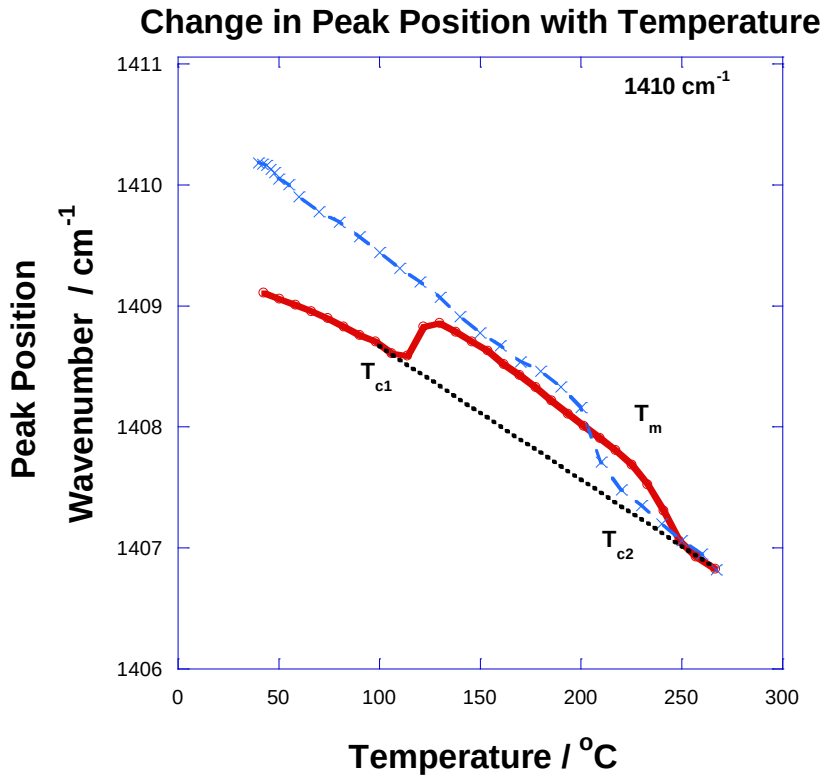

Figure 3.11 The Change in Peak Position of the 1410 cm^{-1} Band with Temperature.
(Red line indicates heating, blue cooling)

The shift in peak position on crystallization is less than 1 cm^{-1} and the crystalline band which develops would almost completely overlap the initial amorphous band. Changes in intensity due to the disappearance of the amorphous band would be minimised by the inverse dependence of the crystalline absorbance

and would cancel one another if the extinction coefficients of the two band were identical.

3.4.5 Special Mode of Type II Behaviour.

The effect of overlapping the two peaks was simulated by summing the intensities of two well separated peaks due to ring stretching modes at 1505 cm^{-1} in the crystalline regions and 1575 cm^{-1} in the amorphous, both of which belong to Type I behaviour and similar to 1470/1450 cm^{-1} pair. The absorbances of the bands increased and decreased to similar extents on crystallizing and melting, see Figure 3.12, such that on adding the two absorbances at each temperature resulted in little or no net change during crystallization or melting, see Figure 3.13, but decreased with increasing temperature followed a linear temperature dependent. To compare directly with the absorption band at 1410 cm^{-1}, these absorbances were added over the full temperature range on heating and cooling. The resulting trend was very similar to that observed with the 1410 cm^{-1} band. In other words, two related but individual Type I behaviour bands can be combined into a special mode of Type II behaviour.

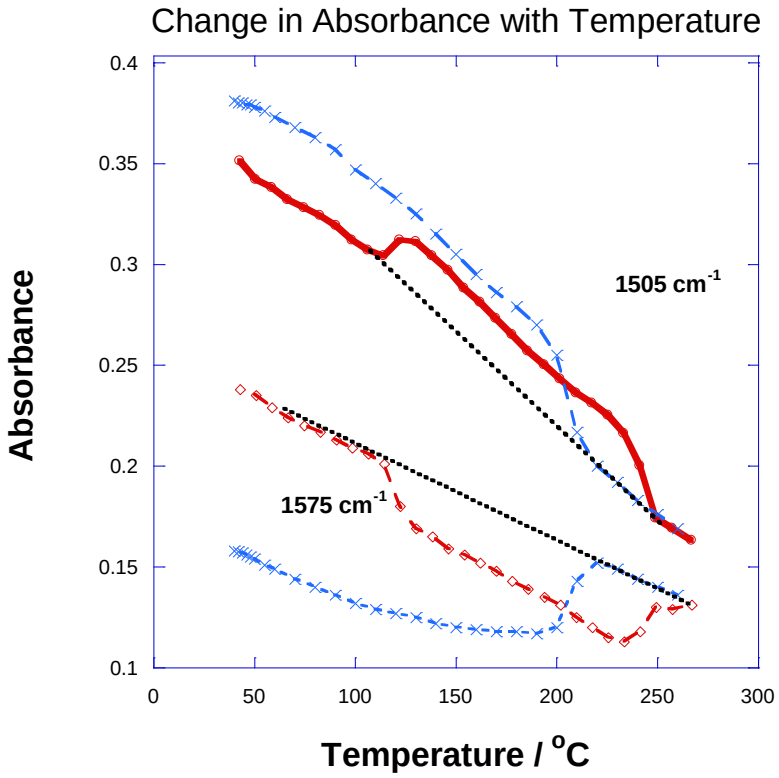

Figure 3.12 The Change in Absorbance of with Temperature and on Crystallization and Manelting at 1575 and 1505 cm^{-1}.
(Red lines indicates heating, blue cooling)

To summarize, Type II behaviour arises when the amorphous and crystalline bands substantially overlap and it is not possible to follow the individual absorbances, but only an average of the two is measured. There is then little or no change associated with crystallization or melting. Nevertheless, the peak position changes on crystallization or melting between the two limits set by the crystalline and amorphous bands.

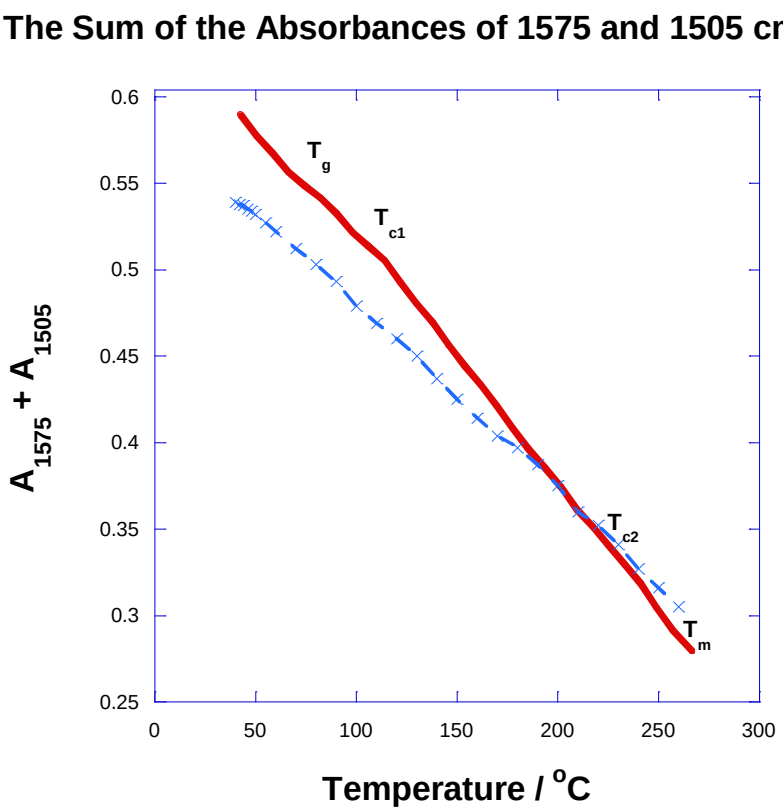

Figure 3.13 Simulation of Type II Behaviour Generated from Summing a Pair of Type I Bands at 1575 and 1505 cm^{-1}.

3.5 Discussion.

3.5.1 Phase Transition Temperature of Individual Functional Group

Close examination of TA-FTIR response of the individual functional groups with temperature show that they exhibit slightly different transition temperatures. Groups which show Type I behaviour indicate that cold-crystallization occurs at 110-120 ^{o}C with a change in absorbance. Those of Type II behaviour were less clear and appeared to crystallize at a lower temperature i.e. at 100 ^{o}C, but this may reflect the

poorer sensitivity of the change in peak position to detect small changes rather than any change in chain conformation. On heating further to melting, some functional groups exhibit changes at a lower temperture (225 ^{o}C) than others. The aliphatic CH_2 stretching band at 2950 cm^{-1}, the carbonyl stretching at 1727/1717 cm^{-1}, the glycol methylene bending at 1470/1450 cm^{-1}, the glycol wagging at 1370/1340 cm^{-1} and the ester bond stretching at 1120/1100 cm^{-1} show the onset of melting to be at 225 ^{o}C. Other functional groups seemed to be less sensitive to the onset of melting, 1575/1525 cm^{-1} aromatic ring stretching, 1410 cm^{-1} aromatic ring stretching and 1020/730 cm^{-1} benzene ring in-plane and out-plane bending. These show the onset of melting to be at the higher temperature of 233 ^{o}C. However, in ever case the last trace of crystallinity was observed to be 230 ^{o}C.

On cooling PET started to re-crystallize at 225 ^{o}C and the bands at 1727/1717, 1120/1100, 1020/730 cm^{-1} respond immediately with a change in absorption while others at 2950, 1575/1505, 1470/1450, 1410 and 1340 cm^{-1} occur later at 215 ^{o}C. The phase transitions and the behaviour of the absorption bands on crystallization and melting are summarised in Table 1.

Table 3.1 Changes to Absorbance and Peak Positions at Phase Transitions.

Wavenumber/ cm^{-1}		Overall	Heating			Cooling
			Tg / ^{o}C	C_{t1}/ ^{o}C	Melting/ ^{o}C	C_{t2} / ^{o}C
2970-2960 Type I	A	↓	80 ↑	115 ↓	260 ↑	220↓
	W	→	─	←	→	←
1730-1710 Type II	A	↓	n,d .	─	260 ↓	220 ↑
	W	←	─	→	←	→
1575-1570 Type I	A	↓	75 ↓	120 ↓	255↑	220↓
	W	→	─	←	→	←
1508-1503 Type I	A	↓	75 ↓	120 ↑	260 ↓	220 ↑
	W	→	─	─	─	─
1470-1475 Type I	A	─	75 ─	115 ↑	255↓	220 ↑
	W	─	─	←	→	←
1458-1438 Type I	A	─	75 ↓	115 ↓	255↑	220↓
	W	─	─	←	→	←
1410 Type II	A	↓	n.d ─	105 ↓	260 ↓	↑
	W	→	─	←	→	←
1370 Type I	A	↓	─	↓	↑	↓
	W	─	─	←	→	← *
1342-1338 Type I	A	─	75 ─	115 ↑	265 ↓	220 ↑
	W	→	─	←	→	←
1130-1120 Type I	A	↓	75 ↑	115 ↓	250 ↑	230↓
	W	→	←	←	→	←
1100-1090 Type I	A	↓	80 ↑	110-120↑	260 ↓	230↑
	W	→	→	←	→	←
1020-1015 Type II	A	↑	75 ↑	100 ↓	250↑	230 ↓
	W	→	─	←	→	←
730-720 Type II	A	↓	75 ↓	100 ↑	265 ↓	230↑
	W	←	←	→	←	→

A is absorbance; W wavenumber at peak; * Splits into two bands; n.d. not detected.

↑ increase and ↓ decrease in absorbance;, ← decrease, → increase in wavenumber, ─ no change.

3.5.2 Thermal Equilibrium of cis/trans Isomers.

Assuming that in the mobile liquid state that an equilibrium exists between the cis and trans isomers, i.e.

$$\text{trans} \Leftrightarrow \text{cis},$$

then which

$$K = [\text{cis}]/[\text{trans}] = A\exp(\Delta H/RT) \qquad (3.1)$$

where K is the equilibrium constant, and [cis], [trans] represents equilibrium concentration of each isomer, A is a pre-exponential factor, R is gas constant, ΔH the heat of isomerisation and T the temperature.

Assuming that Beers-Lambert Law applies to each absorption band then

$$A_t = [\text{trans}]\,\varepsilon_t\, l \quad \text{and} \quad A_c = [\text{cis}]\,\varepsilon_c\, l$$

A is the absorbances of the two bands, ε the two molar extiction coefficients and *l* the sample thickness, then

$$[\text{cis}]/[\text{trans}] = (A_c/A_t)\,(\varepsilon_t/\varepsilon_c) = A\exp(-\Delta H/RT) \qquad (3.2)$$

Unfortunately, $(\varepsilon_t/\varepsilon_c)$ is not independent of whole temperature range since the absorbances of both cis and trans bands decreased with increasing temperature and any trend in which one isomer converts into other at higher temperature is lost by the temperature dependence of the extinction coefficients.

However, in the two temperature regions, from T_g to T_{c1} on heating and from T_m to T_{c2} on cooling, that $(\varepsilon_t/\varepsilon_c)$ is independent of temperature then a plot of log (A_c/A_t) against 1/T would be linear with a slope of -(ΔH/R). A plot of the corresponding ratio gave an activation enthalpies of 1.90 ± 0.5 kJ mol^{-1} for the bending, 3.0 ± 1.0 kJ mol^{-1} for the wagging modes of the ethylene glycol segment. The ring ester conformational enthalpies were also determined from the ratio of the absorbances at 1575 and 1505 cm^{-1} and 1120 and 1100 cm^{-1} as 1.7 ± 0.4 and 1.6 ±0.2 kJ mol^{-1} respectively.

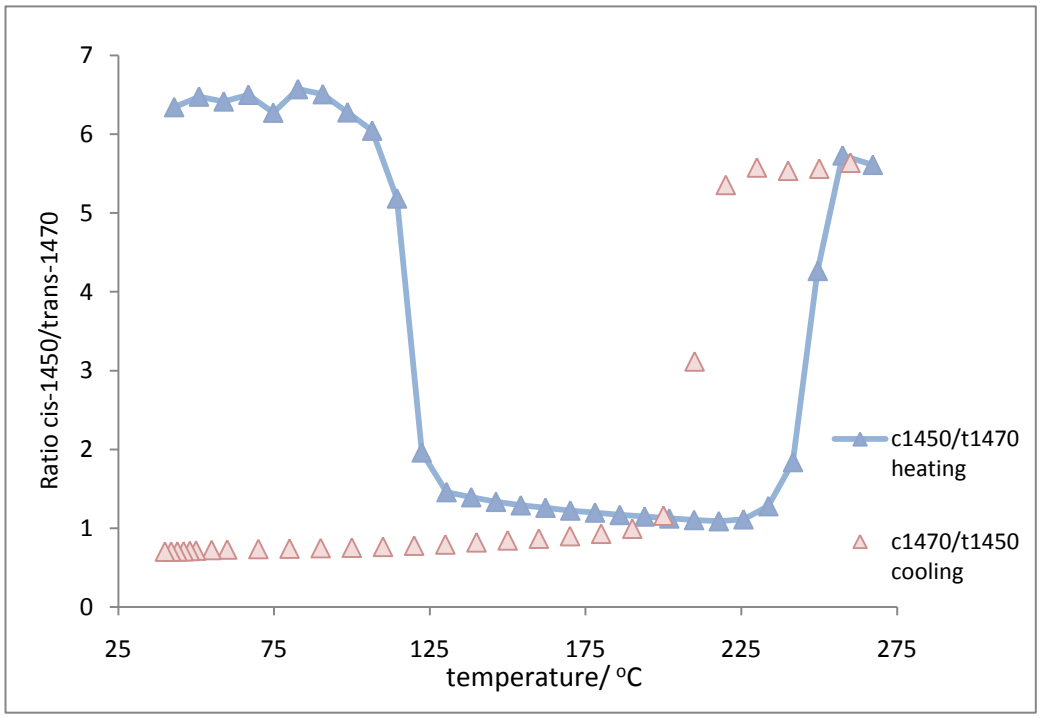

Figure 3.14 Ratio of Constant of 1470 and 1450 cm^{-1} Against Temperature.

3.5.3 Fractional Crystallinity Calculated from TA-FTIR Data

For a two phase partially crystalline polymer, the weight fraction crystallinity, X_c, and the amorphous fraction, X_a, are related since

$$X_c + X_a = 1.0 \qquad (3.3)$$

At constant temperature and a partially crystalline sample the absorbance of the cis or trans bands will both follow the fractional crystallinity and will decrease and increase respectively. Accordingly,

$$A_a = (1-X_c)\, \varepsilon\, l \qquad (3.4)$$

At $X_c = 1.0$, $A_c = 0$ and $X_c = 0.0$, $A_a = A_{a,T}$, where $A_{a,T}$ is the value of the absorbance at temperature T on the extrapolated amorphous line.

The fractional crystallinity of the sample is then

$$X_c = (A_{a,T} - A_a) / A_{a,T} \qquad (3.5)$$

The decrease in the absorbance of the cis isomer in Figure 3.8 on crystallization is consistent with equations [3.4] and [3.5]. From the data presented in Figure 3.5B at 150 ^{o}C, the absorbance on the extrapolated amorphous line is 0.37, on heating is 0.25 and on cooling is 0.20. Substituting these values into Eq.[3.5], the fractional crystallinity of the cold crystallized sample is 0.33, whilst that of the high temperature crystallized material is 0.42 at 150^{o}C. These fractional crystallinity

values are consistent with previous measurements on PET crystallized under similar conditions [103-105].

3.6 Conclusions.

TA-FTIR has certain advantages over conventional thermal analytical techniques in measuring the phase characteristics of polymer materials as has been shown for PET. These lie in being able to measure the crystalline and amorphous fractions directly from the absorbance of separate bands without the need to calibrate with samples of known crystallinity. Absolute values of the crystallinity are measured directly and are not limited by the sensitivity of the detectors since measurements can be made over greater time periods to produce a detectable change. This is not the case with conventional TA instruments which measure the rate of heat evolution and is limited by the sensitivity of the detectors. It has been reported that DSC is not capable of measuring isothermal crystallization of PET with half-lives greater than several hours or indeed of measuring the very much slower secondary crystallization process in PET [102-105]. Instead all measurements are restricted to the primary crystallization process. TA-FTIR by measuring the fractional crystallinity, rather than the rate of change with time, is not restricted in this way and both primary and secondary processes can be measured to a similar degree of accuracy [102].

Unlike DSC, which measures an overall transition temperature, TA-FTIR assigns transition temperature to the onset of rotation or mobility of a particular chain segment and can, in theory, detect the onset of pre-melting and molecular mobility.

The IR spectrum of PET is unduly complicated for its somewhat simple repeat unit and this is undoubtedly due to the chain conformations which it can adopt. Stretching, bending, wagging and deformation modes have been assigned to cis and trans isomers of the ethylene glycol segments, which above the glass transition are in thermal equilibrium and their absorbances changes with temperature, on crystallizing and melting. Similarly the ester unit can adopted cis and trans placement relative to the benzene ring and together with the stretching, in-plane and out-plane bending of the aromatic –C-H groups a large number of bands are present and aromatic substitute effects in the terephthalate group. In addition some of the bands change their peak position according to whether they are associated with amorphous or crystalline regions of the polymer, in particular the carbonyl stretching band occurs at 1727 in the amorphous and 1717 cm^{-1} in the crystalline phase. The wavenumber difference is sufficient to show the decrease in absorbance at the higher wavenumber and the increase at lower, see Figure 3.4, and to deconvolute the overall band into its components part thus enabling the amorphous and crystalline bands to be separately analyzed in a kinetic study of the crystallization in Chapter 5.

Type I and II behaviour are observed in the variation of the absorbance with temperature associated with the onset of rotational modes in the molecular chain and the establishment of a dynamic equilibrium between the conformational isomers. This enables the glass transition of the polymer to be determined from a change in slope of the absorbance with temperature. Since the trans conformation alone can be accommodated in the crystalline phase the absorbance of the trans isomer increases on crystallization and decreases on melting; the overall change being dependent on the fractional crystallinity. In this way the crystallinity of the polymer can be determined along with the stability of the various phases established.

Chapter Four

FTIR Spectroscopic Analysis and Two-dimensional Infrared Correlation Spectroscopy of PET on Isothermal Crystallization

4.1 Introduction.

The IR spectra of PET were found to undergo substantial changes in the position, intensity and breadth of the absorption bands on thermal cycling. However, these changes were accompanied with temperature dependent effects which meant that they increased or decreased with temperature without any phase transitions being involved. They were undoubtedly associated with the thermal equilibrium of the cis/trans isomerization but could also involve changes to the extinction coefficients. To remove the temperature dependence and leave only phase transition effects such

as crystallization and melting, isothermal treatment was chosen at a temperature between the onset of hot crystallization and melting.

The increase and decrease in absorbance, shifting in peak position and change in shape was then due entirely to the transition and not change in temperature. Excluding a few main absorption peaks whose changes can be observed clearly, the behaviour of the weaker peaks were not so obvious. Overlapping of these peaks also produced some difficulty in recognizing and quantifying changes especially where they exhibited different behaviour. Two-dimensional infrared spectroscopy was used to assist in recognizing the trend in behaviour with extent of transformation since it was a novel analytical technique for analyzing a series of FTIR spectra series with time.

4.2 Background Research on FTIR Spectrum of PET

The main absorption bands in the IR spectrum of PET see Figure 3.3 have been assigned as follows; the bands, at 3100 and 2800 cm^{-1} have been attributed to aromatic and aliphatic –C-H bond stretching, 1720cm^{-1} to the ester carbonyl bond C=O stretching, 1470-1350 cm^{-1} to bending and wagging vibrational modes of the ethylene glycol segment, 1235 cm^{-1} to the ester group stretching, 1090 cm^{-1} to the

methylene group and aromatic bands in-plane/out-plane bending at 1016 and 725 cm^{-1}.

Many of the remaining bands depend on the manufacturing procedure and molecular conformation state of PET sample, i.e. whether has been extruded and quenched, heat treated and subsequently drawn, in other word, whether the sample is amorphous or crystalline, or oriented by stretching. Differences are due to conformation of the ethylene glycol group and also phenylene carbonyl bonds (cis/trans isomers).

Many of these absorption bands split as a result of the differences between the force fields in the amorphous and crystalline regions and also between cis and trans isomers. In the crystal, the trans isomer only is present but in the amorphous regions both cis and trans isomers are present in dynamic equilibrium. This in turn is temperature as well as degree of orientation dependent [113].

Since crystallization can also occur on stretching, depending on temperature, the precise assignments of the absorption bands in the IR spectrum in terms of crystallinity and changes in chain conformation have been disputed. Ward et al. [113] have assigned bands at 1470, 1340, 975 and 845 cm^{-1} to the vibrations of the trans isomer of the ethylene glycol segment trans isomer and at 1450, 1370, 1040 and 898 cm^{-1} to the cis. Liang and Krimm [108] have attributed differences to changes in

symmetry and resonance effects of the substituted benzene ring on the basis of model and deuterated compounds. Miyake [111] observed that the bands at 973, 895 and 845 cm^{-1} increase on drawing while those at 1453. 1370, 1337 and 1042 cm^{-1} decreased but Cobbs [109] and Burton used the bands at 1340 and 972 cm^{-1} to follow the crystallization of PET on heating, while Miller and Willis [110] used the 808 cm^{-1} band to follow the decrease in amorphous content. Schmidt [112] observed changes to the 795, 848, 875, 896, 973, 988, 1018, 1022, 1042, 1172 cm^{-1} bands and attributed the cis isomer to 896 and 1042cm^{-1} and the trans to 848 and 973 cm^{-1} bands on heating and stretching.

In a study of physical ageing of amorphous PET, Aref-Azar and Hay [101] used the bands at 896 and 973 cm^{-1} to measure the temperature dependent equilibrium of the rotation of the ethylene glycol segment, assigning these bands to cis and trans conformations respectively while others [95] have used the 1340 cm^{-1} band for trans and 1370 cm^{-1} for the cis conformation. The band at 1340 cm^{-1} was also attributed to crystalline and that at 1370 cm^{-1} to amorphous regions.

Miyake [111] also observed that the bands at 1453, 1370, 1042, and 895 cm^{-1} decreased linearly with draw ratio while those at 1410, 1018, 874 were constant while 1337, 973 and 845 cm^{-1} increased. On heating, peaks at 1453 moves to 1456, 1119 moves to 1126, 1099 to 1101, 873 to 874 and 841 to 848 cm^{-1}. 1475cm^{-1}

appeared on heating while 1453 decreased in intensity. Many of these peaks were assigned by analogy to model compounds and by examination of changes observed on melting and re-crystallization.

Orientation has a marked effect on the IR spectrum of PET and in particular on intensities and shift in the position of the bands [100, 101, 103, 105, 106, 111]. Trans isomers increase with draw ratio at the expense of the cis and have been used to measure degree of orientation. In these studies the band at 973 cm^{-1} is assigned to CH_2 trans; 896 cm^{-1} to cis; 1337 cm^{-1} to the CH_2 cis wagging mode and 1340 cm^{-1} to trans mode; 1020 cm^{-1} to in-plane bending of C-H group and 730 cm^{-1} to out-of-plane bending of the benzene ring. Bands at 749 and 1410 cm^{-1} are also associated with benzene ring vibrations.

In conclusion, crystal field effects produce sharper and more intense bands at 1475, 1387, 988 and 874 cm^{-1}, while bands at 1453, 1370, 1042, 973, 895 and 841 cm^{-1} are due to changes in chain conformation and to the presence of rotational isomers, cis to trans; 909 and 860 cm^{-1} to trans and 898 and 870 cm^{-1} to cis; 848cm^{-1} to the trans -CH_2- rocking and the 895 cm^{-1} to cis. Rotational isomer bands appear as two peaks one increasing and the other decreasing on crystallization or melting, 1453 and 1456 cm^{-1}; 1337 and 1370 cm^{-1} due to -CH_2- wagging. 1042 cm^{-1} is the anti-

symmetrical C-O stretch of cis form. The trans is symmetrical and does not appear in IR spectra of PET [100].

4.3 Two-dimensional Infrared Spectroscopy.

4.3.1 General Two-dimensional Correlation Spectroscopic

Two-dimensional infrared spectroscopy is a novel analytical technique in vibrational spectroscopy which can be used to interpret spectral changes accompanying a change in structure or composition. As such it is useful in analyzing the development of crystallinity within a polymer in which amorphous regions are transformed into crystalline regions involving changes in molecular conformation. Noda [115] proposed to call the procedure two-dimensional infrared (2D IR) spectroscopy by analogy to the 2D correlation techniques used extensively with time-resolved spectral signals in NMR spectroscopy. Later Noda modified the method to analyzing non-oscillating spectra and generalized it to two-dimensional correlation spectroscopy [116-123].

The mathematical procedure to yield 2D correlation spectra can be used to handle arbitrary forms of variable dependent complex spectral signals. Nowadays, 2D correlation methods are widely used in IR, Raman, X-ray, fluorescence and many other spectroscopies for characterizing functional group, conformation change and

complex material structure etc [124-145]. In recent year it has even developed and derived a new concept of sample-sample correlation [146-148].

4.3.2 Principles of Two-dimensional Infrared Spectroscopy

The mathematical procedure involved in obtaining 2D correlation spectra from time or temperature dependent complex spectra has been outlined by Noda and Ozaki in some detail [115-118, 122, 149-151].

If $y(v,t)$ defines the perturbation-induced variations in intensities of spectra observed at fixed intervals (time, temperature or some other external variable), t between t_{min} and t_{max} then the dynamic spectrum of the system, $\tilde{y}(v,t)$ is defined as

$$\tilde{y}(v,t) = y(v,t) - \bar{y}(v) \text{ for } t_{min} \leqq t \leqq t_{max} \tag{4.1}$$

where $\bar{y}(v)$ is the initial or reference spectrum of the system.

The intensity of the 2D correlation spectrum X ($v1$, $v2$) is then represented as

$$\mathrm{X}(v_1, v_2) = \langle \tilde{y}(v_1, t) \cdot \tilde{y}(v_2, t') \rangle \tag{4.2}$$

where X (v_1, v_2) is a quantitative measure of comparative similarities or dissimilarities in the intensities. $\tilde{y}(v,t)$ *is* measured at two separate variables; ν is the wavenumber and time or temperature, t, at fixed intervals.

The symbol < > is the cross-correlation function and is designed to compare the two dependences of the spectra at *t*.

Simplifying Noda treatment, X (v_1, v_2) is a complex number function, such that

$$X\ (v_1,\ v_2) = \Phi\ (v_1,\ v_2) + i\Psi(v_1,\ v_2) \tag{4.3}$$

It includes both real and imaginary components, which are recognized as synchronous and asynchronous 2D correlation intensities. The synchronous 2D correlation intensity $\Phi(v1,\ v2)$ illustrate the overall similarity or coincidental trends of the two separate intensity variations, i.e. it is an in-phase character of the system.

The asynchronous 2D correlation intensity $\Psi(v1,\ v2)$ is considered to be a measure of dissimilarity or, more strictly speaking, out-of-phase character of the spectral intensity variations [116].

The construction of 2D correlation spectra based on sinusoidally varying signals, especially IR dichroism. A sinusoidally varying dynamic spectrum with a fixed frequency Ω has the general form

$$\tilde{y}(v,t) = A'(v)\sin\Omega t + A''(v)\cos\Omega t \tag{4.4}$$

where *A'(v)* and *A''(v)* are the amplitudes of two orthogonal component in-phase and quadrature of the sinusoidal function.

The synchronous $\Phi(v1, v2)$ and asynchronous $\Psi(v1, v2)$ 2D correlation intensity with wavenumber $v1$ and $v2$ are expressed by the following two equations:

$$\Phi(v1, v2) = \frac{1}{2}\left[A'(v1)A''(v2) + A''(v1)A'(v2)\right] \quad (4.5)$$

$$\Psi(v1, v2) = \frac{1}{2}\left[A'(v1)A''(v2) - A''(v1)A'(v2)\right] \quad (4.6)$$

Alternatively, the above equations can be rewritten in term of magnitude and phase angle of the sinusoidal signals, with magnitude $\hat{A}(v) = \sqrt{A'(v)^2 A''(v)^2}$ and phase angle $\beta(v) = \arctan\frac{A''(v)}{A'(v)}$ set to,

$$\Phi(v1, v2) = \frac{1}{2}\hat{A}(v1)\hat{A}(v2)\cos\left[\beta(v1) - \beta(v2)\right] \text{ and}$$

$$\Psi(v1, v2) = \frac{1}{2}\hat{A}(v1)\hat{A}(v2)\sin\left[\beta(v1) - \beta(v2)\right] \quad (4.7)$$

4.3.3 Using Two-dimensional Correlation to Judge Overlapping Peaks.

Figure 4.1A shows the ideal case of two highly overlapping but individual IR absorption bands whose intensities are changing with time, one increasing and the other decreasing but with the same magnitude. The synchronous spectrum, Figure 4.1B, shows a cluster of 2D peaks comprising two autopeaks and two negative cross peaks. This particular and idealized form of peak cluster is called the *four-leaf-clover* pattern. For a common two-band system, the cluster pattern is not always four-way

symmetrical particular when the changing magnitudes of two peaks size are not the same leading to the size of the two autopeaks being different. This peak cluster is illustrated in a later section [116, 152-155].

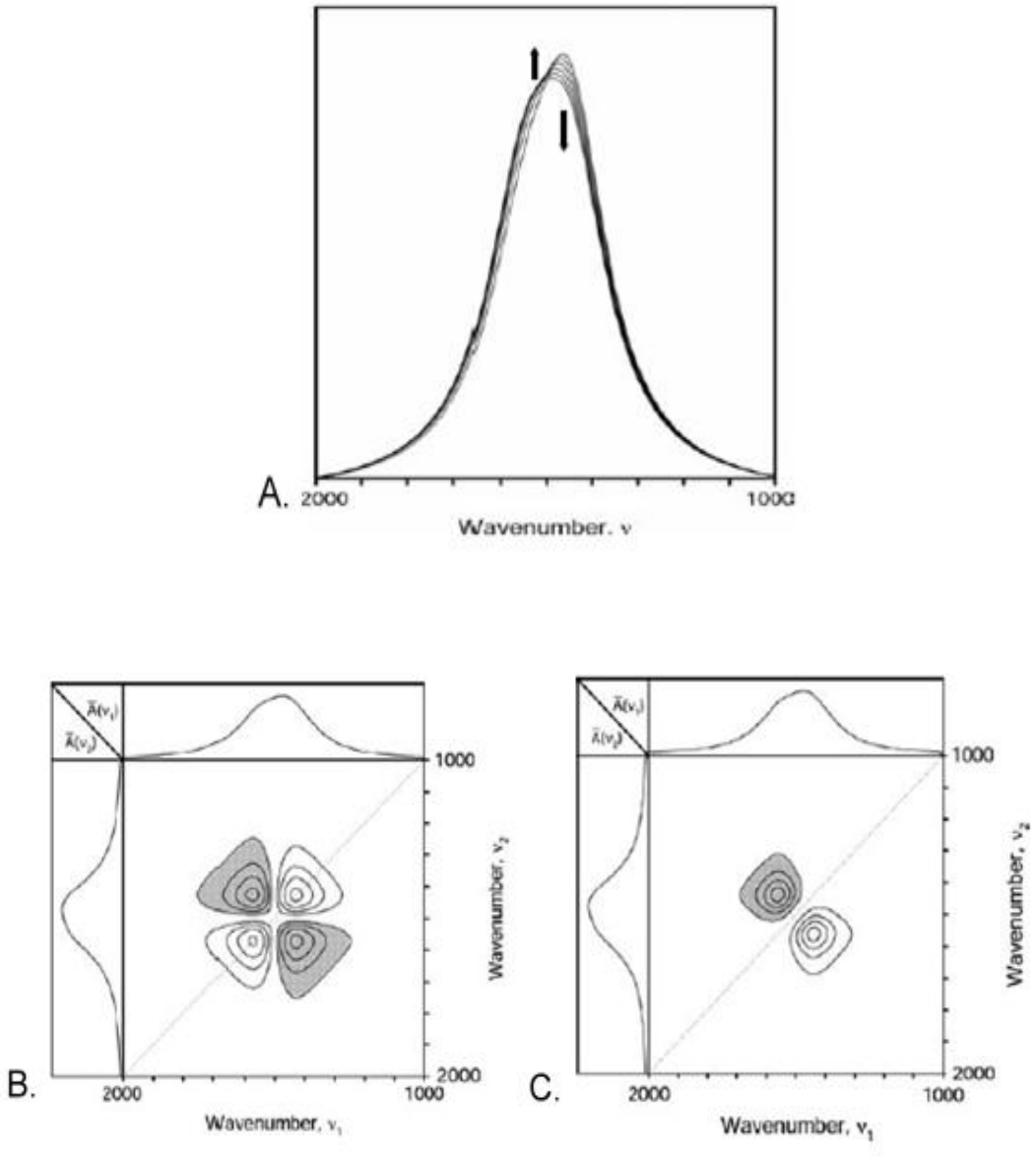

Figure 4.1 Synchronous (B) and Asynchronous (C) 2D Correlation Spectra Based on Two Overlapping Bands Changing Intensity in Opposite Directions (A) [116].

The corresponding asynchronous spectrum, Figure 4.1C, shows two well resolved cross peaks with no other further associated features. This kind of asynchronous 2D spectra is considered as the most reliable indicator that the system contains two overlapping bands and there is no other complicating factor in the system [116, 152, 153].

Other cases of single peaks shifting coupled with intensity changes show very similar spectra as the previous one, however, 2D correlation analysis of them generates synchronous and asynchronous spectra of which two cases can be distinguished.

Figure 4.2A shows the 1-D spectra of a single band whose position shifted to higher wavenumbers with some increase in intensity. The synchronous spectrum, Figure 4.2B, is no longer a four-way symmetrical cluster pattern because the unsymmetrical intensity changes in magnitude lead to two autopeaks with one becoming disproportionately larger than the other. This kind of cluster pattern is called an *angel* pattern with cross peak wings. A similar angel pattern is more commonly observed in the case of two overlapping bands accompanied with changes in intensity. Hence, this synchronous pattern cannot be used as a specific indicator

for distinguishing a position shift coupled with an intensity change and two overlapping bands with intensity changes [116, 152, 153].

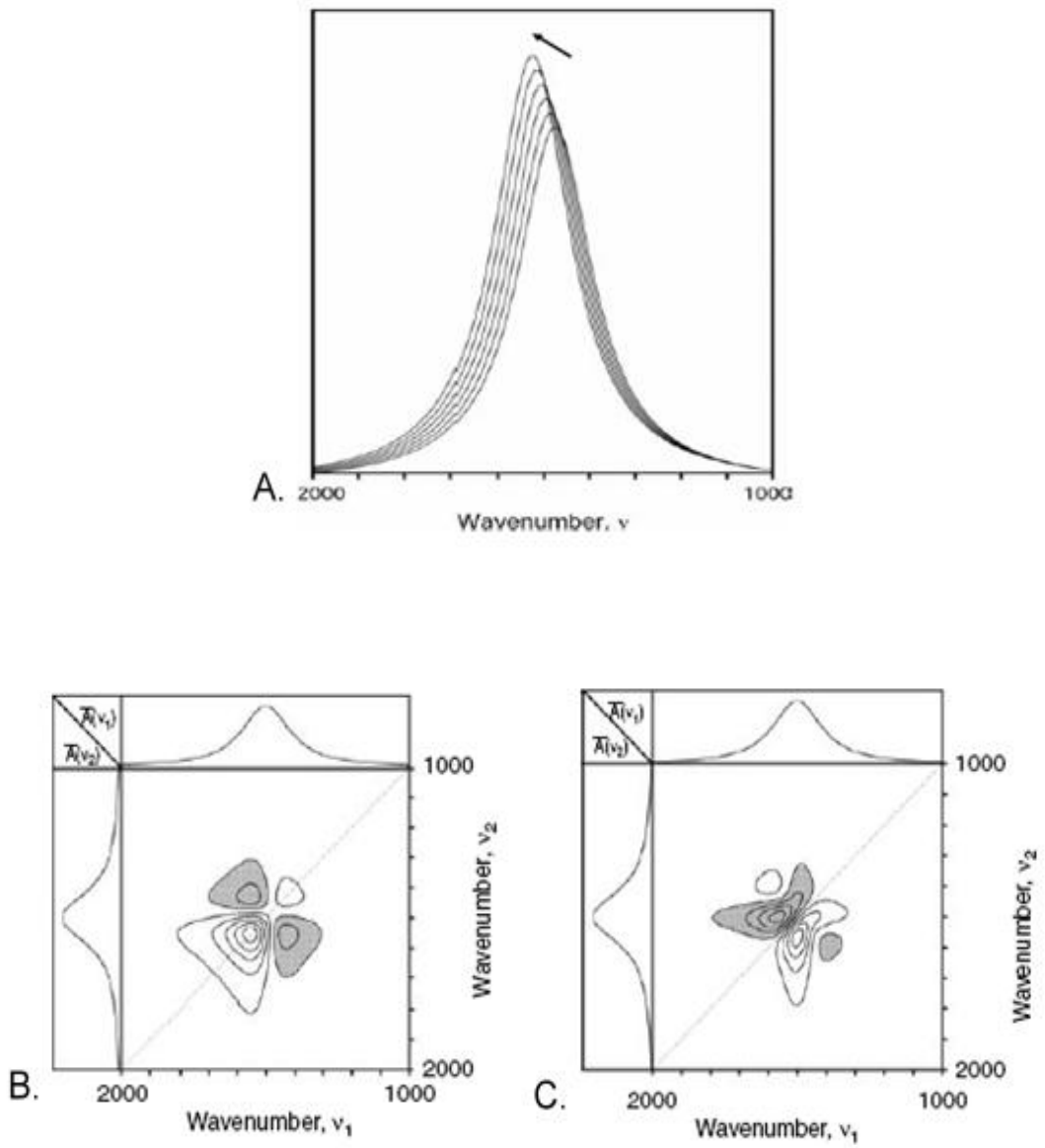

Figure 4.2 Synchronous (B) and Asynchronous (C) 2D Correlation Spectra Based on Single Peaks Shifting Coupled with Intensity Changes (A) [116].

The asynchronous spectrum, Figure 4.2C is represented by a distorted butterfly pattern when the intensity variation is accompanied with a shift in band position. A standard butterfly pattern is normally observed in the asynchronous map of the 1D spectra series with band position shift only. The pair of main asynchronous cross peaks is distributed closer to the stronger synchronous autopeak side and covers the whole range where both positive and negative synchronous autopeaks and cross peaks located [116, 152, 153].

This case is easily confused with the more common case of two overlapping bands with some noise in the spectra which produces secondary cross peaks in the asynchronous map. However, the feature observed above in the main asynchronous cross peaks are a clear indication of this. The asynchronous cross peaks are generated from more complex procedures with less clear internal broad band variations, rather than simple intensity changes of two overlapped bands. Another potential cause is that of a weak secondary pair of cross peaks in the asynchronous spectrum. This pair of cross peaks is located far from the diagonal but inside the range of the main asynchronous cross peaks. In some cases, these weak cross peaks are not obvious and overlooked due to their small magnitude compared with the strong main cross peaks. By adjusting the contour level of the 2D spectrum plots the existence of such weak cross peaks can become more evident [116, 152, 153].

4.4 Isothermal Crystallization on FTIR Spectrum and Two-dimensional Infrared Spectroscopy Correlation of PET.

4.4.1 Isothermal Crystallization on FTIR.

Figure 4.3 shows the selected time-dependent FTIR spectra of PET on rapid cooling from 275^{o}C, above the melting point, to the temperature of onset crystallization as observed to occur by DSC at 234^{o}C [104, 105]. It can be seen that substantial changes in the position, intensity and breadth of the absorption bands occur. These differences result from temperature and conformational effects but the isothermal changes are due to the development of crystallinity only. Significant changes take place to the carbonyl band at 1727 cm^{-1} as it decreases in intensity and a second band at 1717 cm^{-1} develops with isothermal crystallization consistent with the disappearance of the amorphous component and an increase in the crystalline component. A sharper peak develops at 1340 cm^{-1}, which is due to the wagging vibrations of the –CH_2–, associated with the isothermal transformation. Other changes included an increase in intensity, change in shape and shift in wavenumber of the bands at 2960, 1470/1450, 1260, 1100/1090 and 725 cm^{-1} as can be seen in Figure 4.3. The changes with time are displayed to highlight them.

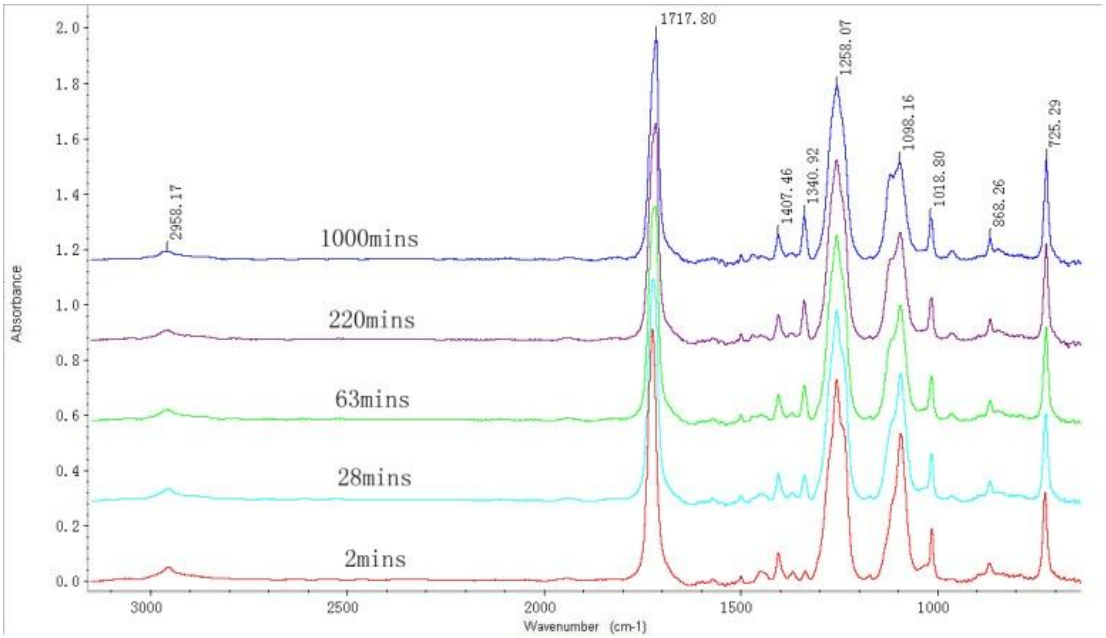

Figure 4.3 Selected FTIR Spectra of PET on Isothermal Crystallization at 234 ^{o}C for 1000 Minutes. 1.5 μm Thick Film.

4.4.2 Overview of 2D-Correlation of Main Region 1800~650 cm^{-1}.

In order to confirm that the changes in the observed spectra are due to the development of crystallinity and to changes in molecular conformation 2D correlation analysis was applied to the whole spectrum and the changes in intensities with time on isothermal crystallization from the melt at 234^{o}C noted. Isothermal conditions were selected in order to eliminate any change in peak intensities or shift in wavenumber with temperature so that the effect of crystallinity alone could be isolated.

Generalized 2D IR correlation spectra based on the IR spectra of the partially crystalline, v_2, and totally amorphous PET samples, v_1, in the reduced range 1800-650cm^{-1} where most of the changes were observed, are shown in Figures 4.4A and B. Seven diagonal peaks, i.e. autopeaks, are present in the regions, 1780-1680 cm^{-1}, 1400 cm^{-1}, 1350-1200 cm^{-1}, 1100 cm^{-1}, 780-730 cm^{-1}, and the change in intensities are clearly associated with the development of crystallinity with time. Many more positive cross or off-diagonal peaks are present; these represent simultaneous changes in the peak intensities at different wavenumbers and as they are increasing in intensities they are due to the development of crystallinity. Negative cross peaks are also present, as light patches, and these are attributed to the reduction in amorphous content in the polymer since their intensities decrease with increasing crystallinity.

The asynchronous 2D correlation spectrum shows sequential changes in the intensities measured at different wavelengths and only develops cross peaks if the absorption bands are out of phase with one other. As expected the asynchronous correlation spectrum in Figure 4.4B shows no autopeaks and only off-diagonal cross peaks of low intensities, suggesting that the changes in peak intensities are closely related to one another, and that the increase in the development of crystalline peaks closely follow the loss in amorphous peaks. Because of the large differences in intensities observed between the bands and the complex nature of the changes

involved in the 2D correlation spectra the individual absorption bands have been separately analyzed in greater detail by adjusting the experimental parameters, such as film thickness, to maximize the differences observed. These are described separately for each absorption band and comparison made with adjacent bands.

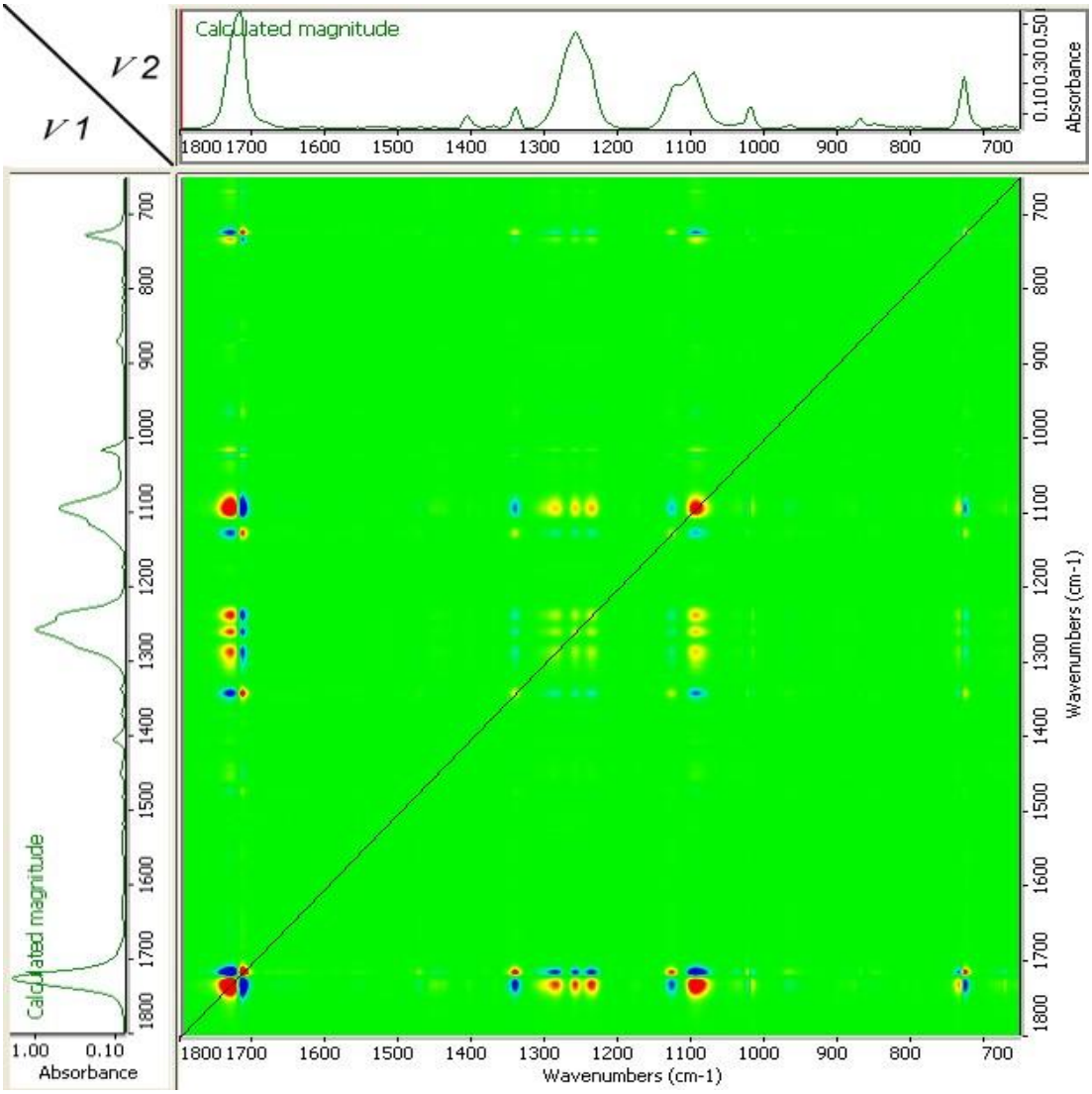

Figure 4.4A Two-Dimensional Synchronous Correlation Spectrum of the Region 1800 - 650 cm^{-1}. 1.5 µm Thick Film.

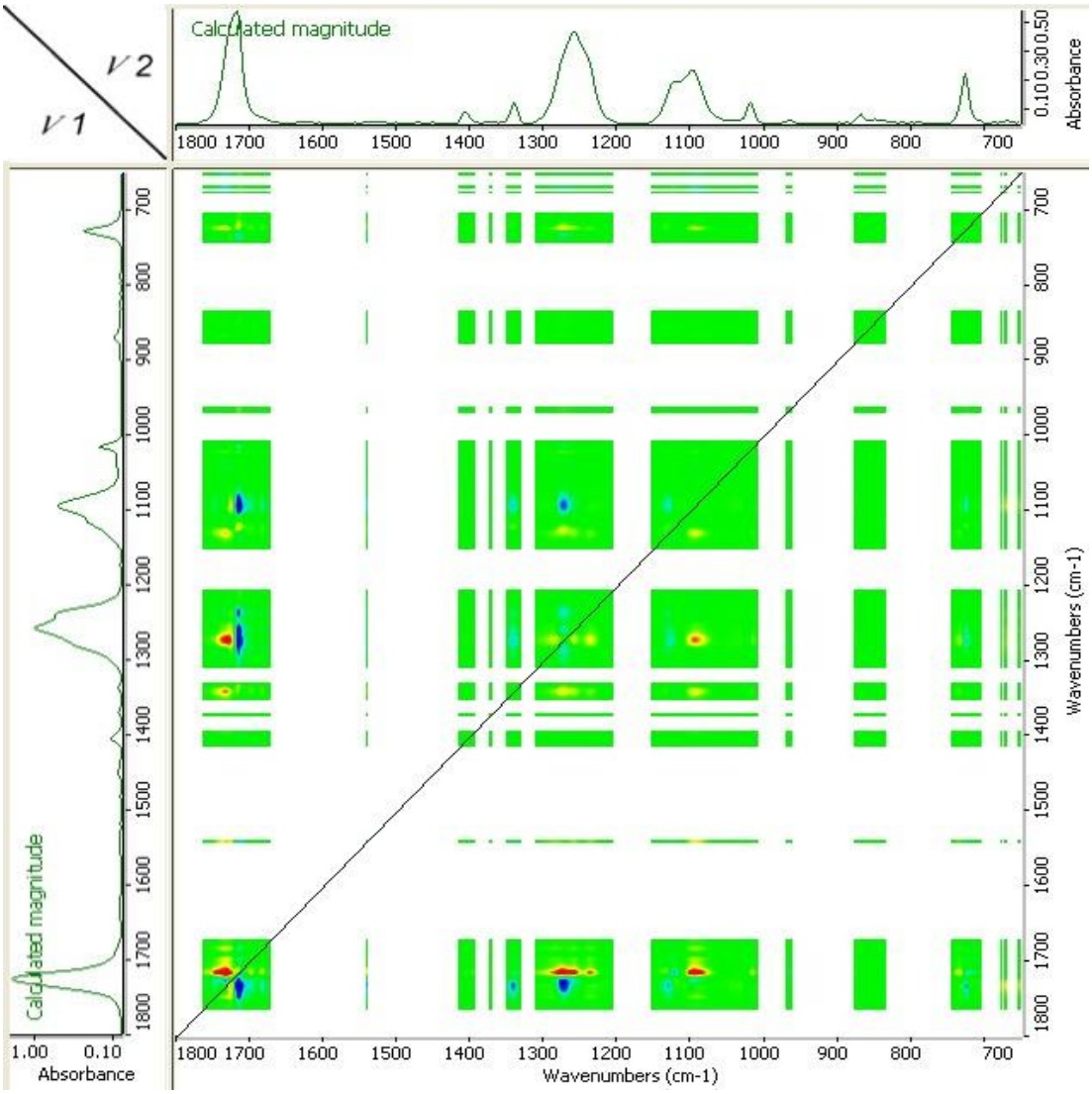

Figure 4.4B The Asynchronous Correlation Spectrum in the Region 1800 - 650 cm^{-1}. 1.5 μm Thick Film.

4.4.3 Methylene and Aromatic Stretching Region – 3500~2800 cm^{-1}.

The weak band at 3440 cm^{-1} as seen in Figure 4.5A increases in intensity, sharpens progressively and shifts to lower wavenumber to 3430 cm^{-1} with time and development of crystallinity. This makes the assignment of the band to the stretching

mode of the H–O bond of the chain end carboxylic acid group unlikely and more consistent with it being an overtone of the carbonyl band which as discussed below shifts on crystallization and develops in intensity with crystallinity.

The higher wavenumber band is assigned to an overtone of the carbonyl band in the amorphous and the 3430 cm^{-1} to that in the crystalline regions.

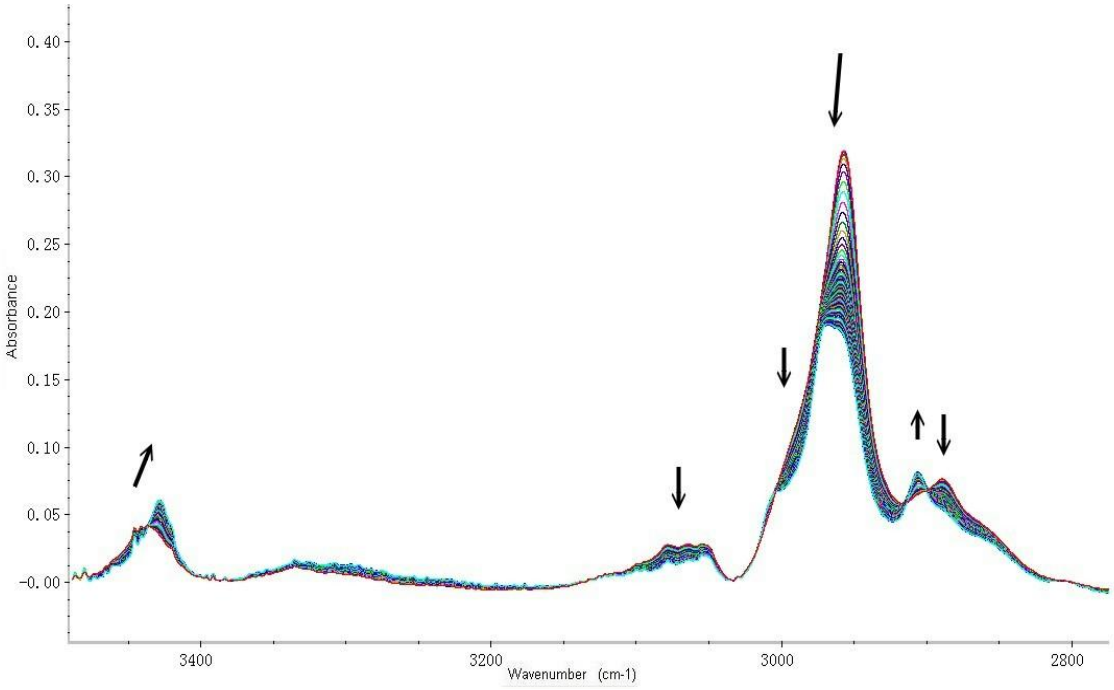

Figure 4.5A. Changes in Absorption in the Region 3500 - 2800 cm^{-1} with Time at 234°C.

12 µm Thick Film.

B.

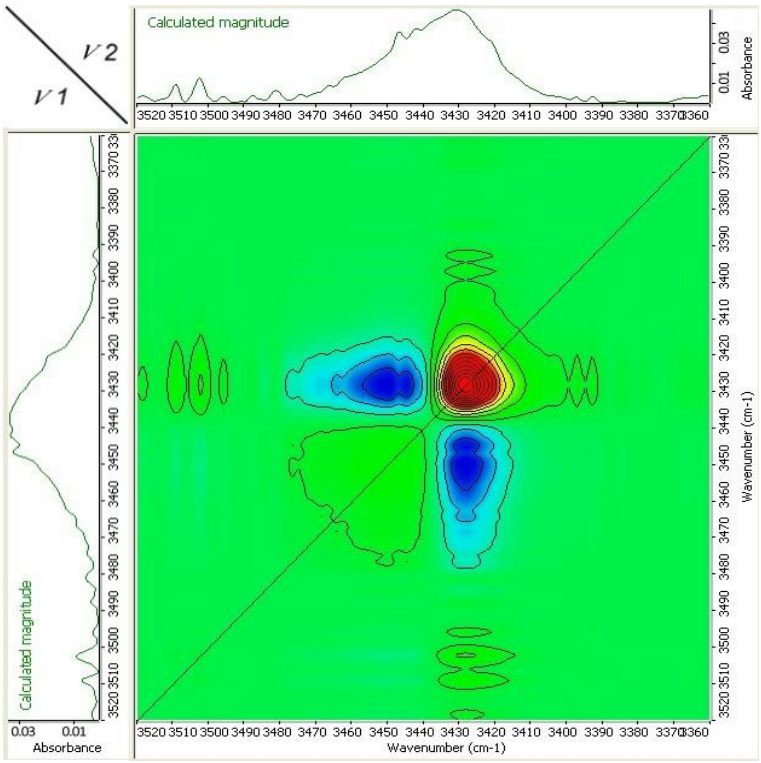

C.

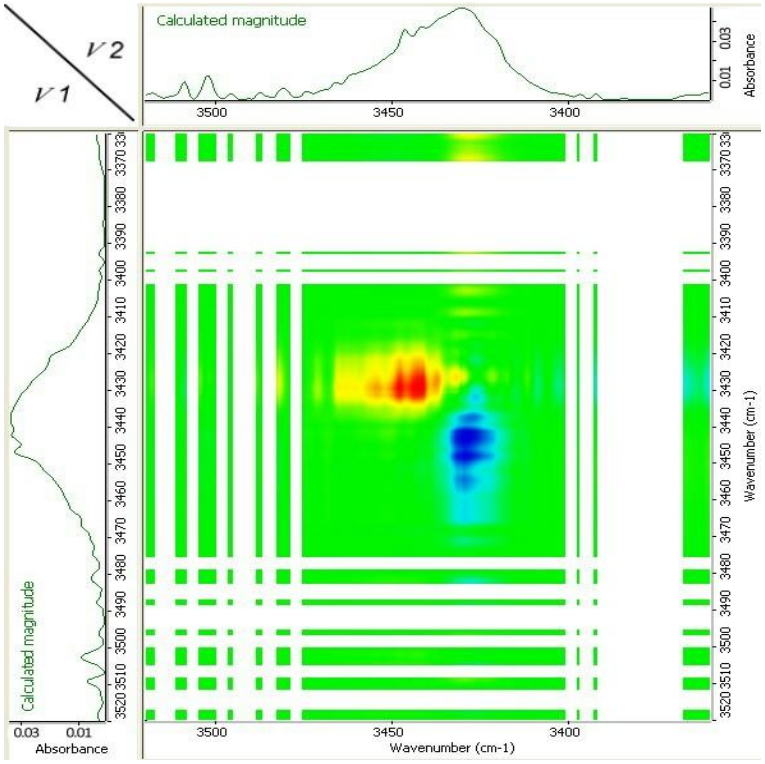

Figure 4.5B and C. Two-Dimensional Synchronous and Asynchronous Correlation Spectra of the Region 3620 - 3360 cm^{-1}.

D.

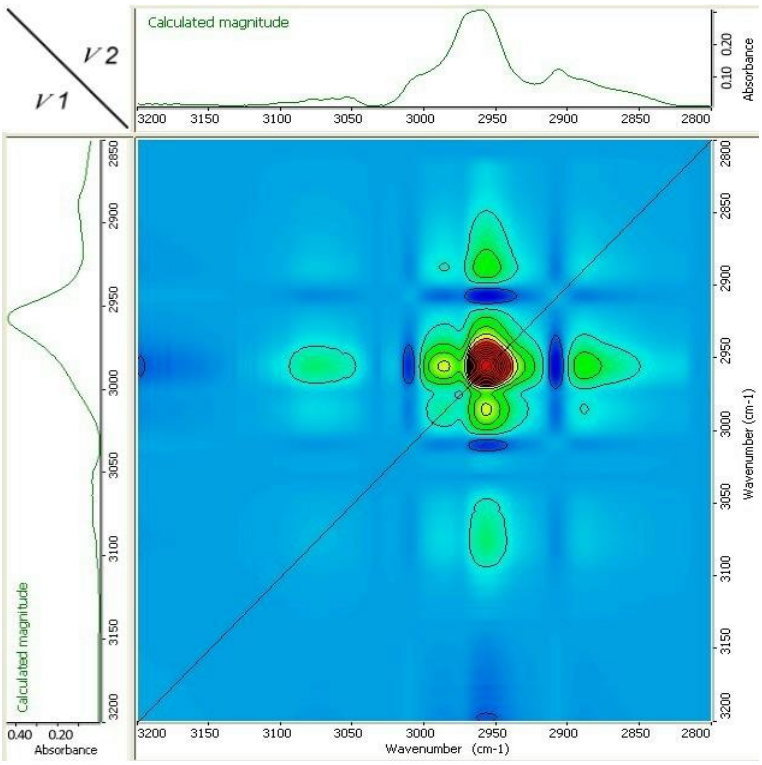

E.

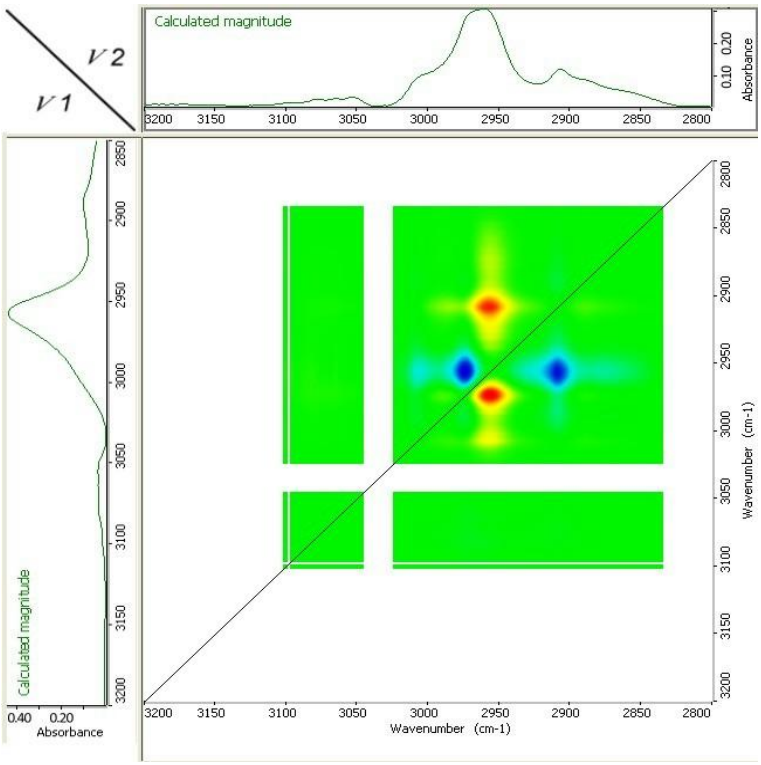

D and E. Two-Dimensional Synchronous and Asynchronous Correlation Spectra of the Methylene Absorption Band in Region 3100 - 2800 cm^{-1}.

Figure 4.5

The 2D synchronous correlation spectrum, see Figure 4.5B, is characteristic of two overlapping bands whose intensities are changing in the opposite direction, the lower wavenumber one increasing while the higher one is decreasing but to a lesser extent. There are accordingly two autopeaks, the lower wavenumber one of which dominates the intensity contours, and two cross peaks both of which are negative. This produces a somewhat distorted clover leaf pattern.

The asynchronous correlation spectrum is somewhat diffuse because of the low intensities of the bands; see Figure 4.5C, but there is clearly two cross peaks, one of which is positive and the other negative, consistent with the changes in peak intensity associated with the transformation being linked together one increasing and the other decreasing.

The four bands between 3100 and 3050 cm^{-1} are attributed to the stretching modes of the four aromatic C–H bonds of the terephthalate ring. The bands do not change position with time but there is a decrease in intensity as crystallinity develops. This decrease is more than can be accounted for in terms of experimental error and is attributed to differences in the extinction coefficients of the C–H bonds in the amorphous and crystalline regions.

The doublet at 2960 and 2910 cm^{-1} is attributed to the stretching mode of the aliphatic -CH_2- groups in the ethylene glycol segment and present in the amorphous

regions. Accordingly, it is assigned to the cis isomer and its intensity drops with time as a result of the phase transformation. It is accompanied with the progressive development of a smaller band at 2890 cm^{-1}, the trans isomer or crystalline band. A second trans peak develops at 3000 cm^{-1} as a shoulder on the cis 2960 cm^{-1} peak.

The contour map of the 2D synchronous correlation spectrum, see Figure 4.5D, is dominated by the intense methylene absorption band at 2960 cm^{-1} such that there appears to be only one autopeak, at 2960 cm^{-1} and four cross peaks, two positive (2960, 2880 and 2960, 2980 cm^{-1}) and two negative (2960, 2910 and 2960, 3010 cm^{-1}) indicating that the change in intensities of the peaks are linked together and occurring as a result of the transformation. The positive cross peak at 2960, 3070 cm^{-1} indicates that the aromatic C–H bands are changing in intensity in the same way as the cis isomer of the methylene group, and is due to crystallization. (Figure 4.5D.)

The asynchronous correlation spectrum shows two cross peaks, one positive and the other negative, indicating that the intensities of the two peaks are changing in different direction but the changes are linked, see Figure 4.5E.

4.4.4 The Carbonyl Stretching Region – 1800~1650 cm^{-1}.

The changes to the carbonyl absorption band at 234^{o}C with time are shown in Figure 4.6A. There is an obvious decrease in intensity of the initial amorphous band at 1727 cm^{-1} followed by a simultaneous increase at 1717 cm^{-1}. An isobestic point appeared in the absorbance at 1720 cm^{-1} consistent with a simultaneous change from amorphous to crystalline.

The corresponding correlation spectra of the carbonyl absorption band in 3 and 2- dimensions, shown in Figure 4.6B and C, are derived from a series of spectra at 234 ^{o}C collected over time characteristic of the amorphous and crystallizing sample. They comprise two positive autopeaks and two negative cross peaks. The 3-dimensional synchronous correlation map, see Figure 4.6B shows a large peak at high wavenumber which progressively decreases in intensity and a second which develops simultaneously at a lower wavenumber. The two are clearly coupled. The 2-dimensional map in Figure 4.6C has the characteristic angel pattern of a single absorption band which shifts from higher to lower wavenumber and with different intensities. The lower symmetry of the angel pattern arises from the difference in breadth of the two bands – the amorphous is broad and the crystalline comparatively sharp - and the maximum intensity of the two autopeaks can be used to define the wavenumber of the initial and final peak, at 1727 and 1717 cm^{-1} respectively.

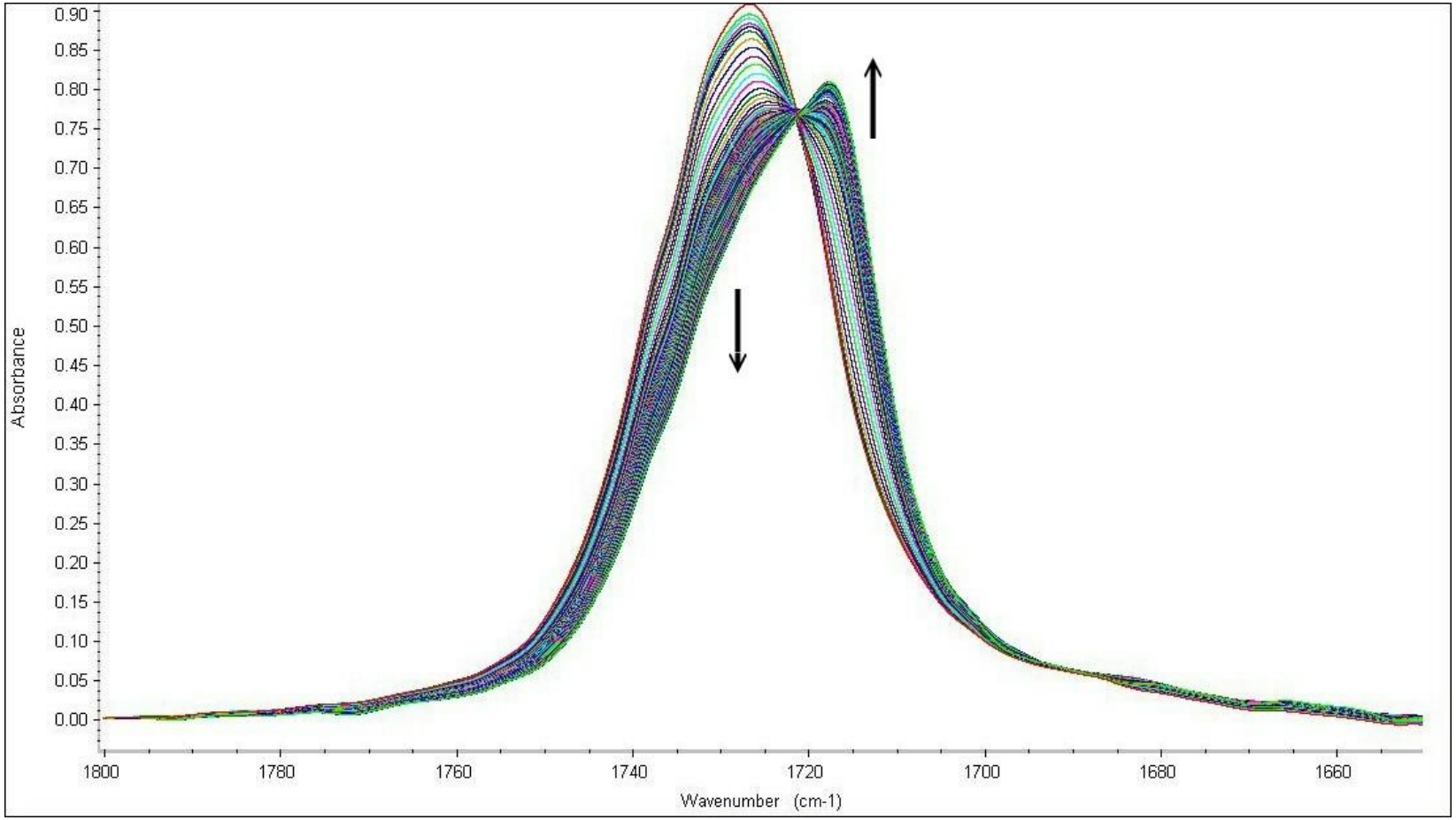

Figure 4.6A. Changes in Carbonyl Absorption with Time at 234 ^{o}C. 1.5 μm Thick Film.

B.

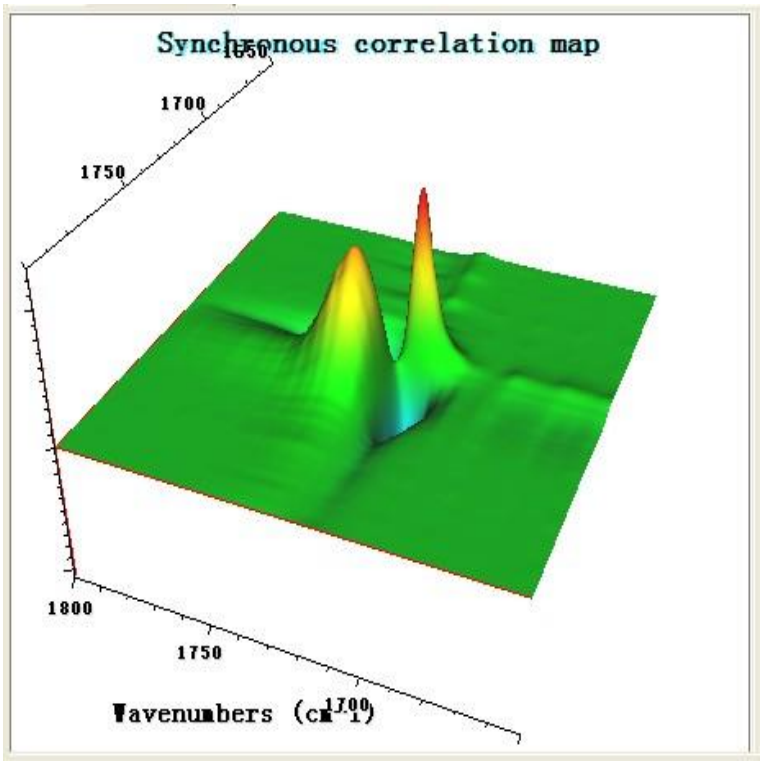

C.

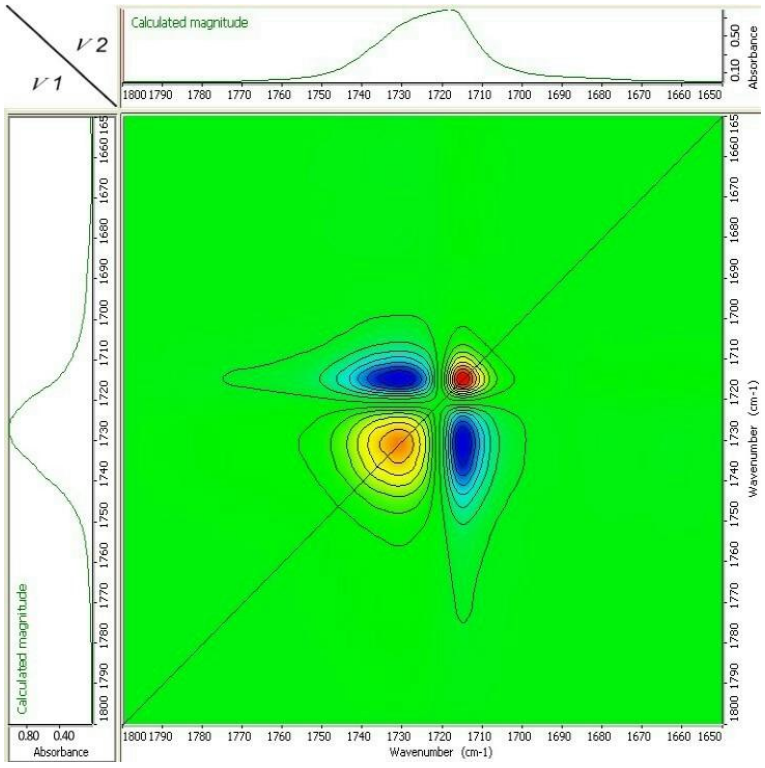

Figure 4.6B and C. Three and Two-Dimensional Synchronous Correlation Intensity Contour Map of the Carbonyl Absorption Band in Region 1800 - 1650 cm^{-1}.

D.

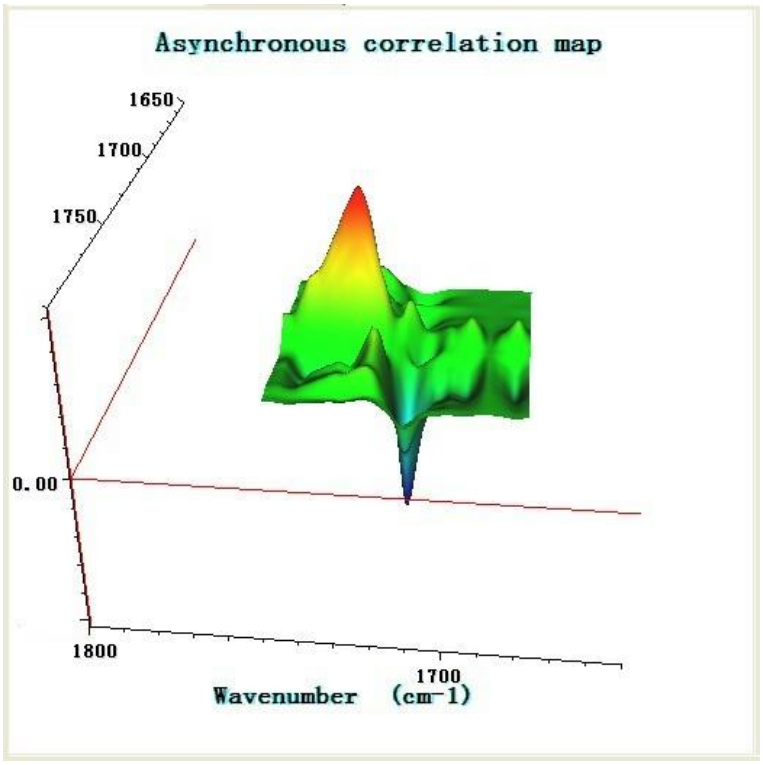

E.

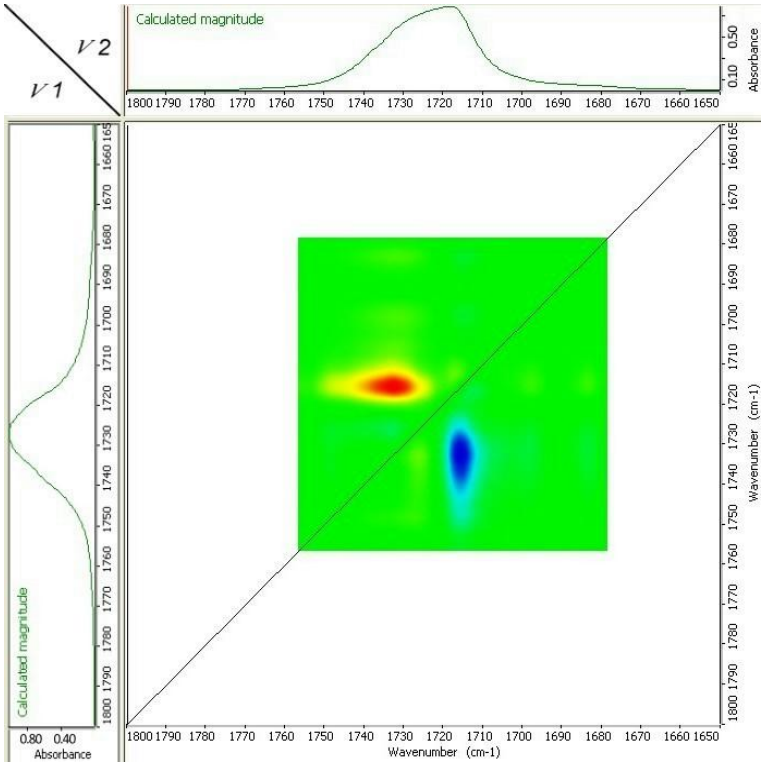

D and E. Three and Two-Dimensional Asynchronous Correlation Map of the Carbonyl Absorption Band in Region 1800 - 1650 cm^{-1}.

Figure 4.6

The asynchronous spectra, Figures 4.6D and E, show one positive (1717, 1727 cm^{-1}) and one negative cross peak (1727, 1717 cm^{-1}) as a two-way pattern reflecting the decrease in intensity of the higher wavelength band as the lower wavelength band intensity increases. The isobestic point, the angel pattern and the two-way pattern are all characteristic of a two component bands, amorphous and crystalline, both changing in intensities in opposite directions.

To conclude the carbonyl absorption band has a maximum absorption in the amorphous regions at 1727 cm^{-1} and 1717 cm^{-1} in crystalline material such that on crystallization the intensity of the higher wavelnumber band decreases and is progressively shifted to lower wavenumber. These changes make the ratio of the two carbonyl absorption bands a convenient method of measuring the fractional crystallinity of PET [156].

4.4.5 The Region 1600~1400 cm^{-1}.

There are considerable alterations to the spectrum of PET in this region on crystallization, see Figure 4.7A. The bands are attributed to p-di-substituted ring stretching modes and the changes are due to differences between amorphous and crystalline phases. A doublet at 1572, 1578 cm^{-1} decreases in intensity with time and is assigned to amorphous while a second at 1502 and 1508 cm^{-1} increases, and is

attributed to the crystalline regions. Single peaks at 1560 and 1470 cm^{-1} also increase and six peaks, in the region 1460-1430 cm^{-1} progressively drop in intensity as crystallinity develops. Others [113] have noted similar changes to the spectrum on crystallization and attributed the change at 1470 cm^{-1} to the bending mode of trans and the 1450 cm^{-1} to the cis rotational isomor. (see Figures 4.7B-E)

The 2-dimensional correlation analysis was carried out on the doublets at the higher wavenumber and on the other peaks by separating them by wavenumbers into higher, 1590 to 1480 cm^{-1}, and lower regions, 1490 to 1420 cm^{-1}. The higher shows two intense autopeaks centred on 1575 and 1505 cm^{-1} and two negative cross peaks, (1505, 1575 and 1575, 1505 cm^{-1}). The asynchronous correlation spectrum has two cross peaks whose intensities have opposite signs indicating that the higher number doublet is decreasing in intensity while the lower is increasing.

The 2-dimension correlation analysis on the lower wavenumber region produced very similar results in that two autopeaks with positive intensities were observed at 1473 and 1455-35 cm^{-1} and two negative cross peaks (1473,1455-35 and 1455-35,1473 cm^{-1}). The square shaped contour reflects the cluster of six cis peaks while the circular contour reflects the single sharp band attributed to the trans isomer with increasing intensity. The narrow but long shape of the cross peaks combines both the long and the sharp aspects of the component peaks.

The asynchronous correlation spectrum has two cross peaks one positive and the other negative consistent with the higher wavenumber peak increasing in intensity and the lower decreasing.

In conclusion the peaks at 1572, 1578 and 1455-35 cm^{-1} are assigned to the cis isomer of the ethylene glycol segment and 1502, 1508 and 1473 cm^{-1} to the trans rotational isomer.

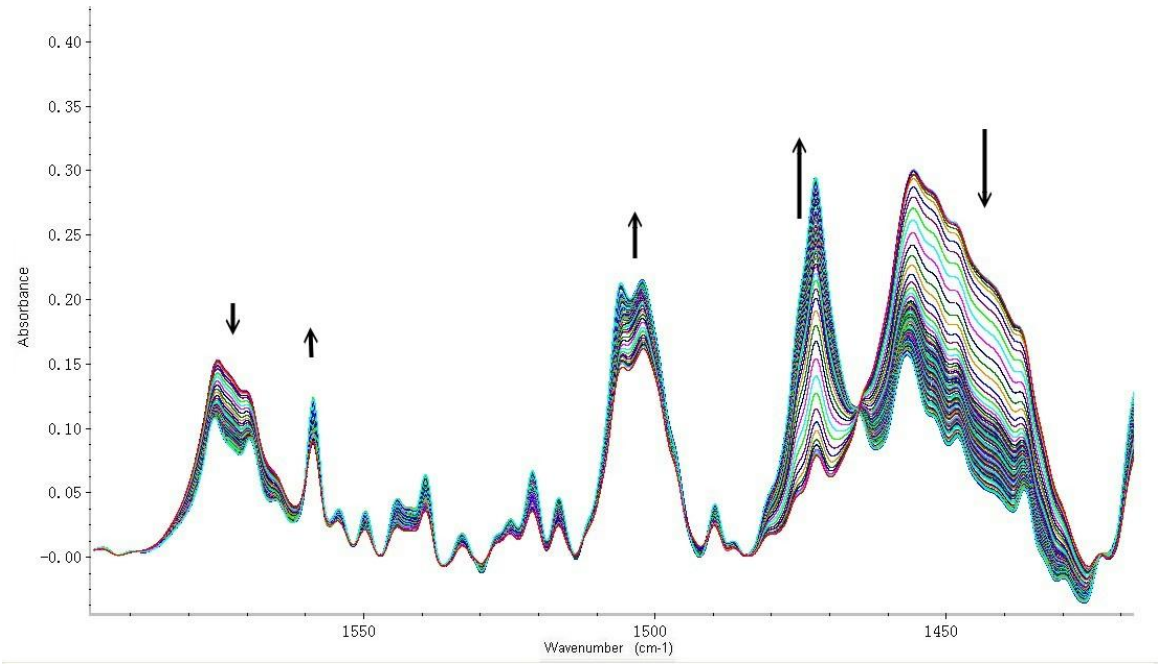

Figure 4.7A. Intensity Changes in Region 1600 - 1420 cm^{-1} Associated with the Development of Crystallinity with Time. 12 μm Thick Film.

B.

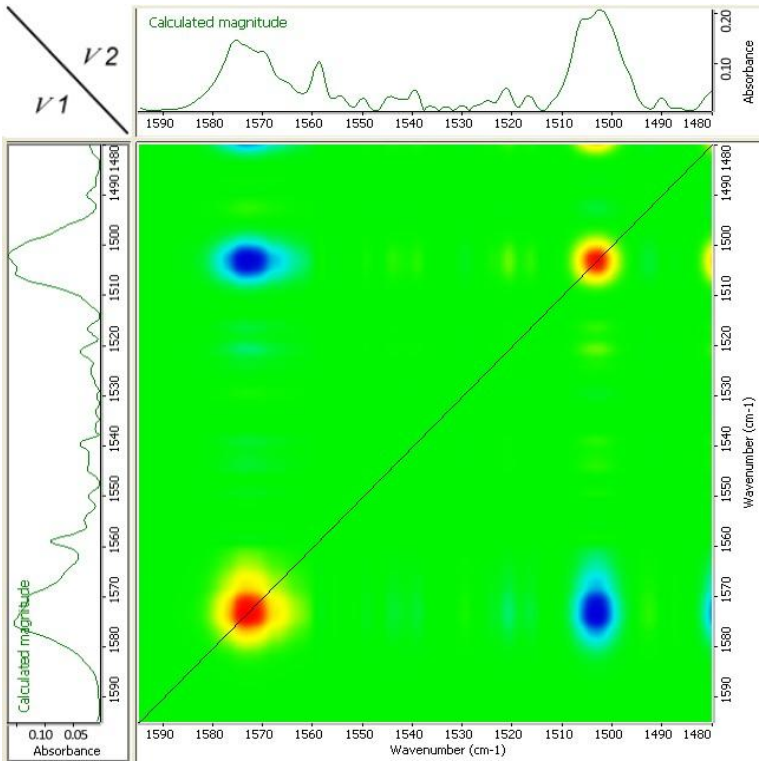

C.

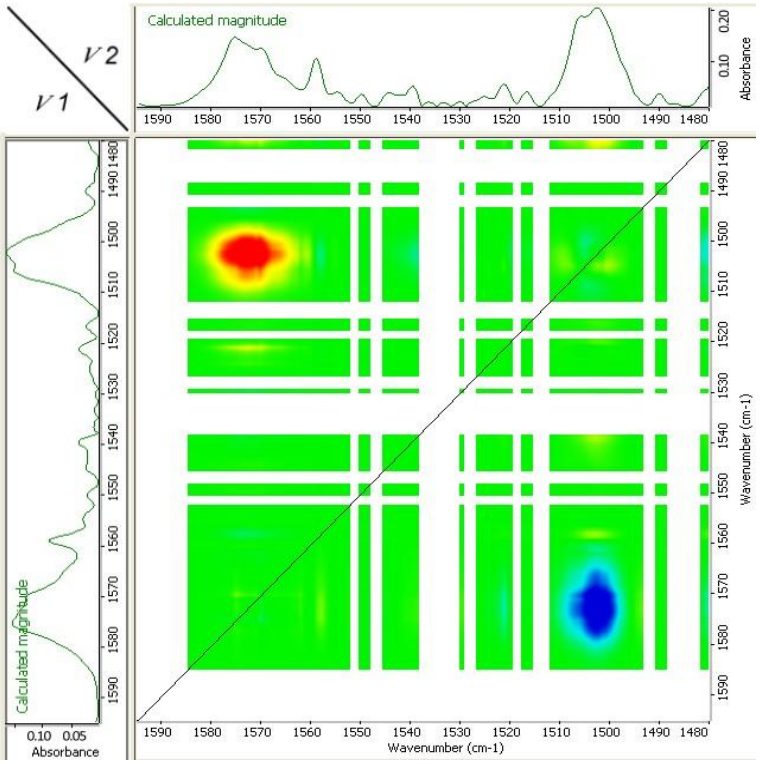

Figure 4.7B and C. Two-Dimensional Synchronous and Asynchronous Correlation Spectra in the Region 1590 - 1480 cm^{-1}.

D.

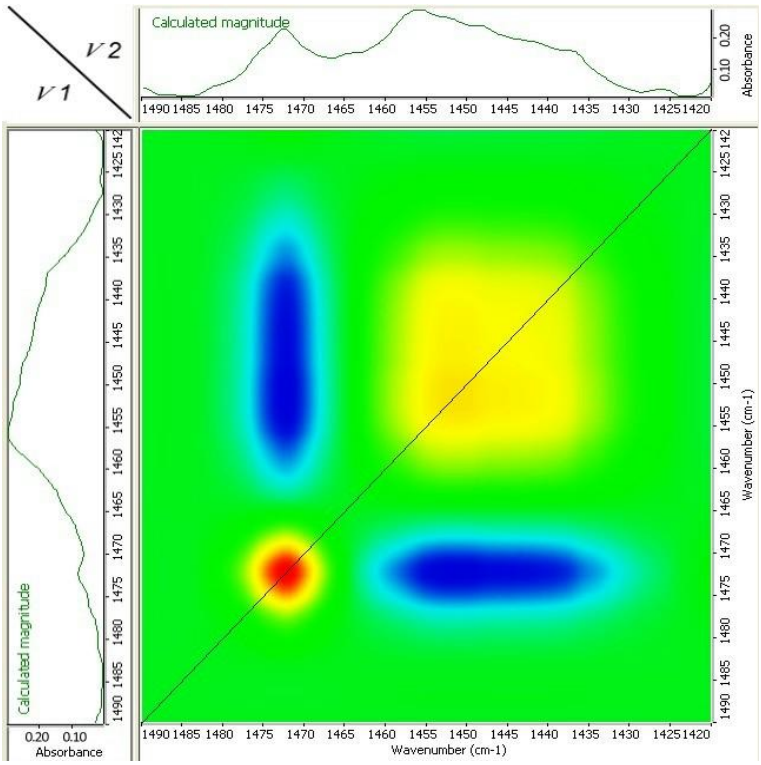

E.

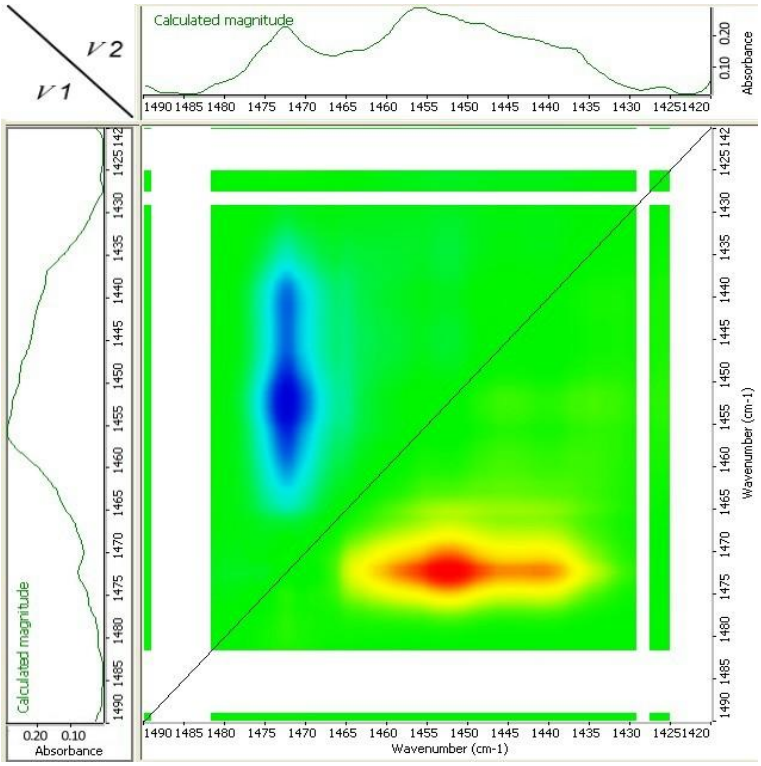

D and E. Two-Dimensional Synchronous and Asynchronous Correlation Spectra in the Region 1490 - 1420 cm^{-1}.

Figure 4.7

4.4.6 The Region 1420~1320 cm^{-1}.

Liang and Krimm [108] have reported that the weak band at 1343 cm^{-1} is sensitive to the degree of crystallinity and is not shifted by deuteration of the polymer. Accordingly they attributed the band to the influence of resonance on the terephthalate group, O-(O=C-C_6H_4-C=O)-O and to the in-plane alignment of the carbonyl groups with the benzene ring in the crystal. However, Ward et al. [157] attributed the 1340 cm^{-1} to the wagging vibrations of the –CH_2- of the trans isomer of the glycol group and the 1370 cm^{-1} to the cis. In line with this later assignment, Figure 4.8A shows the progressive increase in intensity of this band with time and crystallinity. Ward et al. also concluded that the intensity of the band at 1410 cm^{-1} did not change either on stretching or crystallization and used it as an internal standard to standardise the intensities of trans and cis bands. The 3-8% decrease in intensity of this peak is at variance with this as it is outside experimental error but more in line with differences in the extinction coefficient between the amorphous and crystalline regions but with no shift in peak position.

As well as an increase in intensity of the absorption band at 1340 cm^{-1} there is a shift to higher wavenumbers from 1338 to 1342 cm^{-1} on crystallization. The crystalline trans isomer is attributed to 1342 cm^{-1} and the amorphous trans isomer to 1338 cm^{-1}. The cis isomer, only present in the amorphous regions, is considered to

absorb at 1370 cm^{-1}. In the initial amorphous sample both cis and trans peaks have similar intensities but with time the 1370 cm^{-1} peak decreases slightly while the 1342 cm^{-1} increases substantially. Three other bands at 1355, 1380 and 1407 cm^{-1} decrease with time but with much smaller changes in intensity. There are five distinct isobestic points indicating that the changes to the peaks are linked and associated with the phase transformation.

There is one autopeak in the synchronous 2D correlation spectrum consistent with the very much larger increase in intensity of the 1342 cm^{-1}, see Figure 4.7B, and several negative cross peaks indicating these changes are concerted. The cross peaks are negative indicating that their intensities are decreasing along with the 1342 cm^{-1}.

The asynchronous correlation spectrum, see Figure 4.7C, shows one negative and five positive off-diagonal cross peaks indicating that the shift in peak position and change in intensities are synchronous and associated with the loss of amorphous content and increased crystallinity. Five peaks are decreasing in intensity and one increasing.

The 1338 and 1370 cm^{-1} peaks are attributed to the cis isomer of the ethylene glycol segment in the amorphous regions and the 1342 to the trans isomer in the crystalline. The 1408 cm^{-1} absorption band is not constant but decreases with crystallinity, and changes with temperature.

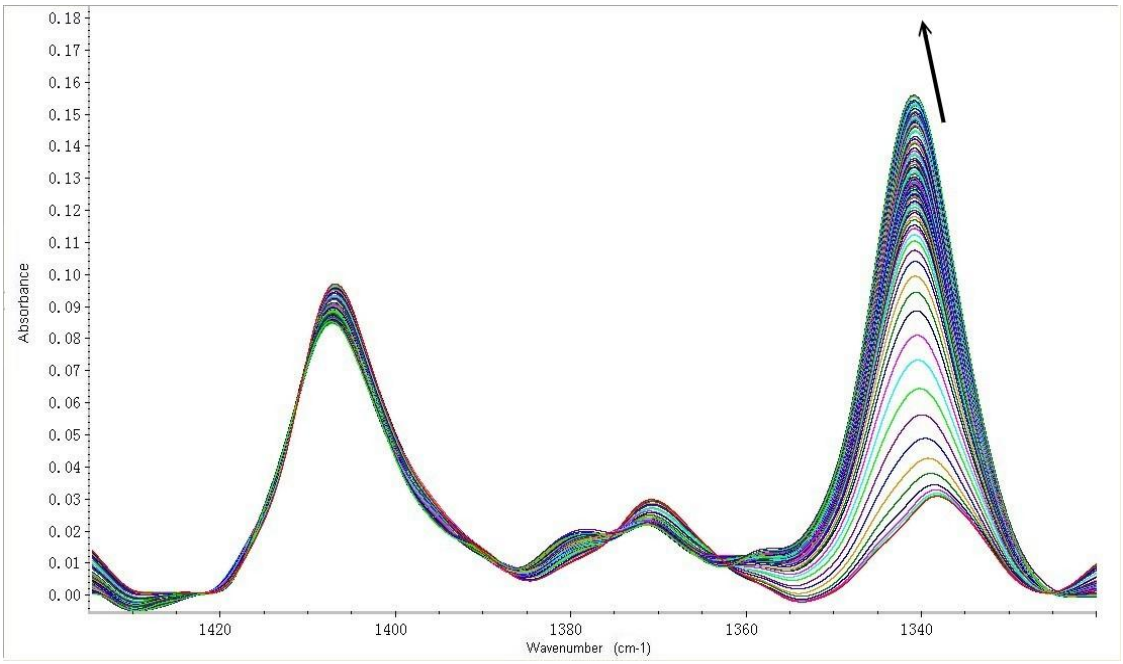

Figure 4.8A. Intensity Changes in Region 1420 - 1320 cm^{-1} Associated with the Development of Crystallinity with Time. 1.5 μm Thick Film.

B.

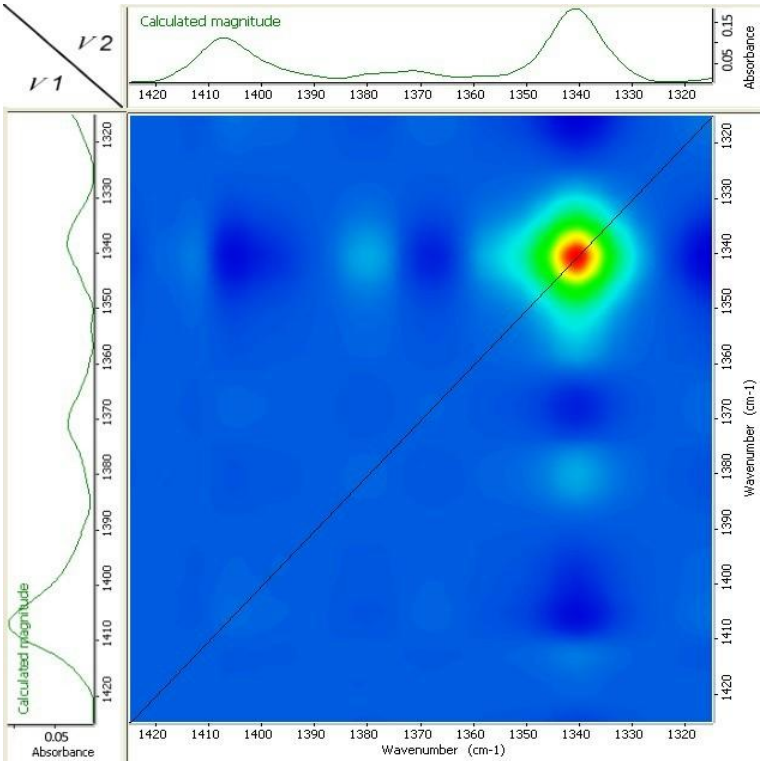

C.

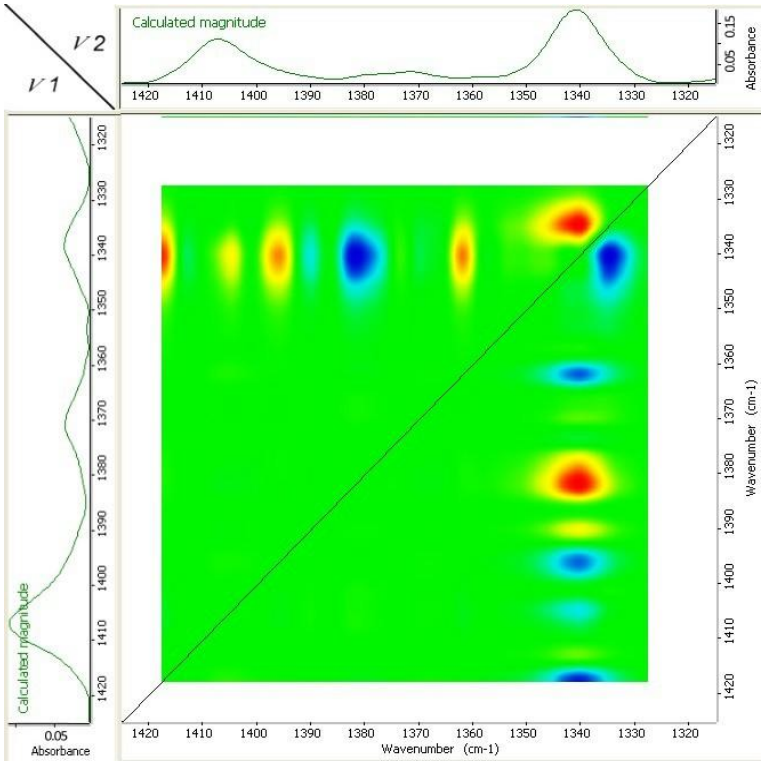

B and C. Two-Dimensional Synchronous and Asynchronous Correlation Spectra in the Region 1420 - 1320 cm^{-1}.

Figure 4.8

4.4.7 The Region 1320~1200 cm^{-1}.

The band at 1255 cm^{-1} has been attributed to the stretching vibration of the ester group, -C-O-C=O and the changes in intensity and peak shape with time are shown in Figure 4.9A. The initial absorption bands have four maxima at 1235, 1255, 1285 and 1307 cm^{-1} associated with amorphous material and these decrease in intensity with time into a featureless broad band with a maximum at 1255 cm^{-1}. The initial bands are assigned to the amorphous and the final to crystalline regions.

The synchronous 2D correlation spectrum, see Figures 4.9B, exhibits three positive autopeaks at 1237, 1260 and 1285 cm^{-1} and six cross peaks which are all

positive, consistent with the original three bands decreasing in intensity as the ester group becomes incorporated within the crystal with time. These peaks can be assigned to the amorphous regions and to the cis isomer. The trans does not appear in the IR spectrum because of its symmetry.

The asynchronous 2D spectrum, see Figure 4.9C, exhibits six off-diagonal positive cross peaks consistent with the three bands all decreasing in intensity with time, linked together and occurring simultaneously.

To summarise, 1235, 1255, 1285 and 1307 cm^{-1} are assigned to the vibration of the ester group in the amorphous phase, and the broad band at 1255 cm^{-1} to the group in the crystalline regions.

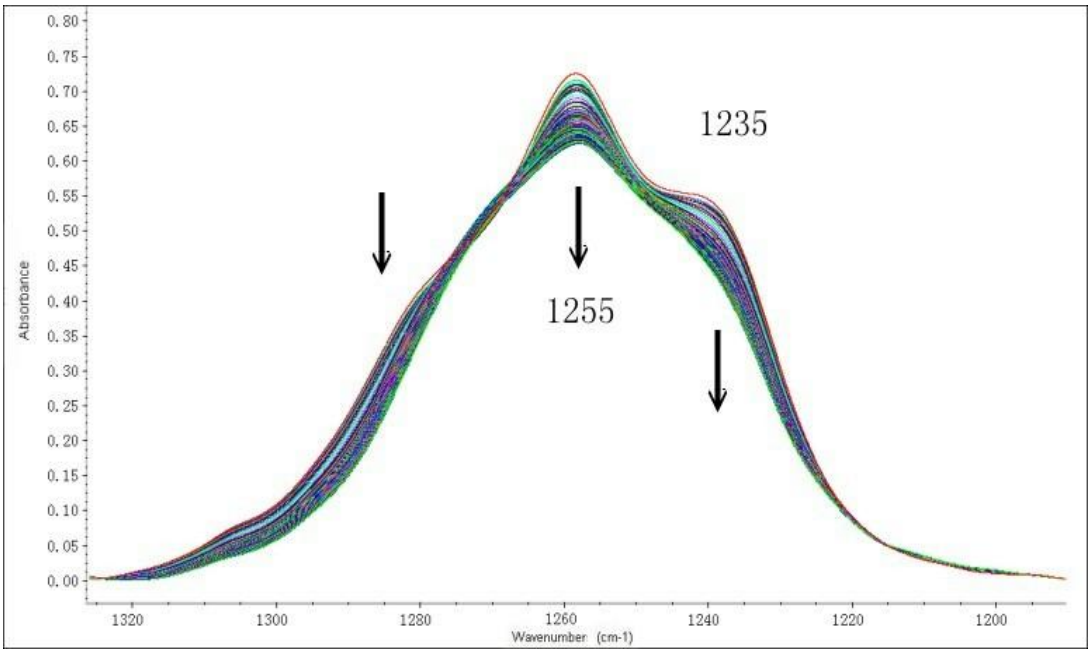

Figure 4.9A. Changes in Intensity in the Region 1320 - 1200 cm^{-1} with Time. 1.5 µm Thick Film.

B.

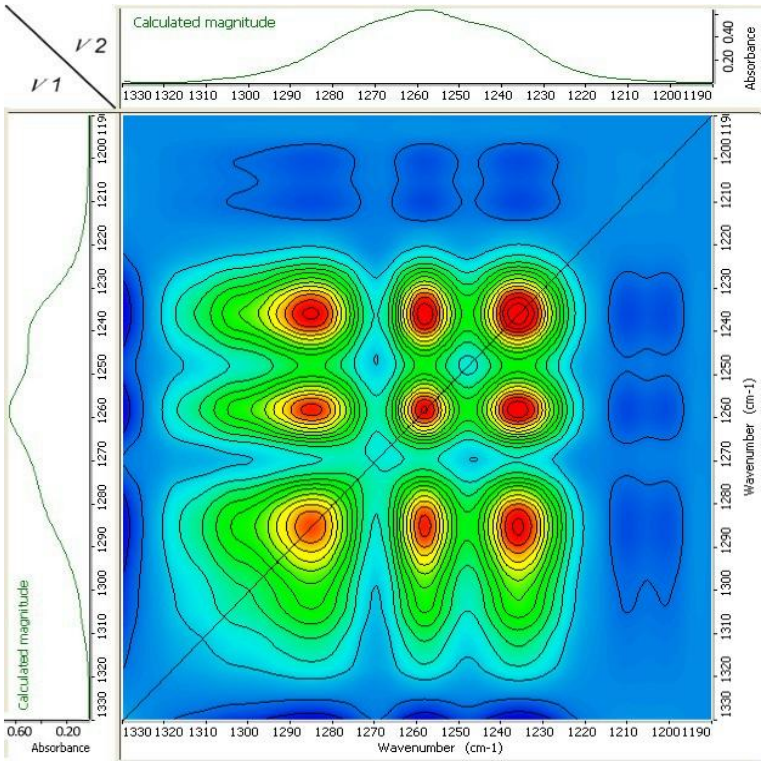

C.

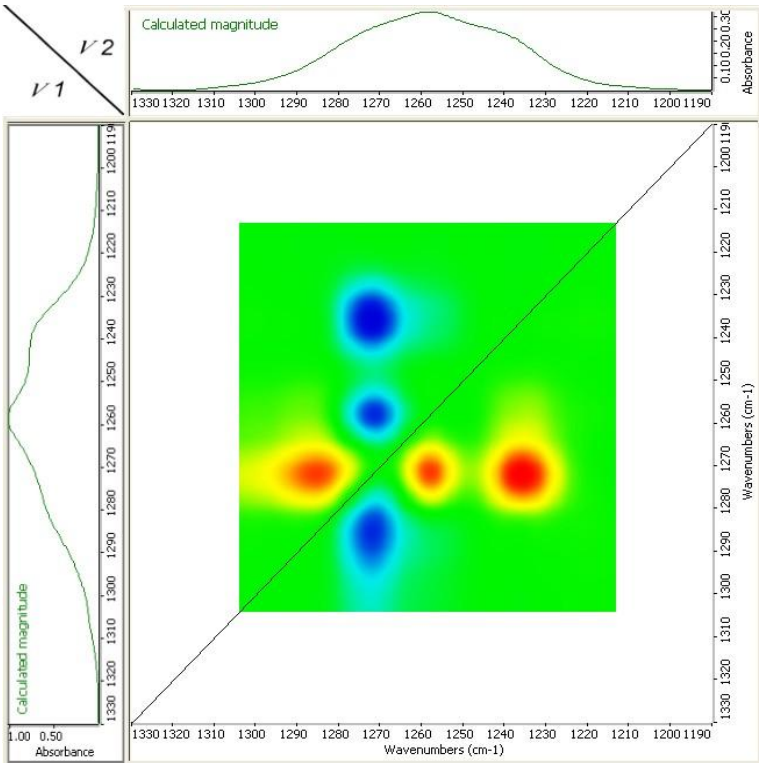

B and C. Two-Dimensional Synchronous and Asynchronous Correlation Spectra in the Region 1320 - 1220 cm^{-1} with Time.

Figure 4.9

4.4.8 The Region 1150~1050 cm^{-1}.

Liang and Krimm [108] have assigned the band at 1100 cm^{-1} to the stretching of the ester C-O-C bond in the amorphous and in the crystalline phase, at 1120 cm^{-1}. This is consistent with the lower wavelength band intensity decreasing and the higher one increasing with time and with the development of crystallinity as is shown in Figure 4.10A. The two absorption bands have also been attributed to the cis to trans transition of the ethylene glycol group. While the amorphous region would be expected to contain both cis and trans forms the crystalline region would be expected to be all trans. As can be seen in Figure 4.10A the intensity of the band with maximum at 1095 cm^{-1} with time the one at 1120 cm^{-1} increases. Since increasing crystallinity is accompanied with a decrease in concentration of the cis form the 1095 cm^{-1} peak is attributed to the cis and 1120 cm^{-1} to the trans isomers.

The 2-dimensional synchronous correlation spectrum, see Figures 4.10B, is dominated by a large decrease in intensity of the band at 1095 cm^{-1}. There are two autopeak, an intense one at 1095 and a much smaller one at 1125 cm^{-1} and two cross peak which are negative, consistent with the intensities of the two changing in the opposite direction with time. This produces an angel pattern which is the inverse of that observed previously since the lower wavenumber peak is

decreasing in intensity but is consistent with the assignment of trans and cis forms of the glycol unit and the change from cis to trans on crystallization. The asynchronous spectrum shows a positive and negative cross peak consistent with the higher wavenumber peak increasing in intensity and the lower decreasing progressively. (See Figure 11C)

In conclusion, the band at 1095 cm^{-1} is attributed to the cis isomer of the ethylene glycol segment and the one at 1120 to the trans isomer.

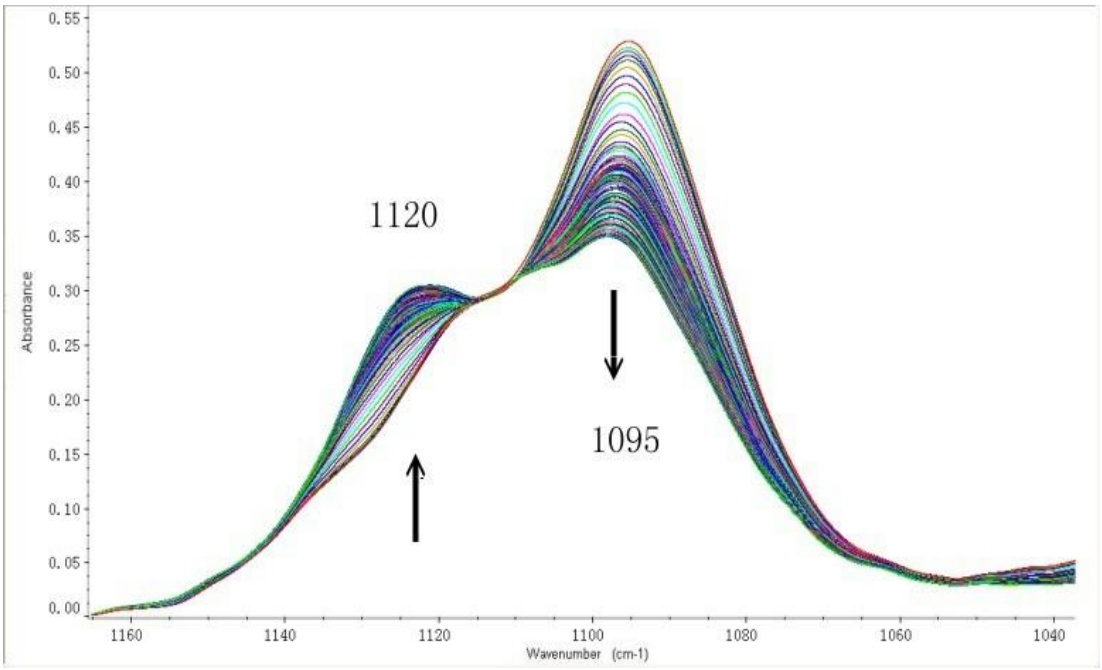

Figure 4.10A. Changes in Peak Intensity with Time in the Region 1150 - 1050 cm^{-1}.
1.5 µm Thick Film.

B.

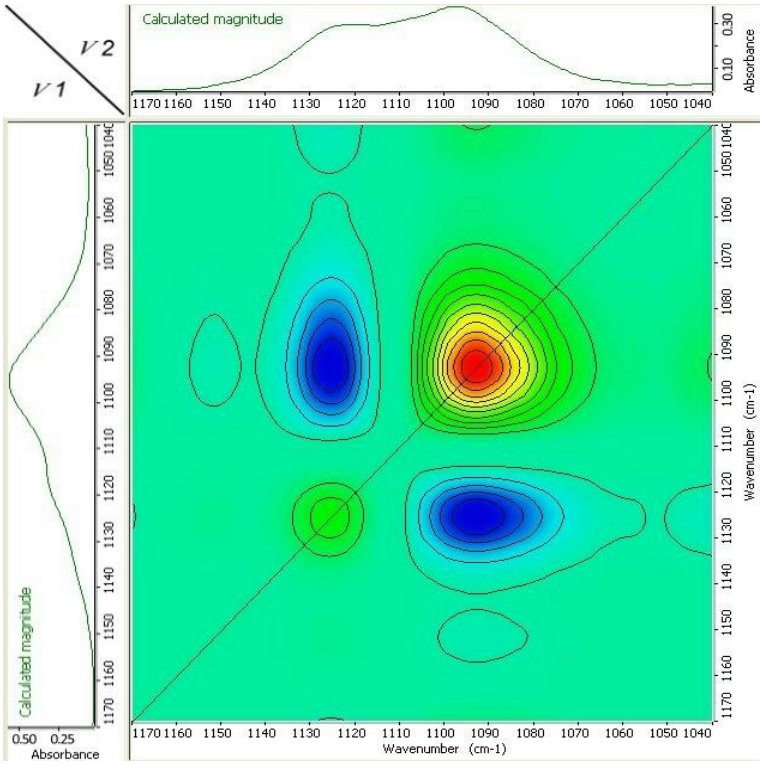

C.

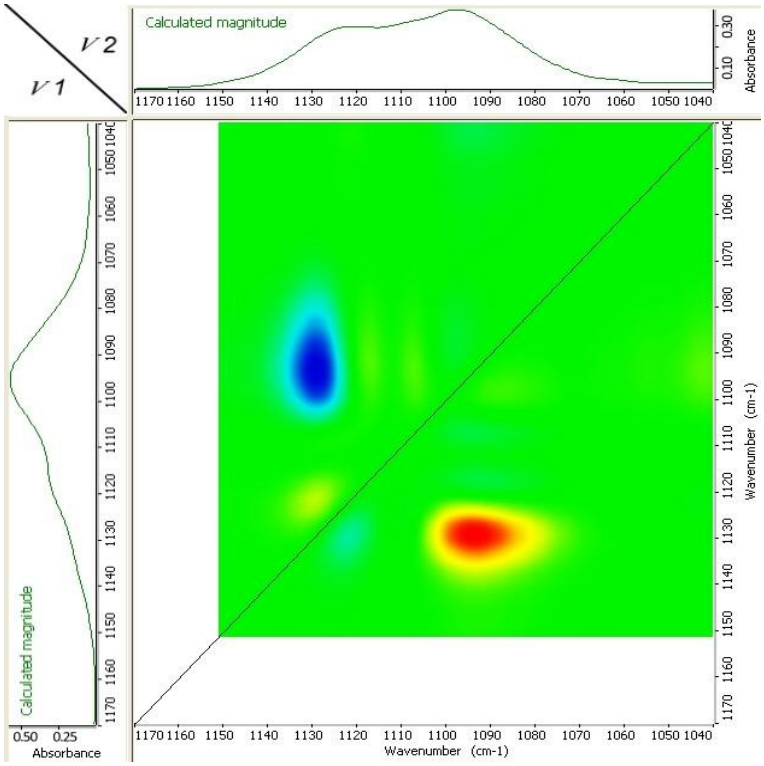

B and C. Two-Dimensional Synchronous and Asynchronous Correlation Spectra in the Region 1150 - 1050 cm^{-1}.

Figure 4.10

4.4.9 1050~990 cm^{-1} Region.

The absorption band with maximum intensity at 1015 cm^{-1} is attributed to the in-plane bending of the C-H bonds of a 1,4- di-substituted aromatic ring [114]. On isothermal crystallization, the initial sharp band progressively broadens and shifts to higher wavenumbers, at 1020 cm^{-1}, see Figures 4.11A. There are isobestic points at 1020 and 1027 cm^{-1} consistent with the changes being concerted.

There are minor decreases in intensity with time in the region 1035 cm^{-1} which have been assigned to the deformation of the cis isomer of ethylene glycol unit. The decrease in intensity is in agreement with it being transformed to the trans isomer.

The 2D synchronous correlation map, Figures 4.11B, shows two positive autopeaks at 1015 and 1022 cm^{-1}, accompanied with a pair of negative off-diagonal cross peaks (1022, 1015 cm^{-1}) producing the characteristic but reversed angel pattern consistent with the amorphous band disappearing and being replaced with a lower intensity crystalline band at a higher wavelength.

In the asynchronous correlation map, see Figure 4.11C, off-diagonal cross peak pairs are present at 1020, 1015 cm^{-1}, producing a butterfly pattern. They are negative and positive consistent with their intensities moving in the opposite

directions with time; the higher wavenumber peak increasing and the other decreasing. There are also three overlapping cross peaks at 1030, 1015 cm^{-1} whose intensities are decreasing simultaneously with the development in crystallinity and is attributed to the cis isomer of the ethylene glycol unit.

The shift to higher wavenumber, from 1020 to 1015 cm^{-1} and the progressive broadening on crystallization indicates that the lower wavenumber peak is assigned to the amorphous regions and higher to crystalline.

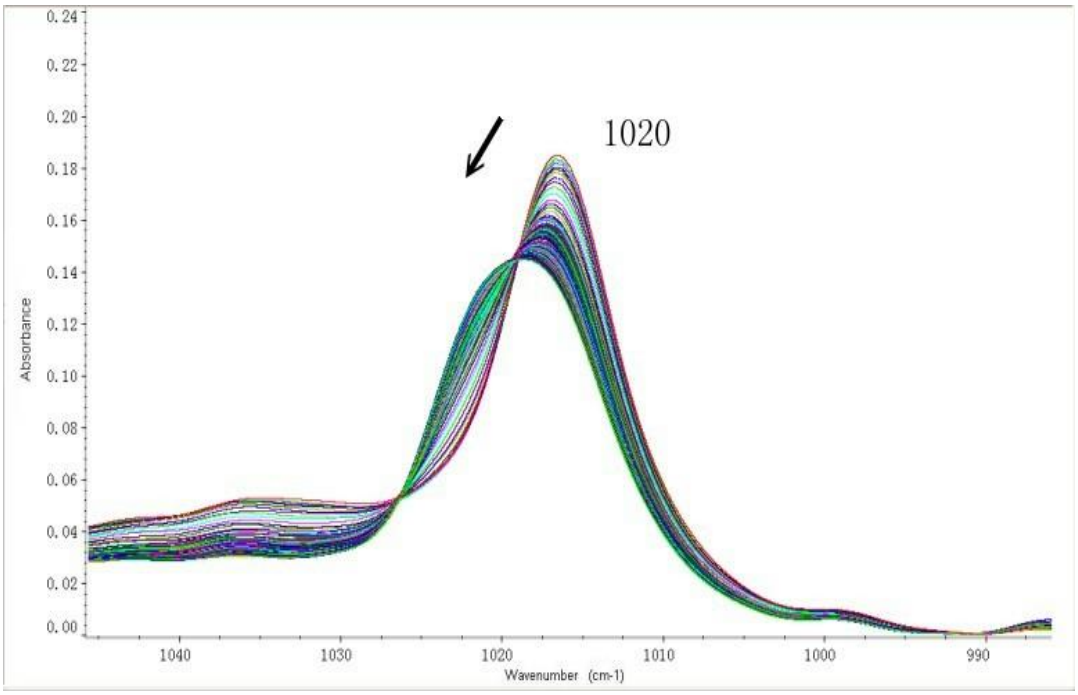

Figure 4.11A. Change in Intensity of the PET Spectrum in Region 1050 - 990 cm^{-1} with Time.

B.

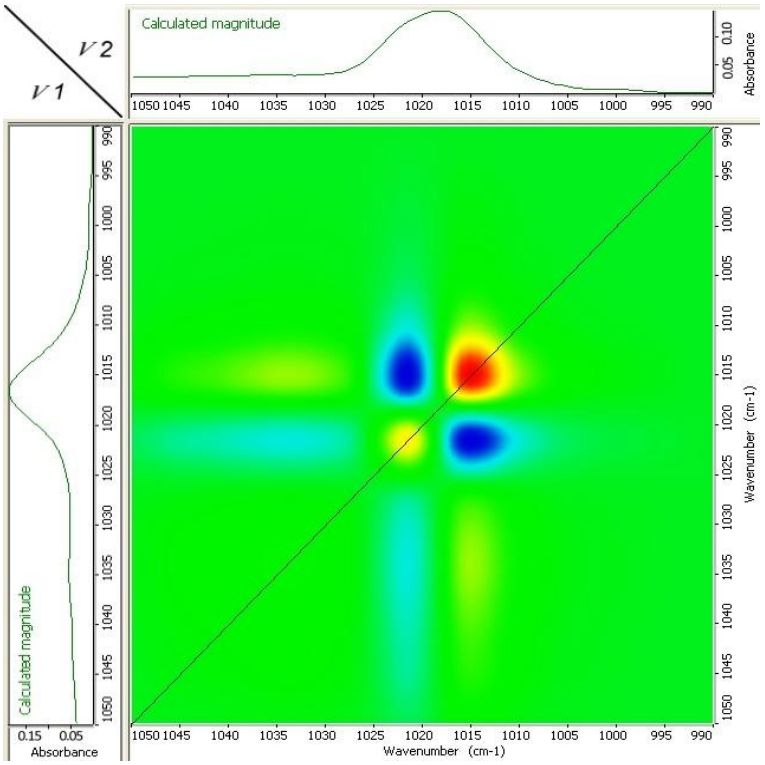

C.

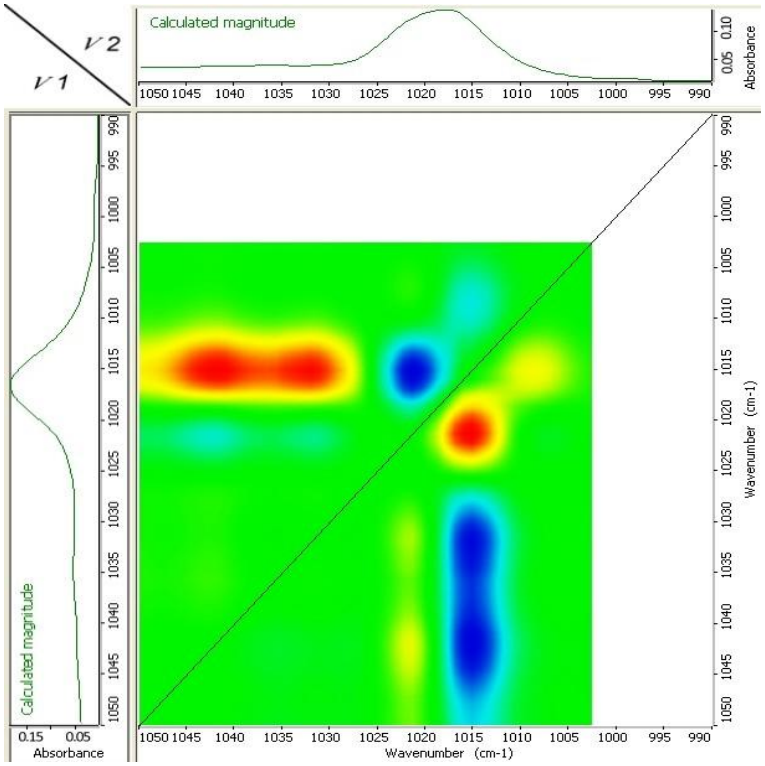

B and C. Two-Dimensional Synchronous and Asynchronous Spectra of the Region 1050 - 990 cm^{-1}. 1.5 µm Thick Film.

Figure 4.11

4.4.10 1000~750 cm^{-1} Region.

The bands in this region are sensitive to the conformation of the ethylene glycol unit, and those at 968 and 848 cm^{-1} have been attributed to the stretching of the -C-H bond of the trans isomer while the band at 894 cm^{-1} is assigned to the cis isomer. This is consistent with the first two bands increasing progressively in intensity with time while the later one decreases. The band at 873 cm^{-1} increases slightly in intensity as well as sharpening and shifting to a lower wavenumber, 870 cm^{-1}. This is attributed to differences in the force fields in the crystal compared to that of the amorphous liquid.

The synchronous correlation spectrum exhibits 4 positive autopeaks centred at 968, 873, 865 and 848 cm^{-1} of very different intensities reflecting the different changes in intensities and three cross peaks of various shapes, two positive (968, 850 and 968, 870 cm^{-1}) and one negative (970, 900-970 cm^{-1}), indicating that the changes occur simultaneously and in opposite direction.

The asynchronous spectrum has two intense cross peaks – one positive and other negative indicative of the intensities changing in opposite directions in line with the above conclusions.

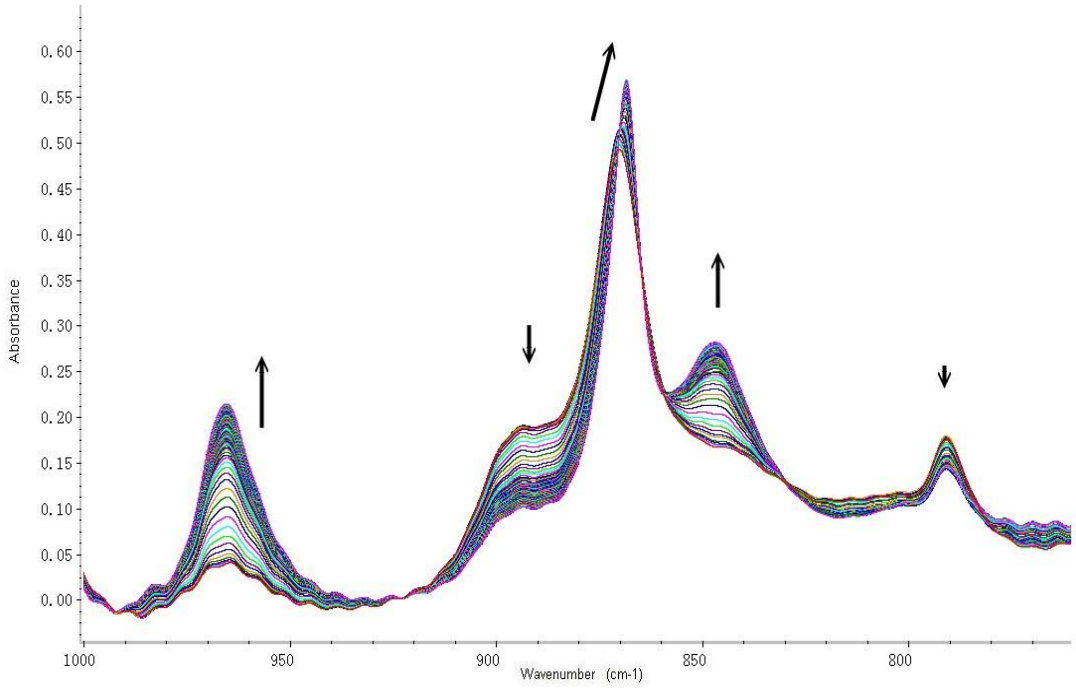

Figure 4.12A. Change in Intensity in Region 1000 - 750 cm^{-1} with Time. 12 µm Thick Film.

B.

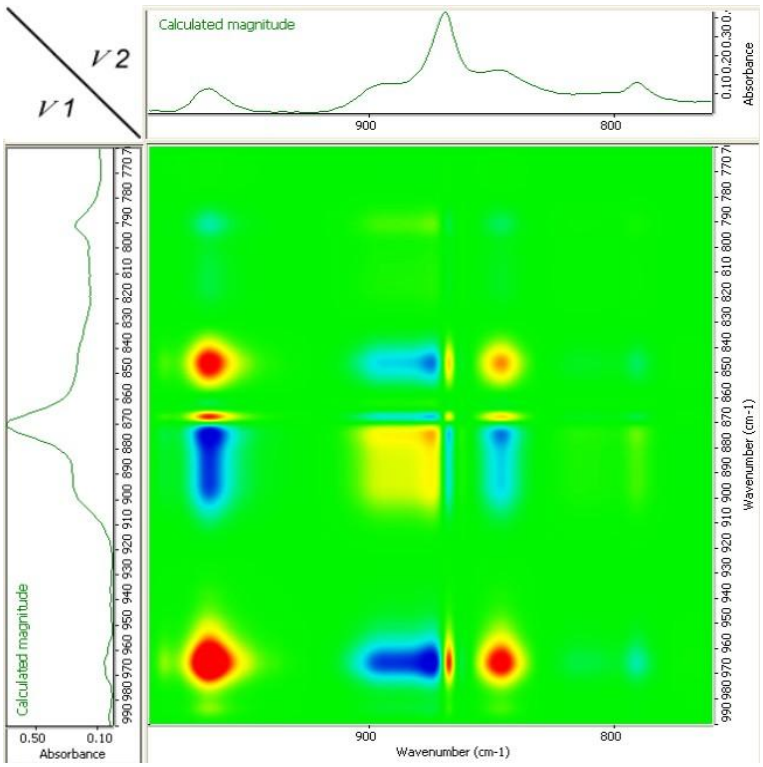

C.

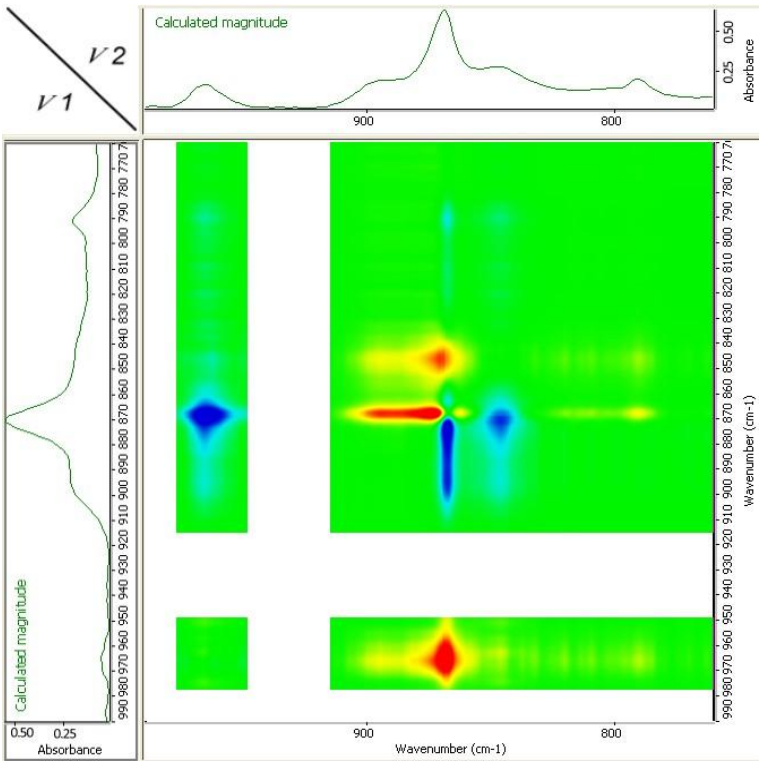

B and C. Two-Dimensional Synchronous and Asynchronous Spectra of the Region 990-760 cm^{-1}.

Figure 4.12

4.4.11 760~690 cm^{-1} Region.

A very different behaviour to that observed above is seen, however, with the absorption bands in this region. While the absorption bands with maximum intensity at 1020 cm^{-1} is attributed [114] to the in-plane bending of the C-H that at 730 cm^{-1} is due either to the out-of-plane bending of the C-H bond or the in-plane bending of the C-C bonds of the benzene ring respectively. Both bond intensities behave in a similar fashion on crystallization at 234 ^{o}C with time, in that the broad band sharpens and shifts to lower wavenumber see Figure 4.13A, in an analogous fashion to that observed with the carbonyl band outlined above.

The synchronous contour map of peak intensities in Figure 4.13B shows two autopeaks at 723 and 730 cm^{-1} accompanied by two negative cross peaks at 723, 730 and 730, 723 cm^{-1} producing the angel pattern consistent with a decrease in intensity at higher and an increase in intensity at lower wavelength. In agreement with this the asymmetric correlation map of out-plane banding of the benzene ring, see Figure 4.13C, shows two pairs of cross peaks at (733, 723 cm^{-1}) and (723, 718 cm^{-1}) producing a butterfly pattern. These are positive and negative indicating that as one increases in intensity the other decreases.

In conclusion the band at 723 cm^{-1} is attributed to the bending of the benzene rings in the crystalline phase and the one at 730 cm^{-1} to the amorphous phase, and to crystal field effects.

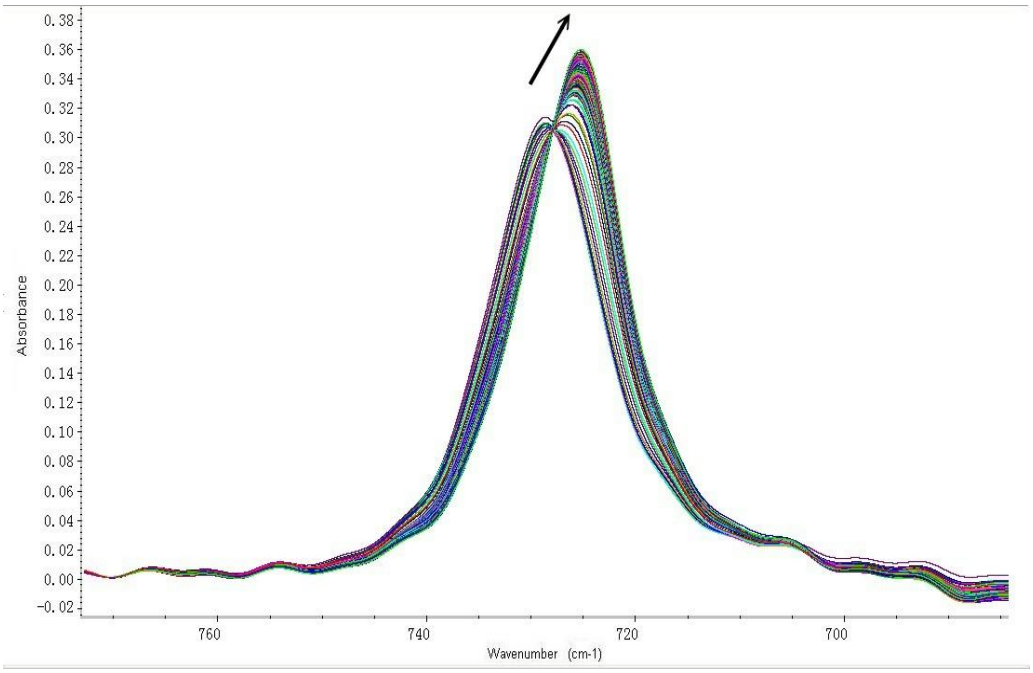

Figure 4.13A. Changes in Region 750 - 690 cm^{-1} with Time. 1.5 µm Thick Film.

B.

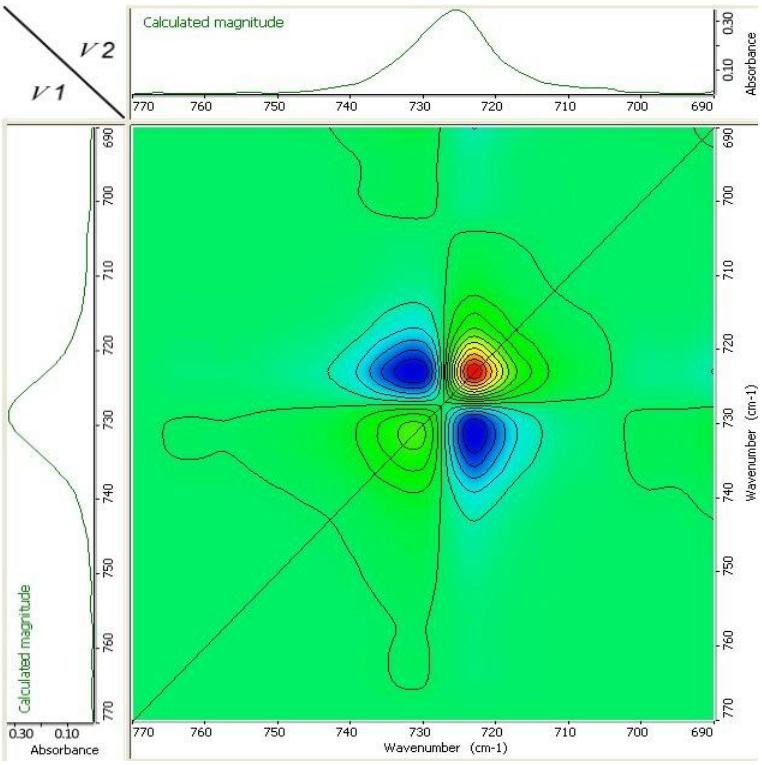

C.

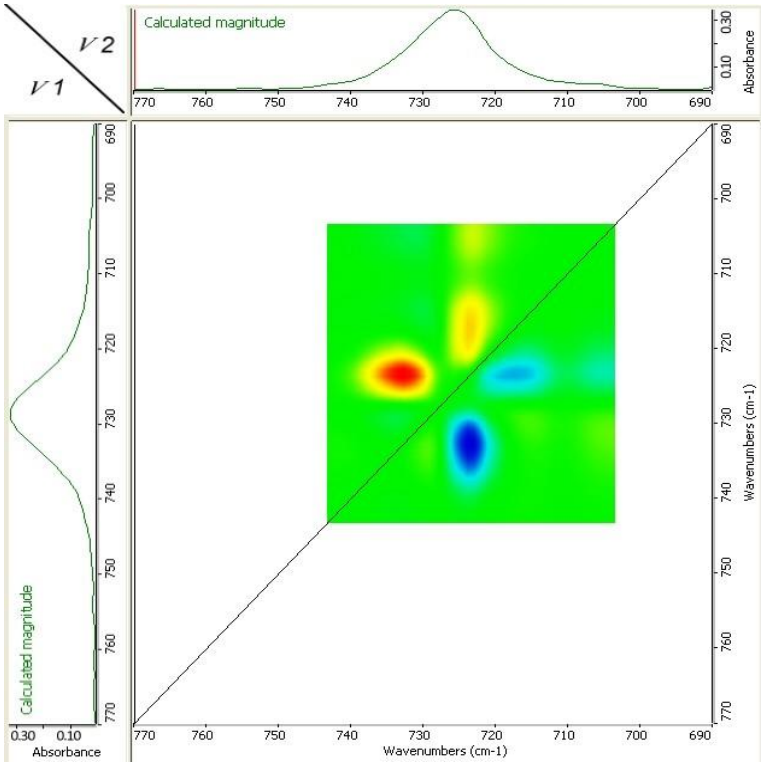

B and C. Synchronous and Asynchronous Correlation Spectra of the Region 750 - 690 cm^{-1}.

Figure 4.13

4.5 Conclusions.

The FTIR spectrum of PET is unduly complicated particularly as it is sensitive to the degree of crystallinity and chain orientation; this is due to presence of rotational isomers of the ester and glycol units and to difference in the force fields between the crystalline unit cell and the amorphous liquid. The first results in changes to pairs of absorption bands attributed to the cis and trans isomers while the second results in a shift in peak position, a sharpening of the band and a change in intensity. The many changes which occur on crystallization are listed in Table 4.1 along with their assignment to crystalline or amorphous bands based on whether the intensity increases (+ve) or decreases (-ve) during the transformation.

In the amorphous phase there is a temperature dependent equilibrium of cis and trans isomers but since the chain structure in the unit cell is all trans crystallization is always accompanied by a decrease in concentration of the cis isomer and a simultaneous increase in the trans. This makes 2-dimensional time depended correlation spectroscopy particularly useful in characterizing these absorption bands.

The broad amorphous absorption band at 3460 cm^{-1} and the crystalline one at 3450 cm^{-1} are attributed, see Table 4.1, to an overtone of the amorphous carbonyl band at 1717 cm^{-1} since it mimics its behaviour on crystallization almost exactly in shifting to lower wavenumber, becoming sharper and progressively increasing in

intensity with time. As a result the synchronous intensity maps are identical showing the characteristic angel pattern, the asymmetry of the pattern arising from the relative difference in extinction coefficient. An alternative assignment to the stretching vibration of an H-O- of a chain end carbonyl group was ruled out as it would not increase in intensity with time on crystallization.

The four very weak intensity bands centred on 3570 cm^{-1} are attributed to the ring C-H bonds stretching vibration. They do not change their position but their intensity is substantially reduced on crystallization. The aliphatic C-H bands at 2960 and 2880 $cm^{-1,}$ however, in the amorphous phase change substantially on crystallization. The intensity of the 2960 cm^{-1} decreases and two distinction shoulders at 3000 and 2970 cm^{-1} develop while the band at 2880 is replaced with one at 2900 cm^{-1}.

The intense carbonyl ester carbonyl band undergoes considerable changes on crystallization in that the broad amorphous band at 1727 cm^{-1} sharpens decreases in intensity and shifts to 1717 cm^{-1}, see Table 4.1. The intensity then increases progressively with time at this lower wavenumber. The amorphous and crystalline band can be separated into the two components and the decrease in amorphous fraction closely follows the increase in fractional crystallinity [156] because of this we attribute the difference in wavenumber of the two bands to environmental

differences between crystalline solid and amorphous liquid rather than the trans and cis positions of the carbonyl groups in the crystal unit cell and the mobile liquid. This makes the changes in the carbonyl band a ready method of determining the fractional crystallinity of a PET sample.

The synchronous and asynchronous correlation spectra of the carbonyl band is characteristic of two bands with different wavenumbers and intensities associated with the initial and final stages of the transformation and is represented by the angel pattern and two cross peaks.

The cis/trans rotational isomerizations of the ethylene glycol and the benzene di-carboxylic ester group exhibit the characteristic angel pattern and this has been useful in assigning the absorption bands of the isomers; bands at 1570, 1430-60, 1370, 1035, 894 cm^{-1} have been assigned to the cis isomer of the ethylene glycol unit while the corresponding trans isomer has been assigned to bands at 1555, 1500-10, 1470, 1340, 962 and 847 cm^{-1}. The cis form of the ester group absorbs at 1255, 1235, 1285 and 1095 cm^{-1} and the trans at 1120 cm^{-1}. The shift in wavenumber, the change in shape of the band and intensity mean that they have characteristic features in their synchronous and asynchronous spectra and this greatly assists in peak assignment.

Other changes to the spectrum are associated with crystal field effects which either shift the characteristic absorption band to different wavenumbers on

crystallization, as shown by the in-plane and out-of plane stretching of C-H bond, or change the intensity of the band, as shown by the aromatic C-H stretching mode. All of which adds greatly to the difficulty in interpreting the spectrum.

Table 4.1 Molecular Assignment – Changes on Crystallization.

Wavenumber / cm^{-1}	Relative Intensity	Assignment	Change in Intensity
3440	w	Amorphous – Carbonyl Overtone	-ve
3430	w	Crystalline – Carbonyl overtone	+ve
3949-2160	w	Aromatic – C–H stretching	-ve
2960, 2880	m,w	Amorphous – Aliphatic CH_2 – stretching; cis	-ve
3000, 2970	w,sh	Crystalline – Aliphatic CH_2 –stretching; trans	+ve
2900	w	Crystalline – Aliphatic CH_2 –stretching; trans	+ve
1727	vs	Amorphous – Carbonyl stretching	-ve
1717	vs	Crystalline – Carbonyl stretching	+ve
1575	w	Amorphous – Ring stretching	-ve
1570	w	Amorphous – Ring – stretching	-ve
1565	w	Amorphous – Ring – stretching	-ve
1558	w	Crystalline – Ring stretching	+ve
1508	m	Crystalline – Ring stretching	+ve
1503	m	Crystalline – Ring stretching	+ve
1472	m	Crystalline – Glycol CH2 – bending; trans	+ve
1465	w	Crystalline – Glycol CH2 – bending; trans	+ve
1458,1452,1449	w	Amorphous – CH2 – bending; cis	-ve
1441,1438	m	Amorphous – CH2 – bending; cis	-ve
1430,1410,1407	w,m,vw	Aromatic skeleton stretching	no change
1370	w	Amorphous – Glycol – CH2 wagging; cis	-ve
1342	w	Crystalline – Glycol – CH2–CH2 wagging; trans	+ve
1338	w	Amorphous – Glycol – CH2 wagging; trans	-ve
1307,1285,1255.1235	s	Amorphous – Ester group stretching; cis	-ve
1275	s	Crystalline – Ester group stretching; trans	+ve
1120,1095	m,m	Aromatic – 1, 4 substituted ring	+ve, -ve
1042	w	Amorphous -CH2– deformation;cis	-ve
1020	w	Crystalline – in-plane stretching of C–H bond	+ve
1015	w	Amorphous – in-plane stretching of C–H bond	-ve
962	w	Crystalline – –C–O– stretching; trans	+ve
895	w	Amorphous – Glycol – CH2- rocking; cis	-ve
848	w	Crystalline – Glycol – CH2– rocking; trans	-ve
790	w		no change
728	m	Amorphous – Out-of-plane bending of C–H bond	-ve
725	s	Crystalline – Out-of-plane bending of C–H bond	+ve

vw very weak, w weak, m medium, s strong, sh shoulder and vs very strong.

Chapter Five

The Kinetics of Crystallization of Poly (ethylene terephthalate) as Measured by FTIR Spectroscopy

5.1 Introduction.

PET has played a unique part in the development of crystallization kinetics as it was one of the first polymers to be studied by dilatometry and the isothermal crystallization time dependence interpreted in terms of the Avrami equation [50]. Since then and because of its commercial importance, its crystallization behaviour has been widely studied by a range of experimental techniques. DSC in particular has been most successful in studying the effect of molecular structure and copolymerization in controlling the rate of primary crystallization but it is deficient in not being sufficiently sensitive to measure to any appreciable extent the development of secondary crystallization with time [103, 105].

Secondary crystallization is important in establishing the final degree of crystallinity and the distribution of lamellar thicknesses achieved during any thermal treatment or drawing process. This has a pronounced effect on the ultimate material properties achieved. In Chapter 4 the application of FTIR spectroscopy to measure the development of crystallinity and the effect on the IR spectra was reviewed, and procedures outlined for separating amorphous and crystalline absorption bands [102]. It was observed by means of two-dimensional correlation spectroscopy that the carbonyl band at 1720 cm^{-1} split into two on crystallization; a band at 1717 cm^{-1} was attributed to the crystalline region and that at 1727 cm^{-1} to the amorphous region and that intensities were inversely related, such that as one increased the other decreased during crystallization and melting. Unlike DSC, FTIR spectroscopy measured the degree of crystallinity directly and the overall conversion could be studied over extended time periods well into the secondary crystallization process.

5.2 Results and Discussion.

5.2.1 Changes in FTIR Spectrum of PET on Crystallization.

Many changes are apparent in the FTIR spectrum of PET in the position of the absorption bands and the increase and decrease of their intensities in the FTIR spectrum of PET with time on crystallizarion, and these have been widely discussed

in terms of chain segment conformational changes (cis/trans isomers) and field effects between crystalline and amorphous regions. While many of these changes follow the progress of the crystallization, a previous study has shown that those associated with the aromatic ester carbonyl stretching band at 1720 cm^{-1} has the potential to be the most accurate in following the development of crystallinity in PET [102].

The change in intensity and shift in the position of the carbonyl absorption band on crystallization at 236 ^{o}C with time is shown in Figure 5.1. There is a decrease in intensity of the initial amorphous band at 1727cm^{-1} followed by a simultaneous increase in the intensity at 1717 cm^{-1} and an isobestic point at 1720 cm^{-1} consistent with the change in the two intensities occurring synchronously. The changes occurred as crystallization was observed to develop by DSC over the same time scale.

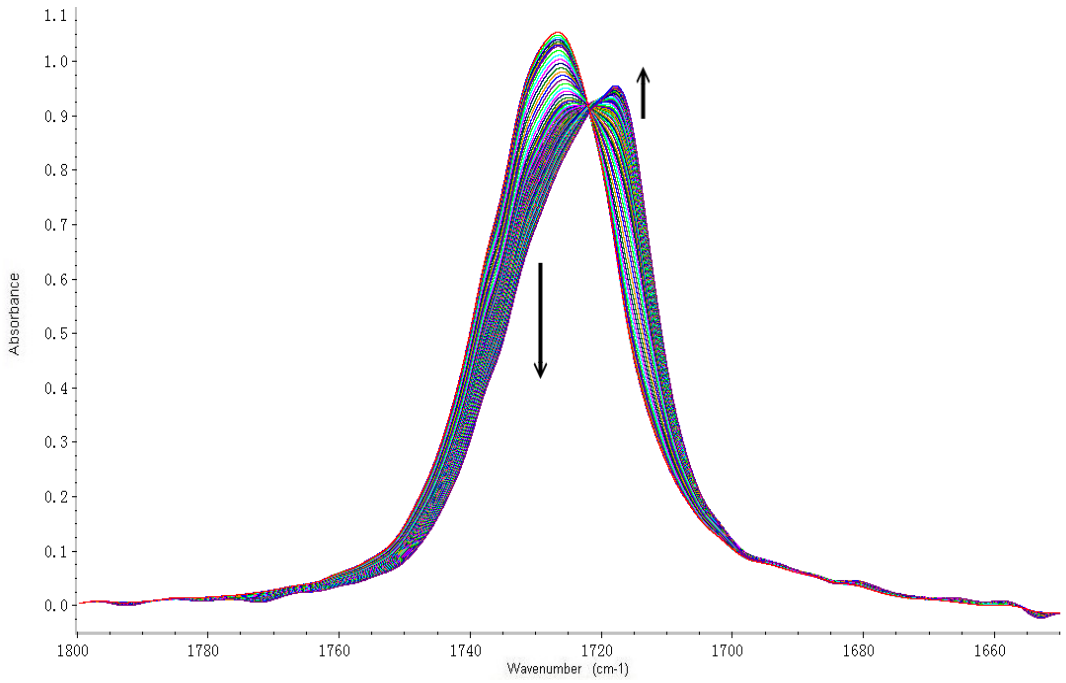

Figure 5.1 Changes to the shape and intensity of the Carbonyl Absorption Band with time at 236^{o}C, 1.5 μm thick film.

After baseline correction at two fixed wavenumbers and auto-smoothing the absorption band was repeatedly de-convoluted by Omnic software into two absorption bands until the best fit was achieved. The analysis was carried out on the basis of two Laurentzian shaped absorption bands with maximum absorbances at 1727 and 1717 cm^{-1} as shown diagrammatically in Figure 5.2A. The resulting resolution of the carbonyl band into its component parts is shown in Figure 5.2B. The changes in absorbance of the two bands as a function of time proceed simultaneously in that as one increases so the other decreases.

A.

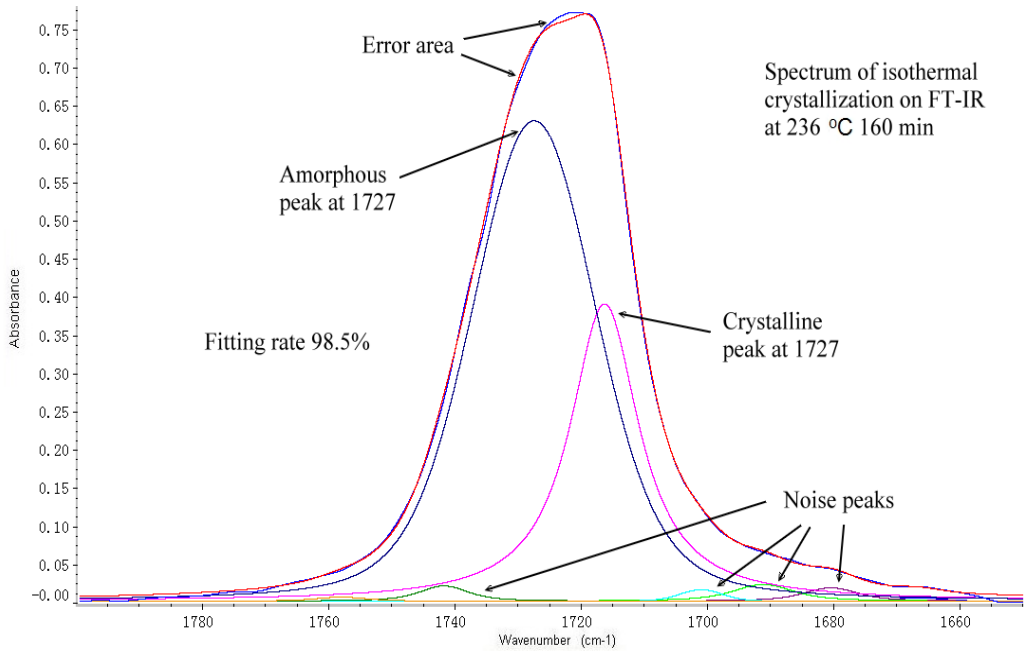

B.

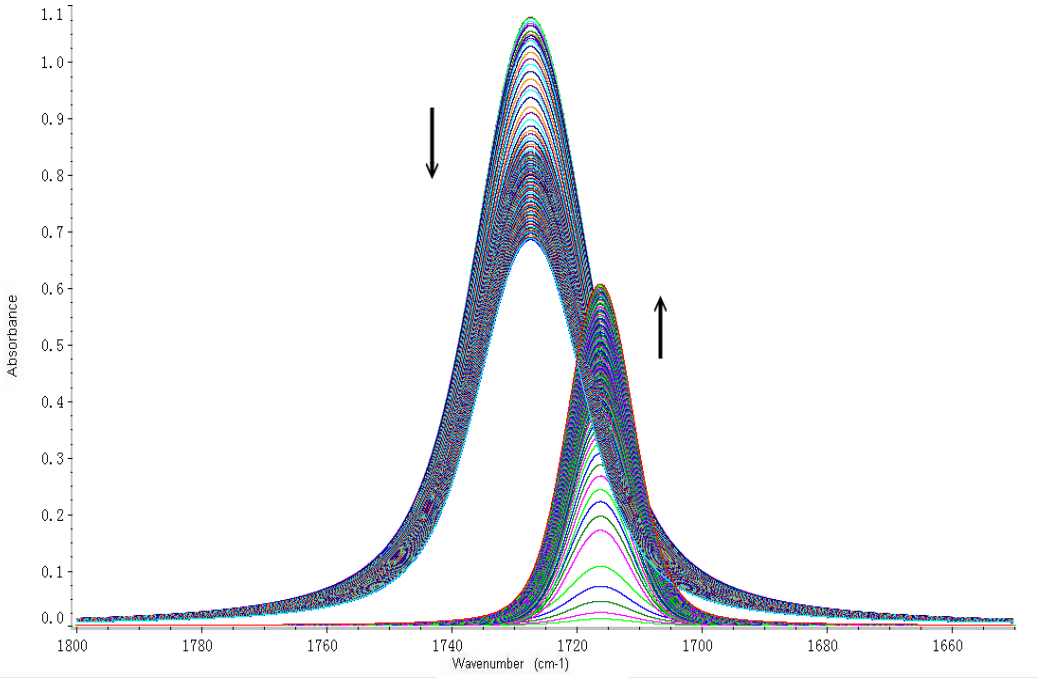

Figure 5.2 Deconvolution of the Carbonyl Absorption Band into Crystalline and Amorphous Absorption Bands.
A. At Time t and B. Peak Changes with Time at 236°C.

The general development of the intensity of the crystalline absorption band with the logarithm of time is shown in Figure 5.3A, isothermally over the temperature range 230-240^{o}C. It has the characteristic dependence on time previously observed in the crystallization of PET measured by a range of experimental techniques, dilatometry and DSC and attributed to the development of primary, i.e. initially exponential and secondary crystallization, i.e. a logarithmic dependence on time.

The amorphous band exhibited the reverse dependence with an instantaneous decrease in intensity with time; see Figure 5.3B, followed by an exponential drop and then a logarithmic decrease consistent with it measuring the amorphous fraction. The initial decrease in intensity followed the temperature drop on cooling to the crystallization temperature occurring before the onset of crystallization. Once the isothermal temperature had been achieved there was an induction period before it decreased exponentially as crystallization developed. After this, the intensity continued to decrease logarithmically with time. These two regions are attributed to primary and secondary crystallization.

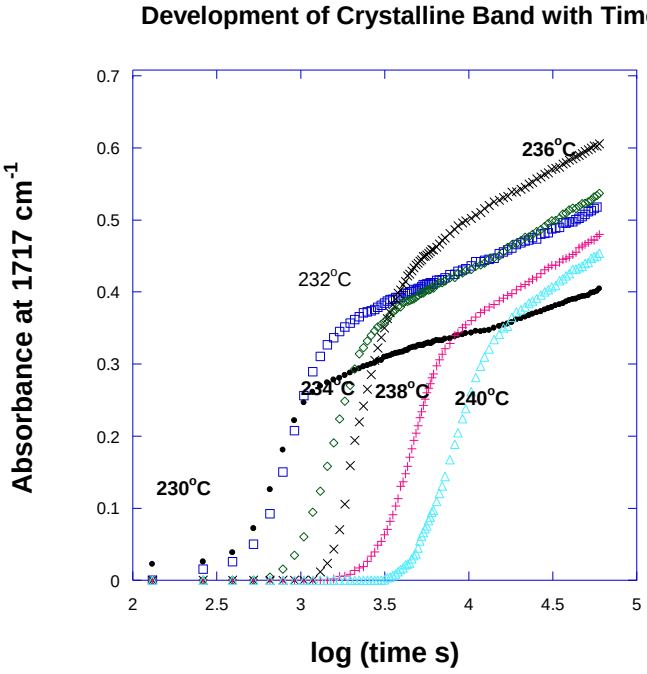

Figure 5.3A. The Increase in Crystalline Absorbance of the Carbonyl Band at 1717 cm^{-1} with Time.
Crystallization Temperatures 230-240°C.

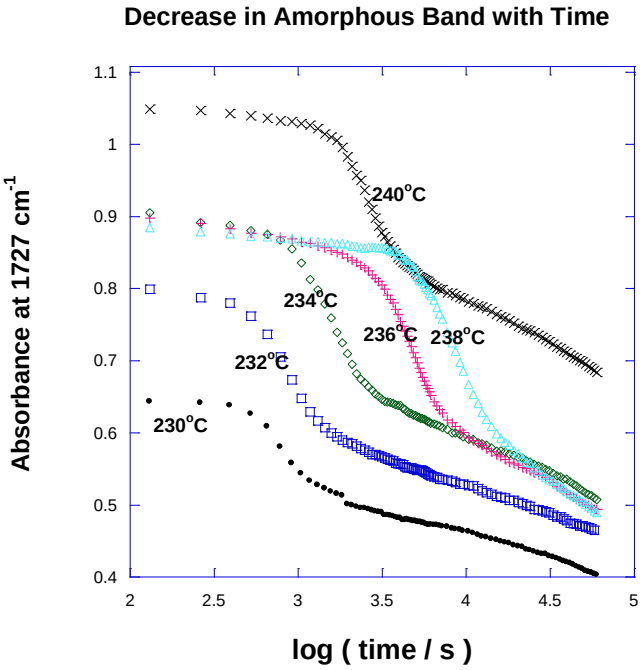

Figure 5.3B. The Dependence of the Relative Absorbance of the Amorphous Band at 1727 cm^{-1} as a Function of Logarithm of Time Over the Range of Crystallization Temperatures.

5.2.2 The Self-Consistency of the Measurements.

For the two phase model of a partially crystalline polymer, the amorphous weight fraction, $X_{a\,t}$, is related to crystalline weight fraction, $X_{c,t}$, at time t,

$$X_{a,t} + X_{c,t} = 1.0 \qquad (5.1)$$

Defining $X_{a,t} = A_{a,t}/A_{a,o}$ where $A_{a,t}$ and $A_{a,o}$ are the absorbances of the amorphous band at time, t, and initially before any crystallinity has developed

$$X_{c,t} = (1 - A_{a,t}/A_{a,o}) \qquad (5.2)$$

For Beer-Lambert law to be obeyed by the crystalline band, the absorbance of the crystalline band, $A_{c,t}$, at time t, $A_{c,t,} = \varepsilon_c l X_{c,t}$

where ε_c is extinction coefficient of the crystalline band and l sample thickness. $A_{c,t}$ is then linearly related to absorbance of the amorphous band, but increasing as the other decreases since,

$$A_{c,t,} = \varepsilon_c\, l\, (1 - A_{a,t}/A_{a,o}) \qquad (5.3)$$

The linear dependence of the absorbance at 1717 cm^{-1}, $A_{1717,t}$, on $(1\text{-}A_{1727,t}/A_{1727,0})$ is shown in Figure 5.4 for each isothermal crystallization and was taken as evidence that the above interpretation of the spectral changes is correcte.

The measured slope is a value of $\varepsilon_c l$ for the crystalline band but since it varied with temperature as well as sample thickness, l, the development of fractional crystallinity with time was determined for each temperature from the ratio of $A_{c.t}/\varepsilon_c l$, The development of the fractional crystallinity with time was calculated for each crystallization temperature, see Figure 5.5, and used to analyze the kinetics of the phase transition.

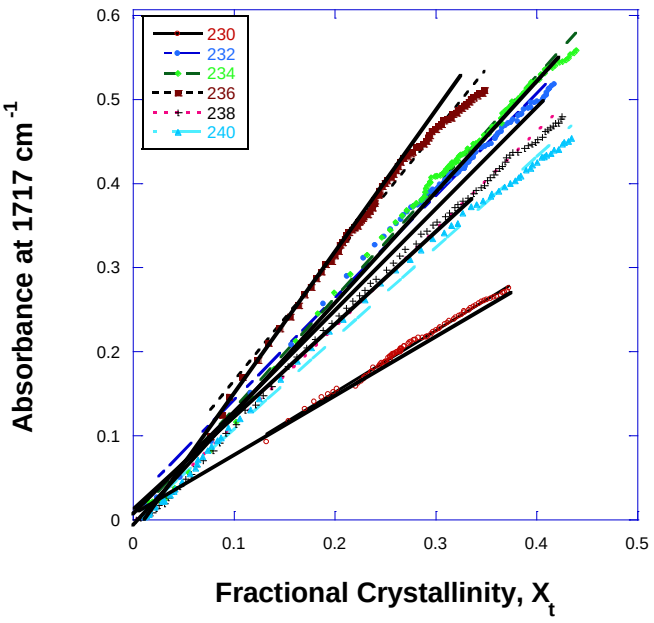

Figure 5.4 The Correlation between Absorbance of the Crystalline Band at 1717 cm^{-1} and the Fractional Crystallinity as Defined by the Absorbance of the Amorphous Band at 1727 cm^{-1}.

In conclusion the carbonyl absorption band of PET changes on crystallization from a broad band with maximum intensity at 1727 cm^{-1} associated with the amorphous region to a narrower band at 1717 cm^{-1} due to the crystalline regions. The

two bands are a quantitative measure of the weight fraction crystallinity and can be used to measure the development of crystallinity with time. It has the added advantage of being able to measure both primary and secondary crystallization processes.

5.2.3 Isothermal Crystallization Rate Study from FTIR Spectroscopy.

The changes in fractional crystallinity as a function of log (t) are shown in Figure 5.5A over a range of crystallization temperatures, from 230-240^{o}C. They have an initial exponential dependence which is characteristic of the extent of crystallinity with time following the Avrami equation[35], i.e.

$$1-X_t= \exp(-Zt^n) \qquad (5.4)$$

where X_t is the crystalline fraction at time t, Z a composite rate constant including growth rate and nucleation characteristics, and n a constant whose value depends on the crystallization mechanism. This was followed by a linear increase in crystallinity with the logarithm of the time, attributed to secondary crystallization. In analyzing the isothermal curves a two-stage crystallization process was adopted consisting of a primary stage in which the crystalline entities grow until they impinged with one another, followed by a secondary stage in which crystallinity further developed but

within the boundaries of the crystalline regions following an Avrami equation with different time dependence.

The primary stage was considered to be limited to the initial stages of the development of crystallinity up to a fractional crystallinity, $X_{p,\infty}$, at which secondary crystallization begins to dominate. The corresponding Avrami equation describing the primary stage is then,

$$X_{p,t} = X_{p,\infty}(1- \exp(-Z_p(t-t_i)^n) \quad (5.5)$$

where $X_{p,t}$, Z_p and n are the fractional crystallinity developed at time t, composite rate constant, exponent of the primary process and t_i the induction time. t_i and $X_{p,\infty}$ were used as adjustable parameters and selected to represent the initial onset and the end of the primary process.

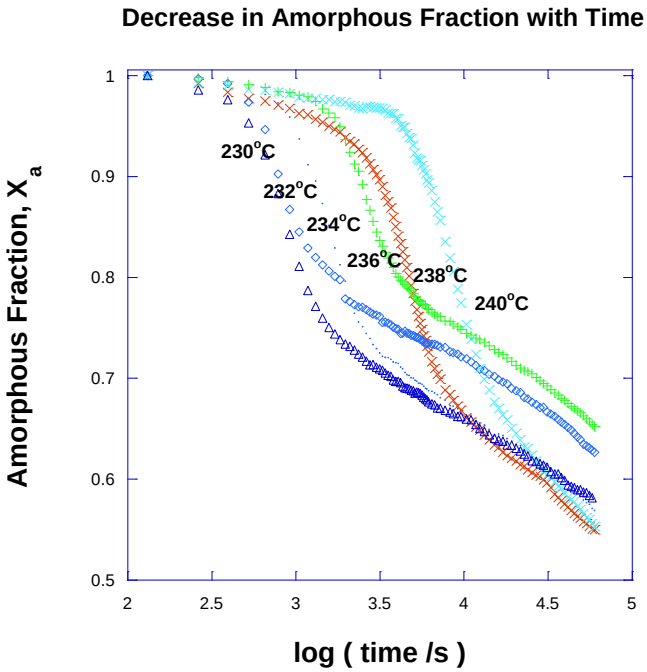

A.

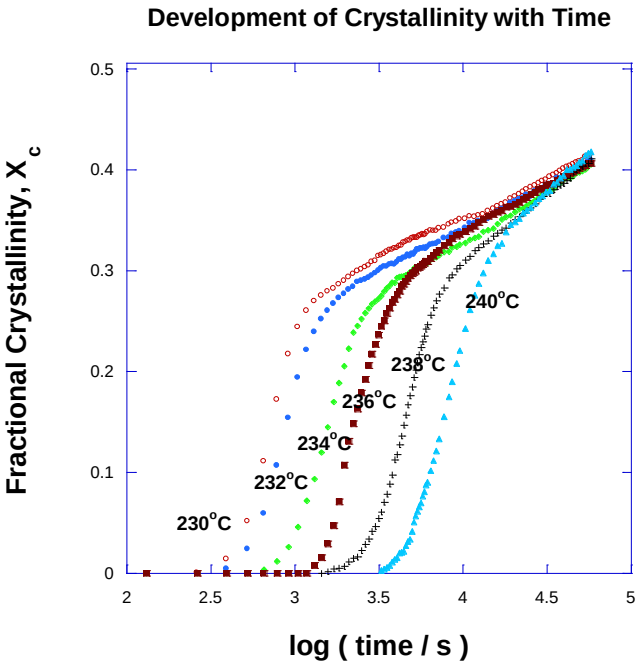

B.

Figure 5.5 The Dependence of the Fractional Crystallinity and Amorphous Content as a Function of Logarithm of Time over the Range of Crystallization Temperatures.
A. Calculated from the Crystalline Band at 1717 cm^{-1} and
B. Amorphous Band at 1727 cm^{-1}.

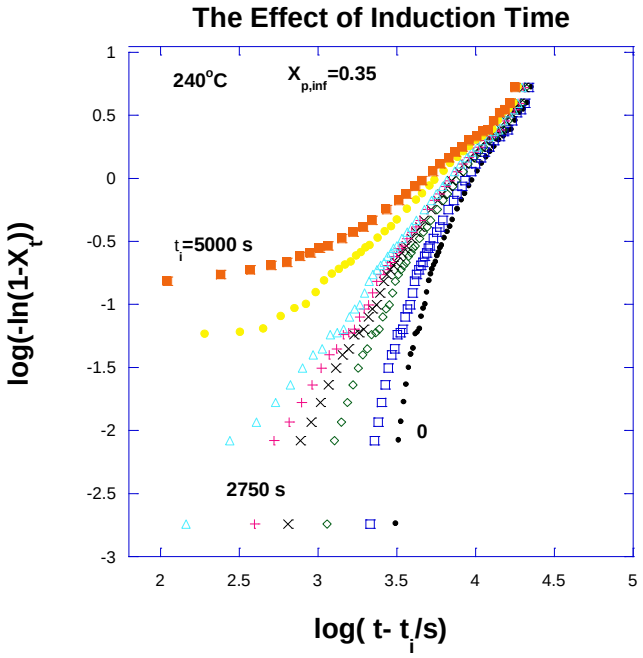
The Effect of Induction Time
240°C
X p,inf =0.35
t i =5000 s
0
2750 s
log(-ln(1-X t))
log(t- t i /s)

A.

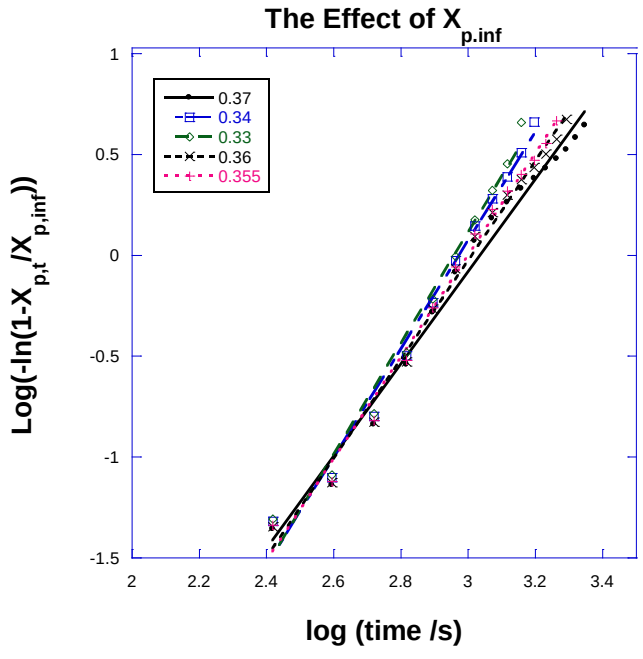
The Effect of X p.inf
0.37
0.34
0.33
0.36
0.355
Log(-ln(1-X p,t /X p,inf))
log (time /s)

B.

Figure 5.6

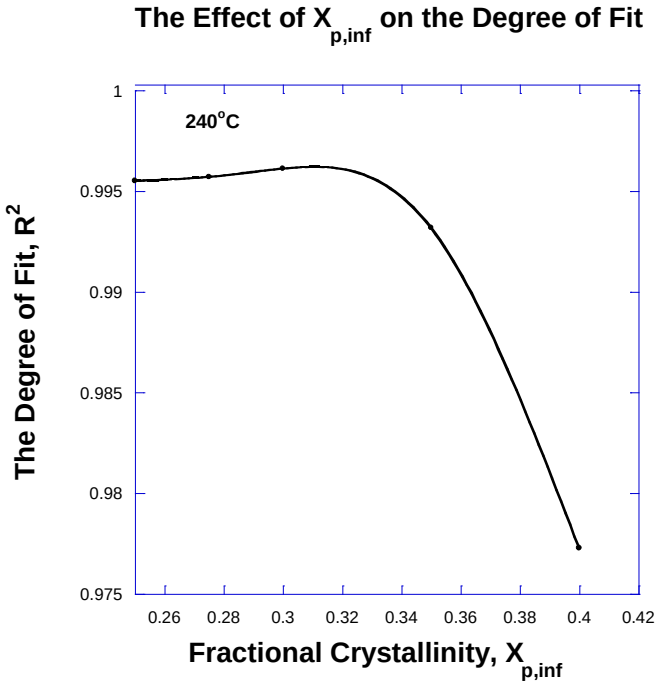

C.

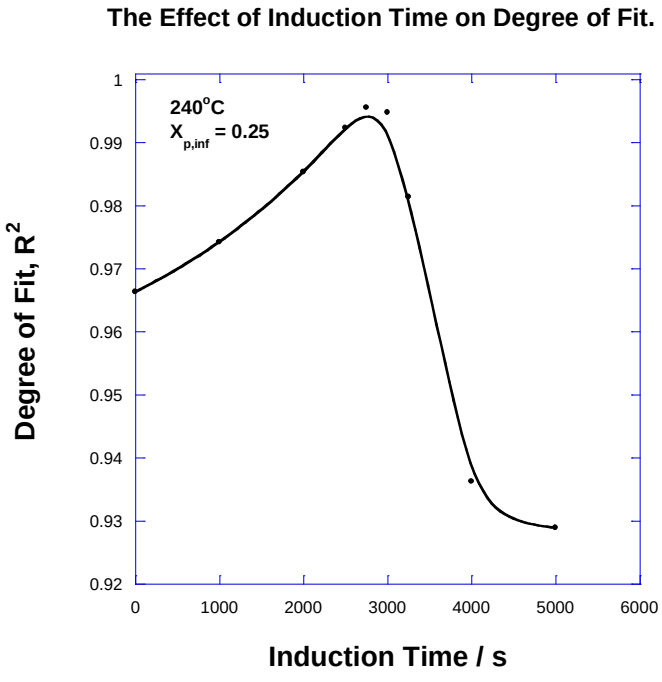

D.

Figure 5.6 Analysis of the Primary Process to Determine Optimum Value by the Effect of the Induction Time, t_i (A) and $X_{p,\,inf}$ (B); $X_{p,inf}$ (C)and t_i (D) on the Degree of Fit.

The optimum values of these parameters were selected as the values which gave the best fit of a linear plot of log [-ln(1-$X_{p,t}/X_{p,\infty}$)] against log(t) using the sum of the square of the residuals, R^2, as shown in Figure 5.6A and B which shows effect of varying $X_{p,\,inf}$ and induction time, t_i, on value on n. This enabled the optimum n value to be determined at each crystallization temperature, as shown in Figure 5.6C and D, for n=2.2 ±0.2. The primary crystallization rate parameters as determined by this procedure are listed in Table 5.1. The primary process was restricted to 30-35 % crystallinity while the secondary process continued to increase for a further 10-15% being limited only by the time over which it was measured.

The average n value obtained for the primary process over the crystallization temperatures measured was 2.0 ±0.4 consistent with the growth of spherical particles, i.e. spherulites, constricted to grow by the thickness of the film, i.e. 1.5-3.0 μm, in two dimensions.

An examination of PET samples crystallized at high temperatures by electron microscopy showed that the spherulites had diameters of 10-20 μm [105, 156] (see figure 5.7) in excess of the film thickness adopted in the present study. The spherulites dimensions exceeded the film thickness early in the crystallization process and thereafter growth spread parallel to the surface of the films with constant thickness.

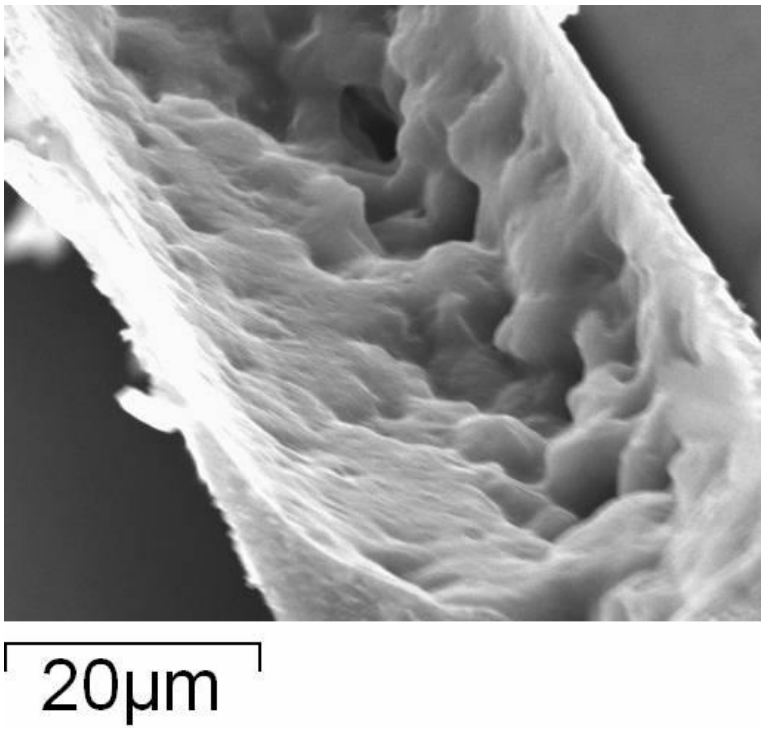

Figure 5.7A. SEM Image of Thin Film Samples without Etching.

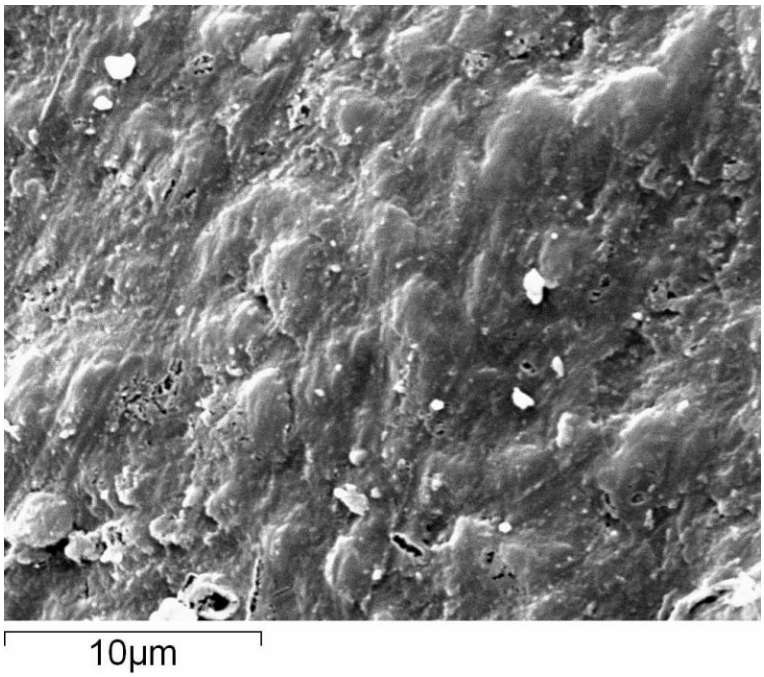

Figure 5.7B. SEM Image of Etched Samples Crystallized in DSC.

The half-life of the primary crystallization increased with the crystallization temperature displaying the characteristics of nucleation control i.e. a reciprocal dependence on the degree of supercooling from the equilibrium melting point, see Figure 5.9.

Table 5.1 The Avrami Rate Parameters for Primary Crystallization.

T_c (^oC)	230	232	234	236	238	240
n $\pm$ 0.2	1.65	2.22	2.10	2.10	1.96	2.20
Z_p (s^{-n}) x10^8	2290	39.5	57.0	31.3	7.46	0.609
$t_{1/2}$ / s	520	650	790	1050	2080	4590
$X_{p,\infty}$	0.275	0.285	0.30	0.35	0.30	0.32
t_i /s	0	131	855	1180	1570	3670

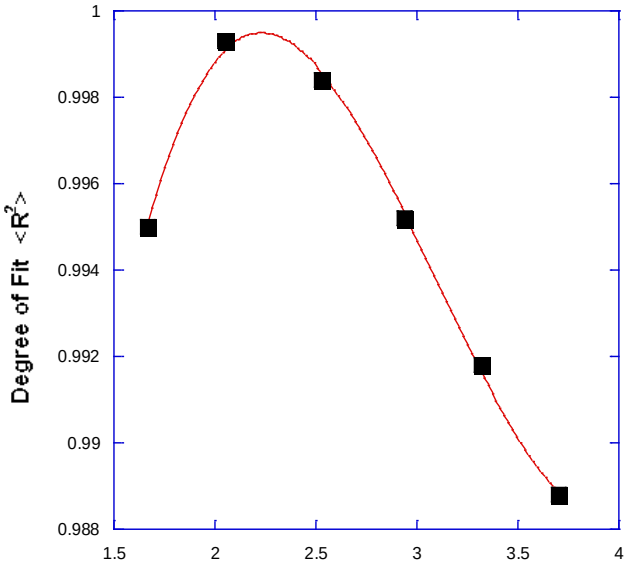

A.

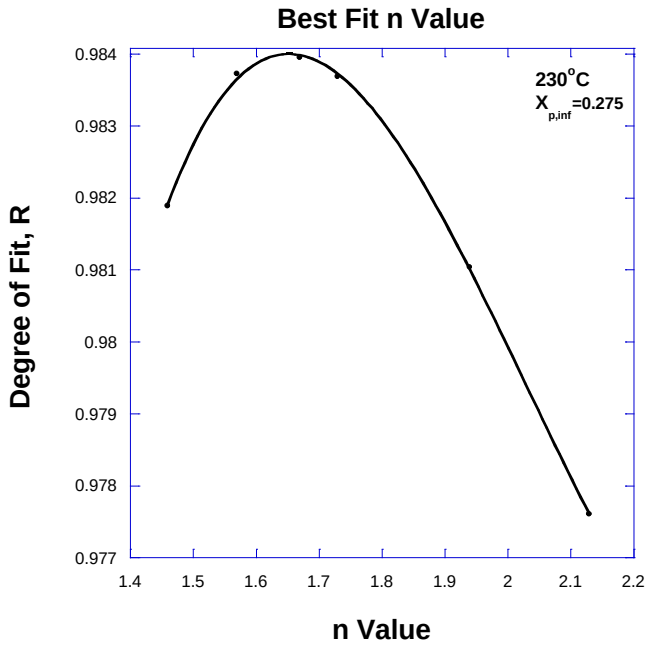

B.

Figure 5.8 Best Fit of n Values.

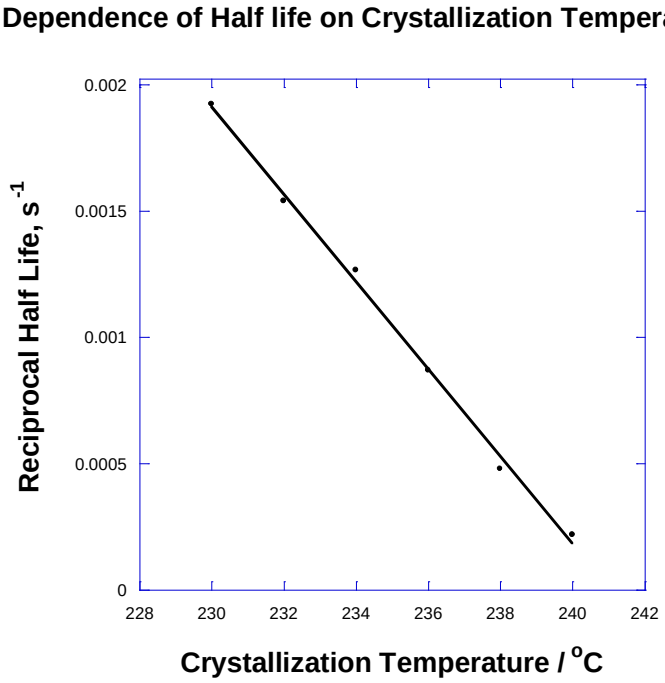

Figure 5.9 Nucleation Control of Primary Crystallization.

5.2.4 Secondary Crystallization.

Bassett and coworkers [158] observed during an electron microscopic examination of the morphology of polymer spherulites that secondary lamellar crystals developed between the frameworks of the initially formed lamellae whose growth and impingement account for the primary crystallization process. The secondary lamellae are thus constrained to grow in one dimension between lamellae and account for the secondary crystallization process. Others have attributed the process to the thickening of the primary lamellae by lateral extension of the fold surface into the amorphous regions. In either case growth is considered to be limited

to one dimension between pre-existing lamellae and should corresponds to an Avrami model for which the n value is 1.0.

The fractional crystallinity, X_t, is accordingly the sum of two Avrami equations for primary and secondary crystallization, modified to incorporate their relative importance, $X_{p,\infty}$, and $X_{s,\infty}$, i.e.

$$X_t = X_{p,t} = X_{p,\infty}\{1 - \exp[-Z(t - t_i)^{n_p}]\} + X_{s,\infty}\{1 - \exp[-Z(t - t_{p,\infty})^{n_s}]\} \quad (5.6)$$

where $X_{p,\infty}$ and $X_{s,\infty}$ are the fractional crystallinity at the end of primary and secondary process respectively.

An additional assumption was made that the secondary process started at the end of the primary process with an induction time of $t_{p,\infty}$. Z_p and Z_s are the corresponding composite rate constants and n_p and n_s the Avrami exponents. The secondary crystallization process was analyzed only when $X_t > X_{p,\infty}$, and accordingly

$$X_t = X_{p,\infty} + X_{s,\infty}\{1 - \exp[-Z(t - t_{p,\infty})^{n_s}]\} \quad (5.7)$$

and the kinetic parameters of the secondary crystallization, i.e. the Avrami constant, n_s, rate constant, Z_s, and the half-life, $t_{1/2,}$ obtained from a plot of $\log(-\ln(1-((X_t-X_{p,\infty})/X_{s,\infty})))$ against $\log(t-t_{p,\infty})$, see Figure 10A. The best fit value of n_s

was determined by varying values of $X_{p,\infty}$ and $t_{p,\infty}$ in the linear region of dependence on log t as described above in the analysis of primary crystallization.

The rate parameters are listed in Tables 5.2, and the linearity of the plots and the success in fitting the data to an Avrami equation can be seen from Figure 10. In most cases the lines were parallel with n= 1.0 ± 0.1 with no systematic change with temperature but differing only in choice of $X_{p,\infty}$ and $t_{p,\infty}$. The half-life were calculated from the Z value since

$$t_{1/2} = (\ln(2)/ Z_s)^{1/n} \qquad (5.8)$$

They exhibiting a reciprocal dependence on temperature, see Figure 5.10B, consistent with nucleation control of the crystallization.

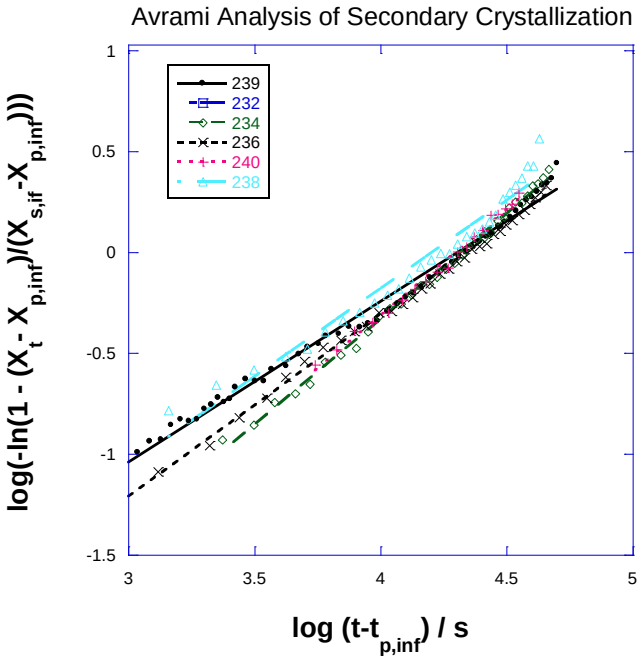

A.

Figure 5.10A The Fit of the Secondary Crystallization to an Avrami Equation.

B.

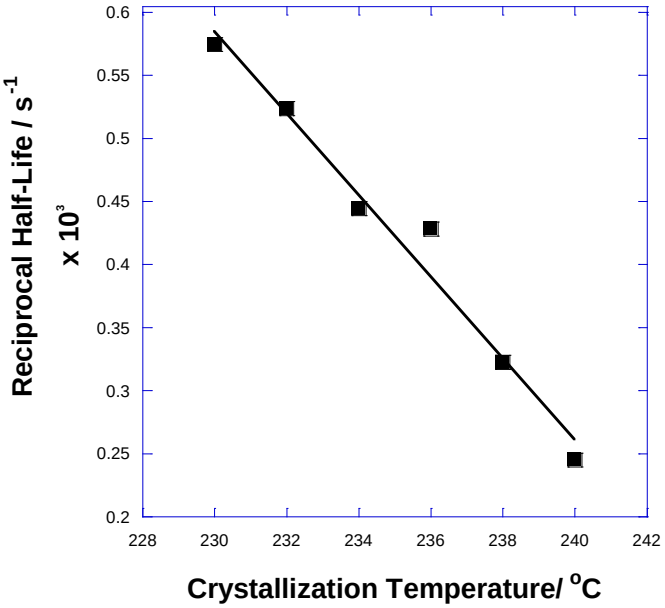

Figure 5.10B The Temperature Dependence of Secondary Crystallization.

Table 5.2 Avrami Rate Parameters for Secondary Crystallization.

T_c (^oC)	230	232	234	236	238	240
$n_s \pm 0.1$	1.03	1.03	1.05	1.02	1.11	0.97
$-\log(Z_s / s^{-n})$	4.40	4.44	4.51	4.58	4.65	4.77
$X_{p,\infty}$	0.350	0.352	0.475	0.505	0.325	0.35
$X_{s,\infty}$	0.100	0.073	0.138	0.094	0.102	0.097
$t_{p,\infty}$ (/s)	3500	8700	7200	12450	16100	22800
$t_{1/2}$ /s x 10^3	17.4	19.1	22.5	22.3	31.0	40.8

5.2.5 The Temperature Dependence of the Crystallization.

The primary and secondary crystallization rates at different temperatures were expressed in the form of reciprocal crystallization half-life, $1/t_{1/2}$, using Hoffman-Lauritzen relationship [48] and following Chan and Isayey [159]; $(1/t_{1/2})$ values were substituted for the crystal growth rates, g and g_0, respectively and the dependence of the crystallization half-life given by,

$$(1/t_{1/2}) = (1/t_{1/2,0}) \exp(-U^*/R(T-T_2).\exp(-K/T_c(\Delta T)) \qquad (5.9)$$

where U* is the activation energy of viscous flow and taken to be 6284 J mol.$^{-1}$ [23], T_2 is the thermodynamic glass transition temperature, K the nucleation constant, T_c the crystallization temperature, and ΔT the super-cooling from the equilibrium melting point, T^o_m.

Plots of $\ln(1/t_{1/2})+U^*/R(T-T_2)$ against $1/(T\Delta T)$ are show in Figure 9 for both primary and secondary crystallization. The data is consistent with two linear relationships for both primary and secondary processes, with $K=4.28x10^5$ and $1.99x10^5$ K^2 corresponding to the two nucleation regimes, I and II. The primary crystallization proceeds by Regime I mechanism of nucleation and the secondary crystallization by Regime II since the ratio of the K values is close to 2:1.

Regime I is considered to occur at high crystallization temperatures and low degree of super-cooling. Surface secondary nucleation is rate determining since coverage of the surface occurs and there is a delay before the next layer is nucleated. For this model, the growing surface is smooth, and

$$K_1 = 4\, b\sigma\sigma_e\, T^o_m \Delta H_v \qquad (5.10)$$

Regime II is normally observed at a higher degree of super-cooling and secondary nucleation is considered to be more rapid such that it occurs before the surface layer is covered. For this model the growing surface has several secondary nuclei and is rough, and

$$K_{11} = 2\, b\sigma\sigma_e T^o_m \Delta H_v \qquad (5.11)$$

where b is the monomolecular layer thickness, taken to be the perpendicular separation of plane [24]. This is 5.53 Å [48], and σ is the side surface free energy of the polymer crystal, σ_e the fold surface free energy and ΔH_v the enthalpy of fusion per unit volume. σ was estimated from [24, 48, 160]

$$\sigma = 0.11 \Delta H_v (ab)^{½} \qquad (5.12)$$

The unit cell dimensions, a and b, were taken to be 4.57 and 5.95 Å [24, 161], ΔH_v 2.10×10^8 Jm^{-3} [103, 105] and T^o_m 562 K [103, 105]. Accordingly, for PET isothermal crystallization, $\sigma = 1.09 \times 10^{-2}$ J m^{-2} and $\sigma_e = 0.076 \pm 0.02$ J m^{-2}. This is in agreement with the value calculated for σ_e for PET of 0.0909 to 0.0936 J m^{-2} [48], and measured from rate studies, 0.0108 J m^{-2} [105].

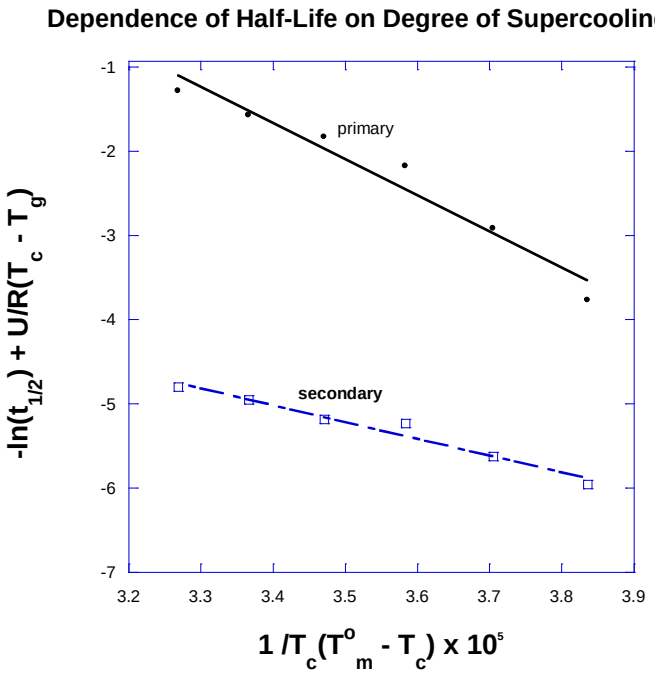

Figure 5.11 Dependence of Half-lives on Degree of Super-cooling.

5.2.6 Research the Crystallization Behaviour by band at 1340 cm^{-1}.

The analysis of the crystallization behaviour of PET by resolving the carbonyl band at 1720 cm^{-1} is quite complex. However, another crystalline peak at 1340 cm^{-1} of due to wagging of the glycol segment exhibited a similar increase with time as the

crystalline component of carbonyl group at 1717 cm^{-1} during isothermal crystallization (see Figure 5.12). Both curves show very similar trends – an initial exponent rise and a final linear increase with log (time) due to the primary and secondary process. Both also had a $t_{1/2}$ value for the primary process of 76 min. after subtraction of an induction time which suggests that they are both measuring the same development of crystallinity.

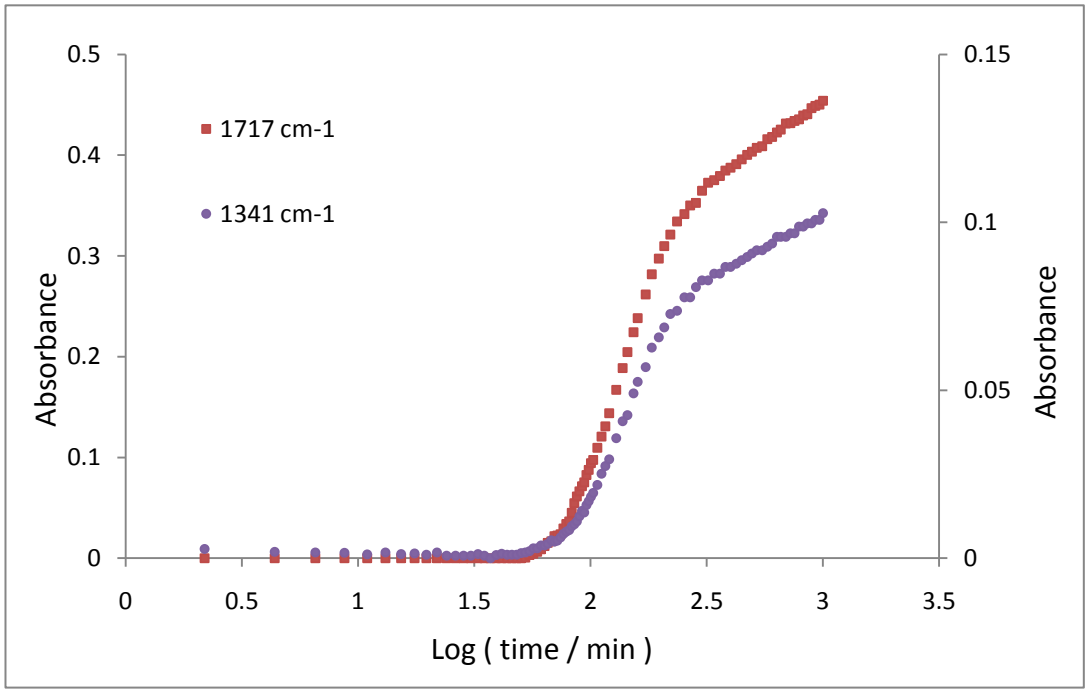

Figure 5.12 Comparison the Changing Tendency of 1717 and 1340 cm^{-1} during Isothermal Crystallization at 240 ^{o}C .

The measurement of absorbance at 1340 cm^{-1} is much simpler than 1717 cm^{-1}, since there is no overlap with the amorphous band. However, it cannot be used

directly to calculate the crystallinity of PET as it relates to the crystalline phase only and there is no crystallinity calibrated reference. The carbonyl absorption band is very intense such that thin films, 1.5-3 μm thick, are required for absorbance values close to 1.0. The much weaker absorbance of the 1340 cm^{-1} band would enable film thicknesses of up 15-30 μm to be used in the FTIR measurements. This could have obvious advantages in measuring effect of film dimensions on the crystallization kinetics, as well as improved accuracy of the measurements.

It would also require a different method of calibrating the fractional crystallinity by similar observations on an amorphous band.

5.3 Conclusions.

The isothermal crystallization of PET has been measured in the temperature range 230-240 ^{o}C by FTIR spectroscopy from the change in absorption of the carbonyl ester group in the region of 1710-1730 cm^{-1}. Absorption bands were attributed both to the amorphous at 1727 and crystalline content at 1717 cm^{-1} and using the power of the Omnic software it was possible to resolve the two overlapping bands and determine their relative contribution. Since both amorphous and crystalline content were separately determined the fractional crystallinity could be measured as a function of time. However, the intensity of both bands at constant

crystallinity decreased with temperature and calibration of the fractional crystallinity was required to be calibrated at each temperature.

Since the fractional crystallinity rather than the rate of crystallization was directly measured by the FTIR spectrometer the procedure was not limited by the sensitivity of the measurements and the crystallization kinetics could be studied to higher temperature, and so to lower rates for extended periods. Accordingly secondary crystallization could be measured in greater detail than has been the case with DSC.

The overall crystallization included two different time dependent steps, attributed to primary and secondary crystallization. These appeared to occur consecutively, such that it was possible to analyze them with two separated Avrami equations - separated at a critical value of the degree of crystallinity, $X_{p,\infty,}$ where the primary process stopped and the secondary started. Separate Avrami exponents, n, were assigned to each; n was 2.0 for the primary process and 1.0 for the secondary consistent with the crystallization mechanism. For the primary crystallization this was growth of discs confined to two dimensions by the thickness of the films, 1.5 to 3 μm. To confirm this point the crystallization of PET sheet samples 1-2 mm thick was measured by DSC over a similar temperature range, 224-234^{o}C, limited by the sensitivity of the calorimeter. Although the measured half-lives were reasonably

similar the n values were very different, i.e. 2.8-3.4 but nevertheless consistent with the growth of heterogeneously nucleated spherical particles in three dimensions. The crystallization rate parameters determined by DSC are listed in Table 5.3.

Table 5.3 Avrami Rate Parameters for PET for Primary Stage of Hot-Crystallization, Measured by DSC.

T_c (^oC)	224	226	228	230	232	234
$n_p \pm 0.1$	3.0	2.8	3.3	3.0	3.2	3.4
$Z_1 \times 10^3$ (min^{-1})	13.7	10.3	1.03	1.60	0.29	0.0846
$t_{1/2}$ / s	223	275	420	466	670	866

Electron micrographs showed that the spherulites were typically 10-20 μm in diameter and so they attained a diameter of the thickness of the film in the early stages of the primary crystallization. This is the first example of a case where the crystallization kinetics is defined by sample dimension and behaves exactly as predicted by Avrami's models for 2- and 3- dimensional growth of spherical particles. The growth rate was nucleation controlled increasing with super-cooling and initiated by secondary nuclei in Regime I.

For the secondary crystallization, the n value was 1.0 and this was consistent with the growth of lamellae between the original lamellae laid down in the formation of the spherulites. Growth was thus confined to the amorphous regions between the parallel lamellae. Unlike primary secondary crystallization, however, was initiated by nuclei in Regime II which may reflect the increased difficulty in accumulating material on the lamellae from the melt constrained between lamellae.

Chapter Six

Melting Behaviour and Seeded Crystallization of PET

6.1 Introduction

The melting behaviour of a polymer is an important physical parameter as it defines the maximum working temperature of a crystalline polymer. Heating close to the observed melting region invariably results in structural alterations to the polymer and a change in physical and mechanical properties. In addition, measurement of the equilibrium melting point of a polymer is important in defining the temperature dependence of the kinetics of crystallization and underpins the theoretical interpretation of all thermodynamic theories of phase transitions.

The melting point of a polymer is not unique since it depends on the crystallization temperature and the thermal history of the sample. Many studies have been made of the melting behaviour of PET but it has been concluded that melting is

complex depending on the experimental conditions chosen [103-106]. One, two and three separate endotherms have been observed and attributed to different lamellae thickness distributions produced on cooling to room temperature, on annealing on heating to the melting point, during primary and secondary crystallization. However, for PET, most of the studies are based on the melting of the lamellae produced during the primary process at various crystallization temperatures [103, 105]. The different heating rate adopted during the melting affects the measured melting temperature since annealing occurred on heating and there is a thermal lag [162]. Secondary crystallization is also important in establishing the final degree of crystallinity and the distribution of lamellae thicknesses achieved during thermal treatment [163]. The thermal history of secondary crystallization is an important factor in determining the shape of the final melting endotherm and the melting point [106, 164].

6.2 Banks and Sharples' model of Seeded Crystallization

Banks and Sharples proposed a procedure of seeded crystallization in order to increase the rate of crystallization of polyethylene [28, 33, 165]. They used the concept of partial melting to produce a large number of crystal seeds on which primary crystallization would develop. This was achieved first by crystallizing

polyethylene at 127.5 ^{o}C, and then partially melting at a temperature 0.9 ^{o}C lower than the previously observed melting point of 136.8 ^{o}C. After partial melting the sample was cooled to 127.5 ^{o}C and subsequently re-crystallized. They found that the half-life of primary isothermal crystallization had been reduced from 100 to 17.5 minutes. Crystallization had developed on seeds of crystalline material which survived the partial melting, and acted as nuclei. In the other word, the number of the primary nuclei had increased and this reduced the half-life of isothermal crystallization and increases the crystallization rate. The nucleation process of seeded crystallization is that of heterogeneous nucleation.

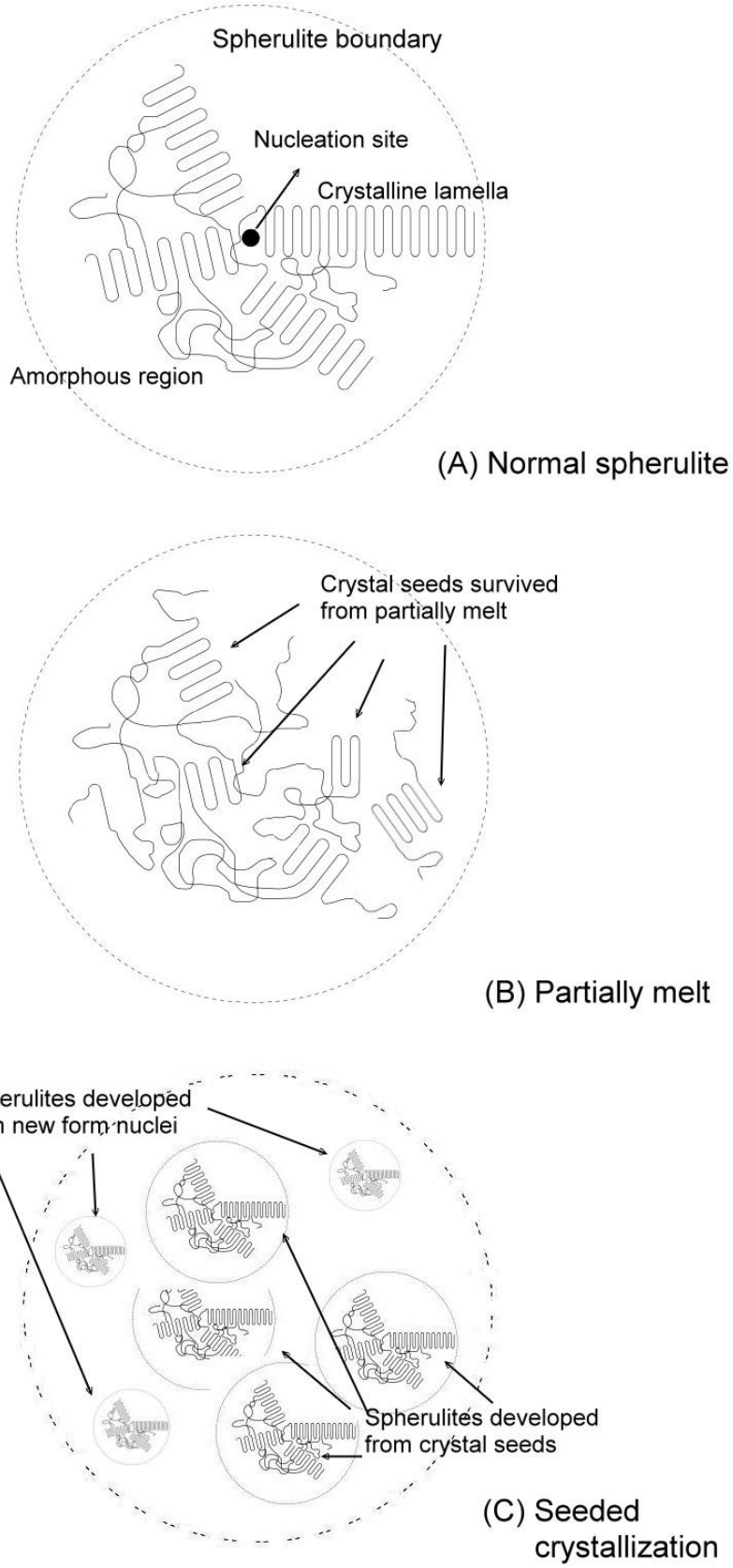

Figure 6.1 A Schematic of Seeded Crystallization.

Figure 6.2 show time lapse micrographs of the seeding procedure adopted by Banks and Sharples showing the change in appearance of the PE spherulites during partial melting, subsequent seeded crystallization and further crystallization. The PE spherulites initially grown from the melt at 118.4 ^{o}C for 8 minutes (Figure 6.2A) were partially melted at 127.6 ^{o}C, which is 0.9 ^{o}C lower than the final melting temperature at which the spherulites disappeared. On cooling to 118.4 ^{o}C again a micro-crystalline texture developed rapidly within the regions initially occupied by the spherulites. The amorphous regions external to the spherulite boundary continued to crystallize retaining a memory of the structure of the original spherulites, see Figure 6.2C.

This technique of seeding was applied to the study of the crystallization of PET but since its spherulites were not resolvable by optical microscopy the process was studied by FTIR spectroscopy and DSC and on samples which had completed their primary crystallization so that the secondary process could be separately studied at higher temperatures.

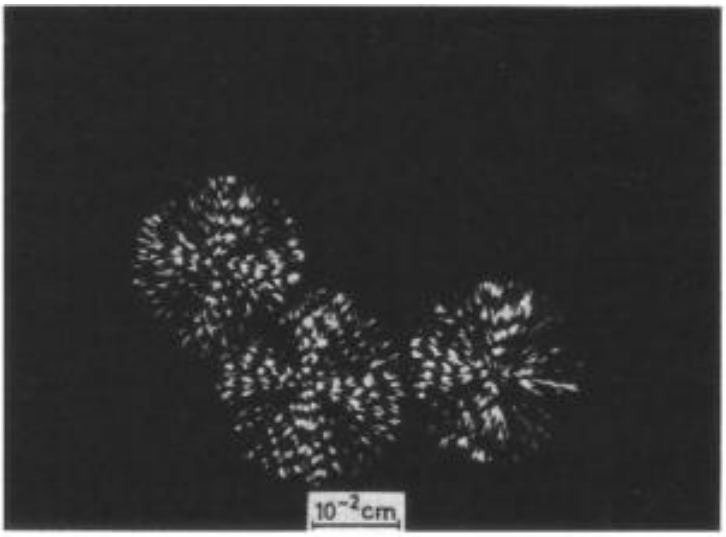

A. Spherulites Grown from the Melt at 118.4 °C for 8min.

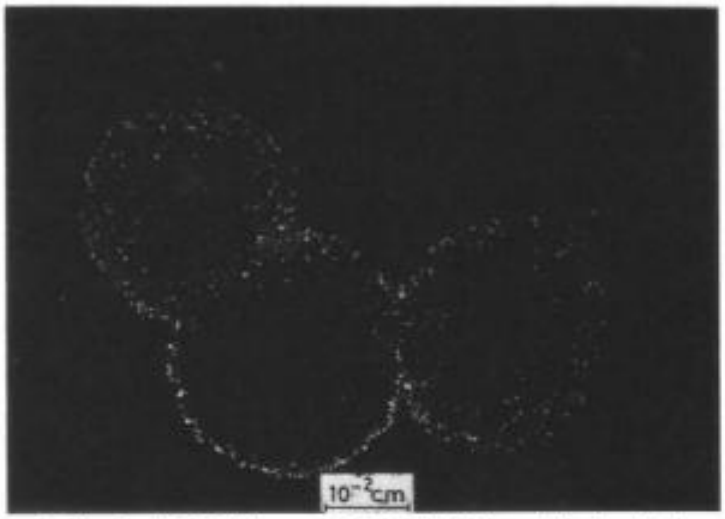

B. by Partial Melting at 127.6 °C Followed by Seeded Crystallization at 118.4 °C for 1 min.

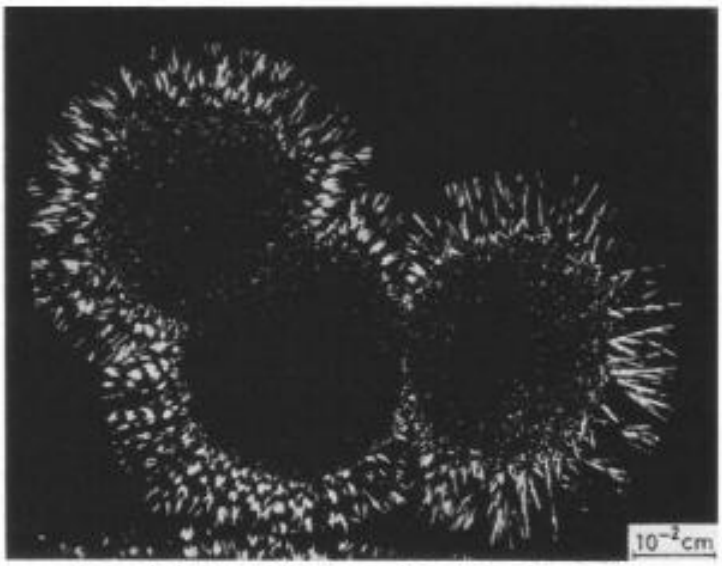

C. Seeded Crystallization at 118.4 °C after 5 min.

Figure 6.2 Microcopy Photo of PE Seeded Crystallization [165].

6.3 The Effect of Crystallization Temperature on Melting.

In order to determine the temperature range in which melting occurred, samples crystallized between 224-234 ^{o}C up to the end of the primary process were melted at 10 K min^{-1}. The DSC endotherms are shown in Figure 6.3 and the temperature corresponding to the last trace of crystallinity was taken as a measure of the melting point, T_m. A broad single endotherm was observed, ranging from 245 to 265 ^{o}C, on samples crystallized at the lowest temperatures but the endotherms narrowed in distribution and at the same time shifted to higher temperatures with increasing crystallization temperature. The last trace of crystallinity was used as a measure of T_m, and following the Hoffman–Week relationship, [12], i.e.

$$T_m = T_m^o(1 - 1/2\beta) + T_c/2\beta \qquad (6.1)$$

with $\beta = (\sigma_e l/\sigma l_e)$ where σ is fold surface free energy, l the lamella thickness and the subscript e refers to equilibrium conditions, the equilibrium melting point, T^o_m, was determined from a plot of T_m against T_c, see Figure 6.3B. This was linear with a slope of 0.5 indicating that equilibrium conditions were present and the samples had not annealed on melting. The extrapolated value of T^o_m was 294±2^{o}C (566 K) in good agreement with the literature values (561±2 and 564±2K) [70, 103, 105]. From

the melting endotherms it was also possible to determine what temperatures could be used for the partial melting studies prior to seeding studies.

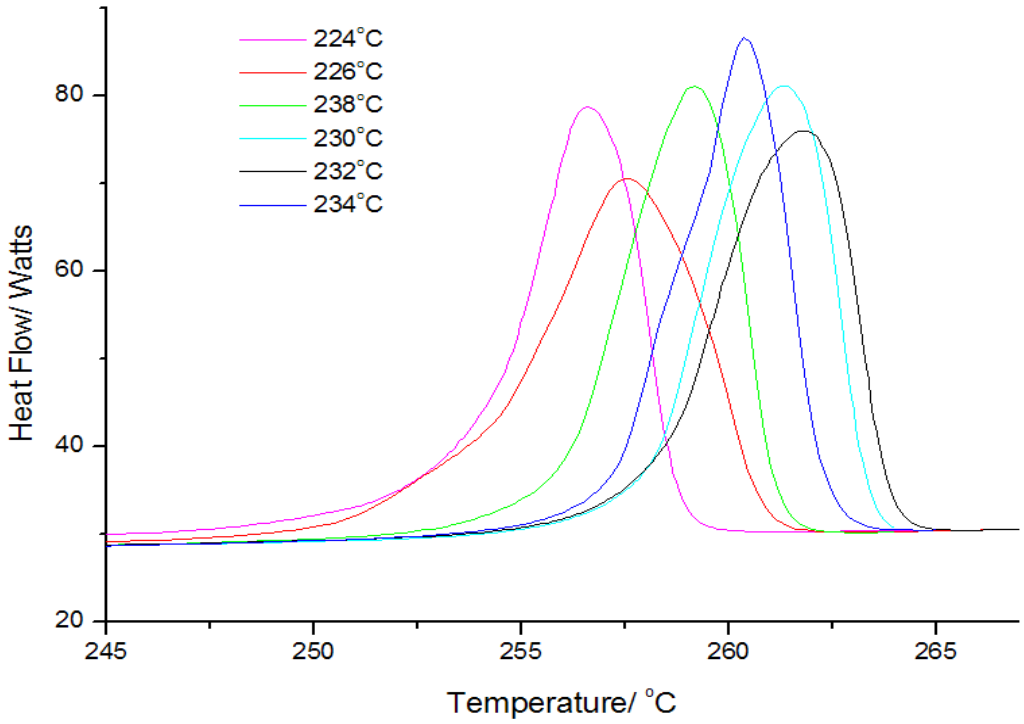

Figure 6.3A The Effect of Crystallization Temperature on Melting Range.

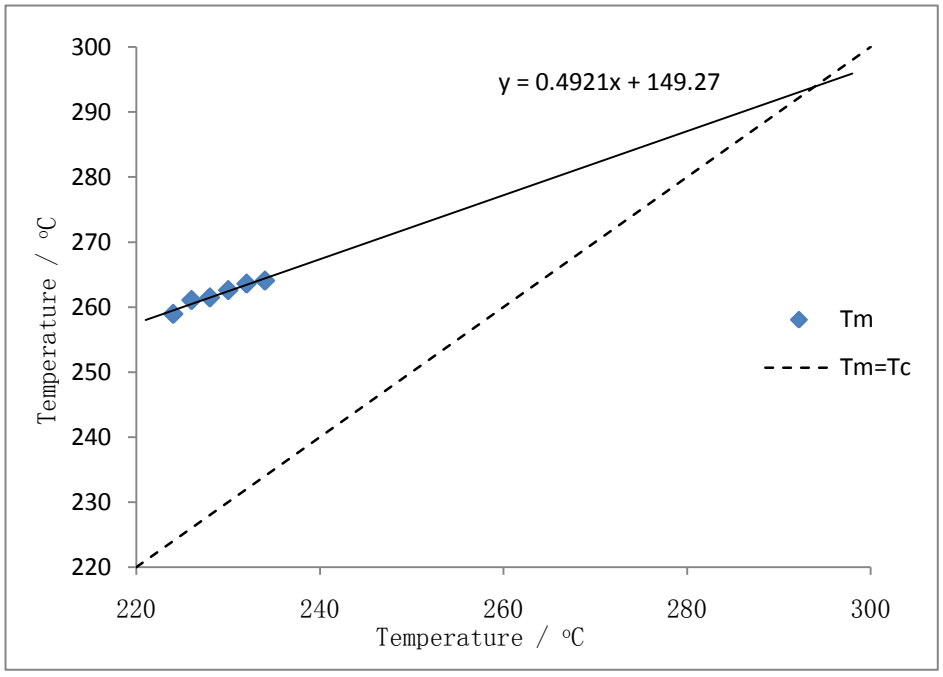

Figure 6.3B Hoffman-Week's plot for PET.

6.4 The Effect of Crystallization Time on Melting Behaviour.

Only two isothermal crystallization series, at 228 and 234 ^{o}C, were selected to study the melting behaviour of PET and in particular determine the effect of the secondary crystallization on the melting behaviour. The melting endotherms for the isothermally crystallized samples as a function of time are shown in Figures 6.4 and 6.5 in the time domain where secondary crystallization dominated, i.e. above 50 minutes. The endotherms were initially broad, melting over 20^{o} but narrowed and progressively moved to a higher temperature with time as secondary crystallization developed.

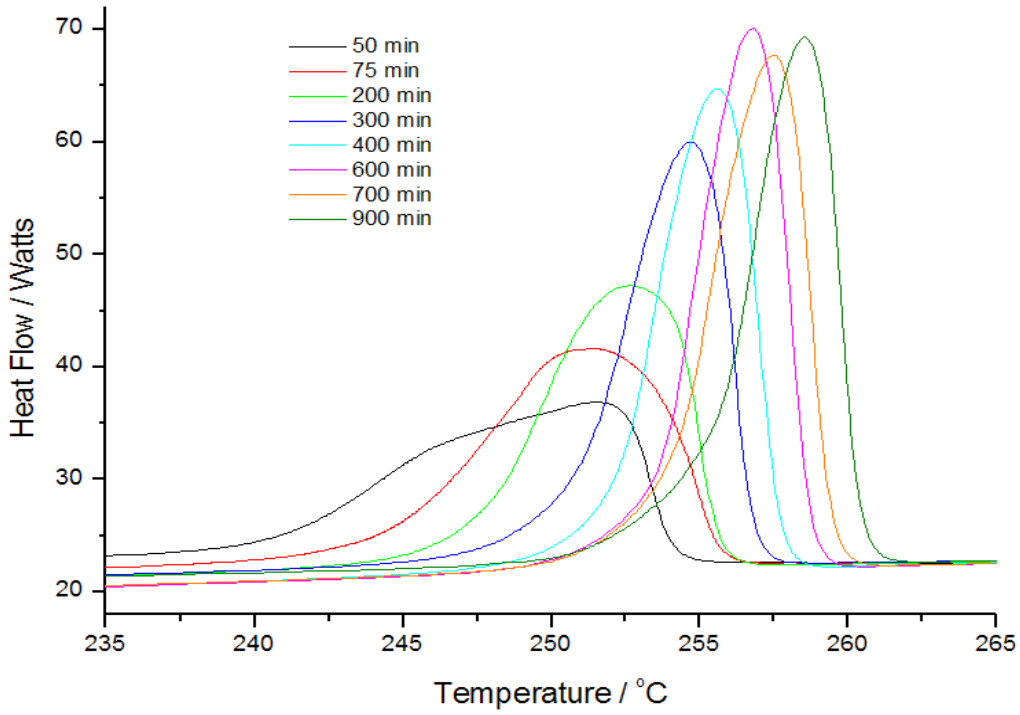

Figure 6.4 The Effect of Time on the Melting of PET crystallized at 228 ^{o}C.

As was shown in Chapter 5, the half-life for primary crystallization at 228 and 234 °C are 12 and 25 minutes. respectively, therefore the extending time scale of 50 to 1000 minutes fell within the secondary crystallization region and the change in melting behaviour is associated with a progressive thickening of the lamella as initially laid down.

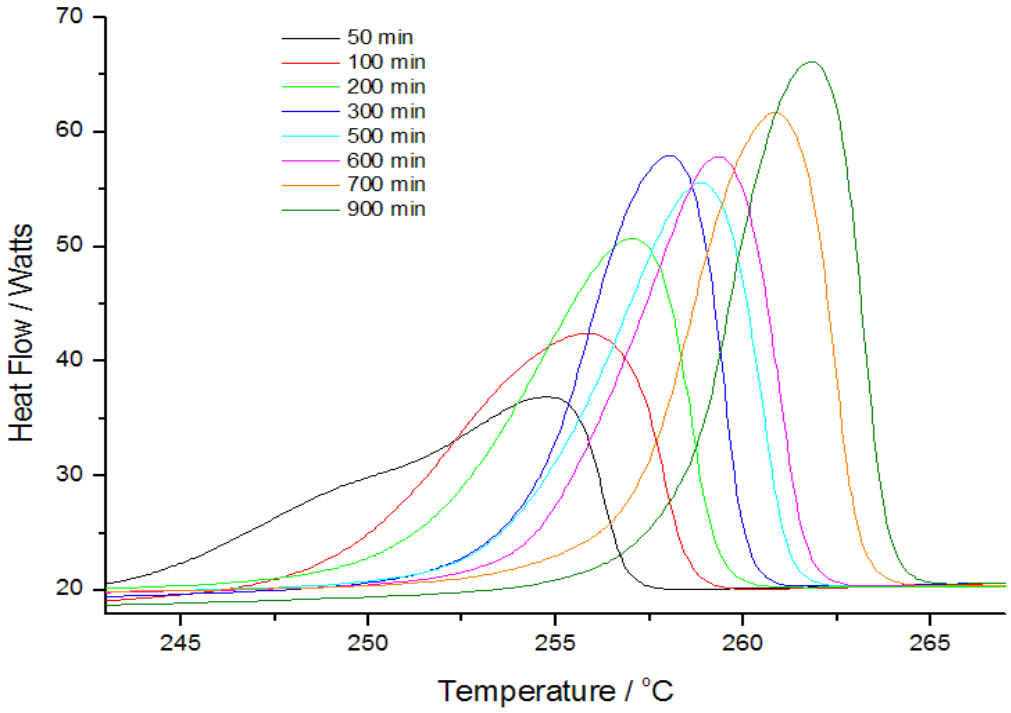

Figure 6.5 The Effect of Time on the Melting of PET crystallized at 234°C

With time the melting point increased from 254 to 262 °C at 228 °C and 257 to 265 °C at 234 °C respectively. The melting temperature defined as the last trace of crystallinity is a measure of the most stable and so thickest lamellae present in the sample. This linear increase in the melting point with time, see Figure 6.6, was

consistent with secondary crystallization being associated with the thickening of the lamellae and the growth of the crystal phase along the c direction of the unit cell.

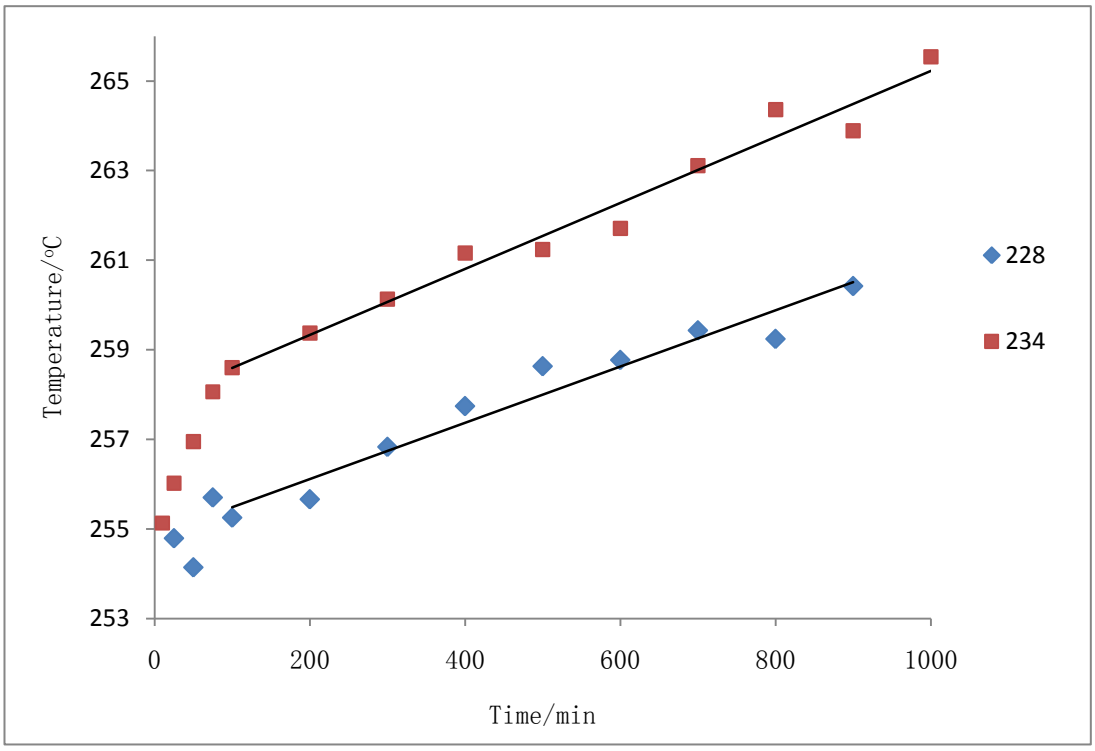

Figure 6.6 Changes in Melting Points with Time

The enthalpy of fusion of each sample was also determined by integrating the melting endotherms with time from the onset of melting to the last trace of crystallinity. This was used as a measure of the relative crystallinity of the samples and as can be seen from Figure 6.7 the heat of fusion or relative crystallinity increased linearly with log (time) above 50 minutes. The increase in crystallinity with log (time), as discussed in Chapter 5, is characteristic of secondary crystallization and dominates the transformation above 50 min.

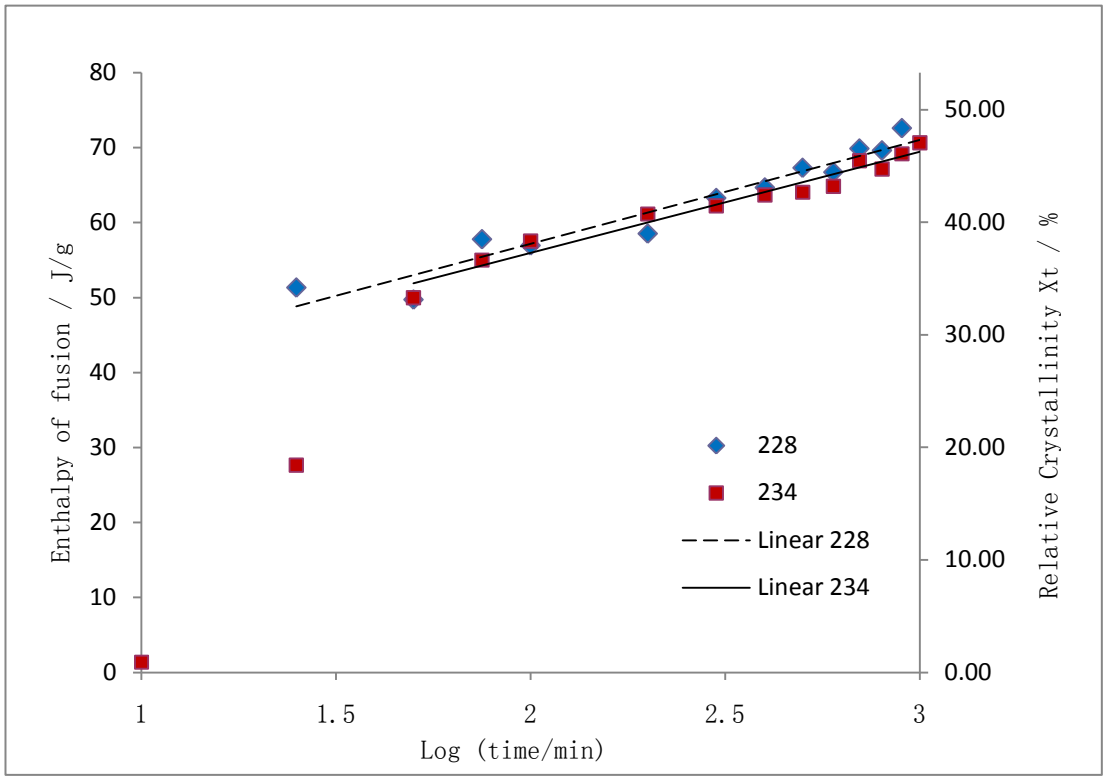

Figure 6.7 The Effect of log (time) on the Enthalpy of Fusion on Crystallizing at 228 and 234 ^{o}C.

6.5 Seeded Crystallization as measured by DSC.

In order to extend the study of secondary crystallization to higher temperatures Banks and Sharples' procedure was modified to enhance crystallization by seeding at these temperatures. The rate of crystallization at 250 and 252 ^{o}C is so low that it could not be detected by DSC in that quenching from the melt to 250 and 252 ^{o}C produced no exotherm but only a return to the calorimeter baseline.

PET was quenched to 234 ^{o}C from the melt and allowed to crystallize until the primary stage had been completed. This took 50 min. The sample was then heated

either to 250 or 252 ^{o}C and partially melted. The surviving crystals in the sample were subsequently used as seeds for crystallizing at 250 and 252 ^{o}C for extended periods of time.

DSC did not have the necessary sensitivity to follow the crystallization with time directly over this extended timescale and the relative crystallization and the change in lamella distribution was followed from the change in melting point and melting endotherms with time at 250 and 252 ^{o}C, see figures 6.8. The melting of PET crystallized at 234^{o}C for 50 minutes is shown as the red dotted line. It has a broad double distribution endotherm from 243 to 257 ^{o}C. However on heating to 250 and 252 ^{o}C the lower temperature melting distribution is removed entirely even after heating for a short period, 1.5 minutes. Further crystallization developed with time up to 1000 minutes. and at the same time the melting point moved to higher values.

On heating, the less stable lamellae melt and the stable ones which persist at the higher temperature act as seeds on subsequent crystallization.

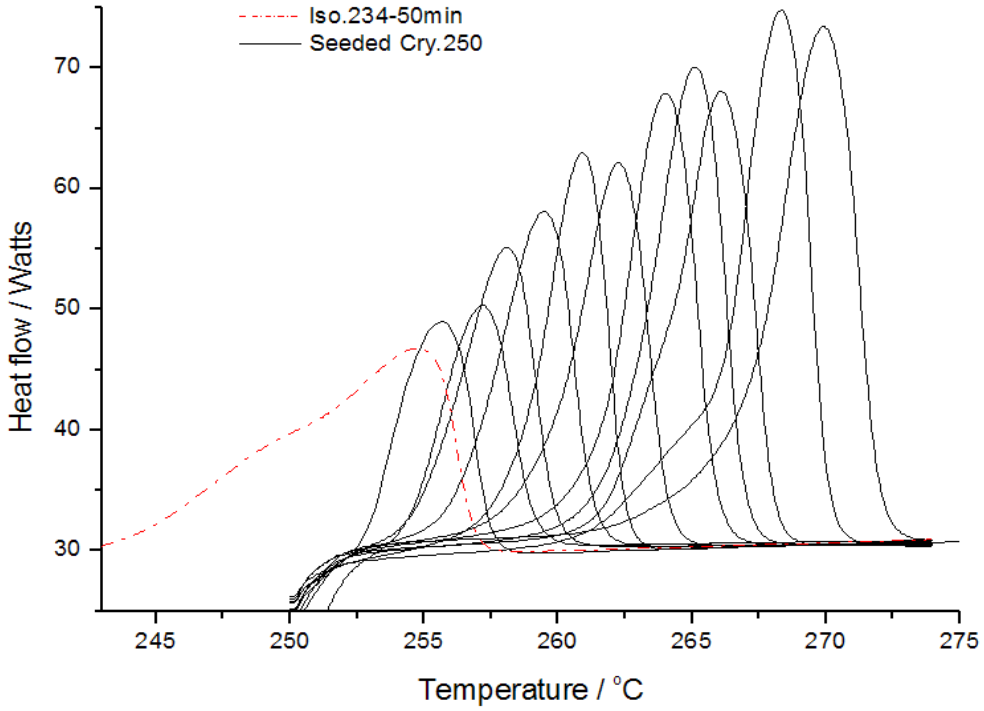

A.

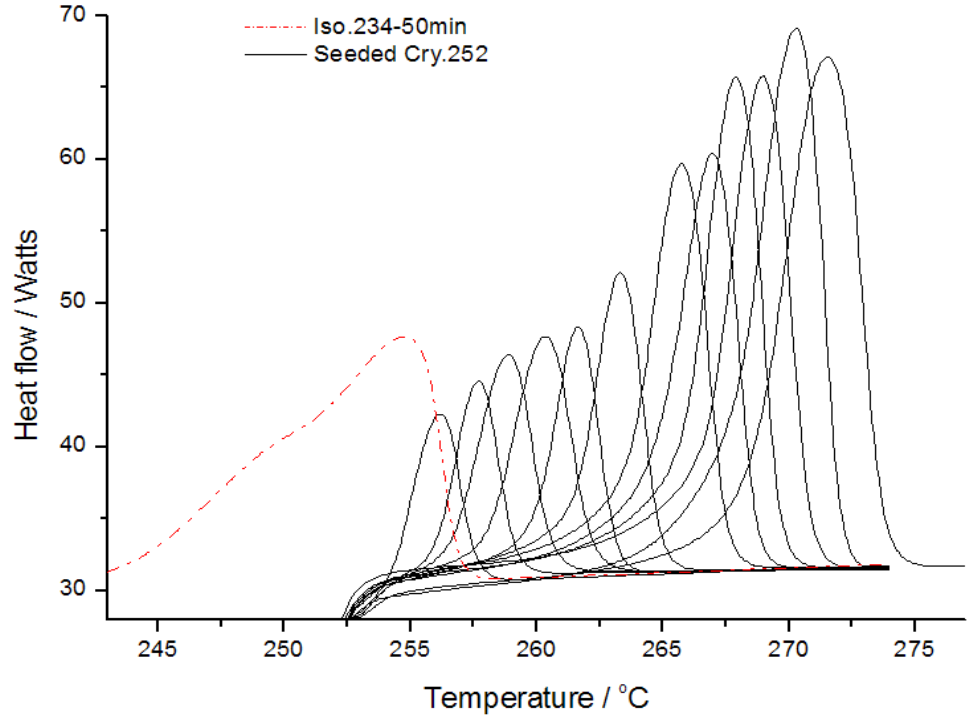

B.

Figure 6.8 Melting Endotherm of Seeded Crystallization of PET Samples. Crystallized at 234 °C for 50 min. (Red Dotted Curve). Crystallized at 234 °C for 50 min. and Heated to 250 °C (A) and 252 °C (B) and Held there for 1.5 to 950 min.

The seeded experiments at 252 ^{o}C were essentially identical in outcome to those carried out at 250 ^{o}C except that more of the crystalline material was removed on first heating to 252 ^{o}C and the lamellae produced melted at higher temperatures consistent with them being thicker and more stable. This can be seen more clearly in Figure 6.9 where the final melting points are plotted against time for both series and the material heated treated at the higher temperature has consistently higher melting points, see Figure 6.9. In both series the melting points increase with time as a result of the lamellae thickening.

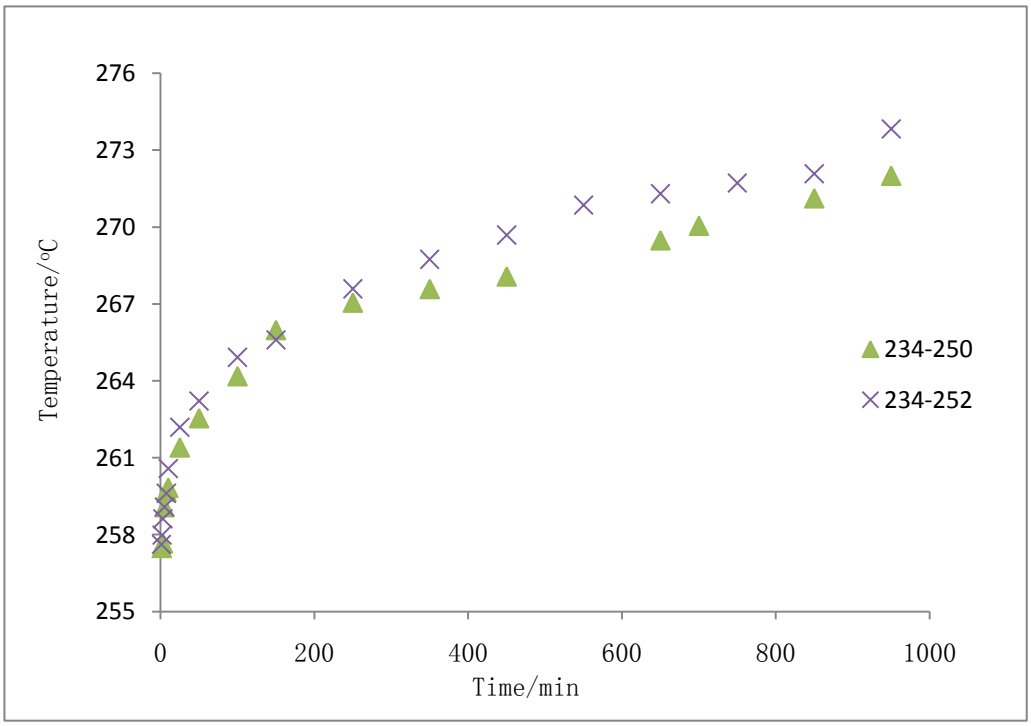

Figure 6.9 The Variation of Melting Point with Time.
Partial Melting at 250/252 ^{o}C.

The enthalpy of fusion of the various PET samples were measured by integrating the melting endotherms against time, as described above and the value used as a measure of relative crystallinity. The increase in enthalpy of fusion, and hence in crystallinity, with log (time) can be seen in Figure 6.10 for both series of seeded crystallizations; this increase was linear after an initial period of 10-30 min., consistent with the seeded crystallization developing by a secondary process.

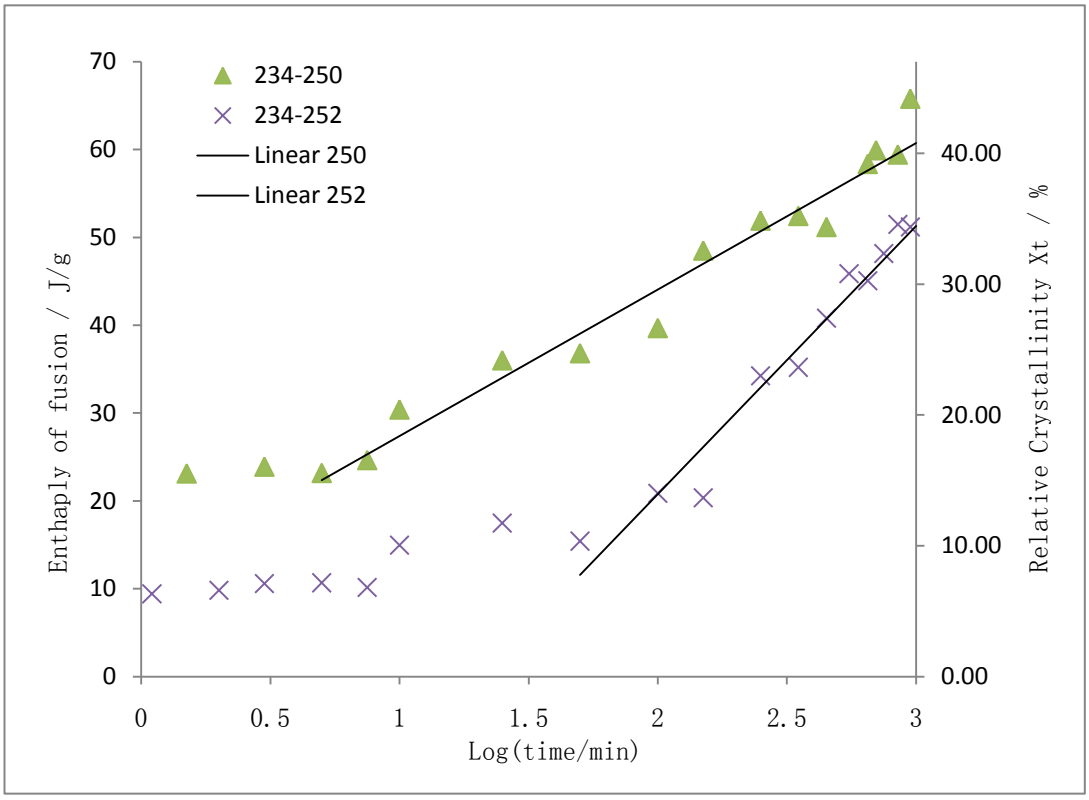

Figure 6.10 The Increase in Enthalpy of Fusion with log (time) on Heating to 250/252 °C.

6.6 Lamella Thickness of PET.

According to a model proposed by Flory and Vrij [166-168] for linear hydrocarbons and later modified by Hay [169, 170] for oligomers in general and for the case of ethylene terephthalate oligomers with uniform end groups, the melting temperature T_m for an oligomer with n repeat monomer units is given by

$$T_m \cong T_m^o[1 - 2RT_m \ln(n)/n\Delta h] \quad (6.2)$$

where Δh is the enthalpy of fusion per repeat unit of a completely crystalline oligomer (equal to 28.8 kJ monomer mol^{-1}) [105, 171] and R is the gas constant (equal to 8.314 $J{\cdot}K^{-1}{\cdot}mol^{-1}$.). T^o_m was taken to be 566 K.

By rearranging,

$$(T_m^o - T_m)/2RT_m^o T_m \Delta h = \ln(n)/n \quad (6.3)$$

For each value of T_m, ln(n)/n was calculated and the value of n read from a table of ln(n)/n values against n to an accuracy of 0.1 repeat units. While n as originally envisaged is the number of repeat units in an oligomer and so is an integer, in the context of polymers, it was considered to be an average value of a distribution of lamellae thicknesses and so could have non-integer values. Two averages values of n were calculated, namely the average lamellae thickness in the distribution as

determined by the maximum in the melting endotherm and also the largest lamellae thickness in the sample as determined by the temperature corresponding to the last trace of crystallinity.

Figures 6.11 and 6.12 show the increase in the number of repeat units in the average thickness with time calculated from the temperature corresponding to the maximum in the endotherm and also in the most stable lamellae calculated from the melting point. In each case the average lamellae are thicker at the higher temperature almost doubling in thickness between 228 and 252 ^{o}C.

From the unit cell dimensions of crystalline PET one repeat unit was taken to be 1.075 nm [172] and the thickness of the average lamellae is then 1.078xn nm.

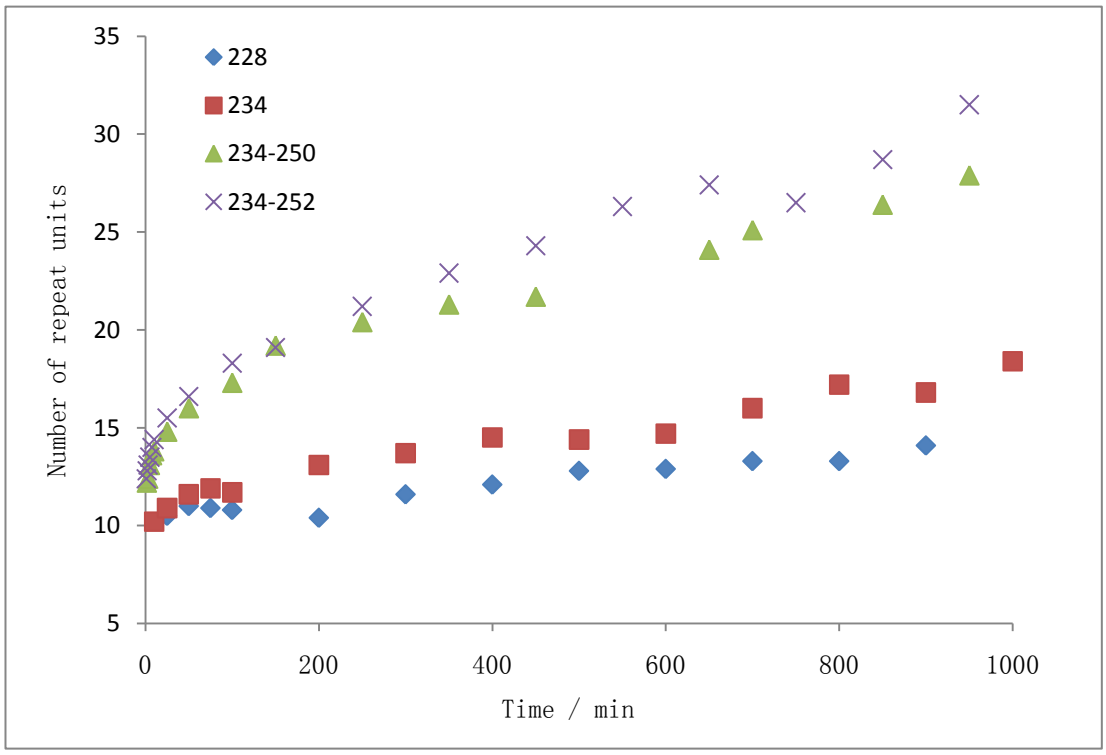

Figure 6.11 Increase in Number of Repeat Units in the Average Lamellae with Time at Different Crystallization Temperatures.

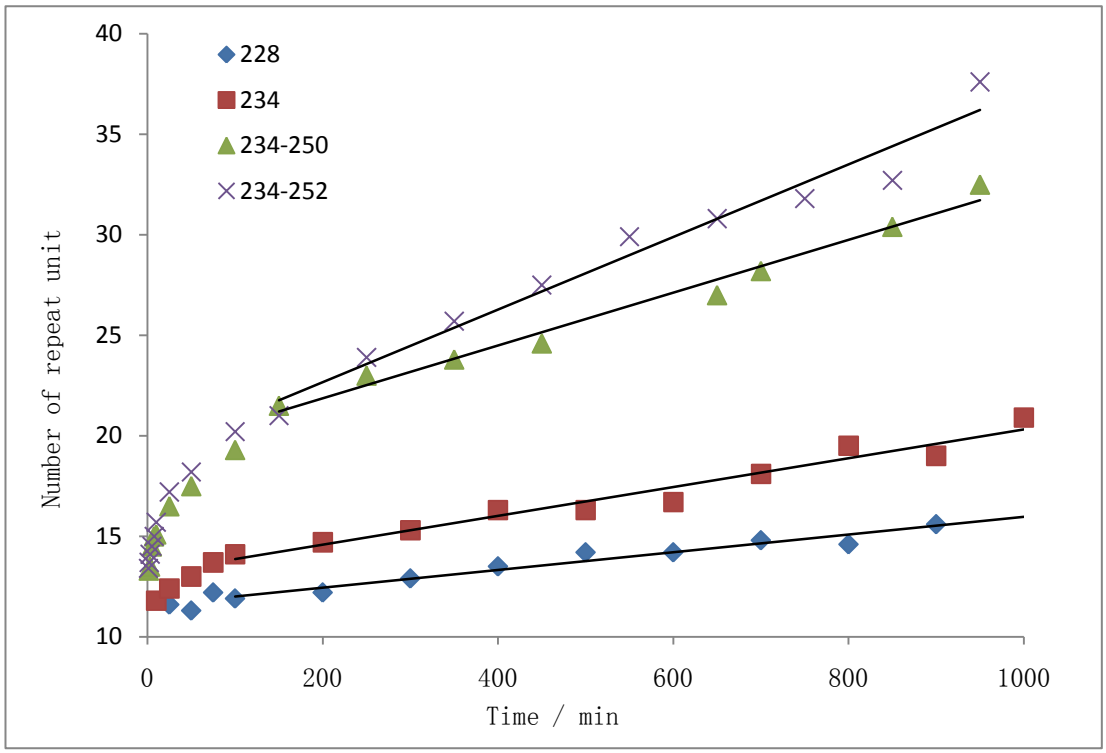

Figure 6.12 Increase in Number of Repeat Units in the Largest Lamellae with Time at Different Crystallization Temperatures.

Table 6.1 The Dependence of Lamellar Growth Rate, g, on Temperature.

Temperature / °C	252	250	234	228
Crystallization type	Seeded crystallization		Secondary crystallization	
Function	y = 0.0181x + 19.061	y = 0.0131x + 19.231	y = 0.0072x + 13.153	y = 0.0044x + 11.558
Crystal growth Rate g / m s^{-1} 10^{9}	0.65	0.23	0.125	0.079
Crystallinity	0.10	0.23	0.33	0.33

The lamellar thickening growth rates, g, were determined from the slopes of linear portions of the curves shown in Figure 6.12. The values obtained are listed in Table 6.1 and show an increase with increasing temperature and in the case of the seeded crystallization with decreasing seed content. This behaviour was unexpected but appears to imply that increasing crystalline content in the melt constrained the melt and slowed the growth rate proportionately.

6.7 Seeded Crystallization as studied by FTIR Spectroscopy.

FTIR spectroscopy has an advantage over DSC in being able to measure the changes in the crystallinity of PET from the absorbance of the crystalline or amorphous carbonyl bands at 1717 and 1727 cm^{-1} respectively. Accordingly the seeded crystallizations discussed above from the point of view of the melting behaviour as measured by DSC were also examined by FTIR spectroscopy.

Two series of seeded crystallization experiment were carried out following the procedure adopted above; firstly a sample was crystallized isothermally up to the end of the primary crystallization at 234 ^{o}C; this was followed by partial melting and re-crystallization at 244 and 250 ^{o}C measuring the change in crystallinity by FTIR spectroscopy. The carbonyl band, in the region 1710-30 cm^{-1} was resolved into its two components, amorphous and crystalline, and the absorbance followed with time,

see Figure 6.13 and 6.14. The initial change in absorbance at 1727 and 1717 cm^{-1} during the isothermal crystallization at 234 ^{o}C, has the inverse and S shape dependence respectively characteristic of the changes in amorphous and crystalline content of the primary process as observed previously and discussed in Chapter 5. On heating to 244 ^{o}C there is a small amount of melting as observed by a drop in crystalline absorbance followed by a linear increase with log (time). The small decrease in crystallinity on heating is consistent with the melting endotherms for the sample crystallized at 234 ^{o}C in Figures 6.5 and 6.8 which shows that little or no melting occurs at 244 ^{o}C. On further heating the crystallinity continued to increase linearly with log (time), consistent with a secondary crystallization process developing on the seeds produced at the lower temperature. These FTIR spectroscopic results are consistent with those observed by DSC in that the crystallinity increases linearly with log (time) at 244 ^{o}C and has the characteristics of a secondary isothermal process at 244 ^{o}C produced after the primary process took place at 234 ^{o}C.

In order to have a better comparison with the DSC seeded experiments the procedure was repeated but the crystallization temperature was raised from 244 to 250 ^{o}C. This enabled more material to melt before crystallization developed further on the residual seeds. The change in the absorption of the crystalline and amorphous

bands with log (time) is shown in Figure 6.14. At the higher temperature the crystallinity initially dropped on heating to 250 ^{o}C to about a third of that which had developed at the end of the primary process. Thereafter on further heating the crystallinity increased linearly with a log (time) dependence characteristic of secondary crystallization,

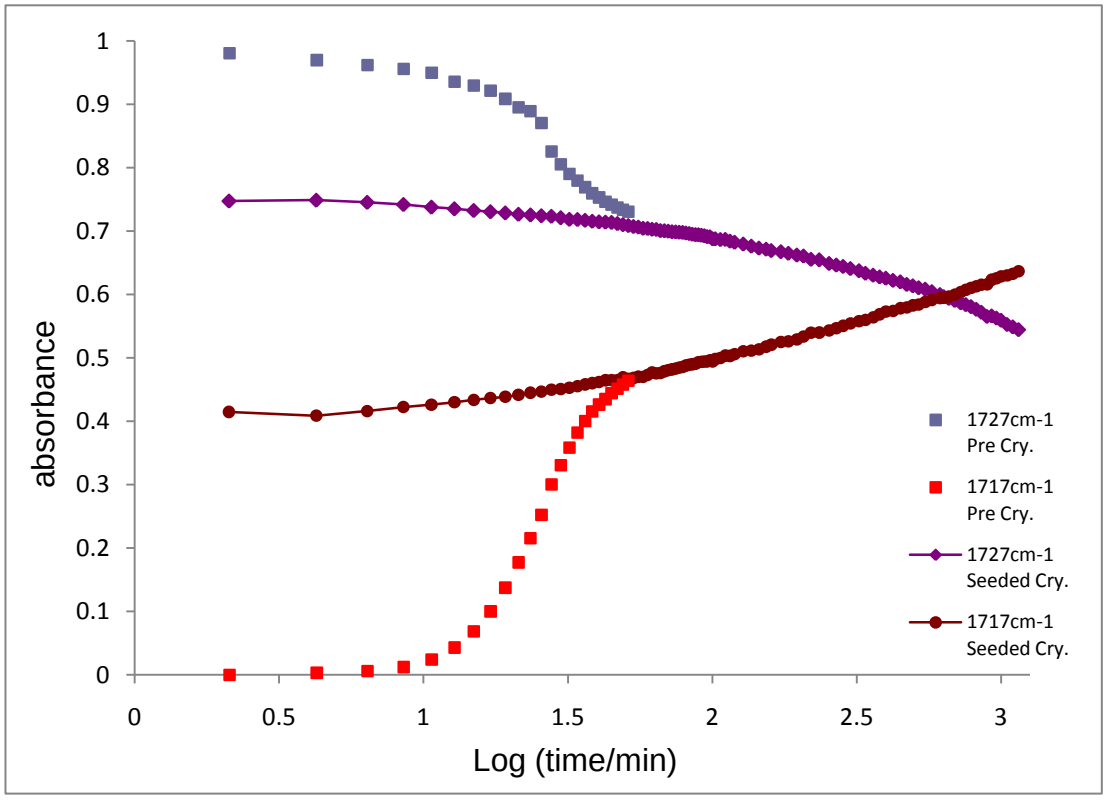

Figure 6.13 The Change in Absorbance of Carbonyl Bands with Log (Time/ min) Crystallization at 234 ^{o}C for 50 min and then at 244 ^{o}C.

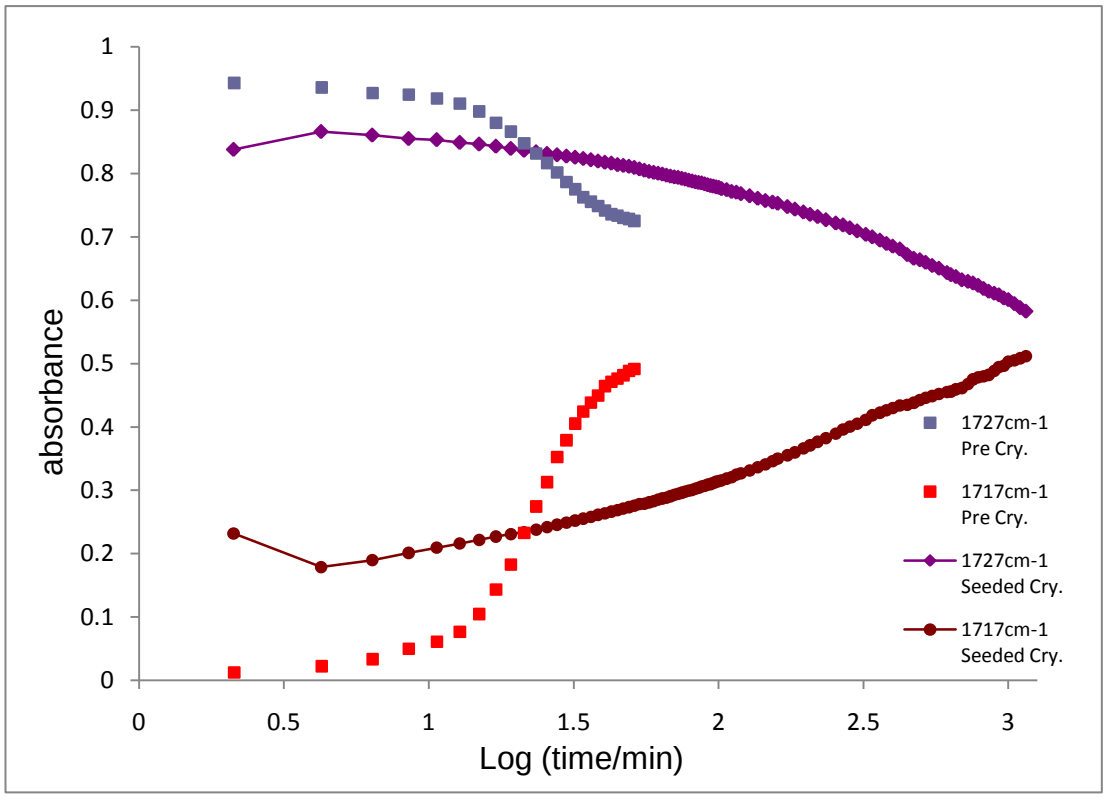

Figure 6.14 The Change in Absorbance of Carbonyl Bands with Log (Time/ min) Crystallized at 234°C for 50 min and then at 250 °C.

6.8 Discussion.

The development of crystallization on seeding with time as measured by the increase in carbonyl absorption band at 1717 cm^{-1}, see Figures 6.13 and 6.14, and was analyzed by a modified Avrami equation, i.e.

$$X_t = X_{p,f} + X_{s,f}(1- \exp -Z(t-t_{p,f})^n) \qquad (6.4)$$

where X_t is the crystallinity developed at time t, $X_{p,f}$ the residual crystallinity left after partial melting and $X_{s,f}$ the final crystallinity achieved by the seeded

crystallization. n is the Avrami constant, Z the composite rate constant, Z_s, and $t_{p,f,}$ the time corresponding to the value of $X_{p,f}$.

Since $X_t = A_t/A_0$, $X_{p,f} = A_{s,f}/A_0$ and $X_{s,f} = A_{s,f}/A_0$, where A_0 is the absorbance of a totally crystalline sample at the crystallization temperature fractional crystallinities were measured from the corresponding absorbances. Rate parameters were obtained from a plot of log (-ln (1-((X_t- $X_{p,f}$)/$X_{s,f}$) against log t, see Figure 6.15 and are listed in Table 6.2. An excellent linear fit of Eq.[6.4] to the data, R^2 = 0.9992, was observed with an n value of 0.7 $\pm$ 0.1 in line with a secondary crystallization process.

Table 6.2 Avrami Rate Parameters for Seeded Crystallizations.

Crystallization Temperature, T_c / ^oC	244	250
n_s $\pm$ 0.1	0.74	0.68
Z_s / s^{-n} x10^3	0.74	1.45
$X_{p,\infty}$	0.415	0.179
$X_{s,\infty}$	0.639	0.512
$t_{1/2}$ /s x 10^3	10.34	9.06

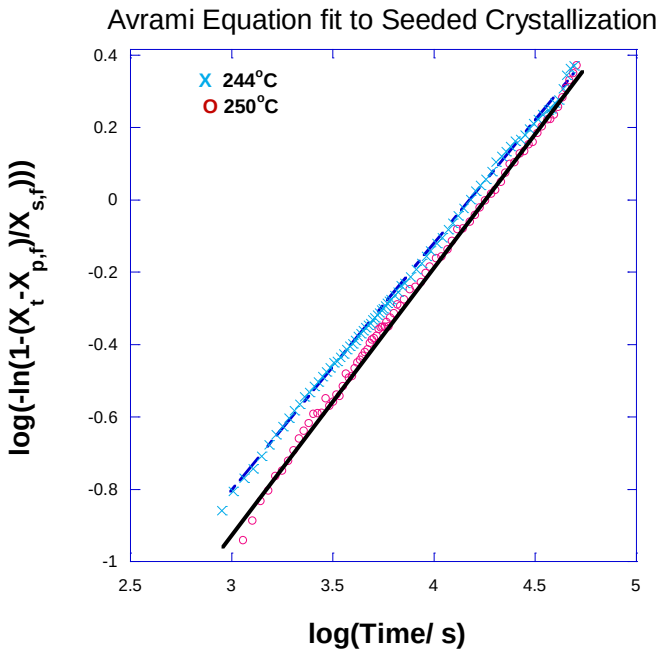

Figure 6.15 Fit of the Avrami Equation to the Development of Crystallinity with Time for the Seeded Crystallization.

In terms of the crystallization mechanism used by Avrami to derive the equation a value of 1.0 for n is consistent with one dimension growth of the lamellae and from the discussion above this is associated with a thickening of the lamellae.

If the cross sectional area of the growth front is A the composite rate constant,

$$Z = ANg \qquad (6.5)$$

where N is the density of heterogeneous nuclei, i.e. the number per unit volume and g the linear growth rate.

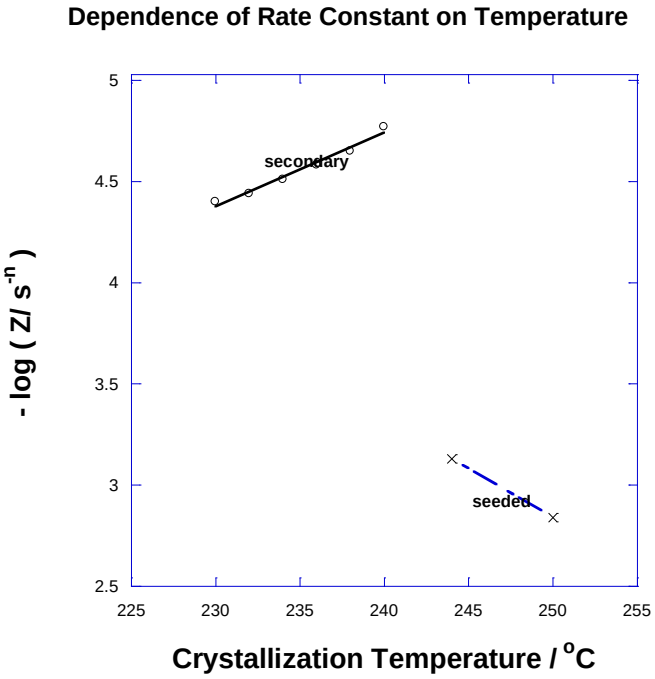

Figure 6.16 Dependence of Composite Rate Constant on Crystallization Temperature.

Unlike secondary crystallization where the crystallization rate constant depended on Regime II nucleation, see Chapter 5, and Z decreased with temperature, Z for the seeded crystallization increased. The increase in Z for seeded crystallization was not marked for the difference of 6 ^{o}C in temperature but could either be due to an increase in number of seed nuclei produced on partial melting or an increase in the of growth rate, g.

If $X_{p,f}$ the degree of crystallinity after partial melting is a measure of the number of seeds present at the beginning of the seeded crystallization Z was, however,

observed to decrease with the seed fraction, see Figure 6.17,which suggests that the nucleation density cannot account for the difference in rate. The growth rate, g, must increase with temperature.

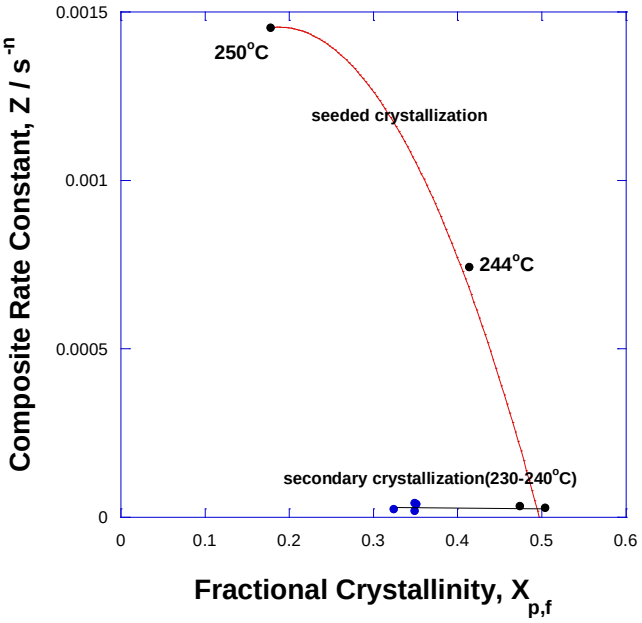

Figure 6.17 The Dependence of Composite Rate Constant (Z / s^{-n}) on the Amount of Residual Crystallinity.

6.9 Seeded Crystallization on Hot-stage Microscopy.

Seeded crystallizations were also carried out using a hot-stage polarized light optical microscope. Thin film samples mounted between glass cover slips were placed in the furnace of the hot stage and melted. They were crystallized at 234 ^{o}C for 50 min. to enable the primary crystallization process to complete. The sample was partially melted by heating to 252 ^{o}C and subsequently left to crystallize at this

temperature. The birefringent structures viewed under cross polarizers are shown in Figure 6.18.

Micrograph A shows the birefringent pattern of the crystallized sample. The texture is non-resolvable but is made up of crystalline particles, perhaps micro-spherulites. On partial melting the birefringence disappears, micrograph B, but with time is replaced with a courser grained birefringent texture, micrograph C. When the sample was cooled to room temperature, the birefringence increased, see micrograph D. This must be due to further crystallinity developing in the PET as it is cooled.

These observations were not inconsistent with the seeded mechanism proposed but since the spherulites were not resolvable evidence for seeded crystallization on partial melting was not obvious.

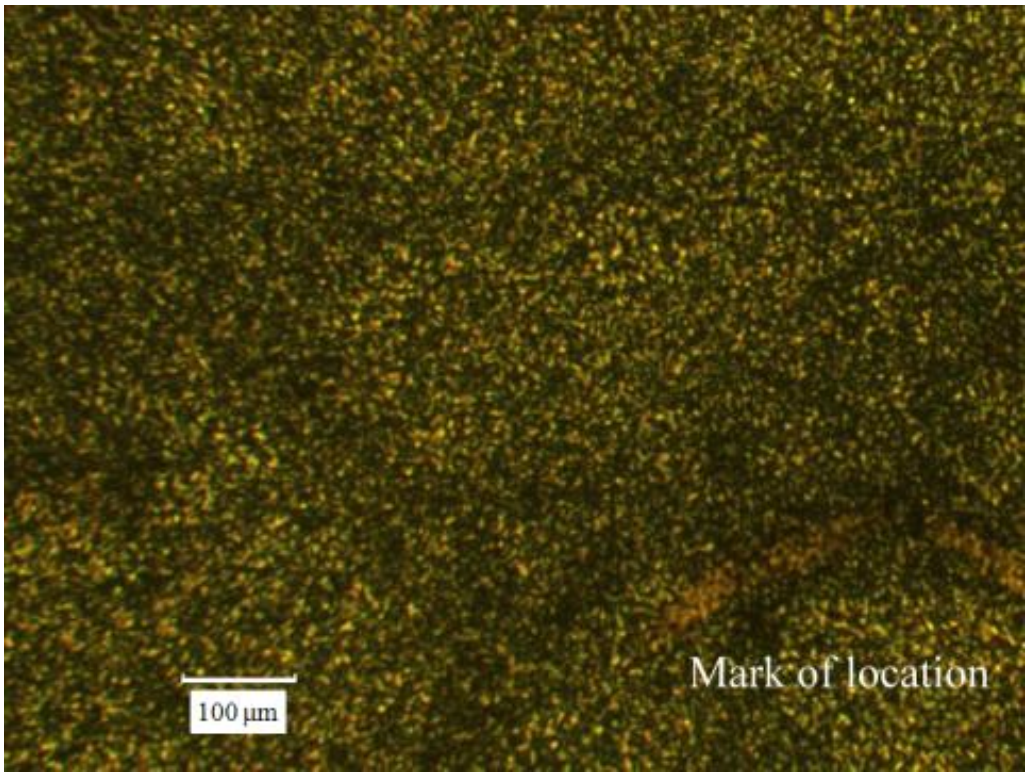

Figure 6.18A. Crystallization at 234^{o}C for 50 min

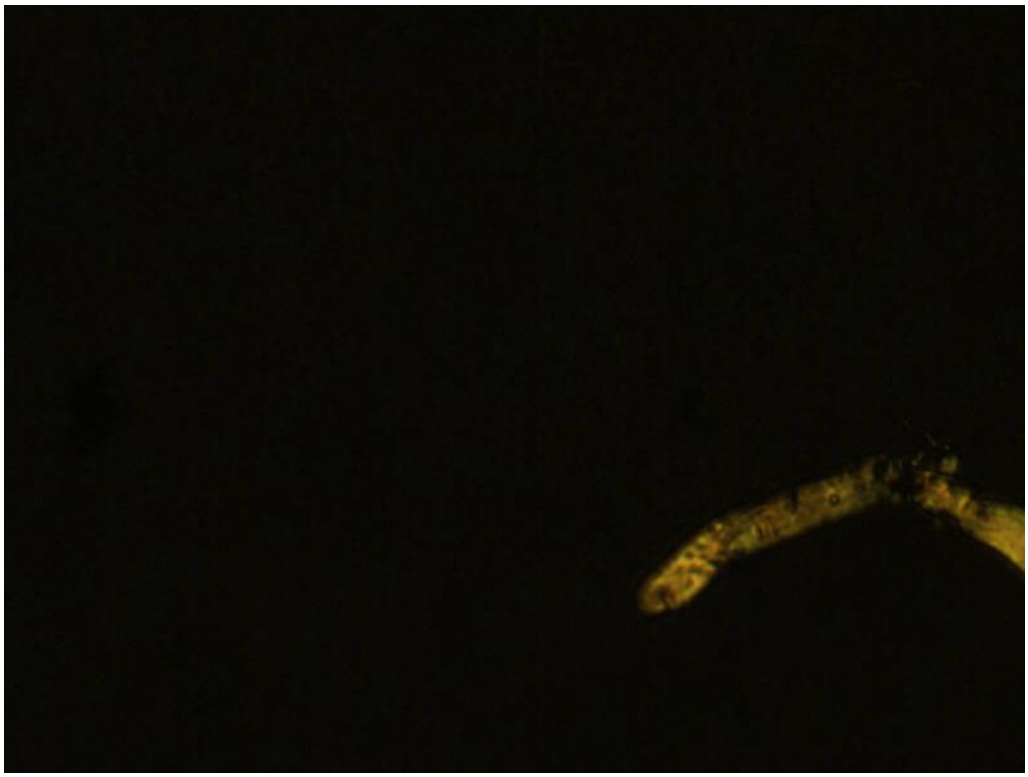

Figure 6.18B. Partial Melting at 252 ^{o}C

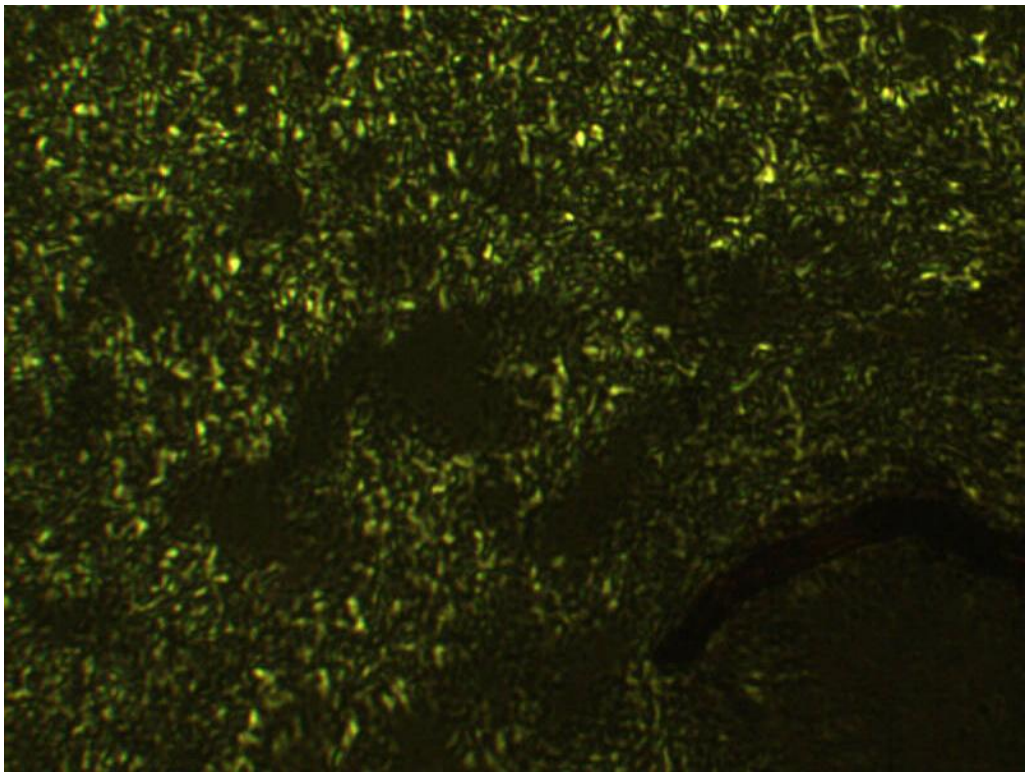

C. Seeded Crystallization at 252^{o}C for 1000 min

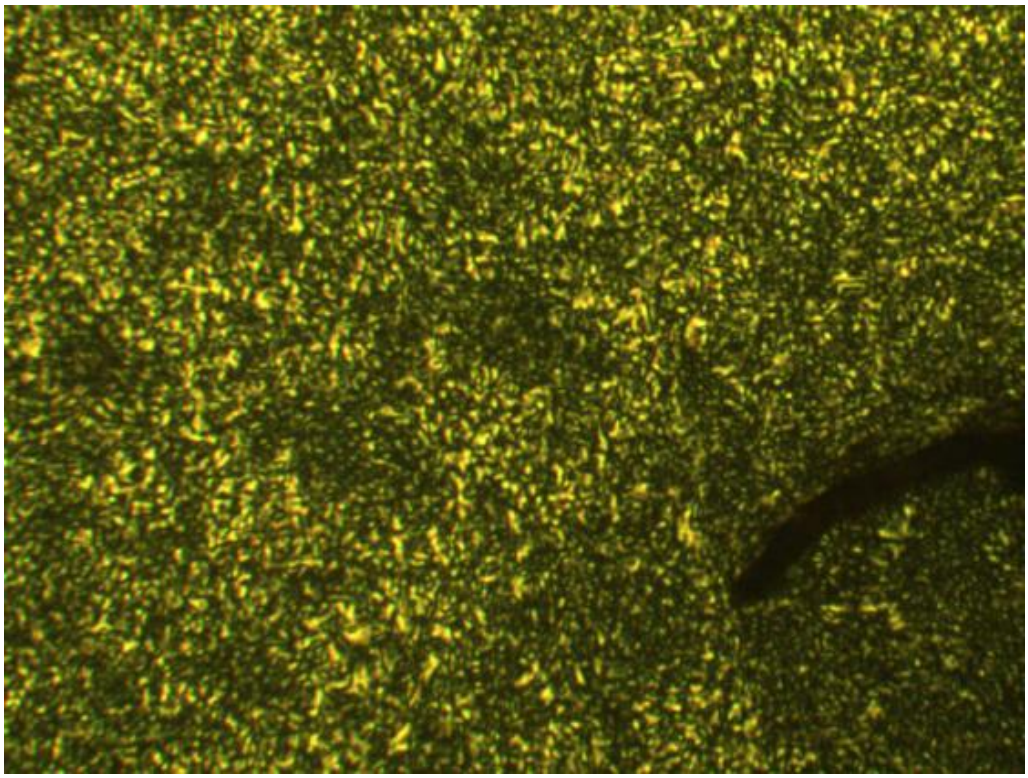

D. Cool Back to Room Temperatture.

Figure 6.18 Hot-stage Microscopy Image of Seeded Crystallization of PET.

6.10 Conclusion

DSC with its limited sensitivity could not be used to measure the rate of secondary crystallization directly with time over the extended periods involved. Nevertheless, by determining the heat of fusion the fractional crystallinity could be determined with temperature and time. A linear dependence of the fractional crystallinity with log (time) was confirmed for the secondary process. The melting point at the end of the primary crystallization was used to determine the equilibrium melting point of PET by extrapolation of the dependence of melting point with crystallization temperature. Analysis of the melting endotherms showed that the lamellae thickened with increasing crystallization temperature and with time at constant temperature. Accordingly, secondary crystallization was attributed to one dimensional thickening of the lamellae. The lamella growth was linear with time during isothermal crystallization and increased with the temperature.

Seeded crystallization was used to increase the temperature range over which the crystallization could be measured and in particular into the melting temperature region. By partial melting the residual crystalline material could be used to develop further crystallinity. However, this developed with all the rate characteristics of secondary crystallization in that the development of the transition corresponded to dependence on time with exponent of 0.7 ± 0.1, compared with 0.8-0.9. Similarly

during seeded crystallization the lamellae thickness increased with temperature and time.

The composite rate constant for seeded crystallization was, however, complicated as it was controlled by the cross sectional area of growth face, the nucleation density and the linear growth rate. Partial melting conditions, melting temperature and time, controlled the initial seed crystallinity and this in turn determined the nucleation area and density. At higher partial melting and temperature, the total area and seed density was small but the composite rate constant and linear growth rate was large. This cannot be explained in terms of nucleation theory which predicts a decrease in rate with increasing crystallization temperature but implies a greater mobility in the melt constrained by the adjacent seed crystals. Such that the lower the seed density the greater the melt mobility and the crystalline growth rate. This assumption has not been considered further in this study.

Chapter Seven

Conclusion and Future Work

7.1 Conclusion.

The study of the thermal properties using TA-FTIR in conjunction with DSC has been most informative and useful in dealing with many interesting crystallization problems in PET. Many of these have been successfully solved, not least of which is the characterization of the IR bands in the spectrum of PET, measuring the fractional crystallinity during crystallization and the kinetics of primary, secondary and seeded crystallization. The novel technique of 2D correlation spectroscopy has been investigated, along with the change in absorbance and peak position as a function of temperature on heating and cooling; both together have been invaluable in explaining the complex IR spectrum of PET in terms of chain conformation and cis/trans isomerization. There is little doubt, however, that such analyses would not have been available but for recent developments in software and data handling associated with FTIR spectroscopy.

TA-FTIR has been used to characterize phase transitions by a change in the absorbance or peak position with temperature in heating and cooling cycles. It has the advantage of assigning the phase transition temperature to an individual chain segment rather than other TA techniques, which averages over all them all.

Two different types of behaviours were observed; type I in which the absorbance changed stepwise at the transition temperature and type II in which there was no change in absorbance but a shift in peak position. The temperature dependence of the absorbance was associated with the change in concentration of rotational modes in the molecular chain and the establishment of a dynamic equilibrium between the conformational cis/trans isomers. The onset of chain mobility and the establishment of this equilibrium enabled the glass transition of the polymer to be determined from the change in slope of the absorbance with temperature. As the trans isomers alone is incorporated in the crystalline regions and the cis and trans isomers exist together in the amorphous phase, changes in absorbance follow the fractional crystallinity. The fractional crystallinity of the polymer can accordingly be determined at any temperature from the ratio of the trans/cis bands.

Type II behaviour is associated with no stepwise change in absorbance on crystallizing or melting but is associate with a change in peak position between the

cis and the trans conformational isomers. It occurs when the absorption bands from the two isomers substantially overlap and have very similar extinction coefficients. Accordingly there is little or no change in absorbance on crystallizing or melting but a change in peak position. In this way it was established that the band at 1410 cm^{-1} was not invariant with temperature or crystallinity and should not be used as an internal standard as it has been in the past. It would be interesting to see if TA-FTIR would be as successful in interpreting the phase transitions in other crystallizable polyesters as it has been in PET.

Many bands in the IR spectrum of PET split into pairs on crystallizing or melting either due to the different environment the molecular groups experience in the crystal from that in amorphous regions or they are associated with the cis or trans conformation of chain segments. In particular the carbonyl stretching band has an amorphous band at 1727 cm^{-1} in the melt and a crystalline band at 1717 cm^{-1}. These two bands have sufficient wavenumber separation for the Omnic software to deconvolute the two components and determine the fractional crystallinity from the absorption ratio. 2-D auto-correlation spectroscopy was successfully applied to these two bands since it showed that the 1727 cm^{-1} band disappeared with time and was progressively replaced by a sharper band at the lower wavenumber. The synchronous and asymmetric correlation spectra had the characteristic “angel” pattern and two

cross peaks associated with the transformation from one IR band to another at different wavenumbers and intensities. The bands could be assigned unambiguously to amorphous and crystalline regions and used to determine the fractional crystallinity with time. There is some evidence that bands at 1727 and 1717 cm^{-1} arose from environmental differences between crystalline solid and amorphous liquid rather than the transition from cis to trans isomers of the carbonyl groups. However, the bands were suitable for a kinetic study of the crystallization of PET.

All the absorption bands in the spectra of amorphous and partially crystalline PET were similarly analyzed by 2D-IR correlation spectroscopy and assigned to crystalline or amorphous molecular grouping in the polymer chains and to cis and trans conformers of various chain segments. Accordingly the complex spectra of PET with almost 50 absorption bands have been assigned. Many of the absorption bands behaved as pairs and increased or decreased in intensity on crystallizing or melting. These behaved in a similar fashion to the carbonyl band and exhibited "angel" and "butterfly" patterns in their synchronous and asynchronous correlation spectra respectively. The technique was useful in characterizing those bands which have multiple components that shift and change intensity during conformation change as this helped to assign them to rotational isomers and crystalline and

amorphous bands. Few of the bands, if any, did not change in this manner particularly the one previously assigned as an internal standard.

The isothermal crystallization kinetics of PET was measured in the temperature range from 230 to 240 ^{o}C by FTIR spectroscopy from the intensities of the crystalline and amorphous bands of the carbonyl ester group. The two overlapping absorption bands were readily deconvoluted by the Omnic software into separated components and the fractional crystallinity determined as a function of time. Since the procedure measured the fractional crystallinity directly and not the rate of crystallinity the analysis was not limited by the sensitivity of the measurements and the temperature range for crystallization kinetics study could have been expanded to higher temperature, slower crystallization rates and longer periods thus the secondary crystallization process could be measured to a reasonable degree of accuracy, unlike in the DSC studies where its limited sensitivity restricted the rates of crystallization which could be measured.

It was possible to analyze the kinetics of both primary and secondary crystallization by assuming that they obeyed Avrami equations, with different n values and that the two occurred one after the other; a value could be assigned to $X_{p,\infty}$ at which the primary process terminated and the secondary started.

The Avrami exponents n were determined as 2.0 for primary and 1.0 for secondary process. This was attributed to the crystallization of predetermined spherical particles, i.e. spherulites limited by the PET film thickness to 1.5 to 3 μm and so constrained to grow in two dimensions for most of their crystallization. SEM measured the diameter of PET spherulites as 10-20 μm. and the diameter of the spherulites attained the thickness of the film in the early stages of the primary crystallization.

DSC kinetic measurement were made on much thicker specimens, 1-2 mm, and the measured n values of 2.6-3.4 were consistent with three dimension growth of spherulites. This is a case where the crystallization kinetics is defined by sample dimension; thin film is dominated by 2-dimensional growth and thicker specimens by three. But nevertheless the crystallization behaves exactly as prediction by the Avrami's models for 2- and 3- dimensional growth of predetermined spherical particles.

A value of 1.0 was obtained for the n value of secondary crystallization and this was interpreted as one dimensional thickening of the lamellae within the internal structure of the spherulites.

The growth rate of the primary process was nucleation controlled increasing with super-cooling and initiated by secondary nuclei in Regime I while that of the

secondary was nucleated in Regime II. The FTIR spectroscopic analysis of the kinetics was consistent with the proposed crystallization mechanism.

While the kinetics of crystallization could only be directly measured over the primary process by DSC due to limiting sensitivity, the increase in crystallinity could be extended into the secondary process by measurement of the enthalpy of fusion, and from this the fractional crystallinity. These measurements were very time consuming and limited by the number of individual measurements which could sensibly be made. Nevertheless the development of crystallinity after the initial primary process followed a linear dependence with log (time) as observed previously for the secondary process.

Melting was also observed to drift to higher temperatures and to narrow with increasing crystallization temperature at constant crystallinity and with increasing crystallization time at constant temperature. This was interpreted firstly as due to an increase in lamellae thickness due to nucleation control of the critical size nuclei and from which the equilibrium melting point of PET was determined and secondly to an increase in lamellae thickness as a result of secondary crystallization such that increasing time periods increased the crystallinity and melting range. Accordingly secondary crystallization was attributed to linear growth of the ab surface of the PET

unit cell along the c direction into the melt between adjacent lamellae within the spherulites.

The melting endotherms were interpreted assuming that the melting point were determined by the thickness of the lamellae and the relative amount present in the crystalline sample was proportional to the height of the endotherm above the baseline at that temperature and accordingly the increase in average thickness and the thickest lamellae were determined as a function of temperature. A linear increase in thickness with time was observed which was taken to be a measure of the growth rate of the lamellae in the chain direction, g. This was observed to increase with increasing temperature. Although the increase was not large it did not agree with nucleation control of growth and suggested that the linear growth of the lamellae was inhibited by increasing crystallinity and increasing constraint imposed by the crystalline lamellae on adjacent regions of the melt.

Self-seeding was used to extend the temperature range over which crystallization rates could be measured and Banks and Sharples' procedure of partially melting the sample and using the residual un-melted material as seeds was adopted. However, these seeds were allowed to re-crystallize at the partial melting temperature rather than cooled to previous crystallization temperature. After an initially settling down period the seeded crystallization followed the same time

dependence of secondary crystallization but the rate constant was much greater and increased with increasing temperature which implied that the kinetics of seeded crystallization much more complicated than expected. It would appear to be controlled by the growth surface area, the number of seeds and the linear growth rate. The effects of these on the kinetics of seeded crystallizations require to be separately studied.

A higher partial melting crystallization temperature leads to lower residual crystallinity and results in a smaller number of seeds and growth area. The first will increase the crystallization rate by increasing the chain mobility and reducing constraints on the melt while the second effect will reduce the crystallization rate. A lower partial melting temperature has the opposite effect since it leads to a higher initial crystallinity, greater surface area and a larger number of seeds. This first reduces the rate of crystallization by increasingly constraining the melt and the second increases the rate proportional to the number of seeds. Experiments have to be designed to eliminate some of these variables before their effect on seeding can be evaluated.

Seeded crystallization provides for the possibility of crystallizing polymers at higher temperatures, even located in the normal melting temperature region, to

produce greater lamellae thicknesses and higher melting temperature and to consider the effect of this morphology on their mechanical and physical properties.

7.2 Future Work.

- **Application of Two-dimensional Infrared Spectroscopy**

Polarized IR and dichroic IR experiments are recommended to be carried out on PET at high yield rate to determine the effect of draw ratio on the IR spectrum. Orientation should increase the amount of trans isomers present in the sample and at high temperatures above T_g encourage the development of crystallinity. This should be followed up by 2D-FTIR analysis to separate the effects of crystallization and orientation of PET on its spectrum and over a wide range of temperature, to establish regimes when they occur together and separately

Once the degree of orientation and fractional crystallinity can be separately kinetic rate studies can be made to determine under what conditions crystallization accompanies orientation and the effect of orientation on the crystallization kinetics.

- **Seeded Crystallization**

Self-seeding appears to be a useful technique to extend the temperature range over which crystallization kinetics can be studied. However, it is more complicated than expected as it is controlled by three additional factors which do not occur in conventional rate studies, namely crystal growth area, number of seeds and the linear growth rate. Their effect on the crystallization rate should be separately studied by controlling the fraction of material melted and the isothermal temperature. By setting the amount of partial melting constant, the temperature dependence of the rate constant can be measured and the effect of super-cooling checked for nucleation control. By varying the amount of partial melting and keeping the crystallization temperature constant the retardation of the growth by increasing crystallinity can be better established.

Since the increased time period for secondary and seeded isothermal crystallization can generate crystalline material with thicker lamellae PET with this morphology may have improved mechanical and physical properties. Tensile specimens with this structure should be prepared for mechanical properties test and compared with conventional samples.

- **SEM Micro structure of Seeded Crystallization**

High resolution SEM is recommended to study the different micro-structures of PET produced by seeded crystallization, isothermal crystallization and on slow cooling to room temperature. It would be interesting to see what differences in morphology are present and determine the size of the crystalline particles present. This would establish the difference in nucleation density between seeded and conventionally crystallized material.

- **Chemical Technology in Industry**

Self-seeding may have advantages over added seeding agents in the temperature range in which they are active, the morphologies produced and should not lead to deleterious effects in thermal and oxidative stability.

Application of the technique in industry may help achieve production of material with higher crystallinity, thicker lamellae and improved mechanical and physical properties. It may also provide a way to reduce the use of nucleating agents, improve the purity of the polymer and be more environmental friendly.

Reference

1. Gumther, B. and H.G. Zachmann, *Influence of Molar Mass and Catalysts on the Kinetics of Crystallization and on the Orientation of Poly(Ethylene-Terephthalate).* Polymer, 1983. **24**(8): p. 1008-1014.
2. Köpnick H., M. Schmidt, W. Brügging, J. Rüter and W. Kaminsky, *Polyesters.* Ullmann's Encyclopedia of Industrial Chemistry, 2005. **A21**: p. 233–238.
3. Hovenkam.Sg, *Kinetic Aspects of Catalyzed Reactions in Formation of Poly(Ethylene Terephthalate).* Journal of Polymer Science Part a-1-Polymer Chemistry, 1971. **9**(12): p. 3617-&.
4. Keller, A., G.R. Lester, and L.B. Morgan, *Crystallization Phenomena in Polymers. I. Preliminary Investigation of the Crystallization Characteristics of Polyethylene Terephthalate* Philosophical Transactions of the Royal Society A, 1954. **A247**: p. 1-12.
5. http://www.goodfellow.com. 1st Otc. 2012
6. Martin, L., *Handbook of Bottle Production and Preforms: Chapter 2-PET Preforms*, ed. O. Brandau. 2012, Norwich, USA: William Andrew Publishing.
7. *PET-Recycling Forum;"Current Technological Trends in Polyester Recycling"; 9th International Polyester Recycling Forum Washington*. 2006, Sao Paulo.
8. Wunderlich, B., *Macromolecular Physics; Volume 2, Crystal Nucleation, Growth*. 1976, London: Anealing Academic Press.
9. Wunderlich, B., *Macromolecular Physics; Volume 2*. 1976, New York: Academic Press.
10. Muthukumar, M., *Nucleation in Polymer Crystallization.* Advances in Chemical Physics, Vol 128, 2004. **128**: p. 1-63.
11. Young R.J and Lovell P.A, *Introduction to Polymers*. 2nd ed. 1991, London: Chapman & Hall.
12. Hoffman, J.D. and J.J. Weeks, *Melting Process and Equilibrium Melting Temperature of Polychlorotrifluoroethylene.* Journal of Research of the National Bureau of Standards Section a-Physics and Chemistry, 1962. **66**(Jan-F): p. 13-&.
13. Turnbull, D. and J.C. Fisher, *Rate of Nucleation in Condensed Systems.* Journal of Chemical Physics, 1949. **17**(1): p. 71-73.

14. Gibbs J.W., *The Scientific Papers of J. Williard Gibbs* 1962, New York: Dover.
15. Lauritze.J.I and J.D. Hoffman, *Extension of Theory of Growth of Chain-Folded Polymer Crystals to Large Undercoolings.* Journal of Applied Physics, 1973. **44**(10): p. 4340-4352.
16. Jenkins, M.J., *Crystallisation in miscible blends of PEEK and PEI.* Polymer, 2001. **42**(5): p. 1981-1986.
17. Cebe, P. and S.D. Hong, *Crystallization Behavior of Poly(Etheretherketone).* Polymer, 1986. **27**(8): p. 1183-1192.
18. Al Lafi, A.G., J.N. Hay, and D.J. Parker, *The effect of proton irradiation on the melting and isothermal crystallization of poly (ether-ether-ketone).* Journal of Polymer Science Part B-Polymer Physics, 2008. **46**(11): p. 1094-1103.
19. Guttman, C.M., J.D. Hoffman, and E.A. Dimarzio, *Monte-Carlo Calculation of Sans for Various Models of Semi-Crystalline Polyethylene.* Faraday Discussions, 1979. **68**: p. 297-309.
20. Hoffman, J.D., C.M. Guttman, and E.A. Dimarzio, *On the Problem of Crystallization of Polymers from the Melt with Chain Folding.* Faraday Discussions, 1979. **68**: p. 177-197.
21. Hoffman, J.D., *Regime-Iii Crystallization in Melt-Crystallized Polymers - the Variable Cluster Model of Chain Folding.* Polymer, 1983. **24**(1): p. 3-26.
22. Hoffman, J.D., *Role of Reptation in the Rate of Crystallization of Polyethylene Fractions from the Melt.* Polymer, 1982. **23**(5): p. 656-670.
23. Lauritzen, J.I. and J.D. Hoffman, *Theory of Formation of Polymer Crystals with Folded Chains in Dilute Solution.* Journal of Research of the National Bureau of Standards Section a-Physics and Chemistry, 1960. **64**(1): p. 73-102.
24. Hoffman, J.D., et al., *Growth-Rate of Spherulites and Axialites from Melt in Polyethylene Fractions - Regime-1 and Regime-2 Crystallization.* Journal of Research of the National Bureau of Standards Section a-Physics and Chemistry, 1975. **79**(6): p. 671-699.
25. Avrami, M., *Kinetics of Phase Change II Transformation-Time Relations for Random Distribution of Nuclei* Journal of Chemical Physics, 1940. **8**(212-224).
26. Avrami, M., *Kinetics of Phase Change and Microstructure Kinetics of Phase Change III Journal of Chemical Physics.* Journal of Chemical Physics 1940:8:212-224 1941. **9**: p. 177-184.

27. Velisaris, C.N. and J.C. Seferis, *Crystallization Kinetics of Polyetheretherketone (Peek) Matrices.* Polymer Engineering and Science, 1986. **26**(22): p. 1574-1581.
28. Banks, W., M. Gordon, R. J. Roe and A. Sharples, *The Crystallization of Polyethylene .1.* Polymer, 1963. **4**(1): p. 61-74.
29. Hay, J.N. and M. Sabir, *Crystallization Kinetics of High Polymers . Polyethylene Oxide .2.* Polymer, 1969. **10**(3): p. 203-&.
30. Hay, J.N. and P.J. Mills, *The Use of Differential Scanning Calorimetry to Study Polymer Crystallization Kinetics.* Polymer, 1982. **23**(9): p. 1380-1384.
31. Hillier, I.H., *Modified Avrami Equation for Bulk Crystallization Kinetics of Spherulitic Polymers.* Journal of Polymer Science Part a-General Papers, 1965. **3**(9pa): p. 3067-&.
32. Price, F.P., *A Phenomenological Theory of Spherulitic Crystallization - Primary and Secondary Crystallization Processes.* Journal of Polymer Science Part a-General Papers, 1965. **3**(9pa): p. 3079-&.
33. Banks, W., A. Sharples, and J.N. Hay, *The effect of simultaneously occurring processes on the course of polymer crystallization.* Journal of Polymer Science Part a-1-Polymer Chemistry, 1964. **2**(9): p. 4059–4067.
34. Verhoyen, O., F. Dupret, and R. Legras, *Isothermal and non-isothermal crystallization kinetics of polyethylene terephthalate: Mathematical modeling and experimental measurement.* Polymer Engineering and Science, 1998. **38**(9): p. 1594-1610.
35. Hay, J.N., *Application of modified Avrami equations to polymer crystallization kinetics.* British Polymer Journal, 1973. **3**: p. 74-82.
36. Evans, U.R., *The Laws of Expanding Circles and Spheres in Relation to the Lateral Growth of Surface Films and the Grain-Size of Metals.* Transactions of the Faraday Society, 1945. **41**(7): p. 365-374.
37. Qin, J.L., S.Q. Guo, and Z.T. Li, *Melting behavior and isothermal crystallization kinetics of PP/mLLDPE blends.* Journal of Polymer Research, 2008. **15**(5): p. 413-420.
38. Charles, E. and J. Carraher, *Seymour/Carraher's polymer chemistry.* 2003: CRC Press.
39. McCrum, N.B., C.P.Buckley, and C.B.Bucknall, *Principles of Polymer Engineering*. 1988: Oxford University Press.
40. Mandelkern, L., *Characterization of Materials in Research: Ceramics and Polymers*. 1975, New York: Syracuse University Press, Syracuse.

41. Raimo, M., *"Kinematic" analysis of growth and coalescence of spherulites for predictions on spherulitic morphology and on the crystallization mechanism.* Progress in Polymer Science, 2007. **32**(6): p. 597-622.
42. Granasy, L., T. Pusztai, G. Tegze, J. A. Warren and J. F. Douglas, *Growth and form of spherulites.* Physical Review E, 2005. **72**(1).
43. Hartshorne, N.H. and A. Stuart, *Crystals and the Polarising Microscope*. 4th ed. 1970, London: Edward Arnold Ltd.
44. Sawyer, L.C., D.T. Grubb, and G.F. Meyers, *Polymer microscopy*. 2008: Springer.
45. Bassett, D.C., *Principle of Polymer morghology*. 1981, New York: Cambridge university press.
46. R.W.Cahn, P. Haasen, and E.J. Kramer., *Materials science and technology series : a comprehensive treatment*. Processing of polymers, ed. H. E.H. Vol. 18. 1997, Weinheim, Chichester: Wiley-VCH.
47. Hay, J.N., *"Crystallization from the Melt" in "Flow-Indusced Crystallization in Polymer Systems"*. 1979, London: Gordon and Breach Sci. Publishers Ltd.
48. Hoffman J.D, Davis GT, and L. JI., *Treatise on solid state chemistry. Crystalline and non-crystalline solids*, ed. H. NB. Vol. 3. 1976, New York: Plenum.
49. Lim, J.S., I. Noda, and S.S. Im, *Effects of metal ion-carbonyl interaction on miscibility and crystallization kinetic of poly(3-hydroxybutyrate-co-3-hydroxyhexanoate)/lightly ionized PBS.* European Polymer Journal, 2008. **44**(5): p. 1428-1440.
50. Hartley, F.D., F.W. Lord, and L.B. Morgan, *Crystallization Phenomena in Polymers. III. Effect of Melt Conditions and the Temperature of Crystallization on the Course of the Crystallization in Polyethylene Terephthalate.* Philosophical Transactions of the Royal Society A, 1954. **A247**: p. 23-34.
51. Van Antwerpen, F. and D.W.V. Krevelen, *Influence of crystallization temperature, molecular weight, and additives on the crystallization kinetics of poly(ethylene terephthalate).* Journal of Polymer Science: Polymer Physics Edition, 1972. **10**(12): p. 2423-2435.
52. Jabarin, S.A., *Crystallization kinetics of polyethylene terephthalate. II. Dynamic crystallization of PET.* Journal of Applied Polymer Science, 1987. **34**(1): p. 97-102.
53. Mitsuishi, Y. and M. Ikeda, *Studies on crystallization of poly(ethylene terephthalate) by differential thermal analysis. Special consideration of the*

two exothermic peaks in the thermogram of crystallization. Journal of Polymer Science Part A-2: Polymer Physics, 1966. **4**(2): p. 283-288.
54. Bell, J.P. and T. Murayama, *Relations between dynamic mechanical properties and melting behavior of nylon 66 and poly(ethylene terephthalate).* Journal of Polymer Science Part A-2: Polymer Physics, 1969. **7**(6): p. 1059-1073.
55. McGraw, G.E., *Study of molecular orientation in poly(ethylene terephthalate) fibers by fluorescence polarization.* Journal of Polymer Science Part A-2: Polymer Physics, 1970. **8**(8): p. 1323-1336.
56. Miller, G.W., *Thermal analyses of polymers. XIII. Crystalline character of the 70 ℃ transition of poly(ethylene terephthalate).* Journal of Polymer Science: Polymer Physics Edition, 1975. **13**(9): p. 1831-1844.
57. Nealy, D.L., T. G. Davis, and C.J. Kibler, *Thermal history and melting behavior of poly(ethylene terephthalate).* Journal of Polymer Science Part A-2: Polymer Physics, 1970. **8**(12): p. 2141-2151.
58. Ozawa, T., *Kinetics of non-isothermal crystallization.* Polymer, 1971. **12**(3): p. 150-158.
59. Misra, A. and R.S. Stein, *Light scattering studies of the early stages of the crystallization of poly(ethylene terephthalate).* Journal of Polymer Science Part B: Polymer Letters, 1972. **10**(6): p. 473-477.
60. Stein, R.S. and A. Misra, *Kinetics of growth of developing spherulites.* Journal of Polymer Science: Polymer Physics Edition, 1973. **11**(1): p. 109-116.
61. Reinsch, V.E. and Ludwig Rebenfeld, *Crystallization processes in poly(ethylene terephthalate) as modified by polymer additives and fiber reinforcement.* Journal of Applied Polymer Science, 1994. **52**(5): p. 649-662.
62. Jackson, J.B. and G.W. Longman, *The crystallization of poly(ethylene terephthalate) and related copolymers.* Polymer, 1969. **10**: p. 873-884.
63. Lu, X. and J.N. Hay, *The effect of physical aging on the rates of cold crystallization of poly(ethylene terephthalate).* Polymer, 2000. **41**(20): p. 7427-7436.
64. Abdesselam, M., J.P. Stoquert, S. Chami, M. Djebara and A.C. Chami, M. Siad, *Method to measure composition modifications in polyethylene terephthalate during ion beam irradiation.* Nuclear Instruments and Methods in Physics Research Section B: Beam Interactions with Materials and Atoms, 2009. **267**(1): p. 108-112.
65. Yoshii, T., Hirohisa Yoshida, and Tadashi Kawai, *Effect of structural relaxation of glassy PET on crystallization process observed by the*

simultaneous DSC–XRD and DSC–FTIR. Thermochimica Acta, 2005. **431**(1-2): p. 177-181.

66. Zhu, P. and D. Ma, *Study on the double cold crystallization peaks of poly(ethylene terephthalate) (PET): 2. Samples isothermally crystallized at high temperature*. European Polymer Journal, 1999. **35**(4): p. 739-742
67. Zhang, Z., M. Ren, J. Zhao, S. Wu and H. Sun, *Kinetics of non-isothermal cold crystallization of uniaxially oriented poly(ethylene terephthalate).* Polymer, 2003. **44**(8): p. 2547-2551.
68. Li, G., S.L. Yang, J.M. Jiang and C. X. Wu, *Crystallization characteristics of weakly branched poly(ethylene terephthalate).* Polymer, 2005. **46**(24): p. 11142-11148.
69. Avramov, I. and N. Avramova, *Kinetics of relaxation and crystallization of poly(ethylene terephthalate).* Journal of Non-Crystalline Solids, 1999. **260**(1-2): p. 15-20.
70. Dangseeyun, N., P. Srimoaon, P. Supaphol and M. Nithitanakul, *Isothermal melt-crystallization and melting behavior for three linear aromatic polyesters.* Thermochimica Acta, 2004. **409**(1): p. 63-77
71. Brandrup, J., E.H.Immergut, *Polymer Handbook.* Third ed. 1989: John Wiley & Sons.
72. Mark, J.E., *Polymer Data Handbook.* Second ed. 2009: Oxford University Press.
73. Speight, J.G. and N.A. Lange, *Lange's handbook of chemistry* 16 ed, ed. McGraw-Hill. 2005.
74. Dominghaus, H., *Plastics for Engineers: Materials, Properties, Applications*. 3rd ed. 1993, Munich Vienna New York Barcelona: Hanser Publishers.
75. Smith, B.C., *Fundamentals of Fourier Transform Infrared spectroscopy*. 1996, Boca Raton: CRC press.
76. Fawcett , H., A., *Polymer Spectroscopy*. 1996: John Wiley & Sons.
77. Stuart, B., *Infrared Spectroscopy: Fundamentals and Applications*. 2004: John Wiley & Sons.
78. Mackenzie, M.W., *Advances in applied Fourier transform infrafred spectroscopy* 1988 Chichester: Wiley
79. Ingle, J.D.J. and S.R. Crouch, *Spectrochemical Analysis*. 1988, New Jersey: Prentice Hall.
80. Bernhard, S., *Infrared and Raman spectroscopy: methods and applications*. 1994, Cambridge: Weinheim, VCH.
81. Scheuing, D., *Fourier transform infrared spectroscopy in colloid and interface science*. 1990, Washington, DC: American Chemical Society.

82. Planck, M., *The Theory of Heat Radiation*. 2nd ed, ed. M. Masius. 1914: P. Blakiston's Son & Co.
83. http://www.thermo.com.20th Feb 2012
84. Jiang, E.Y., *Advanced FT-IR Spectroscopy, Principles, Experiments and Applications Based on Research-Grade Nicolet ™ FT-IR Spectrometers*. 2008: Part of Thermo Fisher Scientific.
85. Oneill, M.J., *Analysis of Temperature-Controlled Scanning Calorimeter*. Analytical Chemistry, 1964. **36**(7): p. 1238-&.
86. Wunderlich, B., *Thermal Analysis*. 1990, New York: Academic Press.
87. http://www.perkinelmer.co.uk.20th Feb 2012
88. http://www.sintef.no/.5th May 2012
89. http://www.linkam.co.uk/.8th May 2012
90. Stieger, N., M. Aucamp, S.W. Zhang and M.M. de Villiers, *Hot-stage Optical Microscopy as an Analytical Tool to Understand Solid-state Changes in Pharmaceutical Materials.* American Pharmaceutical Review, 2012.
91. Vitez, I.M., A.W. Newman, M. Davidovich and C. Kiesnowski, *The evolution of hot-stage microscopy to aid solid-state characterizations of pharmaceutical solids.* Thermochimica Acta, 1998. **324**(1-2): p. 187-196.
92. Schonherr, H., R.M. Waymouth, and C.W. Frank, *Nucleation and crystallization of low-crystallinity polypropylene followed in situ by hot stage atomic force microscopy.* Abstracts of Papers of the American Chemical Society, 2003. **226**: p. U521-U521.
93. Krumme, A., *Measuring crystallization kinetics of high density polyethylene by improved hot-stage polarized light microscopy.* Polymer Testing, 2004. **23**(1): p. 29-34.
94. Wang, X., W.M. Hou, J.J. Zhou, L. Li, Y. Li and C.M. Chan, *Melting behavior of lamellae of isotactic polypropylene studied using hot-stage atomic force microscopy.* Colloid and Polymer Science, 2007. **285**(4): p. 449-455.
95. Atkinson, J.R., F. Biddlestone, and J.N. Hay, *An investigation of glass formation and physical ageing in poly(ethylene terephthalate) by FT-IR spectroscopy.* Polymer, 2000. **41**(18): p. 6965-6968.
96. Levchik, S.V., L. Costa, and G. Camino, *Effect of Ammonium Polyphosphate on Combustion and Thermal-Degradation of Aliphatic Polyamides.* Makromolekulare Chemie-Macromolecular Symposia, 1993. **74**: p. 95-99.
97. Holland, B.J. and J.N. Hay, *Thermal degradation of nylon polymers.* Polymer International, 2000. **49**(9): p. 943-948.

98. Holland, B.J. and J.N. Hay, *The kinetics and mechanisms of the thermal degradation of poly(methyl methacrylate) studied by thermal analysis-Fourier transform infrared spectroscopy.* Polymer, 2001. **42**(11): p. 4825-4835.
99. Holland, B.J. and J.N. Hay, *The thermal degradation of PET and analogous polyesters measured by thermal analysis-fourier transform infrared spectroscopy.* Polymer, 2002. **43**(6): p. 1835-1847.
100. Holland, B.J. and J.N. Hay, *The thermal degradation of poly(vinyl alcohol).* Polymer, 2001. **42**(16): p. 6775-6783.
101. Arefazar, A. and J.N. Hay, *Physical Aging in Glassy-Polymers - an Ir Spectroscopic Investigation of Poly(Ethylene-Terephthalate).* Polymer, 1982. **23**(8): p. 1129-1132.
102. Chen, Z.Y., J.N. Hay, and M.J. Jenkins, *FTIR spectroscopic analysis of poly(ethylene terephthalate) on crystallization.* European Polymer Journal, 2012. **48**(9): p. 1586-1610.
103. Kong, Y. and J.N. Hay, *Multiple melting behaviour of poly(ethylene terephthalate).* Polymer, 2003. **44**(3): p. 623-633.
104. Lu, X.F. and J.N. Hay, *Crystallization orientation and relaxation in uniaxially drawn poly(ethylene terephthalate).* Polymer, 2001. **42**(19): p. 8055-8067.
105. Lu, X.F. and J.N. Hay, *Isothermal crystallization kinetics and melting behaviour of poly(ethylene terephthalate).* Polymer, 2001. **42**(23): p. 9423-9431.
106. Kong, Y. and J.N. Hay, *The measurement of the crystallinity of polymers by DSC.* Polymer, 2002. **43**(14): p. 3873-3878.
107. Geur, U., S. Lau, B.B. Wunderlich and B. Wunderlich, *Heat Capacity and Other Thermodynamic Properties of Linear Macromolecules. VIII. Polyesters and Polyamides.* Journal of Physical and Chemical Reference Data, 1983. **12**(1): p. 65-89.
108. Liang, C.Y. and S. Krimm, *Infrared Spectra of High Polymers .9. Polyethylene Terephthalate.* Journal of Molecular Spectroscopy, 1959. **3**(5): p. 554-574.
109. Cobbs, W.H. and R.L. Burton, *Crystallization of Polyethylene Terephthalate.* Journal of Polymer Science, 1953. **10**(3): p. 275-290.
110. Miller, R.G.J. and H.A. Willis, *An Independent Measurement of the Amorphous Content of Polymers.* Journal of Polymer Science, 1956. **19**(93): p. 485-494.

111. Miyake, A., *The Infrared Spectrum of Polyethylene Terephthalate .1. The Effect of Crystallization.* Journal of Polymer Science, 1959. **38**(134): p. 479-495.
112. Schmidt, P.G., *Polyethylene Terephthalate Structural Studies.* Journal of Polymer Science Part a-General Papers, 1963. **1**(4): p. 1271-&.
113. Grime, D. and I.M. Ward, *The Assignment of Infra-Red Absorptions and Rotational Isomerism in Polyethylene Terephthalate and Related Compounds.* Transactions of the Faraday Society, 1958. **54**(7): p. 959-971.
114. Ward, I.M. and M.A. Wilding, *Ir and Raman-Spectra of Poly(M-Methylene Terephthalate) Polymers.* Polymer, 1977. **18**(4): p. 327-335.
115. Noda, I., *Two-Dimensional Infrared-Spectroscopy.* Journal of the American Chemical Society, 1989. **111**(21): p. 8116-8118.
116. Noda I and Ozaki Y, *Two-dimensional correlation spectroscopy - applications in vibrational and optical spectroscopy*. 2004, Chichester: John Wiley and Sons.
117. Noda, I., *Kernel analysis for two-dimensional (2D) correlation spectroscopy.* Journal of Molecular Structure, 2006. **799**(1-3): p. 34-40.
118. Noda, I., *Cyclical asynchronicity in two-dimensional (2D) correlation spectroscopy.* Journal of Molecular Structure, 2006. **799**(1-3): p. 41-47.
119. Marcott, C., A.E. Dowrey, and I. Noda, *Dynamic 2-Dimensional Ir Spectroscopy.* Analytical Chemistry, 1994. **66**(21): p. A1065-A1075.
120. Wu, Y.Q., I. Noda, F. Meersman and Y. Ozaki, *Orthogonal signal corrected two-dimensional (OSC 2D) correlation infrared spectroscopy.* Journal of Molecular Structure, 2006. **799**(1-3): p. 121-127.
121. Shinzawa, H., S. Morita, I. Noda and Y. Ozaki, *Effect of the window size in moving-window two-dimensional correlation analysis.* Journal of Molecular Structure, 2006. **799**(1-3): p. 28-33.
122. Noda, I., *Progress in two-dimensional (2D) correlation spectroscopy.* Journal of Molecular Structure, 2006. **799**(1-3): p. 2-15.
123. Noda, I., *Scaling techniques to enhance two-dimensional correlation spectra.* Journal of Molecular Structure, 2008. **883**: p. 216-227.
124. Zhong, Z.M., G.F. Wang, and M.L. Geng, *Probing strong adsorption of individual solute molecules at solid/liquid interfaces with model-based statistical two-dimensional correlation analysis.* Journal of Molecular Structure, 2006. **799**(1-3): p. 204-210.
125. Esmonde-White, F.L.W. and D.H. Burns, *Visualization of N-way data using two-dimensional correlation analysis.* Vibrational Spectroscopy, 2004. **36**(2): p. 287-292.

126. Gregoriou, V.G., S.E. Rodman, B.R. Nair and P.T. Hammond, *Two-dimensional correlation infared analysis (2D-IR) based on dynamic infrared spectroscopy used as a probe of the viscoelastic behavior of side chain liquid crystalline polyurethanes.* Journal of Physical Chemistry B, 2002. **106**(43): p. 11108-11113.
127. Palmer, R.A., P.Y. Chen, and M.H. Gilson, *Step-scan two-dimensional Fourier transform infrared (S-2 2D FT-IR) spectroscopy applied to the dynamic mechanical analysis of block copolymers.* Abstracts of Papers of the American Chemical Society, 1996. **212**: p. 26-Pmse.
128. Chen, P.C. and C.C. Joyner, *Coherent 2D Resonance Raman Spectroscopy as a tool for studying molecular structure.* Journal of Molecular Structure, 2006. **799**(1-3): p. 23-27.
129. Mello, C., A.E.M. Crotti, R. Vessecchi and W.R. Cunha, *2D Raman spectroscopy as an alternative technique for distinguishing oleanoic acid and ursolic acid.* Journal of Molecular Structure, 2006. **799**(1-3): p. 141-145.
130. Jung, Y.M. and I.S. Yang, *Analysis of Raman modes of YNi2B2C by two-dimensional correlation spectroscopy.* Journal of Molecular Structure, 2006. **799**(1-3): p. 173-176.
131. Noda, I., Y.L. Liu, and Y. Ozaki, *Two-dimensional correlation spectroscopy study of temperature-dependent spectral variations of N-methylacetamide in the pure liquid state .1. Two-dimensional infrared analysis.* Journal of Physical Chemistry, 1996. **100**(21): p. 8665-8673.
132. Noda, I., Y.L. Liu, and Y. Ozaki, *Two-dimensional correlation spectroscopy study of temperature-dependent spectral variations of N-methylacetamide in the pure liquid state .2. Two-dimensional Raman and infrared-Raman heterospectral analysis.* Journal of Physical Chemistry, 1996. **100**(21): p. 8674-8680.
133. Noda, I., Y.L. Liu , Y. Ozaki , M.A. Czarnecki, *Two-Dimensional Fourier-Transform near-Infrared Correlation Spectroscopy Studies of Temperature-Dependent Spectral Variations of Oleyl Alcohol.* Journal of Physical Chemistry, 1995. 99(10): p. 3068-3073.
134. Padermshoke, A., H. Sato, Y. Katsumoto, S. Ekgasit, I. Noda and Y. Ozaki, *Crystallization behavior of poly(3-hydroxybutyrate-co-3-hydroxyhexanoate) studied by 2D IR correlation spectroscopy.* Polymer, 2004. **45**(21): p. 7159-7165.
135. Padermshoke, A., Y. Katsumoto, H. Sato, S. Ekgasit, I. Noda and Y. Ozaki, *Surface melting and crystallization behavior of polyhydroxyalkanoates*

studied by attenuated total reflection infrared spectroscopy. Polymer, 2004. **45**(19): p. 6547-6554.

136. Wu, Y.Q., F. Meersman, and Y. Ozaki, *A novel application of hybrid two-dimensional correlation infrared spectroscopy: Exploration of the reversibility of the pressure- and temperature-induced phase separation of poly(N-isopropylacrylamide) and poly(N-isopropylmethacrylamide) in aqueous solution.* Macromolecules, 2006. **39**(3): p. 1182-1188.
137. Pastrana-Rios, B., *Simulation of FT-IR spectra and 2D-COS analysis for the thermal perturbation of apo-centrin.* Journal of Molecular Structure, 2006. **799**(1-3): p. 163-167.
138. Thomas, A.C. and H.H. Richardson, *2D-IR correlation analysis of thin film water adsorbed on alpha-Al2O3(0001).* Journal of Molecular Structure, 2006. **799**(1-3): p. 158-162.
139. Wang, L.X., Y.Q. Wu, and F. Meersman, *Two-dimensional correlation infrared spectroscopic study on the conformational changes occurring in the thermally induced pretransition of ribonuclease A.* Journal of Molecular Structure, 2006. **799**(1-3): p. 85-90.
140. Wang, L.X., Y.Q. Wu, and F. Meersman, *Clarification of the thermally-induced pretransition of ribonuclease A in solution by principal component analysis and two-dimensional correlation infrared spectroscopy.* Vibrational Spectroscopy, 2006. **42**(2): p. 201-205.
141. Nakashima, K., H. Fukuma, Y. Ozaki and I. Noda, *Two-dimensional correlation fluorescence spectroscopy V: Polarization perturbation as a new technique to induce intensity changes in fluorescence spectra.* Journal of Molecular Structure, 2006. **799**(1-3): p. 52-55.
142. Ashton, L., C.M.B. Boguslawa, and E.W. Blanch, *Application of two-dimensional correlation analysis to Raman optical activity.* Journal of Molecular Structure, 2006. **799**(1-3): p. 61-71.
143. Dluhy, R., S. Shanmukh, and S.I. Morita, *The application of two-dimensional correlation spectroscopy to surface and interfacial analysis.* Surface and Interface Analysis, 2006. **38**(11): p. 1481-1496.
144. Ji, H., H, Hwang, S.B. Kim, I. Noda and Y.M. Jung, *Characterization of spin-coated films of biodegradable poly(3-hydroxybutyrate-co-3-hydroxyhexanoate) copolymers by two-dimensional correlation spectroscopy.* Journal of Molecular Structure, 2008. **883**: p. 167-172.
145. Zhang, J.M., H. Sato, H. Tsuji, I. Noda and Y. Ozaki, *Differences in the CH3 center dot center dot center dot O=C interactions among poly(L-lactide), poly(L-lactide)/poly(D-lactide) stereocomplex, and poly(3-hydroxybutyrate)*

studied by infrared spectroscopy. Journal of Molecular Structure, 2005. **735**: p. 249-257.

146. Sasic, S., J.H. Jiang, and Y. Ozaki, *Potentials of variable-variable and sample-sample, generalized and statistical, two-dimensional correlation spectroscopies in investigations of chemical reactions.* Chemometrics and Intelligent Laboratory Systems, 2003. **65**(1): p. 1-15.
147. Sasic, S., A. Muszynski, and Y. Ozaki, *A new possibility of the generalized two-dimensional correlation spectroscopy. 1. Sample-sample correlation spectroscopy.* Journal of Physical Chemistry A, 2000. **104**(27): p. 6380-6387.
148. Sasic, S., A. Muszynski, and Y. Ozaki, *A new possibility of the generalized two-dimensional correlation spectroscopy. 2. Sample-sample and wavenumber-wavenumber correlations of temperature-dependent near-infrared spectra of oleic acid in the pure liquid state.* Journal of Physical Chemistry A, 2000. **104**(27): p. 6388-6394.
149. Noda, I., *2-Dimensional Infrared (2d Ir) Spectroscopy - Theory and Applications.* Applied Spectroscopy, 1990. **44**(4): p. 550-561.
150. Jiang, E.Y. and R.A. Palmer, *Comparison of phase rotation, phase spectrum, and two dimensional correlation methods in step-scan Fourier transform infrared photoacoustic spectral depth profiling.* Analytical Chemistry, 1997. **69**(10): p. 1931-1935.
151. Jiang, E.Y. and A. Grenov, *Extension of two-dimensional global phase difference correlation analysis to step-scan FT-IR photoacoustic spectral depth profiling of layered systems.* Journal of Molecular Structure, 2006. **799**(1-3): p. 188-195.
152. Morita, S., H. Shinzawa, I. Noda and Y. Ozaki, *Effect of band position shift on moving-window two-dimensional correlation spectroscopy.* Journal of Molecular Structure, 2006. **799**(1-3): p. 16-22.
153. Morita, S., H. Shinzawa, R. Tsenkova, I. Noda and Y. Ozaki, *Computational simulations and a practical application of moving-window two-dimensional correlation spectroscopy.* Journal of Molecular Structure, 2006. **799**(1-3): p. 111-120.
154. Czarnik-Matusewicz, B., et al., *Potential pitfalls concerning visualization of the 2D results.* Journal of Molecular Structure, 2006. **799**(1-3): p. 253-258.
155. Wang, Y.W., W.Y. Gao, I. Noda and Z.W. Yu, *A modified mean normalization method to reduce the effect of peak overlap in two-dimensional correlation spectroscopy.* Journal of Molecular Structure, 2006. **799**(1-3): p. 128-133.

156. Chen, Z.Y., J.N. Hay, and M.J. Jenkins, *The kinetics of Crystallization of Poly(ethylene terephthalate) measured by FTIR Spectroscopy.* European Polymer Journal, 2012 submitted for publication.
157. Padibjo, S.R. and I.M. Ward, *A Structural Study of the Tensile Drawing Behavior of Poly(Ethylene-Terephthalate).* Polymer, 1983. **24**(9): p. 1103-1112.
158. Bassett, D.C., R.H. Olley, and I.A.M.A. Raheil, *On crystallization phenomena in PEEK.* Polymer, 1988. **29**(10): p. 1745–1754.
159. Chan, T.W. and A.I. Isayev, *Quiescent polymer crystallization: Modelling and measurements.* Polymer Engineering & Science, 1994. **34**(6): p. 461-471.
160. Miller, R.L. and R.F. Boyer, *Chain folding and cross-sectional area per chain.* Journal of Polymer Science: Polymer Physics Edition, 1978. **16**(2): p. 371-374.
161. Miller, R.L. and R.F. Boyer, *Regularities in x-ray scattering patterns from amorphous polymers.* Journal of Polymer Science: Polymer Physics Edition, 1984. **22**(12): p. 2043-2050.
162. Brown, M.E., *Introduction to Thermal Analysis - Techniques and Applications*. 2nd ed. 2001, Netherlands: Kluwer Academic Publishers.
163. Kolb, R., C. Wutz, N. Stribeck, G. von Krosigk and C. Riekel, *Investigation of secondary crystallization of polymers by means of microbeam X-ray scattering.* Polymer, 2001. **42**(12): p. 5257-5266.
164. Yagpharov, M., *Thermal-Analysis of Secondary Crystallization in Polymers.* Journal of Thermal Analysis, 1985. **31**(5): p. 1073-1082.
165. Banks, W., M. Gordon, and A. Sharples, *The Crystallization of Polyethylene after Partial Melting.* Polymer, 1963. **4**(3): p. 289-302.
166. Flory, P.J. and A. Vrij, *Melting Points of Linear-Chain Homologs - Normal Paraffin Hydrocarbons.* Journal of the American Chemical Society, 1963. **85**(22): p. 3548-&.
167. Flory, P.J., R.A. Orwoll, and A. Vrij, *Statistical Thermodynamics of Chain Molecule Liquids .2. Liquid Mixtures of Normal Paraffin Hydrocarbons.* Journal of the American Chemical Society, 1964. **86**(17): p. 3515-&.
168. Flory, P.J., R.A. Orwoll, and A. Vrij, *Statistical Thermodynamics of Chain Molecule Liquids .I. Equation of State for Normal Paraffin Hydrocarbons.* Journal of the American Chemical Society, 1964. **86**(17): p. 3507-&.
169. Hay, J.N. and M. Wiles, *Surface Free-Energy of Extended Chain Crystals of Polyethylene.* Makromolekulare Chemie-Macromolecular Chemistry and Physics, 1977. **178**(2): p. 623-630.

170. Mills, P.J. and J.N. Hay, *The Lamella Size Distribution in Nonisothermally Crystallized Low-Density Polyethylene.* Polymer, 1984. **25**(9): p. 1277-1280.
171. Mehta, A., U. Gaur, and B. Wunderlich, *Equilibrium Melting Parameters of Poly(Ethylene-Terephthalate).* Journal of Polymer Science Part B-Polymer Physics, 1978. **16**(2): p. 289-296.
172. Daubeny, R.D. and C.W. Bunn, *The Crystal Structure of Polyethylene Terephthalate.* Proceedings of the Royal Society of London Series a-Mathematical and Physical Sciences, 1954. **226**(1167): p. 531-542.

Appendix

Supported Publications:

1. Chen, Z.Y., J.N. Hay, and M.J. Jenkins, *FTIR spectroscopic analysis of poly(ethylene terephthalate) on crystallization.* European Polymer Journal, 2012. **48**(9): p. 1586-1610.

   Received 22th Apr. 2012. Received in revised form 1st Jun. 2012. Accepted 11th Jun. 2012.

2. Chen, Z.Y., J.N. Hay, and M.J. Jenkins, *The thermal analysis of poly(ethylene terephthalate) by FTIR spectroscpy.* Thermochimica Acta, 2013. **552**: p. 123–130

   Received 11th Jul. 2012. Received in revised form 2nd Oct. 2012. Accepted 1st Nov. 2012.

3. Chen, Z.Y., J.N. Hay, and M.J. Jenkins, *The kinetics of crystallization of poly(ethylene terephthalate) measured by FTIR Spectroscopy*. European Polymer Journal, In Press, Corrected Proof, Available online 28 March 2013

   Received 28th Jun. 2012. Received in revised form 11th Mar. 2013. Accepted 17th Mar. 2013.

European Polymer Journal 48 (2012) 1586–1610

Contents lists available at SciVerse ScienceDirect

European Polymer Journal

journal homepage: www.elsevier.com/locate/europolj

FTIR spectroscopic analysis of poly(ethylene terephthalate) on crystallization

Ziyu Chen, J.N. Hay *, M.J. Jenkins

The School of Metallurgy and Materials, College of Physical Science and Engineering, The University of Birmingham, Edgbaston, Birmingham B15 2TT, UK

ARTICLE INFO

Article history:
Received 22 April 2012
Received in revised form 1 June 2012
Accepted 11 June 2012
Available online 29 June 2012

Keywords:
Poly(ethylene terephthalate)
Two-dimensional FTIR correlation spectroscopy
Synchronous and asynchronous mapping
Crystallization

ABSTRACT

The vibrational spectrum of partially crystalline poly(ethylene terephthalate), PET, appears to be unduly complex in that the absorption bands are split into amorphous and crystalline modes and are sensitive to chain configuration and orientation. Assignment of the bands has accordingly proved to be difficult and lead to differences in interpretation. Two-dimensional infrared spectroscopy is a recent novel analytical technique in vibrational spectroscopy which can be used to interpret differences in the spectra with time or temperature accompanying changes in structure and morphology and has been used to analyze the development of crystallinity within a polymer in which amorphous regions are transformed into crystalline regions and involving changes in molecular configuration.

Two-dimensional IR correlation spectroscopy has been successfully applied to these problems in the attempt to measure the fractional extent of crystallinity in PET as a function of time and crystallization temperature as well as changes to molecular configuration.

1. Introduction

Poly(ethylene terephthalate), PET, is an important commercial polymer and widely used in fibre production and in the manufacture of pressurized bottles. Since the development of physical and mechanical properties is closely associated with the degree of crystallinity and orientation the development of crystallinity and/or fibre morphology substantially improves dimensional stability and gas permeability. In the commercialization of the polymer it has been important to develop rapid analytical procedures to determine the degree of crystallinity and fibre orientation during processing in order to maintain material properties. Various IR spectroscopic techniques have been extensively used to determine crystallinity and orientation in PET [1–12] but many limitations have been cited which have restricted their application, not least of which have been the assignment of the molecular characteristic of the absorption bands which are observed in the vibrational spectrum of PET and their assignment to crystalline and amorphous regions.

This paper attempts to use recent developments, such as two dimensional correlation spectroscopy [13–15] to resolve many of the issues of band assignments as well as using the increased accuracy and speed of data acquisition of rapid scan FT IR spectroscopy to measure isothermal crystallization and melting behaviour of PET.

2. Experimental

Commercial PET films, 1–15 μm thick, were obtained from Goodfellow Ltd., UK. These were dried in a vacuum oven at 100 °C for 12 h prior to use and stress relieved by melting between KBr plates. Amorphous samples were produced by quenching into ice/water from above the melting point and subsequently dried in a vacuum oven below the glass transition temperature.

FTIR spectra were measured on Nicolet spectrophotometers, models 1860 and 8700 with a DTGS-KBR detector, on thin film samples mounted between KBr plates in an

* Corresponding author. Tel.: +44 121 414 4544; fax: +44 121 414 5232.
E-mail address: j.n.hay@bham.ac.uk (J.N. Hay).

0014-3057/$ - see front matter © 2012 Elsevier Ltd. All rights reserved.
http://dx.doi.org/10.1016/j.eurpolymj.2012.06.006

Thermochimica Acta 552 (2013) 123–130

Contents lists available at SciVerse ScienceDirect

Thermochimica Acta

journal homepage: www.elsevier.com/locate/tca

The thermal analysis of poly(ethylene terephthalate) by FTIR spectroscopy

Ziyu Chen, J.N. Hay*, M.J. Jenkins

The School of Metallurgy and Materials, The College of Physical Sciences and Engineering, The University of Birmingham, Edgbaston, Birmingham B15 2TT, UK

ARTICLE INFO

Article history:
Received 11 July 2012
Received in revised form 2 October 2012
Accepted 1 November 2012
Available online 28 November 2012

Keywords:
Poly(ethylene terephthalate)
DSC
FTIR spectroscopy
Trans/*cis* isomers
Crystallization
Melting

ABSTRACT

Thermal analysis-FTIR spectroscopy, TA-FTIR, has been used to characterize the phase transitions in thin films of poly(ethylene terephthalate) and it has been shown to have distinct advantages over other TA techniques in particular it was not so limited in sensitivity. Since the technique measured property, such as amorphous content or fractional crystallinity directly rather than the rate of change of the properties with time or temperature, it was not so restricted in the time scale over which measurements were made. It also had the advantage of measuring the change in concentration of different functional groups with temperature and determining the temperature range over which chain mobility set in and defining the type of molecular groups involved in the configurational changes.

The change in absorbance and shift in peak position with temperature are discussed in terms of the separation of crystalline and amorphous bands as well as defining the *cis*/*trans* ratio as a function of temperature.

Depending on the change in absorbance or peak position with temperature of the IR bands, they have been characterized as type I or type II behaviour. Measurements on both have been used to characterize the glass transition, crystallization and melting behaviour of PET.

1. Introduction

Thermal analysis-FTIR spectroscopy, TA-FTIR, has been used to study the chemical reactivity and physical properties of polymers at a molecular level. Polymer degradation, in particular, has been widely studied since it enables changes in the polymer structure to be followed as a function of temperature and time, the kinetics of reactions have been followed by the change in intensity of functional groups [1–7] and any significant change in chemical composition determined from the appearance and disappearance of absorption bands. In this way the relative importance of competing reactions have been established as well as the build-up and disappearance of transient species involved in the decomposition reactions.

Recently [8], the kinetics of isothermal crystallization of poly(ethylene terephthalate) has been measured by TA-FTIR by separating the crystalline and amorphous components of the carbonyl absorption bands as a function of time over a range of temperatures. This enabled the weight fraction crystallinity to be measured well into the secondary crystallization process over a greater time scale and wider temperature range than was possible by differential scanning calorimetry, DSC. The later technique by measuring the rate of crystallization rather than the fractional crystallinity was limited by the sensitivity of the calorimeter to measure heat flow and could not measure the secondary process directly [9–12].

This paper considers the value of TA-FTIR to measure phase and molecular transitions which occurs in an amorphous/crystallizable polymer, PET, and makes a direct comparison with DSC.

2. Experimental

Commercial PET films, with thickness between 1.5 and 13 μm, were obtained from Goodfellow Ltd, UK. They were stress relieved by melting between KBr plates or in aluminum pans, and then quenched into ice/water to produce amorphous samples as determined by DSC [11]. They were dried in a vacuum oven below the glass transition temperature, T_g, prior to use.

A Perkin-Elmer differential scanning calorimeter, DSC-7, interfaced to a computer was used as described elsewhere [9–12] to follow the variation of the rate of heat evolution with time. The temperature scale of the DSC was calibrated from the melting point of high purity metals: tin (230.06 °C); indium (154.58 °C). The power response of the calorimeter was calibrated from the enthalpy of fusion of indium, taken to be 28.47 J g^{-1}. Disc shaped samples of PET, cut from a moulded sheet, were weighted and enclosed in aluminum pans. An empty aluminum pan was used as reference. Samples were initially heated from room temperature to 275 °C at a heating rate of 10 °C min^{-1} and kept for 2 min at 275 °C. They were subsequently cooled to 30 °C at 10 °C min^{-1}. The thermal procedure

* Corresponding author. Tel.: +44 121 414 4544; fax: +44 121 414 5232.
E-mail address: j.n.hay@bham.ac.uk (J.N. Hay).

0040-6031/$ – see front matter © 2012 Elsevier B.V. All rights reserved.
http://dx.doi.org/10.1016/j.tca.2012.11.002

European Polymer Journal xxx (2013) xxx–xxx

Contents lists available at SciVerse ScienceDirect

European Polymer Journal

journal homepage: www.elsevier.com/locate/europolj

The kinetics of crystallization of poly(ethylene terephthalate) measured by FTIR spectroscopy

Ziyu Chen, J.N. Hay *, M.J. Jenkins

The School of Metallurgy and Materials, College of Physical Sciences and Engineering, The University of Birmingham, Edgbaston, Birmingham B15 2TT, UK

ARTICLE INFO

Article history:
Received 28 June 2012
Received in revised form 11 March 2013
Accepted 17 March 2013
Available online xxxx

Keywords:
Poly(ethylene terephthalate)
FTIR spectroscopy
Isothermal crystallization
Primary and secondary crystallization

ABSTRACT

The kinetics of crystallization of poly(ethylene terephthalate), PET, have been measured by FTIR spectroscopy using the absorbances of the crystalline and amorphous phase carbonyl bands at 1717 and 1727 cm^{-1} to determine the fractional crystallinity as a function of time and isothermally over the temperature range 230–240 °C. Both primary and secondary crystallization could be measured with similar accuracy limited only by the length of time over which the measurements were made.

The primary and secondary crystallization time dependences were fitted to Avrami equations with n values of 2.0 and 1.0, respectively. The initial primary process was interpreted as due to two-dimensional spherulites restricted early in the crystallization by the thickness of the film sample, 1.5–3.0 μm. Secondary crystallization was considered to be due to one dimensional thickening of lamellae produced in the initial production of the spherulites.

FTIR spectroscopy was considered to have some advantages in measuring the development of crystallinity over other techniques, such as DSC and DTA, which measure the rate of crystallization and are limited by the sensitivity of the calorimeter to measure the rate of heat evolution.

1. Introduction

Poly(ethylene terephthalate), PET, has played a unique part in the development of crystallization kinetics as it was one of the first polymers to be studied by dilatometry [1] and the isothermal crystallization-time dependence interpreted in terms of the Avrami equation [2]. Because it is a commercially important engineering polymer, as a molding material, as fibers and in the manufacture of pressurized bottles, whose material properties are markedly dependent on microstructure, morphology and degree of orientation, its crystallization behavior has been widely studied by a range of other experimental techniques, including calorimetry, X-ray diffraction, light scattering and vibrational spectroscopy [1,3–20]. Differential scanning calorimetry (DSC) in particular has been most successful in studying the effect of molecular structure and copolymerization in controlling the rate of primary crystallization but it is deficient in not being sufficiently sensitive to measure to any appreciable extent the development of secondary crystallization with time [21,22].

Secondary crystallization is important in establishing the final degree of crystallinity and the distribution of lamellar thicknesses achieved during any thermal treatment or drawing process. This has a pronounced effect on the ultimate material properties achieved. We have recently reviewed the application of FTIR spectroscopy to measure the development of crystallinity and the effect on the IR spectra, outlining procedures for separating amorphous and crystalline absorption bands [23]. It was observed by means of two-dimensional correlation spectroscopy that the carbonyl band at 1720 cm^{-1} split into two, at 1717 and 1727 cm^{-1}, attributed to crystalline and amorphous content and that the absorbance of each are in-

* Corresponding author. Tel.: +44 121 414 4544; fax: +44 121 414 5232.
E-mail address: j.n.hay@bham.ac.uk (J.N. Hay).

0014-3057/$ - see front matter © 2013 Elsevier Ltd. All rights reserved.
http://dx.doi.org/10.1016/j.eurpolymj.2013.03.020